JAVIER GRACIA-TABUENCA

Impedance Pneumography for the Nocturnal Assessment of Lower Airway Obstruction

JAVIER GRACIA-TABUENCA

Impedance Pneumography for the Nocturnal Assessment of Lower Airway Obstruction

ACADEMIC DISSERTATION
To be presented, with the permission of
the Faculty of Medicine and Health Technology
of Tampere University,
for public discussion at Tampere University,
on 4 December 2020, at 12 o'clock.

ACADEMIC DISSERTATION
Tampere University, Faculty of Medicine and Health Technology
Finland

Responsible supervisor and Custos	University Lecturer Jari Viik Tampere University Finland	
Pre-examiners	Professor Philipp Latzin University of Bern Switzerland	Assistant professor Ilkka Laakso Aalto University Finland
Opponents	Professor Pasi Karjalainen University of Eastern Finland Finland	Professor Tuomas Jartti University of Turku Finland

Cover design: Roihu Inc.

ACKNOWLEDGEMENTS

"I cannot remember the books I've read any more than the meals I have eaten; even so, they have made me."

Ralph Waldo Emerson

I cannot remember the all the personal interactions that I've had during my PhD; even so, they have made this thesis and made who I'm today.

On the latest of these interactions, I'd like to express my gratitude to pre-examiners Professor Philipp Latzin from Bern and assistant professor Ilkka Laakso from Helsinki, who kindly help polishing this thesis.

On the longest of these interactions, I'd like to thank my supervisor Jari Viik for his guidance, his continuous help, and his sorcery to always finding the financial support for this work. Likewise, I shall thank the founding instances, Tampere University of Technology's Graduate School and Tampere Tuberculosis Foundation.

The most essential interactions have been, undoubtedly, the countless times that Ville-Pekka Seppä has directly or intermediately helped me. Seppä redesigned the almost forgotten impedance pneumography technology, put it into clinical practice, and I'm confidence he will soon lead it into clinical routine. All articles forming this thesis were carried using technology and recordings lead by him. I'm also greatly thankful to the many people helping Seppä in his endeavour. Particularly, to all the co-authors of my publications. I have especially learnt the most from the corrections made by Pekka Malmberg and Jussi Karjalainen, which gave clinically value to the manuscripts. I also wish to thanks the younger researchers Milla Jauhiainen for her hard work, and Anton Hult for allowing me to include his first authored manuscript in this dissertation.

Other short of interactions have been essential to stay sane during the frustration and uncertainty that research occasional inflicts. There are several friends from different countries that have kept my soul warm while being far from own origins. There are few that brace me while being far from my close ones. There is one that has been my wonderwall and forced me to live other lives. Lastly, an honourable mention goes to my son Samuel, who's imminent arrival squeezed the last strength to end this thesis before his birth.

ABSTRACT

Tidal breathing analysis is a lung function technique suggested for infants and children who are unable to cooperate with forced spirometry. This technique aims to quantify lower airway obstruction from average changes in the shape or the breath-to-breath variations of the tidal breathing flow-volume loop (TBFV) profiles. If tidal airflow is recorded with a mouth pneumotachograph (PNT), tidal breathing analysis finds the same limitations as other alternatives to spirometry. These are typically the need for sedation and the assessment of lung function only for sort times at the hospital. Recent improvements in impedance pneumography (IP) enable for the first time the continuous non-invasive monitoring of respiratory airflow overnight. This can improve the analysis of tidal breathing by capturing circadian and nocturnal worsening in lower airway obstruction. However, due to the lack of previous methods recording nocturnal airflow, little is known about how the interaction of sleep physiology and lower airway obstruction is reflected in the shape and variability of tidal breathing.

This thesis reviews the literature regarding shape and variability analysis of tidal breathing during lower airway obstruction, sleep, or maturation. The thesis also extends this knowledge by presenting four original publications. The first publication describes a technical improvement in the IP method. The other three study the nocturnal TBFV's shape in wheezing infants and children, and the nocturnal TBFV's variability in healthy children.

Both the literature and the results agree that for the TBFVs' shape, increasing lower airway obstruction advances the peak of expired flow and turns the middle part from convex to concave. However, these changes occur at a different degree of obstruction for different subjects depending on the compensation strategy that they have chosen. In infants, changes putatively occur at a higher degree of obstruction because most of the expiration is controlled by the respiratory musculature. During rapid eye movement (REM) sleep, changes putatively occur at a lower degree of obstruction because muscle atony limits the compensation strategies. For the variability of TBFVs, increasing lower airway obstruction decreases the variability in the early part of expiration in the long term (the whole night).

However, the short-term variability is dominated by the stage-dependent variations in the respiratory drive.

The thesis concludes that, at the present, tidal breathing analysis can estimate lower airway obstruction but cannot quantify its degree with accuracy. However, nocturnal IP recordings are easy to conduct and can serve as a first-line diagnosis or for the monitoring of disease progression. Nonetheless, future improvements in signal processing and the understanding of the tidal airflow signal can easily increase the accuracy and find new applications.

CONTENTS

ABBREVIATIONS

BD   bronchodilator

BP   bronchial provocation

CF   cystic fibrosis

CGO   cardiogenic oscillation

CLD   chronic lung disease

COPD   chronic obstructive pulmonary disease

DRG   dorsal respiratory group

E2   expiration neural phase

ECG   electrocardiogram

EEG   electroencephalogram

EMG   electromyogram

EVI   expiratory variability index

ExBr   expiration breaking

ExIn   expiration interruption

ExPa   passive expiration

FOT   forced oscillation technique

FRC   functional residual capacity

HR	high risk
IBI	interbreath intervals
ICS	inhaled corticosteroids
Insp.	inspiration neural phase
IP	impedance pneumography
IP-HRSG	IP heart rate Savitzky-Golay
IP-NLPF	IP non-linear local projection filter
IR	intermediary risk
LR	low risk
mAPI	modified asthma predictive index
MSE	multi-scale entropy
N1	NREM substage 1
N2	NREM substage 2
N3	NREM substage 3
NLPF	non-linear local projection filter
NREM	non-rapid eye movement
PCA	posterior cricoarytenoid
PIIA	post-inspiratory inspiratory activity
PIRCM	paradoxical inward rib cage motion
PNT	pneumotachograph
Post-I	post-inspiration neural phase
PRG	pontine respiratory group

PSG   polysomnograph

REM   rapid eye movement

rEMG   respiratory electromyogram

RIP   respiratory inductance plethysmography

RQA   recurrence quantification analysis

RTC   rapid thoracoabdominal compression

SG   Savitzky-Golay

SOT   single breath occlusion technique

TA   thyroarytenoid constrictor

TBFV   tidal breathing flow-volume loop

TUT   Tampere University of Technology

VRG   ventral respiratory group

x

SYMBOLS

Respiratory mechanics

C_{rs}	compliance of the respiratory system	l/Pa
FRC	functional residual capacity	L
P_{ao}	alveolar pressure	Pa
R_{rs}	resistance of the respiratory system	$Pa \cdot l^{-1} \cdot s$
τ_{rs}	time constant of the respiratory system	s
$\dot{V}$	airflow	l/s
V_r	resting lung volume	l

Respiratory indices

IBI	interbreath interval	s
P_{CO_2}	carbon-dioxide pressure	mmHg
P_{O_2}	oxygen pressure	mmHg
pH	acidic or basic indicator	1
RR	respiratory rate	min^{-1}
V_t	tidal lung volume	l

Lung function indices

FEV1	forced expired volume in one second	l

FEV1/FVC	relative forced expired volume in one second	l
FRC_{pleth}	functional residual capacity (Plethysmograph)	l
PD40	provocative dose at 40% of $z\dot{V}_{maxFRC}$	μg
R_{aw}	airway resistance (Plethysmograph)	$kPa{\cdot}l^{-1}{\cdot}s$
$R_{rs}5$	respiratory system resistance at 5Hz (FOT)	$kPa{\cdot}l^{-1}{\cdot}s$
$R_{rs}(f)$	respiratory system resistance (FOT)	$kPa{\cdot}l^{-1}{\cdot}s$
$X_{rs}(f)$	respiratory system reactance (FOT)	$kPa{\cdot}l^{-1}{\cdot}s$
sGaw	specific airway conductance (Plethysmograph)	$kPa{\cdot}s$
$\dot{V}_{maxFRC}$	maximum flow at FRC (RTC)	L/s
$z\dot{V}_{maxFRC}$	adjusted maximum flow at FRC (RTC)	L/s

Tidal breathing shape indices*

EV	extrapolated volume	s
PTEF	peak tidal expiratory flow	l/s
P_{FV}	exponential decrease from PTEF to TEF05	1
τ_{RS}	time constant of the respiratory system	s
T_E	time of expiration	s
T_I	time of inspiration	s
TEF50	tidal expiratory flow at 50% tidal volume	l/s
TEF50/PTEF	relative tidal exp. flow at 50% tidal volume	1
TEF25	tidal expiratory flow at 25% tidal volume	l/s
TEF25/PTEF	relative tidal exp. flow at 25% tidal volume	1
TEF10	tidal expiratory flow at 10% tidal volume	l/s
TEF05	tidal expiratory flow at 5% tidal volume	l/s
TEF05/PTEF	relative tidal exp. flow at 5% tidal volume	1
T_{PTEF}	time to peak tidal expiratory flow	s

T_{PTEF}/T_E	relative time to peak tidal exp. flow	1
$\dot{V}_{b-o}$	end expiratory break-off	l/s
V_{PTEF}	expired volume at peak tidal expiratory flow	l
V_{PTEF}/V_E	relative volume to peak tidal exp. flow	1

Variability indices

ApEn	approximate entropy	1
CD	correlation dimension	n
CSR_{min}	expiratory minimum curve shape correlation	1
CV	coefficient of variation	1
DFA	detrended fluctuation analysis	1
EVI	expiration variability index	1
IQR	interquartile range	x
kd	harmonic distortion	%
KSE	Kolmogorov-Sinai entropy	1
LLE	largest Lyapunov exponent	1
MAD	median absolute deviation	x
MFDFA	multifractal detrended fluctuation analysis	1
NL	noise limit	1
RC	repeatability coefficient	%
REC	recurrent points for a given radius in RQA	n
$r_{15-45}IQR$	IQR of correlations on the 15-45% exhaled volume	1
RPDEn	recurrence period density entropy	1
s	slope of a line fitted the airflow power	mL
SampEn	sample entropy	1
SD	standard deviation	x

Bioimpedance

U	electrical voltage	V
I	electrical current	A
Z	electrical impedance	Ω
ρ	resistivity	$\Omega \cdot m$
A	area of current flow	m^2
l	length of the conductor	m
J_{LU}	voltage lead field	m^{-2}
J_{LI}	current lead field	m^{-2}

Non-linear projection filter test indices*

Dss	absolute sample-by-sample difference	l/s
D_L	absolute mean value of linearity	l/s
$\Delta P_{f_1 - f_2}$	difference in power in the range $f_1 - f_2$ range	l^2/s
r	noise reduction factor	1

Non-linear projection filter parameters

i	iterations	n
m_p	projection dimension	n
rad	radius	s
τ_s	downsampling rate	1
τ_w	time window	s

* If absolute indices are measured with impedance pneumography, units are expressed in Ohms (Ω) instead of litres (l)

LIST OF PUBLICATIONS

This thesis is based on the following four publications hereafter referred as P.*N*, where *N* stands for the publication number. All the publications are reprinted in this thesis with permission from the publisher.

P.I J. Gracia, V.-P. Seppä, A. Pelkonen, A. Kotaniemi-Syrjänen, M. Mäkelä, P. Malmberg and J. Viik (2017). Nonlinear Local Projection Filter for Impedance Pneumography. *EMBEC & NBC 2017*. IFMBE Proceedings. Springer, Singapore, 306–309. DOI: 10.1007/978-981-10-5122-7_77

P.II J. Gracia-Tabuenca, V.-P. Seppä, M. Jauhiainen, A. Kotaniemi-Syrjänen, K. Malmström, A. Pelkonen, M. J. Mäkelä, J. Viik and L. P. Malmberg (2019). Tidal Breathing Flow Volume Profiles during Sleep in Wheezing Infants Measured by Impedance Pneumography. *Journal of Applied Physiology* 126.5, 1409–1418. DOI: 10.1152/japplphysiol.01007.2018

P.III J. Gracia-Tabuenca, V.-P. Seppä, M. Jauhiainen, M. Paassilta, J. Viik and J. Karjalainen (2020). Tidal Breathing Flow Profiles during Sleep in Wheezing Children Measured by Impedance Pneumography. *Respiratory Physiology & Neurobiology* 271, 103312. DOI: 10.1016/j.resp.2019.103312

P.IV A. Hult, R. G. Juraški, J. Gracia-Tabuenca, M. Partinen, D. Plavec and V.-P. Seppä (2019). Sources of Variability in Expiratory Flow Profiles during Sleep in Healthy Young Children. *Respiratory Physiology & Neurobiology* 274, 103352. DOI: 10.1016/j.resp.2019.103352

AUTHOR CONTRIBUTIONS

All named authors in all four publications approved and made contributions to the writing. The author of the present thesis made the following specific contribution to each publication.

In publication P.I, he was the main author, designed and implemented the signal processing and the protocol to validate it.

In publication P.II, he was the main author, analysed the recorded signals, designed and implemented the signal processing, and produced the statistical analysis.

In publication P.III, he was the main author, analysed the recorded signals, designed and implemented the signal processing, and produced the statistical analysis.

In publication P.IV, he contributed to the analysis of the results and the writing of the discussion.

The implemented signal processing tools are available in:

github.com/javier-gracia-tabuenca.

1 INTRODUCTION

Asthma is the most common chronic respiratory disease among children, and chronic obstructive pulmonary disease (COPD) is the fifth leading cause of mortality worldwide (World Health Organization 2018). These two diseases are characterised by the narrowing of the lower airway causing wheezing, chest tightness, and shortness of breath. The lower airway narrowing, or obstruction, is conventionally assessed with a spirometer. During a spirometer test, the subject conducts a forced exhaling manoeuvre and features of the airflow recorded at the mouth are analysed. However, young children, infants, as well as the elderly and unconscious or heavily sedated patients, cannot adequately perform the forced exhaling manoeuvre. For this reason, the current assessment of these groups is based on qualitative methods which are susceptible to subjective interpretations. For instance, childhood asthma is diagnosed by considering the presence of allergies, history of symptoms, or family asthma.

Considerable efforts have been made to find quantitative techniques for measuring lung function in uncooperative patients. Attempted techniques can be grouped into two broad categories. Firstly, these techniques that assess the response of the respiratory system to an imposed external stimulus, such as rapid thoracoabdominal compression (RTC) or forced oscillation technique (FOT). Secondly, techniques that assess the undisturbed tidal breathing, conventionally recorded at the mouth using a pneumotachograph (PNT). Within this second category, the most common method has been to analyse features from the shape of the expiratory flow or the tidal breathing flow-volume loop (TBFV) profiles. Shape features are commonly derived from several breaths and averaged. More recently, with the advances in the field of systems biology, new methods have been proposed based on the analysis of the breath-to-breath variations. Nonetheless, none of these techniques has yet reached a wide acceptance into clinical routine. The reasons for this include the need for expensive equipment, patients' sedation, or the lack of repeatability. Moreover, the bulky instrumentation used by these techniques only allows for a short assessment of lung function at the hospital missing circadian changes in diseases such as asthma (Sutherland 2005).

Previous research at Tampere University of Technology (TUT) has brought a series of improvements to an old instrumentation technique, namely impedance pneumography (IP). These improvements enable for the first time the continuous monitoring of tidal flow for long periods. Recording long-term airflow opens up new possibilities for the analysis of tidal breathing and therefore the quantitative assessment of lower airway obstruction. IP uses skin surface electrodes to derive respiratory flow from the changes in thoracic electrical impedance caused by lung aeration. Unlike conventional PNT recording airflow through a mouthpiece, IP does not alter breathing (Dolfin et al. 1983; Emralino and Steele 1997) and therefore, it does not interfere in the shape (P. J. Fleming, Levine and Goncalves 1982; Perez and Tobin 1985) nor variability analysis (Fiamma, Samara et al. 2007). Unlike other non-invasive instruments recording changes in thorax diameter, such as respiratory inductance plethysmography (RIP), IP can reliably derive tidal flow (Hollier et al. 2014). Before the present work, Vuorela 2011 utilised modern electronics to reduce IP instrumentation into a portable recording device. V.-P. Seppä 2014 developed novel signal processing and validated it and the new device in multiple clinical trials. Consequently, the new IP technology was utilised in several clinical studies at Helsinki, Tampere, and Zagreb university hospitals (Malmberg et al. 2017; V.-P. Seppä, Hult et al. 2019; V.-P. Seppä, Paassilta et al. 2018). These studies propose using IP technology for the analysis of tidal breathing during the night in children and infants. Recording during sleep ensures physiological and psychological stability, provides longer recordings, and more importantly, it allows us to monitor the symptoms of obstructive diseases overnight, when they are known to worsen (Mortola 2004).

However, due to the previous lack of technology able to record long-term airflow, little is known about how sleep physiology affects the shape and variability of the TBFV profiles, and therefore if sleep undermines the ability of tidal flow analysis to detect obstruction in asthmatic children and infants. Moreover, on the technical side, new methods are needed to ensure a low noise IP-derived airflow from long-term recordings. Shape analysis is commonly performed in visually accepted TBFV profiles (Beydon et al. 2007) which becomes infeasible in nocturnal recordings with hundreds of profiles.

This thesis summarises the latest knowledge on the mechanics of the respiratory system and the neural control of respiration, as well as their behaviour during sleep, maturation, and airway obstruction (section 3.1). Consequently, the thesis reviews the literature on these works, which study changes in tidal breathing associated with airway obstruction, maturation, or sleep for shape and variability analysis (subsection 3.2.2 and 3.2.3 respectively).

The literature's lack of studies on obstruction during sleep was completed with three original articles studying changes in tidal breathing in sleeping healthy and wheezing infants and children. An additional technical article describes a processing method to increase the signal-to-noise ratio in long IP recordings (chapter 4 and 5). Finally, this thesis discusses the possible mechanisms behind the empirical associations found in our studies and the literature. Limitations and possible improvements for the use of IP to detect airway obstruction overnight are also discussed (chapter 6).

2 AIMS OF THE THESIS

The general objective of this thesis was to study the ability to detect airway obstruction from tidal breathing recorded overnight using IP, and whether sleep and maturation influence this ability. This general aim can be divided into four partial aims as follow:

- to develop a signal processing method that increases the signal-to-noise ratio of the IP signal, thus allowing for more accurate long-term analyses (P.I).

- to study the changes in shape on the IP-derived TBFV profiles during sleep in wheezing infants with different asthma risks and degree of respiratory obstruction determined by conventional lung function (P.II).

- to study the changes in shape on the IP-derived TBFV profiles in wheezing children during sleep under medical treatment for lower airway obstruction, and two and four weeks after the interruption of the treatment (P.III).

- to study the variability on the IP-derived TBFV profiles in healthy children between different sleep stages, within the same sleep stage, and before and after a body position change (P.IV).

3 BACKGROUND

This chapter is divided into three main sections. The first section introduces the anatomy and functioning of respiratory mechanics and respiratory control in humans. Subsequently, it describes how mechanics and control adapt to natural changes during sleep, maturation, and obstructive lung diseases. The second section summarises the existing methods to assess airflow obstruction in infants and children with an emphasis on these based on the analysis of tidal breathing. The third section describes the working principle and the current state of the IP technology.

3.1 The respiratory system

In essence, the respiratory system is a $50\,\text{m}^2$ to $70\,\text{m}^2$ contact surface between the atmosphere and the bloodstream, where metabolic gases are exchanged (Notter 2000). For convenience, this surface is crinkled into two sacks (lungs) and fitted inside the thorax. A piping system (airway tree) and a pump (respiratory muscles) ensure the air circulation along the packed surface. Exchange of gases must work efficiently from the moment of birth to the last gasp. Hence, a robust feedback system adjusts air pumping to the changing metabolic demands of the body, the environment, and to developmental and pathological changes.

   The next sub-sections summarise the minimum knowledge needed to understand the rest of the thesis. However, each of these subjects is sufficiently deep and complex to have produced several books and reviews. To gain a deeper understanding of these subjects, the reader is encouraged to consult the following: Levitzky 2018 for background on respiratory physiology; Feldman, McCrimmon and Morrison 2013 and Del Negro, Funk and Feldman 2018 for an up-to-date view on respiratory control; Chapter 21 and 22 in Horner 2017, and Krimsky and Leiter 2005 for the control of breathing during sleep; Chapter 23 in Carroll and Donnelly 2013 for respiration during sleep on children; and Ballard 1999 for nocturnal asthma in adults.

3.1.1 Mechanics of respiration

The lungs and the chest wall are tightly connected by a thin layer of fluid between the parietal and visceral pleurae. This connexion prevents the former from collapsing under its own recoiling force. Under null muscle activity, the outward recoil of the chest wall opposes the inward recoil of the lungs, thus keeping the lungs partially inflated and ensuring a negative intrapleural pressure (Sahn, S.A. 1988). The lung volume at this balancing point is known as resting lung volume (V_r) (subsection 3.1.4 Figure 3.4). In a resting individual, there is a small tonic muscle activity that slightly elevates lung volume over the passive V_r. This lung volume is known as functional residual capacity (FRC) (Muller, Volgyesi et al. 1979). V_r changes with posture (Lumb and Nunn 1991) and body size (Gillespie 1983). FRC is closer to V_r during sleep (subsection 3.1.3), and is farther apart for infants (subsection 3.1.4).

During inspiration, the diaphragm and the external intercostal muscles contract. Thoracic volume increases as the diaphragm descends its dome into the abdominal cavity, external intercostal muscles enlarge the rib cage, and the scalene muscle elevates the thorax (Troyer and Loring 2011). Expansion of the thorax farther decreases the pressure of the pleural cavity. This pressure drop propagates mechanically through the alveolar septa dilating alveoli across the lungs. At this point, subatmospheric pressure at the alveoli drives the external air into the body through the nasal cavity and the mouth. Inhaled air crosses, the pharynx, the larynx, the trachea, and branches across a tree of size-decreasing bronchi and bronchioles. Around the 17th branch generation, inhaled air starts to fill the first alveoli. By the 20th to the 23rd generations, the air ends in a region densely populated by alveolar tracts and alveolar sacs (Weibel, Cournand and Richards 1963). The walls of the alveoli are surrounded by capillaries. Oxygen from the inhaled air diffuses into the bloodstream, and metabolic carbon dioxide is released into the alveoli.

During expiration, the inspiratory muscles relax and the elastic energy stored in the distended alveoli returns the diaphragm and the rib cage to their resting position. Consequently, alveoli shrinkage increases pressure above atmospheric pressure, driving an air rich in carbon dioxide from the alveoli through the airway tree back to the environment. In this scenario, without active muscular intervention (passive expiration (ExPa)), the rate of exhaled air is defined by a balance between the combined toraco-pulmonary recoil pushing the air out of the lungs and the resistance of the airways slowing the flow of air (subsection 3.2.2 Figure 3.6-A) (Otis, Fenn and Rahn 1950). Total airways resistance depends on the calibre of the tree's airways and the upper conducts.
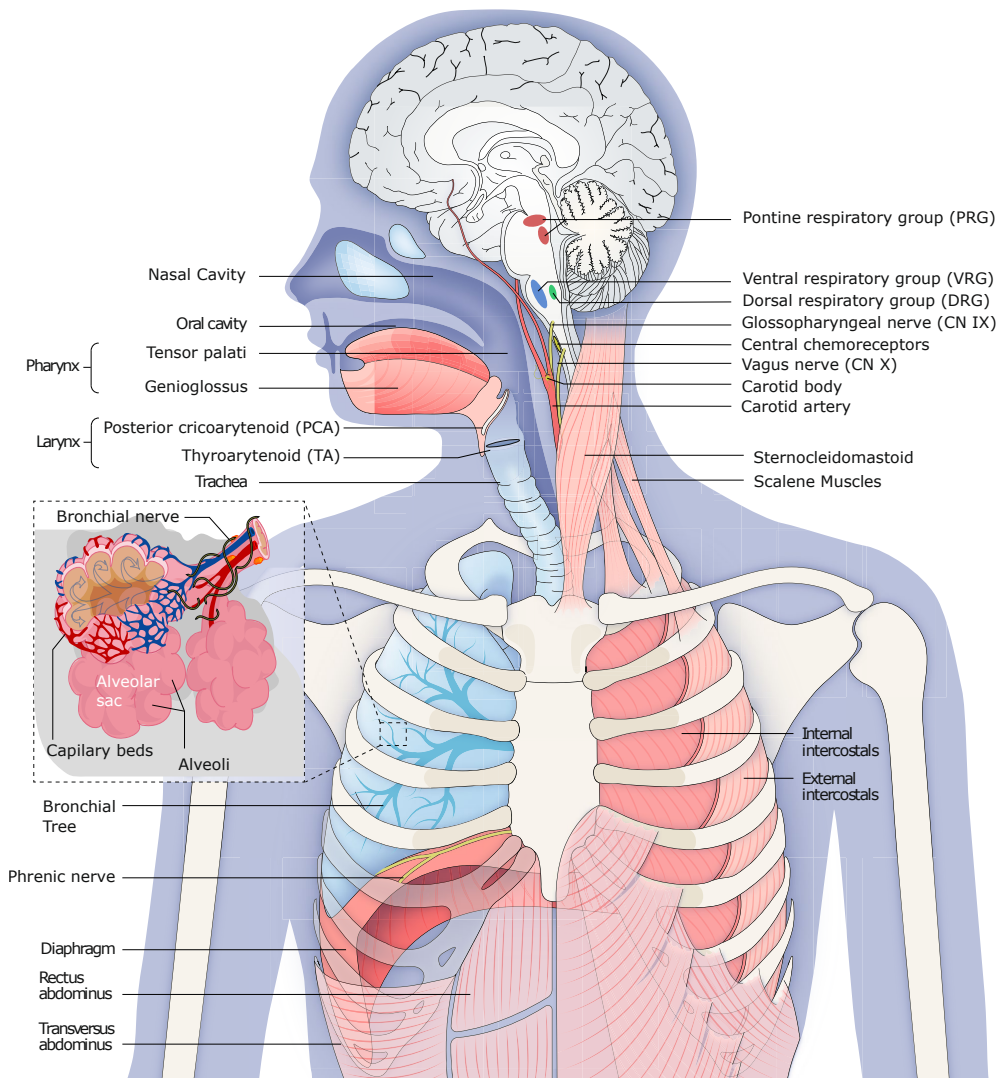
Figure 3.1 **The anatomy and physiology of respiration.** Section of the human body indicating the different elements involved in the mechanics and control of respiration referenced in the text. Body drawing adapted with permission from Del Negro, Funk and Feldman 2018. Alveoli drawing adapted from Wikimedia Commons.

However, expiration is not completely passive. Mammals actively slow down passive expiration to allow the possibility for a prolonged gas exchange and a smoother transition from inspiration to expiration (subsection 3.2.2 Figure 3.6-B) (Levitzky 2018). This is known as expiration breaking (ExBr) and may combine two different mechanisms, post-inspiratory inspiratory activity (PIIA) and laryngeal breaking. For the first, the diaphragm

and the external intercostal muscles do not stop suddenly at the end of inspiration, but their activity fades progressively to slow the recoiling forces of the thorax (Ent et al. 1998). For the second, the glottal aperture narrows to increase the upper airways' resistance and reduce airflow. The glottal narrowing can result from the relaxation of laryngeal abductor muscles, mainly posterior cricoarytenoid (PCA) (T. P. Brancatisano, Dodd and Engel 1984), or from the activation of laryngeal adductors, such as the thyroarytenoid constrictor (TA) (Tully et al. 1990). In healthy wake adults, ExBr is primarily controlled by PIIA. PCA is active during inspiration and relaxed in expiration, which makes upper resistance higher but relatively constant during the entire duration of the expiration (England, Ho and Zamel 1985). In contrast, PIIA only affects the first part of expiration with a duration that changes breath-to-breath. PIIA takes on average 23 % of the expiratory time to reach the 50 % of the peak activity and 79 % time to cessation Shee, Ploy-Song-Sang and Milic-Emili 1985. Contribution of laryngeal abductors, adductors, and PIIA to ExBr varies with sleep, maturation and disease, as detailed later. Moreover, during sleep, relaxation of pharyngeal abductors, such as genioglossus and tensor palatini, may also impact upper airway resistance. Although, this is more common in adults.

In addition to ExBr controlling the beginning of expiration, expiration interruption (ExIn) may control the end of expiration. In ExIn expiration is interrupted by the start of the following breath before the resting state (V_r) is reached. This leads to an elevation of the FRC (subsection 3.2.2 Figure 3.6-C) (Morris, R. Madgwick et al. 1998). Occasionally, under high metabolic demand, such as exercising, abdominal and external intercostal muscles are recruited to actively push air out of the lungs. This leads to an increase in tidal volume (V_t) and a decrease of the FRC under the V_r (Aliverti, Cala et al. 1997).

3.1.2   Control of respiration

The control of respiration is directed by the central nervous system. The respiration control centres are located in three groups of neurons within the brainstem: pontine respiratory group (PRG), dorsal respiratory group (DRG) and ventral respiratory group (VRG) (Figure 3.1). These centres interact with each other, with the body sensory receptors, and with the spinal and cranial motoneurons, forming a feedback control system (Figure 3.2-A). In essence, a sub-region in the VRG generates an oscillating inspiratory–expiratory rhythm. This spontaneous rhythm serves as a reference to generate the multiple stimulation patterns sent to the different respiratory muscles. The characteristics of the base rhythm and

the stimulation patterns are modulated by the lung inflation and the levels of metabolic gases in the blood respectively sensed by mechanoreceptors and chemoreceptors. Moreover, rhythm and stimulation patterns may be readjusted by higher brain centres for a variety of behaviours such as speech production, sleep, or response to exercise (Feldman, McCrimmon and Morrison 2013).

Generation of the respiratory rhythmicity is not yet fully understood since the invasiveness of the measurements restricts in vivo experimentation in humans. The contemporary view describes three coupled oscillators located in VRG that delimit three different phases of the breathing cycle: inspiration neural phase (Insp.), post-inspiration neural phase (Post-I), and expiration neural phase (E2). The inspiration oscillator is the indispensable initiator of the breathing cycle, whereas post-inspiration and expiration oscillators are subordinated to the former (Del Negro, Funk and Feldman 2018).

These three phases mark the stimulation and inhibition of subregions on the DRG and the VRG which build the firing patterns relayed to spinal and cranial motoneurons respectively. In the Insp. phase, the inspiration oscillator provides a ramp-up reference pattern that is relayed to the phrenic and the recurrent laryngeal nerves stimulating the diaphragm, the internal intercostal muscles, and the laryngeal abductors (PCA) respectively. In the Post-I phase, reference pattern switches into a declining burst. This declining stimulus is markedly stronger in the adductor laryngeal muscles (TA). It also stimulates the diaphragm, although with less intensity than the inspiration ramp-up stimulus. The E2 phase is typically silent, except during high metabolic demand (see Richter and Smith 2014 for details). Although these three neural phases relate to the mechanical phases described above, it is important to emphasise that the neural and the mechanical phases are not synchronised (Figure 3.2-B). The duration of each neural phase and the contribution of the patterns to each nerve group are modulated by stimuli arriving from chemoreceptors and mechanoreceptors.

Chemoreceptors are specialised neuronal units that sense the blood's partial pressure of carbon-dioxide (P_{CO2}), oxygen (P_{O2}), or hydrogen ions (pH). Acidity directly relates to P_{CO2} increase. Most chemoreceptors are concentrated in two regions of the body. Peripheral chemoreceptors sense gas and ions concentration directly from the bloodstream in the carotid and aortic bodies, whereas central chemoreceptors measure P_{CO2} and pH from the cerebral spinal fluid in the medulla (Cunningham 1973). Spinal and arterial P_{CO2} and pH stimuli are the strongest influence on the rhythm and pattern generators (Mitchell and Severinghaus 1967). An elevation of carbon-dioxide in the blood (hypercapnia) causes a linear

A

Posture
Emotion
Exercise
Pronation
Sleep

Rhythm generator(s)

Pattern generator

Mechano

Chemo

Spinal Motoneurons

Cranial Motoneurons

Central nervous system

Motor nuclei

Pump

Alveoli

Blood gases, pH

Gas exchange

Diaphragm

Airway muscles

Air

Breathing plant

B

Mechanic

Insp.
Expiration

Volume

20 ml

ExBr
ExPa
ExIn

Flow

50 ml/s
-50 ml/s

EMG TA

EMG PCA

EMG Dia

Insp
Post-I
E2

Neural

12

Figure 3.2   **A: Feedback control of respiration.** Patterns stimulating pumping and upper airways muscles are based on an oscillatory rhythm modulated by physical and chemical body receptors. Higher brain functions may also alter the patterns by mediating receptors' influence or intercepting them at the motoneurons. Adapted with permission from Del Negro, Funk and Feldman 2018.

B: Neural and mechanical phases of respiration. In vivo recordings in a newborn lamb during tidal breathing. Colour boxes mark the neural and mechanical phases of respiration. Inspiration neural phase (Insp.) stimulates pumping and laryngeal dilator muscles, diaphragm (Dia) and posterior cricoarytenoid (PCA). Post-inspiration neural phase (Post-I) stimulates laryngeal constrictor muscles thyroarytenoid constrictor (TA). expiration neural phase (E2) is silence. Air inflow and outflow define mechanical inspiration and expiration respectively. The three subphases in expiration are expiration breaking (ExBr), passive expiration (ExPa), and expiration interruption (ExIn). Noti that healthy human adults typically break expiration by diaphragmatic post-inspiratory inspiratory activity (PIIA) rather than TA (see text). Adapted with permission from Hutchison et al. 1993.

increase in minute ventilation. The slope of this linear relationship (sensitivity) varies with P_{O2} and awareness state (Knill and Clement 1985). Another consequence of hypercapnia is the decrease in respiratory variability (Fiamma, Straus et al. 2007). The arterial stimulus to P_{O2} is less strong, but is nonetheless still a relevant influence on the breathing control. A decrease in P_{O2} (hypoxia) has little influence on ventilation at normal levels of P_{CO2} (38 mmHg to 40 mmHg). However, if P_{CO2} decreases below 50 mmHg to 60 mmHg, the minute ventilation increases rapidly with the decrease in P_{O2} (Berger 1977).

Mechanoreceptors sense physical changes in the lungs, the cardiovascular system, muscles and tendons. Their activation may trigger protective reflexes which alter the control of breathing. Some reflexes, such as coughing or sneezing, respond to temporal irritation of the airways. Others, such as Hering-Breuer inflation and deflation reflexes, have a continuous influence on the breathing cycle (Iber et al. 1995). The Hering-Breuer inflation reflex is evoked by stretch receptors located within the smooth muscle of large and small airways. These sense slow pulmonary inflation. If an overdistension of the lung is suspected, inspiration is interrupted, expiration starts, and airway smooth muscle relax to facilitate the deflation. The Hering-Breuer deflationary reflex is triggered by abrupt deflation of the lungs, presumably sensed by irritant and pulmonary C-fiber receptors. As a response, expiration is shortened to prevent airway closure. Although these reflexes are an essential part of the

control of breathing in mammals, it is believed that for human adults they only provide fine tuning of the respiratory cycle (Widdicombe 1961). Nonetheless, reflexes still play an important role in human newborns and infants (subsection 3.1.4), and speculatively, in obstructive lung diseases (subsection 3.1.5).

Higher brain centres may alter the automatic behaviour of PRG, DRG and VRG , or may even bypass them by directly stimulating motoneurons. For instance, emotions can cause yawning, laughing or sighing (Homma and Masaoka 2008); speech production consciously manipulates glottal aperture and lung volume (Sears 1977); and sleep stage influences motoneurons' sensitivity, as described in the following subsection 3.1.3.

3.1.3   Changes in respiration due to sleep

During normal sleep, humans alternate between two main sleep stages, rapid eye movement (REM) and non-rapid eye movement (NREM). Neurological changes during these stages translate into distinct physiology when compared to each other and wakefulness. NREM is associated with a synchronous electroencephalogram (EEG), low skeletal muscle tone, and parasympathetic dominance. NREM can be further divided into three subgroups (NREM substage 1 (N1), NREM substage 2 (N2), and NREM substage 3 (N3)) attending to the EEG activity, although muscular tone remains relatively similar between them. In contrast, REM is characterised by a variable EEG, sympathetic dominance, and muscle atonia. REM's atony is episodically interrupted by bursts of muscular stimulation and rapid eye movements.

Sleep-dependent variations in neuronal activity and skeletal muscle tone have a direct effect on the phasic and tonic control of respiratory musculature. These effects on respiratory control lead to consequent changes in respiratory mechanics.

Control   Respiratory and postural motoneurons receive behavioural stimuli during wakefulness and a tonic stimulus modulated by sleep-wake related regions of the brain. As illustrated in Figure 3.3-A, respiratory motoneurons receive an additional source of stimulus, the respiratory phasic pattern generated in the brainstem (subsection 3.1.2). When the sum of the multiple premotor excitatory and inhibitory stimuli elevates the membrane potential above a threshold, motoneurons activate the skeletal muscles that they innervate. Therefore, respiratory muscle activation depends on the magnitude of the sleep-wake tonic drive, the magnitude of the respiratory phasic drive, and the threshold of activation set by
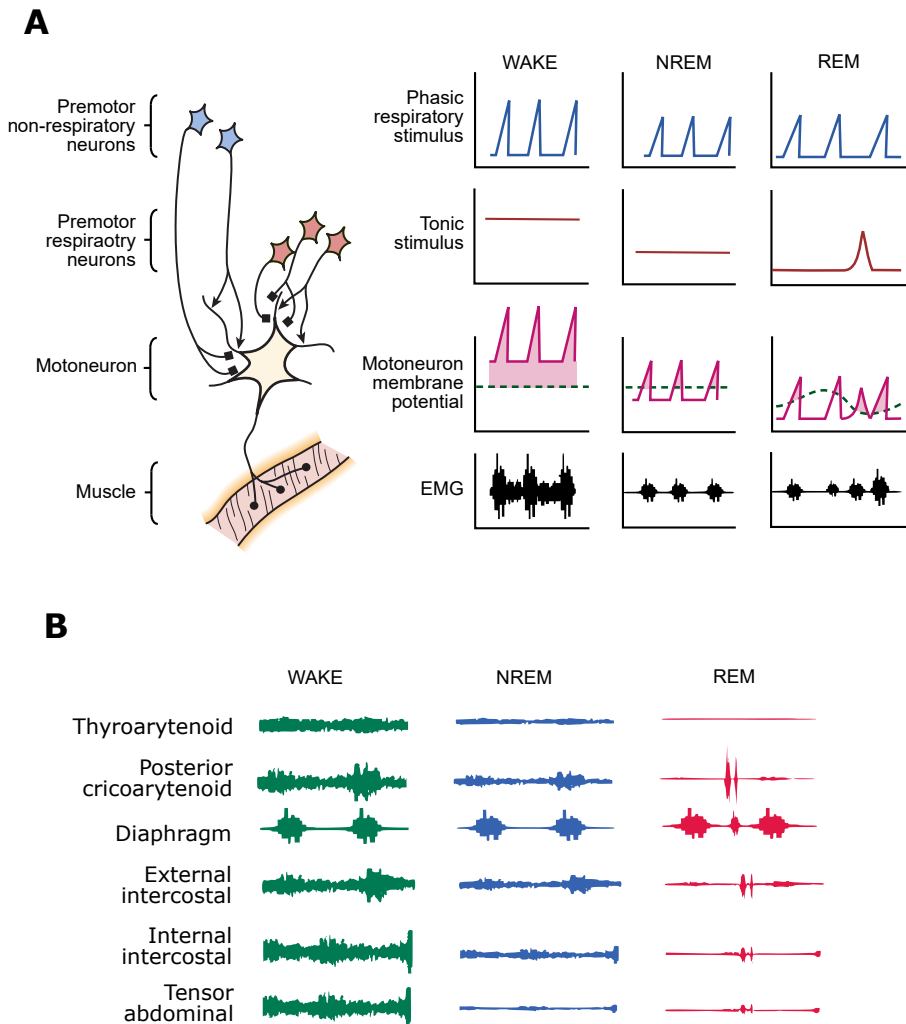
Figure 3.3 **A: Formation of the muscular stimulation pattern in a respiratory motoneuron during awareness state.** A motoneuron (left) stimulates the muscle (black) if the sum (pink) of phasic respiratory stimuli (blue) and tonic sleep-related stimuli (red) surpasses a threshold (dashed green). Neuronal changes during wake, non-rapid eye movement (NREM), and rapid eye movement (REM) result in different muscular stimulation patterns (see text). **B: Stimulation patterns for different respiratory muscles and awareness state.** The contribution of the phasic and tonic drives to the stimulation pattern differs for each respiratory muscle. Therefore, each respiratory muscle presents a different stimulation pattern (rows) and sleep-related changes in both drives affect each patternn differently (columns). During wake, most muscles receive a tonic stimulus, which lowers during NREM and almost disappears during REM. Episodic bursts of activity interrupt REM's atony. Neuron drawing and Figure B modified with permission from Chase and Morales 2005

the input resistance of the motoneurons' membrane (Kosch, Davenport et al. 1986).

The tonic drive decreases in strength from wake to NREM and decreases further from NREM to REM. During REM, however, the tonic drive presents episodic bursts of activity. The phasic drive decreases in frequency and amplitude during both sleep stages. This decrease in frequency is due to lower sensitivity in the chemoreceptors during sleep which accentuates in REM. During sleep, the body experiences a 5 % and a 10 % drop in P_{CO2} respectively for NREM and REM compared to wake (Joseph, Pequignot and Van Reeth 2002). Finally, the input resistance decreases considerably ($\sim$40 %) and presents time fluctuations during REM compared to NREM and wake (Chase and Morales 2005).

These sleep-related neural changes lead to characteristic changes in breathing for each sleep stage. From wake to NREM, minute ventilation decreases due to a reduction in lung volume and respiratory rate; respectively caused by the lower tonic drive and the lower phasic drive rate. Moreover, the breathing signal is markedly regular, especially during N3 (Phillipson 1978). This regularity in the respiratory drive is likely to be associated to the also regular brain activity characteristic of NREM (Burioka et al. 2003). From NREM to REM, minute ventilation decreases further due to an even lower lung volume, but a fairly similar respiratory rate (Douglas et al. 1982). In opposition to NREM, during REM, the breathing signal is highly irregular. Figure 3.3-A shows that this irregularity is less dependent on the properties of the phasic drive and more on the fluctuations in the tonic drive and the input resistance. These distinct differences in variability in the breathing signal can be employed to estimate NREM and REM stages as described in the literature (Haddad, Jeng et al. 1987; Willemen et al. 2014) and in publications P.II and P.III.

Mechanics   Tonic and phasic drives do not contribute equally to the stimulation of all the respiratory muscles. Muscle stimulation depends on the net sum of excitatory and inhibitory innervations a motoneuron receives from each drive (Figure 3.3-A). Muscles combining respiratory and non-respiratory functions, receive a lesser influence from the phasic drive. As a result, when the tonic drive decreases during sleep, these muscles experience a greater reduction in their participation in respiration (Figure 3.3-B). Abdominal and external intercostal muscles are barely stimulated during sleep. Internal intercostal muscles undergo a small reduction of activity during NREM, but during REM, the withdrawal of the tonic drive almost suppress completely its participation in respiration. The diaphragm, as the main respiratory muscle, is largely saved from the tonic reduction of NREM and inhibition of REM sleep (Tusiewicz et al. 1977). In the upper musculature, laryngeal dilator

posterior cricoarytenoid (PCA) experiences a loss in tone, and a 77 % decrease in peak inspiration phasic activity from wake to NREM (Kuna, Smickley and Insalaco 1990). Moreover, PCA's tonic and phasic stimulus presumably lowers during REM (Orem, Norris and Lydic 1978). Pharyngeal dilator genioglossus behaves similarly to PCA. Its activity decreases during NREM and it only presents non-respiratory bursts during REM (Sauerland and Harper 1976). Laryngeal constrictor PCA is silenced during both sleep stages except for sporadic bursts in REM (Kuna, Smickley and Vanoye 1997).

Decreased stimulation of the respiration pump muscles during sleep translates into the following mechanical changes. Firstly, the lower intercostal tone leads to a more compliant chest wall. A compliant chest makes respiration less efficient, as the diaphragm needs to apply more work to move the same amount of air. Tusiewicz et al. 1977 reported a 44 % contribution of the rib cage to tidal volume during wake and NREM in adults, which fell to 19 % of the tidal volume during REM sleep. Secondly, the overall tone decrease in both diaphragm and intercostal muscles leads to a reduction in lung volumes during sleep which accentuates during REM. Two studies, Ballard, Irvin et al. 1990 and Hudgel and Devadatta 1984, measured a small but significant 8 % to 16 % decrease in functional residual capacity (FRC) during NREM, and a 12 % to 19 % decrease during REM compared to wake. Douglas et al. 1982 reported a 6 % to 15 % reduction in tidal volume during NREM, and a 25 % reduction during REM compared to wake in healthy individuals. The decrease in lung volume is tightly connected to the increase in lower airway resistance. However, in healthy adults the decrease in volume does not lead to a proportional decrease in lower resistance (Bellia et al. 1989; Hudgel, R. J. Martin et al. 1984), but it does in subjects with lower airway obstruction (subsection 3.1.5).

In the upper respiratory muscles, sleep-related decreased in tone in laryngeal and pharyngeal dilators leads to a reduction in upper airways calibre, hence increasing resistance. By placing a catheter in the retroepiglottic space Hudgel, R. J. Martin et al. 1984 measured an average increase in the upper resistance of 50 % and 55 % during NREM and REM compared to wake. Collapsibility of the pharyngeal track during sleep is also a common reason for increased upper resistance. This has been largely studied concerning sleep obstructive apnoea (Senaratna et al. 2017), but it out of the scope of this thesis as infants and children are more resilient to this phenomenon, see Katz, Marcus and White 2006.

The abovementioned studies report sleep changes in respiratory mechanics during the whole respiratory cycle. To the best of our knowledge, the specific effects of sleep on the different parts of expirationhave not been studied in adults.

3.1.4 Changes in respiration due to maturation

In young children, the developing chest wall is relatively flexible, and therefore less effective at opposing the inward recoil of the lungs. As a result, passive deflation is faster and reaches a lower resting volume than in adults. To compensate for these mechanical deficiencies, infants rely on active expiration control mechanisms and respiratory reflexes more than adults. Active control of expiration becomes more challenged during sleep, particularly during REM, due to the decrease in muscular tone. For this reason, alterations in respiration caused by sleep are more exaggerated in young children than in adults. Developmental changes in respiration typically stabilised by the age of two.

Mechanics   Over the first two years of life rapid ossification and muscle growth stiffen the rib cage to adult-like levels (Papastamelos et al. 1995). At the same time, rib cage geometry transitions from a spherical cross-sectional shape with ribs perpendicular to the spine to an ovoid shape and descended ribs (Openshaw, Edwards and Helms 1984). In contrast to this, lung compliance remains similar during maturation despite a multiplication in the number of alveoli (Thurlbeck 1982). As a consequence, during infancy, chest wall compliance is several-fold higher than lung compliance. Chest wall compliance decreases with advancing post-natal age, reaching adult levels by the age of two (Sharp et al. 1970)

The highly compliant chest wall in infants has two mechanical implications (Figure 3.4). Firstly, it increases the total respiratory system compliance, which results in a shorter τ_{RS}. Hence, if expiration was passive, the lungs would deflate at a faster rate (Mortola et al. 1982). Secondly, the outward recoil of the chest wall and the inward recoil of the lungs balance at a lower relative resting volume (V_r) than in adults (Agostoni 1959). Breathing under such fast deflation and low lung volumes may lead to reduced oxygen levels and airways closure. To compensate for this, infants employ expiration breaking (ExBr) and expiration interruption (ExIn) mechanisms to actively slow deflation and maintain an elevated tidal breathing (Kosch and Stark 1984). Putatively, in infants, passive expiration (ExPa) is shorter that in adults.

Another consequence of the highly compliant chest is the low contribution of the rib cage to respiration which causes a phenomena known as paradoxical inward rib cage motion (PIRCM) (Hershenson et al. 1990). In normal healthy infants, the chest may collapse under the inspiration effort of the diaphragm causing a paradoxical decrease in chest diameter during inspiration (Hammer and Newth 2009). PIRCM decreases during the first 31 months
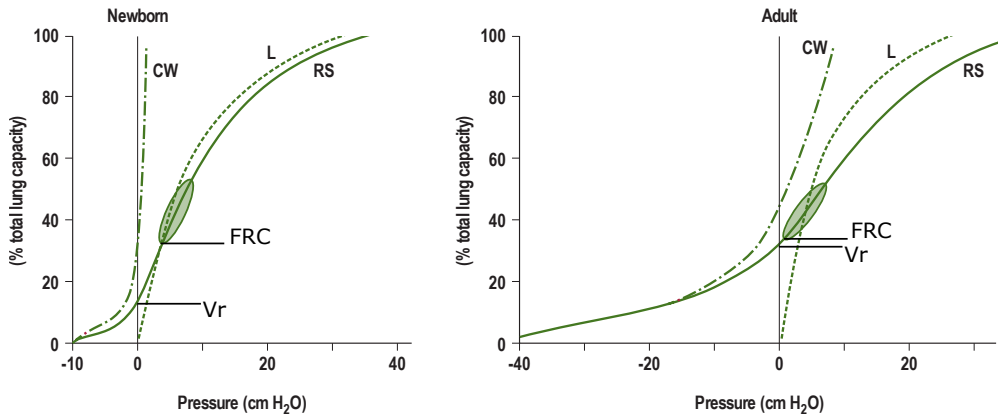
Figure 3.4 **Comparison of the chest wall and lung compliance between infants and adults.** Both plots show the static compliance for the chest wall (CW), the lung (L), and respiratory system (RS) which is the sum of the other two. An ellipse marks the range for tidal volume, where the lowest point corresponds to the functional residual capacity (FRC). The point where chest and lung compliance balances corresponds to the resting volume (V_r). In adults (right plot) FRC is close to resting volume. In infants (left plot), V_r is lower and therefore FRC needs to be actively elevated. Reproduced with permission from Chase and Morales 2005

of life (Gaultier et al. 1987). If PIRCM is still present in subjects older than three years, it and may be an indicator of upper airway resistance (Gaultier 1995).

Control   As mentioned, in infants, ExBr plays a crucial role in prolonging gas exchange. As with adults, intercostal post-inspiratory inspiratory activity (PIIA) stiffens the chest wall, diaphragmatic PIIA holds lung deflation, and laryngeal abductors' relaxation increases the upper airways resistance (Eichenwald, Ungarelli and Stark 1993). Moreover, it is suspected that human newborns also constrict the larynx via thyroarytenoid constrictor (TA) muscle (Kosch, Hutchinson et al. 1988), as seen in other mammal newborns (Figure 3.2-B). ExBr, combined with the passive recoil, maintains an elevated lung volume during the early part of tidal expiration. However, it is ExIn that eventually keeps FRC above V_r in infants (Kosch and Stark 1984). Kosch, Davenport et al. 1985 speculate that ExIn is mediated by a mechanism similar to Hering-Breuer deflation reflex. Stretch receptors would sense accumulated expired volume history and trigger inspiration when certain level is reached, thus expiration duration depends on ExBr and τ_{RS}. The same authors, suggest a similar reflex terminating inspiration, this time based on the sensed cumulative inspired volume (Kosch, Davenport et al. 1986). The transition from the elevated FRC to the adult-like relaxed late

exhale has been estimated to occur around the 12 months of age (Colin et al. 1989), which coincide with the decrease of mechanoreceptors' influence in respiration (Rabbette et al. 1994).

Another sign of maturation is the decrease in respiratory rate (Haddad, Epstein et al. 1979), and respiration variability (Parmelee, Stern and Harris 1972). Sachis et al. 1981 hypothesise that the decrease in respiration variability with postnatal age is due to an increase in myelination strengthening the neural input to the respiratory oscillator.

Sleep   During sleep, the work of ExBr and ExIn to keep an elevated FRC is compromised by the loss of muscular tone, particularly during REM's muscle atony. This decrease in control during REM compared to NREM has been directly observed in pre-term newborns from simultaneous diaphragmatic electromyogram (EMG) and mouth airflow recordings (Stark et al. 1987). The decrease in ExBr showed as the shortening of the diaphragmatic PIIA. However, in another study Harding, Johnson and McClelland 1980 hypothesises that lower laryngeal breaking also contributes to decrease ExBr during REM. The absence in ExIn during REM also reflects in the EMG recording and as a lower extrapolated volume (EV) in tidal flow-volume loops.

There is a lack of studies directly measuring the effects of sleep respiratory muscle activity in full-term infants or young children. However, the following studies suggest that sleep affects breathing control in the same manner as described for pre-term. A shorter expiration time (T_E) during REM compared to NREM while tidal volume (V_t) remains similar suggests a faster deflation due to a less effective ExBr (Haddad, Epstein et al. 1979). A decrease in the thoracic gas volume of a 31% from NREM to REM in newborns suggest that ExIn is also lowered (Henderson-Smart and Read 1979). In addition, the increase of PIRCM during REM also reflects the lowering in the intercostal muscle tone (Gaultier 1995).

In newborns, respiratory frequency has been reported to be higher during REM than during NREM, but this difference decreases over the first year of life (Parmelee, Stern and Harris 1972). Respiration variability, however, remains distinctively high during REM and low during NREM at all ages (Isler et al. 2016).

3.1.5 Changes in respiration due to obstructive lung diseases

Obstructive lung diseases cause a narrowing in the lower airway which reduces respiratory airflow. In such a scenario, individuals employ different strategies that modify the control of respiration to compensate for this mechanical deficiency. During the night obstructive diseases worsen. Several circadian factors and the decrease in lung volume accentuate the narrowing of the lower airway. Moreover, sleep-dependent changes in the control of respiration limit the application of the compensation strategies.

Mechanics   COPD and asthma are the most common obstructive lung diseases. COPD is associated with a homogeneous, progressive, and not fully reversible degradation of the lung tissue. Tissue reparation causes inflammation and secretions that narrows the airways. COPD is more frequent in smokers and the elderly (Brandsma et al. 2017; Celli et al. 2004). In contrast, in asthma, airflow limitation is reversible and heterogeneously distributed across the lung (Teague, Tustison and Altes 2014). Airways narrowing is caused by a hyperresponse to a variety of chemical and physical stimuli which have little or no effects in healthy subjects. Typically, airflow is restored when the stimuli retreat. This thesis focuses on asthma as it is more frequent in infants and children. Nonetheless, in practice, a significant proportion of patients have overlapping characteristics associated with both conditions (Gibson and McDonald 2015).

It is believed that airway hyperresponsiveness results as the combination of multiple factors. These factors include a genetic predisposition to inflammatory and mucosal secretion stimuli, and the shortening of the airway smooth muscle (Gauthier, Ray and Wenzel 2015). The narrowing caused by the latter depends on genetic factors defining its structure, autonomic neural factors regulating its tone, and the load defined by the surrounding elastic structures (M. J. Lewis, Short and K. E. Lewis 2006). The major source of this load is provided by the lung elastic recoil which decreases with lung deflation. Hence, a decrease in lung volume, a loss in lung elasticity, and a reduced number of deep breaths favour airway narrowing (Brusasco and Pellegrino 2003).

Despite lower airway narrowing being heterogeneous in its causes and its distribution across the lung, the effects on the large scale are similar. At the respiratory system level, lower airway obstruction increases airway resistance which extends τ_{RS} and slows passive lung deflation. (Polak, Wysoczański and Mroczka 2019; Venegas et al. 2005).

Control The literature discusses two different strategies to compensate for lower airway obstruction. These are hereafter referred as hyperinflation and ExBr-relaxation strategies. These two strategies seem seem contradictory at first, specifically on how ExBr is used. The hyperinflation strategy suggests that individuals increase ExBr to maintain breathing over an actively elevated FRC, and thus dilating the lower airway. Individuals may achieve this thought an increase in PIIA (Muller, Bryan and Zamel 1981) and/or a paradoxical increase in upper airway resistance (Collett, T. Brancatisano and Engel 1983). This has been studied on adults and children during natural and induced obstruction (Greenough, Pool and Price 1989; J. Martin et al. 1980; Wheatley et al. 1990). The ExBr-relaxation strategy suggests that individuals relax ExBr to compensate for the retardation in the passive lung deflation produced by obstruction. Studies in tracheotomized cats suggest that ExBr is relaxed by a vagally mediated shortening of the PIIA (Ent et al. 1998; Walraven et al. 2003). As simply put by Beydon et al. 2007: *"[Speculatively,] individuals with airway obstruction sense that they do not need as much braking of expiration, and relax their inspiration muscles more promptly at the end of inspiration"*. ExBr-relaxation has been studied in adults with chronic airway obstruction which also showed the use of hyperinflation (Citterio et al. 1981; Morris, R. G. Madgwick, Frew et al. 1990).

Pellegrino and Brusasco 1997 present a hypothesis that unites these two seemingly contradictory strategies. They suggest that *"rather than the cause of hyperinflation, the increase in ExBr is the result"*. Patients with mild bronchoconstriction do not need to resort to hyperinflation (Figure 3.5). They can compensate for the retardation in expiration by applying the ExBr-relaxation strategy. It is when the obstruction is high enough to cause airway limitation at the end of expiration that individuals react by applying hyperinflation. Breathing at the new elevated FRC causes a twofold shortening in the expiration time constant. The dilated lower airway reduces the lower resistance and the expanded chest increases the recoiling force of the respiratory system ($\tau_{RS} = C_{RS} \cdot R_{RS}$). If the new time constant is too short, then increasing ExBr is necessary to maintain a prolonged expiration. In the case of acute obstruction, individuals may need to apply both strategies; hyperinflation to shorten the expiration time constant, and ExBr-relaxation to avoid a slow expiration.

It is important to emphasise that individuals do not necessarily employ these two strategies in the same proportion at the same level of obstruction. Balancing between both strategies may depend on multiple subjective factors such as physiology, pathology, or posture (Pellegrino, Violante, Nava et al. 1993). In infants, where the FRC is already actively elevated, understanding how these strategies are combined is more challenging (Hutten et al. 2010).
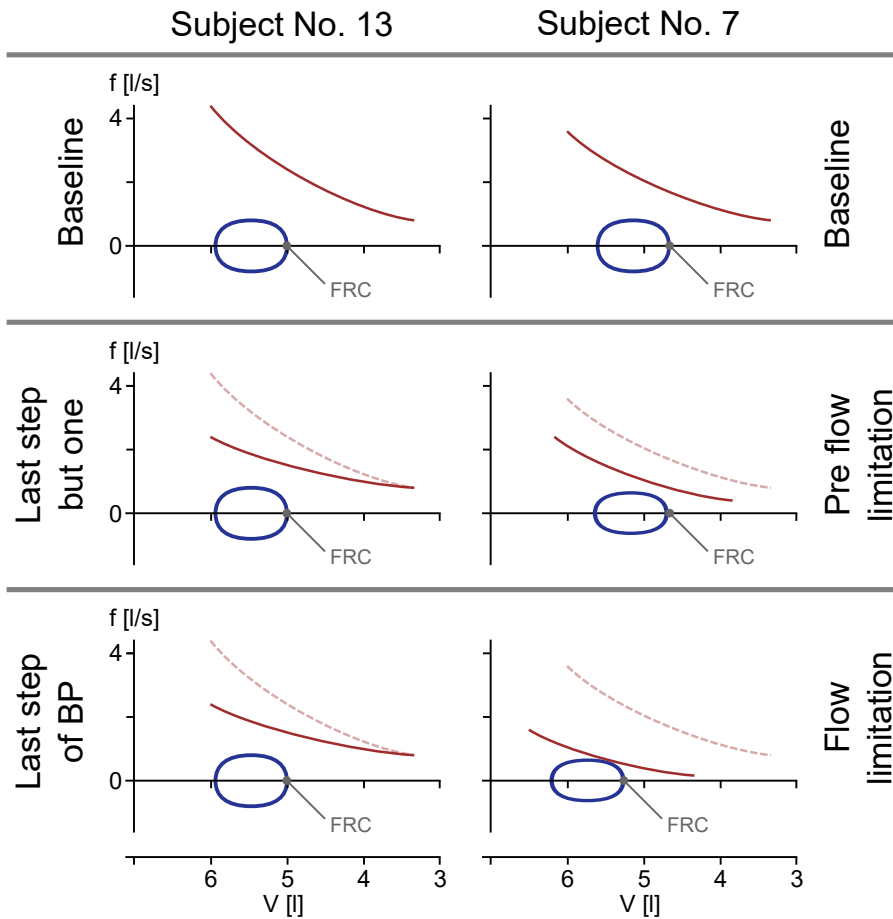
Figure 3.5 **Tidal flow and airflow limitation during three steps of a bronchial-provocation test in two representative adult subjects.** Each flow-volume plot shows in dark blue a tidal breathing flow-volume loop (TBFV) loop, in solid red the edge of airflow limitation measured by spirometry, and in dashed red the edge at the baseline. Lower airway resistance is medically increased from baseline (upper plots) to the last step of the test (lower plots). For subject No. 7 (right plots) the increase in resistances causes airflow limitation at the end tidal expiration, thus triggering hyperinflation (functional residual capacity (FRC) increases). For subject No. 13 (left plots) airflow limitation does not occur at the end tidal expiration, and thus does not trigger hyperinflation. Adapted with permission from Pellegrino, Violante, Nava et al. 1993

Sleep Like many human functions, airways resistance is not constant but varies over the course the day. Hetzel and Clark 1980 measured the circadian variation in peak expiratory flow and showed that the highest and the lowest values occur around 16:00 and 4:00 respectively. Moreover, the difference between these two was more pronounced in asthmatic

patients. Catterall et al. 1986 demonstrated that nocturnal increase in peak expiratory flow also occurs in sleep-deprived subjects, and is therefore not caused by sleep. Bellia et al. 1989 used an oesophageal and an supraglottic catheter to confirm that most of the increase in resistance comes from the lower airway. These circadian variations in the lower airway resistance emerges from the interaction of several factors whose effects are amplified in asthmatic patients (Bohadana, Hannhart and Teculescu 2002). These factors include variations in the hormonal levels (Sutherland 2005), in the immune system (Durrington et al. 2014), and in the hyperresponsiveness (Oosterhoff et al. 1993).

Although these circadian factors are sleep-independent, sleep also contributes increasing the lower airway resistance in healthy and asthmatics (Catterall et al. 1986). Perhaps, the most evident reason for a sleep-dependent increase in lower resistance is the decreases in the FRC caused by the drop in muscle tone (subsection 3.1.3). Ballard, Irvin et al. 1990 demonstrated that, indeed, the FRC and the conductance drops immediately after sleep onset, but they also showed that the specific airway conductance (sGaw) continues to decrease during the first hour of sleep. Therefore, the FRC drop contributes but does not account for all the increase in the resistance. The same authors (Ballard, Pak and White 1991) suggest that another contributor is the pooling of blood due to a sustained supine posture. In a posterior study, Irvin, Pak and R. J. Martin 2000 suggest that the dependency between airways resistance and lung volume diminishes during sleep, and therefore after sleep onset resistance increases independently from the FRC decrease.

Regarding the effects of sleep stages in the lower resistance, Bellia et al. 1989 are, to the best of our knowledge, the only researchers to have directly measured this. They reported that bronchoconstriction episodes are more common and more severe during NREM that during REM in asthmatic adults. This seems counterintuitive, considering that asthmatics can maintain hyperinflation during NREM, but they lack the muscle tone to do so during REM (Ballard, Irvin et al. 1990). Two factors may contribute to lower airway obstruction during REM despite the absence of hyperinflation. Firstly, the uncoupling between airways resistance and lung volume suggested by Irvin, Pak and R. J. Martin 2000. Secondly, the bronchodilation properties of deep breaths (Pellegrino, Violante and Brusasco 1996) which are quite common during REM due to the irregular respiratory drive. Either due to the airway-parenchyma uncoupling or the muscle atony, the hyperinflation strategy is putatively less common during REM than during NREM and wake.

3.2 Assessment of airflow obstruction in infants and children

As described in subsection 3.1.1, the respiratory airflow is driven by the difference between the alveolar and the environmental pressures and is restricted by the calibre of the airway tree. The most intuitive way to calculate airway resistance is therefore to measure the alveolar pressure and the mount airflow ($R_{rs} = P_{ao} / \dot{V}$). However, estimating the former is either invasive (introducing a pressure sensor through the oesophagus) or challenging (see methods below).

Fry et al. 1954 discovered that while transmural pressure dictates airflow during tidal expiration, forced expiration turns the low airway into a Starling resistor and airflow became solely dependent on the airway resistance. This phenomenon is known as flow limitation and is the principle behind spirometry (Hyatt, Schilder and Fry 1958). During a spirometry test, patients are asked to exhale through a PNT from total vital capacity to residual volume as hard as possible. Exhaled flow plot against volume typically displays a sharp increase to maximum flow followed by a monotonic decrease. Values during this decrease reflect the mechanical properties of the different bronchial segments of the airway tree. For example, obstructed lower airway collapses at relatively high lung volumes, and therefore it draws a concave shape and a delayed lung emptying. Multiple indices have been proposed to quantify the type and degree of airflow obstruction. The more commonly used indices are forced expired volume the first second (FEV1) or expired flow at different levels of expired volume (Miller 2005).

Nowadays, spirometry is the most common of the lung function tests to assess lower airway obstruction, as well as other respiratory conditions. Nonetheless, this test is not suitable for infants or young children who are unable to comprehend and follow the given instructions. The following subsections describe alternative methods to assess airflow obstruction in this group of patients. The first subsection discusses methods which, like spirometry, rely on some sort of manoeuvre or external stimulus to derive mechanical properties of the respiratory system. In contrast, the other two are based on the analysis of tidal breathing. Hence, these two depend not only on the respiratory mechanics but also on the control of respiration.

3.2.1   Methods based on an external stimulus

Like spirometry, the methods in this group interpret the respiratory system as a classic mechanical system. They apply a known stimulus into the body, measure the reaction, and derive mechanical properties of the system. These methods only allow to measure for a few minutes and, often, require sedation and bulky equipment.

The following list describes the basic working principle, advantages and limitations of each method. More emphasis is given to these indices mentioned in the literature (Table 3.1 and Table 3.2) and in publication P.II. For further details on these methods or other lung function techniques for infants and children, see Czovek 2019.

Rapid thoracoabdominal compression (RTC)   RTC is based on the same principle as spirometry, but the forced expiration is induced by means of an inflatable jacket. Sedated infants breath through a PNT. Three tidal breathe are recorded to determine the end of inspiration and the FRC, and the jacket is inflated at the end of the fourth inspiration. This procedure is repeated with increasing inflation pressures until no further increase in airflow at the FRC is detected ($\dot{V}_{maxFRC}$) (Peterson-Carmichael et al. 2016). Other indices have been proposed, but conventional spirometry indices, such as FEV1, have been shown to fail to detect obstruction in young children (Gaffin et al. 2010). The major limitation for this method is the need for sedation and the difficulty to determine the FRC in infants.

Plethysmography   A plethysmograph estimates the alveolar pressure from the changes in volume and pressure in a sealed box enclosing the patient. The patient, inside a box, breathes through a PNT connected to the exterior. According to Bernoulli's principle, the product of volume and pressure in the box equals the product of volume and pressure in the lungs ($P_{box} \cdot V_{box} = P_{ao} \cdot FRC$). By occluding the PNT the plethysmograph can also estimate the FRC and derive the airway resistance (R_{aw}). However, this measurement is less reliable in children (Bisgaard and Nielsen 2005). For this reason the airway resistance is expressed in relation to FRC as the specific airway conductance:

$$\text{sGaw} = \frac{1}{R_{aw} \cdot FRC} = \frac{\dot{V}}{P_{box} \cdot V_{box}} \tag{3.1}$$

The instrumentation used by this method is bulky, the box needs to fit at least the child and often also the parent. Moreover, SGaw may be altered by changes in the FRC, and the accuracy of results in nasally breathing infants are still vague (Robinson et al. 2015).

Interruption technique   In the interruption technique, a PNT records the child's tidal airflow and the alveolar pressure is estimated by measuring the mouth pressure during a brief occlusion of the PNT. In theory, during this short occlusion, the alveolar pressure propagates to the mouth sensor, and the resistance is calculated as mentioned ($R_{rs} = P_{ao}$ / $\dot{V}$). In practice, the pressure propagation following occlusion produces several rapid oscillations before reaching equilibrium. If the occlusion is too short, pressures may have not yet balanced. If the occlusion is too long, P_{ao} does not correspond with the $\dot{V}$ measured pre-occlusion. Alveolar and mouth pressures equilibrium requires more time in the presence of lung inhomogeneities. Therefore, this method typically underestimates obstruction.

Single breath occlusion technique (SOT)   The SOT relies on the Hering-Breuer reflex to evoke an apnoea in infants and record airflow during a completely passive expiration. A PNT recording the infant's tidal airflow is occluded at end inspiration. This occlusion has two purposes. Firstly, it estimates the change in alveolar pressure which together with inspired volume serves to calculate the compliance of the respiratory system ($C_{rs} = \Delta V/\Delta P_{ao}$). Secondly, it triggers a Hering-Breuer reflex that relaxes all inspiratory muscles. Recording flow during a passive expiration serves to estimate τ_{RS} (subsection 3.2.2 Figure 3.6-A) (Gappa et al. 2001). The resistance of the respiratory system is then calculated as:

$$R_{rs} = \tau_{RS} \cdot \frac{\Delta P_{ao}}{\Delta V} \tag{3.2}$$

SOT is one of the most common lung function tests in infants. However, the Hering-Breuer reflex diminishes with postnatal age, thus limiting its application in children (Marchal and Crance 1987). As with the interruption technique, SOT may underestimate obstruction in the presence of lung inhomogeneities. Although, in SOT occlusion times are allowed to be longer.

Forced oscillation technique (FOT)   In FOT, a multi-frequency pressure signal is superimposed over tidal breathing at the airway opening and the airflow response is measured. The cheeks and the floor of the mouth are firmly supported to minimize the upper airway shunt. The complex ratio of the pressure and airflow signals is defined as the input mechanical impedance ($Z_{in}(f) = P_{ao}(f)/\dot{V}(f)$). In theory, the real part $R_{rs}(f)$ of the impedance is associated with the airway and tissue resistance, and the imaginary part $X_{rs}(f)$ with the elasticity of the chest wall and the lungs and the inertance of the airway tree

$(Z_{in}(f) = R_{rs}(f) + j \cdot X_{rs}(f))$. However, in practice, the response of all mechanical components of the respiratory system overlap in the input impedance (J. H. Bates, Irvin et al. 2011). Although several models have been proposed, it is difficult to extract the value of a single component from the input impedance. This difficulty has been the major limitation to reaching clinical routine (Goldman 2001).

3.2.2 Shape analysis of tidal breathing

Shape analysis of tidal breathing is based on the intuitive idea that obstruction must not only be reflected in the forced exhale but also in the shape of relaxed expiration. However, interpreting the shape of tidal expiration is far from intuitive (Beydon et al. 2007). Truly relaxed expiration (ExPa) depends on the airway resistance (R_{rs}), but also on the respiratory system compliance (C_{rs}) (Figure 3.6-A). The respiratory compliance may vary with lung volume, lung volume history, body mass, and disease (Ferris and Pollard 1960; Mols et al. 1999; Naimark and Cherniack 1960). Moreover, expiration is rarely completely passive. Respiratory musculature controls a significant part of the beginning (ExBr) (Figure 3.6-B) and the end (ExIn) (Figure 3.6-C) of expiration (subsection 3.1.2), where ExBr and ExIn may vary with obstruction (subsection 3.1.5) as well as other factors (subsection 3.1.3 and subsection 3.1.4).

As accurately explained by J. H. Bates 1998: *"[due to the many interacting factors that form the tidal flow], similar shapes may originate under dissimilar circumstances. Therefore, [unlike the previous methods,] shapes indices cannot be taken as direct surrogates of the mechanical respiratory resistance"*. Although efforts have been made to relate the shape indices to the underlying mechanical properties or the respiratory control processes, the connection between these two primarily remains based on empirical observations.

The following subsection describes the most commonly used shape indices and how these are thought to relate to respiratory mechanics or respiratory control. Consequently, we review the literature studying empirical connections of shape indices with airway obstruction, sleep, maturation, and other factors. Advantages and disadvantages on this method are discussed further in section 6.2.

3.2.2.1 Tidal expiration shape indices

For clarity, indices are divided into three groups: *early*, *middle*, and *late expiration*. In practice, all factors shaping tidal expiration have an influence in the indices of these three

groups. For instance, a large ExBr in the *early expiration* will shorten ExPa in the *middle expiration* and vice versa. However, indices in the *early expiration* receive a putatively larger influenced from ExBr; indices in the *middle expiration* from ExPa; and indices in the *late expiration* from ExIn. European Respiratory Society Task Force recommends that linear indices are calculated for several individual breaths, and then expressed as a mean (J. H. Bates, Schmalisch et al. 2000).

We omitted some shape indices sporadically used in individual studies, but included the indices that were newly introduced in P.II, (grey text in Figure 3.6-D). For a more comprehensive list of indices the reader is referred to V.-P. Seppä 2014.

- *Early expiration:* As suggested by Figure 3.6, peak tidal expiratory flow (PTEF) and time to PTEF (T_{PTEF}) are influenced by a combination of the passive mechanical properties and the strength and duration of the ExBr. In tracheostomized cats, Ent et al. 1998 proved that faster exponential decay in the diaphragm's EMG relates to a shorter T_{PTEF}. Moreover, in a similar setup, Walraven et al. 2003 showed that adding a resistive load did not change T_{PTEF} but decreased PTEF.

  Absolute T_{PTEF} may depend on the respiratory rate, which is subject-dependant (S. Fleming et al. 2011). More often T_{PTEF} is expressed in relation to total expiratory time (T_{PTEF}/T_E). However, this should also be interpreted with care as T_E can be influenced by passive retardation during the ExPa or an early ExIn. V_{PTEF}/V_E has been suggested to be a more robust alternative to these timing differences. Putatively, a larger V_{PTEF}/V_E relates to a longer ExBr.

- *Middle expiration:* Morris, R. G. Madgwick and Lane 1995 suggested to estimate τ_{RS} from the slope of a line fitted to the ExPa part of the TBFV. They assumed this part to be the longest linear portion of the profile. Although, they found this slope to correlate with R_{aw} in adults, they also recognised that finding the longest linear portion on the TBFV was often subjective, as in many cases *middle expiration* was not linear but concave or convex.

  These differences in the shape of the *middle expiration* have been employed by multiple researchers that visually classified the TBFV profiles as concave, convex, linearly-decreasing, or constant (often called "flat" expiration) (Filippone et al. 2000; Morris and Lane 1981). Nonetheless, visual classification is subjective and does not quantify the degree of concavity or convexity.

  Relative tidal exp. flow at 50% tidal volume (TEF50/PTEF) and relative tidal exp.

flow at 25% tidal volume (TEF25/PTEF) are an attempt to objectively quantify concave and convex shapes (Lodrup-Carlsen and K. H. Carlsen 1993). Absolute TEF50 and TEF25 alone has been also proposed as a measurement of flow at lower volumes, but these may lack significance if total lung volume is unknown (Totapally et al. 2001). TEF50/PTEF and TEF25/PTEF are solely based on two points of the TBFV profile and are therefore subjected to noise. Moreover, the reference point PTEF alone is highly influenced by *early expiration*.

The solve these drawbacks, we presented in P.II and P.III a new shape index, namely P_{FV}. It is calculated as the exponent of a power function fitted to the section between PTEF and TEF05. P_{FV} is robust to noise and independent of PTEF. P_{FV} is 1 for a linear decrease; between 1 and 0 for a convex decrease; and over 1 for a concave decrease.

- *Late expiration:* Morris, R. Madgwick et al. 1998 also suggested that prolonging the line fitted to longest linear portion of the TBFV profile until it cuts the volume axes. They named the distance between this point and the end of expiration, extrapolated volume (EV). They found EV to correlated to predicted FRC. This has the same limitation that τ_{RS}. Schmalisch, R. R. Wauer et al. 2003 suggested measuring the point of maximal change in the descent of the TBFV in the transition from expiration to inspiration on infants, namely end expiratory break-off ($\dot{V}_{b-o}$). This point was defined visually, which makes the index subjective. In P.II and P.III, we propose to use relative tidal exp. flow at 5% tidal volume (TEF05/PTEF). A larger $\dot{V}_{b-o}$ or TEF05/PTEF putatively reflects an earlier ExIn.

3.2.2.2 Studies on tidal expiration shape indices

Table 3.1 presents a review of the studies investigating the changes in tidal expiration shape indices associated to airway obstruction, maturation, and sleep. This table is partially based on a similar table in V.-P. Seppä 2014.. The results column on this table, however, emphasises the association, or lack of it, between the studied factors and the indices. Moreover, this table includes later studies and excludes these studies in preterm infants for being outside of the scope of this thesis. An exception is made for study (27) as sleep-related studies are so rare. For studies on preterm infants, we recommend the review conducted by Baldwin et al. 2006.
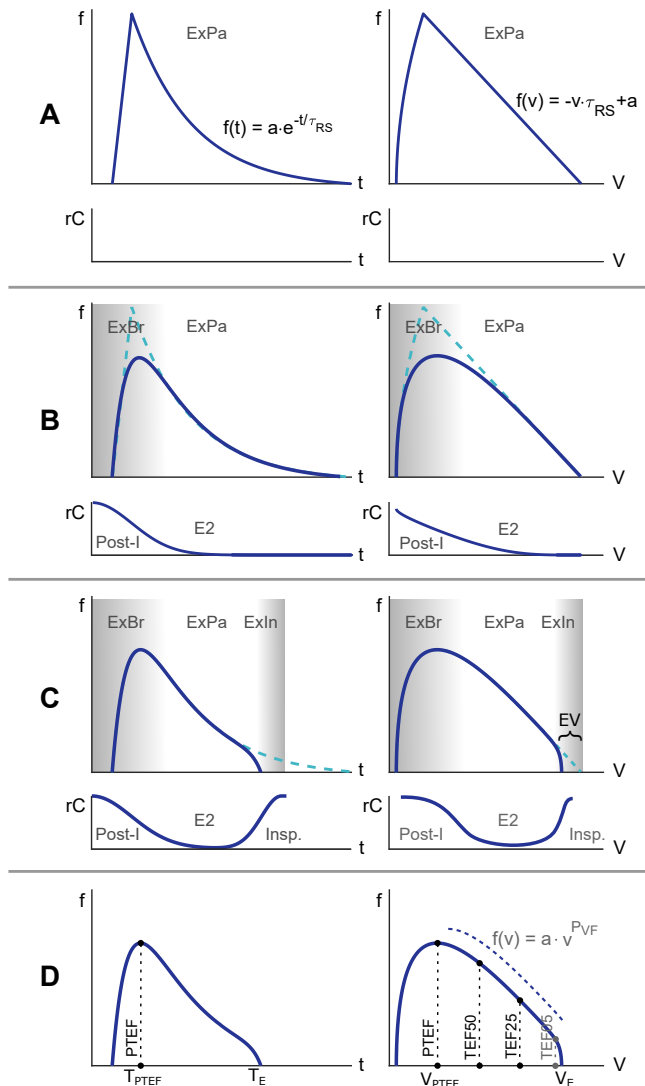
Figure 3.6 **Factors shaping tidal expiration and shape indices:** The groups of plots **A**, **B**, and **C** shows how the shape of tidal expiration changes as factors are added. Dashed lines overlaps the upper plot group for reference. Plots in **D** shows different shape indices on the expiration shape resulting from **C**. For each group of plots, flow-time plots show airflow during a tidal expiration. Respiratory control (rC)-time plots symbolise the strength and duration of the stimulation of the respiratory musculature, including pump and upper airways muscles. This strength is also overlapped as a grey gradient on the corresponding flow-time plot. On the right, the same plots are mirrored on the flow-volume domain. In **A**, expiration is completely passive passive expiration (ExPa) and flow can be described by the mechanical properties of the respiratory system ($\tau_{rs} = C_{rs} \cdot R_{rs}$). In **B**, post-inspiration neural phase (Post-I) causes expiration breaking (ExBr) which shapes the *early expiration*. In **C**, the beginning of inspiration neural phase (Insp.) causes expiration interruption (ExIn) which shapes the *late expiration*.

Table 3.1 **Clinical studies on tidal expiration shape indices:** Studies grouped by the main factor of study and sorted by the age of the participants. Column *Compared Groups* indicates the groups compared within the study, such as, healthy, chronic lung disease (CLD), cystic fibrosis (CF), asthmatic, or other respiratory conditions. Column *Interv./Cofac.* indicates if other intervention or cofactors are compared within groups, such as bronchial provocation (BP), bronchodilator (BD), age, or sleep stages. In the *Results* column r refers to the correlation coefficient (Pearson unless otherwise indicated) and ROC-AUC to area under the received operation characteristic curve

| Authors | Population | | Methods | | | Results |
	Compared Groups(n)	Age	Interv./ Cofac.	Device	Indices	
Airflow limitation						
1. Morris, R. G. Madgwick and Lane 1995	Asthma (20)	29-71 years	BP	PNT	V_{PTEF}/V_E, τ_{RS}, EV	τ_{RS} and EV increased significantly after BP. T_{PTEF}/T_E showed <u>no</u> changes. τ_{RS} and EV were calculated visually which may include biases.
2. Morris, R. Madgwick et al. 1998	Suspected airway obstruction (118)	7-85 years	BP	PNT	τ_{RS}, EV	τ_{RS} showed a good positive correlation with R_{aw} (r = 65). EV showed a good positive correlation with FRC% predicted (r = 68). τ_{RS} and EV were calculated visually which may include biases.

3.	Morris and Lane 1981	Healthy (15), Obstruction (51), Restriction (24)	Children and adults	None	PNT	T_{PTEF}/T_E, V_{PTEF}/V_E, convex vs. concave	T_{PTEF}/T_E, V_{PTEF}/V_E correlated well with FEV1/FVC. Within the obstruction group TBFV expiration turned from a convex to a concave shape with increased obstruction.
4.	Cutrera et al. 1991	Healthy (24) Asthma (60)	5.3-17.5 years	BP	PNT	V_{PTEF}/V_E	V_{PTEF}/V_E did not differ for asthmatics and controls. However, it showed low correlations ($r = [0.4-0.6]$) with multiple lung function indices and their variations after BP.
5.	V.-P. Seppä, A. S. Pelkonen, Kotaniemi-Syrjänen, Mäkelä et al. 2013	Asthma (21)	3-7 years	BP, BD	PNT, IP	T_{PTEF}/T_E, V_{PTEF}/V_E	Both indices decreased with BP and returned to pre-BP levels after BD. Both indices showed low negative correlation with FOT indices ($r = [0.4-0.6]$ for FEV1). Results were similar for both recording devices.
6.	K. H. Carlsen and K. L. Carlsen 1994	Healthy (26) Asthma (26)	3-85 months	BD	PNT	T_{PTEF}/T_E, V_{PTEF}/V_E, TEF25/PTEF	All indices were higher for controls compared to asthma. All indices increased after BD in asthmatic and controls, except for TEF25/PTEF which did not changed in controls.

#	Reference	Population	Age			Indices	Findings
7.	Filippone et al. 2000	Healthy (15), Respiratory symptoms (95)	15-48 months	None	PNT	T_{PTEF}/T_E, convex vs. concave vs. constant expiration	A convex expiration TBFV was observed in the 15 healthy subjects and 47 subjects with laryngomalacia from which 44 presented an irregular inspiration pattern. A concave expiration was present in 20 subjects with lower airways obstruction. A constant expiration profile was present in 46 subjects with upper airways obstruction.
8.	Malmberg et al. 2017	Respiratory symptoms (44)	5-28 months	BP, BD	PNT, IP	T_{PTEF}/T_E, V_{PTEF}/V_E	Only V_{PTEF}/V_E recorded with PNT showed a significant decreases with BP. Both indices showed a low, positive correlation with $z\dot{V}_{maxFRC}$ ($r = [0.35 - 0.4]$) under both recording devices.
9.	K. C. L. Carlsen, Pettersen and K.-H. Carlsen 2004	Healthy (251), Recurrent bronchial obstruction (265)	26±3.7 months	BD	PNT	T_{PTEF}/T_E	T_{PTEF}/T_E increased significantly after BD, with a larger increase in subjects with recurrent bronchial obstruction.
10.	Lodrup-Carlsen and K. H. Carlsen 1993	Healthy (38), Wheezers (41)	2-26 months	BD	PNT	T_{PTEF}/T_E, V_{PTEF}/V_E	T_{PTEF}/T_E, V_{PTEF}/V_E were lower in wheezers than controls. This difference disappeared after BD.

11.	Hevroni et al. 2018	Absent to mild obstruction ($z\dot{V}_{maxFRC} < -2$) (104), Severe obstruction ($z\dot{V}_{maxFRC} \geq -2$) (52)	3–24 months	None	PNT	T_{PTEF}/T_E, TEF50/PTEF, TEF25/PTEF	The three indices were significantly lower for the severe obstruction group ($p < 0.0001$), with a ROC-AUC of 0.81, 0.79, and 0.79 respectively. The three indices showed a good positive correlation ($r = [0.61, 0.67, 0.65]$ respectively) with $z\dot{V}_{maxFRC}$ when using an s-curve correlation.
12.	Leonhardt, Ahrens and Kecman 2010	Healthy (37), Various respiratory diseases (158)	3-24 months	None	PNT	T_{PTEF}/T_E, V_{PTEF}/V_E, TEF50/PTEF, TEF25/PTEF, Others	A support vector machine could classify the subjects into ten clinical categories using the TBFV indices. Linear decreasing expiration was associated with asthma and bronchitis, a convex expiration with healthy, and a constant expiration with upper airways conditions.
13.	Benoist et al. 1994	Recurrent wheezers (55)	16±5.2 months	BP	PNT	PTEF, T_{PTEF}/T_E, convex vs. concave	PTEF and T_{PTEF}/T_E respectively increased and decreased after BP.TBFV expiration profiles changed from convex pre-BP to concave (32/42) or decreasing straight line (10/42) post-BP.
14.	Banovcin, Seidenberg and Der Hardt 1995	Various obstructive diseases (26)	6-14 months	None	PNT	T_{PTEF}/T_E, V_{PTEF}/V_E	Both indices showed good positive correlation with $\dot{V}_{maxFRC}$ ($r > 0.63$), but no correlation with R_{aw}.

15.	Aston, J. Clarke and Silverman 1994	BP responders (18), Non-responders (19)	6-12 months	BP	PNT	τ_{RS}, T_{PTEF}/T_E, Others	In responders, BP decreased τ_{RS}. T_{PTEF}/T_E showed <u>no</u> significant changes.
16.	Totapally et al. 2001	Syncytial bronchitis (20)	Under 12 months	BP	PNT	PTEF, T_{PTEF}/T_E, V_{PTEF}/V_E, TEF25/PTEF, TEF10	PTEF increased, TEF25/PTEF and TEF10 decreased significantly after BP. Whereas T_{PTEF}/T_E and V_{PTEF}/V_E did <u>not</u> experienced a significant change.
17.	Schmalisch, Wilitzki and R. Wauer 2005	Healthy (48), CLD (48)	36-42 weeks	None	PNT	T_{PTEF}/T_E, V_{PTEF}/V_E, TEF50, TEF25, Convex vs. concave vs. linear, Others	TEF50 and TEF25 was lower for subjects with CLD. Whereas T_{PTEF}/T_E and V_{PTEF}/V_E presented <u>no</u> significant difference. Expiration shape was convex for 10 healthy and 9 CLD; linear decrease for 31 and 13; concave for 1 and 15; and undefined for the rest.

| 18. | Schmalisch, R. R. Wauer et al. 2003 | Healthy (54), CLD (32) | 3-162 days | None | PNT | T_{PTEF}/T_E, V_{PTEF}/V_E, TEF25/PTEF, $\dot{V}_{b-o}$, Convex vs. concave vs. linear, Others | T_{PTEF}/T_E, V_{PTEF}/V_E, and TEF25/PTEF were lower for subjects with CLD. Whereas $\dot{V}_{b-o}$ presented <u>no</u> significant difference. Expiration shape was convex for 8 healthy and 6 CLD; linear decrease for 36 and 12; and concave for 2 and 9. |

Maturation (and some also airflow limitation)

| 19. | van der Ent et al. 1996 | Healthy (26), Asthma (26), CF (12) | 3-11 years | BD, Age | PNT | T_{PTEF}/T_E | In healthy subjects, T_{PTEF}/T_E showed a negative correlation with age, but this was <u>too weak</u> to draw conclusions. T_{PTEF}/T_E was lower for asthmatics compared to controls and increased after BD, but not so for CF. T_{PTEF}/T_E showed low positive correlation with forced expiration indices ($r = 0.50$ for FEV1). |
| 20. | Colin et al. 1989 | Healthy (27) | 1 month to 8 years | Age | RIP | Interrupted vs. uninterrupted expiration | The TBFV expiration profiles were predominantly classified as interrupted below 6 months of age and predominantly uninterrupted over 1 year of age. Mixed profiles were observed in children 6-12 months of age. |

#	Reference	Subjects	Age		Method	Parameters	Results
21.	Frey, Silverman and Suki 2001	Healthy (10); Weezers (10); CLD (10)	1-18 months	BP, Age	PNT	T_{PTEF}/T_E, Others	T_{PTEF}/T_E decreased from 1 month to 6 months, but change was <u>not</u> significant from 6 months to 12 months. T_{PTEF}/T_E was <u>not</u> significantly different between age-matched healthy and symptomatic. BD, carried out only in the healthy, did <u>not</u> changed T_{PTEF}/T_E at any age. (Variability analysis showed more differences, see Table 3.2)
22.	J. R. Clarke, Aston and Silverman 1994	Healthy (22), Lower respiratory illness (32)	1-12 months	Age	PNT	T_{PTEF}/T_E	T_{PTEF}/T_E was found to decrease from the age of 1 to 6 months of age, but <u>not</u> from age 6 to 12 months of age in healthy infants. <u>No</u> changes were seen in subjects with lower respiratory illness..
23.	Young et al. 1994	Healthy (252)	1-12 months	BP, Age	PNT	T_{PTEF}/T_E	T_{PTEF}/T_E was found to decrease from 1 to 6 months of age. A sub-group of 19 infants with flow limitation showed significantly lower T_{PTEF}/T_E than controls at 1 month. However T_{PTEF}/T_E, at 6 and 12 months was <u>no</u> significant differences between these groups.
24.	Dezateux et al. 1994	$\leq$13weeks (73), >13weeks (68), >13weeks+ wheeze (79)	5-78 weeks	Age	PNT	T_{PTEF}/T_E	T_{PTEF}/T_E showed a weak association with sGaw in infants above 3 months of age, independently of prior wheezing status. However, this relationship was <u>not</u> significant in healthy younger infants, in whom a significant but weak association with FRC_{pleth} was found.

25.	K. L. Carlsen, Magnus and K. H. Carlsen 1994	Healthy (803)	1-9 days	Age	PNT	$PTEF$, T_{PTEF}/T_E, V_{PTEF}/V_E, $TEF25/PTEF$	These indices decreased with postnatal age, but only $PTEF$ depended on bodyweight. All these indices were higher in males.

Sleep

26.	Lødrup, Mowinckel and K. H. Carlsen 1992	Healthy (19)	1-5 days	Awake, Sleep	PNT	T_{PTEF}/T_E, $TEF50$	Both indices decreased from awake to sleep.
27.	Stark et al. 1987	Preterm (6)	4-7 days	NREM, REM	PNT, rEMG	Visual analysis of TBFV and rEMG	During NREM, TBFV expiration profiles presented a later T_{PTEF}, an interrupted expiration, and a higher diaphragm activity compared to REM.

3.2.2.3   Summary of observed influences in the shape indices

The common results from Table 3.1 are summarised next. To avoid repetition, the numbers in parenthesis refer to the studies on the Table 3.1. The possible mechanisms behind the associations of the following factors with the change in the shape indices are discussed together with the results of publications P.II and P.III in section 6.1.

Influence of lower airway obstruction

a. When an association is found, results suggest that an increase in lower airway obstruction leads to a decrease in the *early expiration* indices T_{PTEF}/T_E and V_{PTEF}/V_E. This association appears between symptomatic and controls (3, 10, 13, 18, 19), induced bronco-constriction or bronco-dilation (5, 9, 19), and correlation to lung function (3, 4, 5, 8, 11, 14, 19, 21).

b. However, correlations are weak, groups typically present a high overlap, and many studies researchers have not found significant differences between the compared groups (1, 4, 8, 15, 16, 17, 21, 22, 23).

c. Results suggest that an increase in lower airway obstruction leads to a linear decrease or a concave *middle expiration* (3, 7, 12, 13, 17, 18). This also reflect as a decrease in TEF50/PTEF and TEF25/PTEF with increased obstruction (6, 11, 16, 18).

d. As with *early expiration* indices, *middle expiration* indices also present weak correlations and high overlaps between the compared groups.

Influence of sleep

e. From awake to NREM, the *early expiration* shows a decrease in T_{PTEF}/T_E, and the *middle expiration* decrease in TEF50/PTEF (26). From NREM to REM, *late expiration* transitions from interrupted to uninterrupted expiration (27). These observations should be interpreted with care as the studies correspond to newborn and preterm infants.

Influence of maturation

f. Over the first six months of life T_{PTEF}/T_E decreases and the *late expiration* is less often interrupted. Both changes become stable by the age of one (20, 21, 22, 23).

g. Maturation seems to overlap with obstruction when shaping expiration. Most of the studies that failed to associate shape indices to obstruction are those carried out on infants below 12 months of age (15, 16, 17, 21, 22, 23).

Other influences

h. Other respiratory conditions may alter the shape of the expiration profile, thus making the interpretation of the shape indices difficult. For instance, a constant (or "flat") expiration shape seems associated with an increased upper airways resistance, either due to upper obstruction (7, 12) or to grouting (17).

3.2.3 Variability analysis of tidal breathing

All the previous methods follow a reductionist paradigm. The respiratory system is simplified to a linear system where the inaccessible mechanical properties can be inferred from the measured variables. Systems biology has a more holistic view of the human body. It understands the respiratory system as a set of multiple regulatory subsystems interacting with each other and the environment in order to maintain a homeostatic equilibrium (Coveney and Fowler 2005; Thamrin et al. 2016). The inherent delays, feedback loops, and non-linear interactions of these subsystems result in complex temporal fluctuations of the measured variables. Variability analysis has collected a set of mathematical tools from multiple disciplines to quantify the degree of complexity and variation on these fluctuations (Bravi, Longtin and Seely 2011; Seely and Macklem 2004). Deviations from the normal levels of variability indicate limitations on the system to adapt to environmental changes or the loss in the control of the homeostatic equilibrium. These deviations may reflect the presence of disease or serve as a predictor for illnesses worsening (Frey, Maksym and Suki 2011; Suki, J. H. T. Bates and Frey 2011).

As int the case with shape analysis, in variability analysis, it is difficult to know the real physiological mechanisms leading to a change in the variability of respiration. In addition to this, in variability analysis, it is sometimes also difficult to know how the variability of the respiratory signals is reflected in some of the variability indices. Variability analysis applied to systems biology is a young approach. Some concerns have been raised regarding whether indices arriving from chaos and information theory are suitable for the noisy and the non-stationary properties of the biological signals (Gao, Hu et al. 2012; Shashidhar 2006; Small et al. 1999). Nonetheless, as expressed by Kantz and Schreiber 2004: "*We feel that people*

have already spent too much of their time trying to find an answer to the question is it chaos or is it noise?. Often it is much more fruitful to ask which is the most useful approach for a given experiment. That a data set is stochastic to some degree does not mean that we have to use stochastic methods exclusively.". For these reasons, the connection between variability indices and the factors influencing respiration are mostly based on empirical observations. The following section briefly describes these variability indices that have been applied to respiratory signals. Consequently, we review the literature studying the empirical connections of shape indices with airway obstruction, sleep, maturation, and other factors.

3.2.3.1 Variability analysis indices

This section follows the classification suggested by Bravi, Longtin and Seely 2011, which groups the variability indices in five domains based on the field from which they originate. These five domains are described together with a short explanation of these indices mentioned on the thesis. Each domain is labelled with a letter later used in Table 3.2. For further details on these indices, more indices, or other classifications the reader is referred to the works of Seely and Macklem 2004 and Bravi, Longtin and Seely 2011.

- *Statistical [s]:* Indices in this domain treat the time series as a collection of independent samples produced by a stochastic variable. Hence, they derive features from its probability distribution. This includes measures of dispersion from classic statistics, such as coefficient of variation (CV) and standard deviation (SD), or more robust to outliers, such as median absolute deviation (MAD) or interquartile range (IQR).

- *Geometric [g]:* The time series is transformed into a certain multidimensional space and indices are derived from the shape of the new transformation. A clear example of this is the Poncaire plots used in heart rate variability analysis (Brennan, Palaniswami and Kamen 2001). A more advanced method is recurrence quantification analysis (RQA). RQA embeds the signal into a time-delayed phase space, calculates a threshold distance matrix from the embed samples, and derives geometrical features from this matrix, such as recurrence period density entropy (RPDEn) and recurrent points for a given radius in RQA (REC) (Marwan et al. 2007). A somewhat similar method, specific of tidal breathing, is the family of expiration variability index (EVI). In this case, the distance matrix is built from the Pearson correlation between TBFV profiles and the IQR is calculated from all values in the matrix. Correlation may be calculated from the whole expiration limb, such as CSR_{min} (V.-P. Seppä, A. S. Pelkonen,

Kotaniemi-Syrjänen, Viik et al. 2016), or only from a section of the TBFV, such as r_{15-45}IQR (V.-P. Seppä, Paassilta et al. 2018), later renamed to EVI. Publication P.IV uses EVI in the 15 % to 45 % and 55 % to 85 % exhaled volume ranges.

- *Energetic [e]:* The time series is typically transformed into the frequency domain and indices related to the energy or the power spectrum are derived. Frey, Silverman and Suki 2001 suggest two indices measuring how similar tidal airflow is to a sinusoid. Index s is the slope of a line fitted to the flow power frequency in log-log scale, and the harmonic distortion (kd), inspired by Suki, Hantos et al. 1991. A higher s and lower kd indicate lower harmonics relative to the fundamental frequency and, hence, a more regular flow signal similar to an ideal sinusoidal wave.

- *Informational [i]:* Unlike statistical indices, information indices consider samples to be statistically dependent, and hence derive statistical features from the repeatability or predictability of similar time patterns. Indices are inspired by the concept of entropy coming from information theory (Shannon 1948). A regular signal has low entropy as future samples can be predicted by looking at the pass, e.g. a sine wave. In contrast, an irregular signal has high entropy as future samples may be less dependent on the pass, e.g. a Gaussian process. The exact entropy can be measured by regularity statistics, such as Kolmogorov-Sinai entropy (KSE). However, accurate entropy calculation requires long datasets and is sensitive to measurement noise. For this reason, Pincus 1991 introduced approximate entropy (ApEn). In short, $ApEn(m, r)$ reflects the conditional probability that a section of length m samples, repeated along the time series within a tolerance r, will repeat itself when the length is increased one sample $m + 1$. Sample entropy (SampEn) is modification of ApEn to correct the bias on data length (Richman and Moorman 2000). Multi-scale entropy (MSE) proposes to calculate SampEn at different timescales (M. Costa, Goldberger and Peng 2005).

- *Fractal [f]:* Temporal patterns may not only repeat over time but also at different time and size scales within the same time series. This self-similarity at different scales is known as fractality and is an emerging property of complex systems. Fractal indices measure the repeatability/predictability of patterns invariant with scale. There are two radically different approaches to measure self-similarity which arise from two different branches of mathematics: *deterministic chaos* and *stochastic processes*.

The former assumes that the time series is the output of a deterministic low-dimension chaotic system. It transforms the time series into a multidimensional time

delay phase space and measures fractal properties of the chaotic attractor (Kantz and Schreiber 2004). These include correlation dimension (CD) which measures the fractal dimension of the attractor and largest Lyapunov exponent (LLE) which measures the sensitivity to initial conditions. A periodic signal will yield a low CD and LLE= 0 (J. L. Kaplan and Yorke 1979), whereas increasing degrees of freedom and variability of the system results in higher CD and LLE. Unfortunately, when the dimensionality of the system becomes large, it is not possible to differentiate *deterministic chaos* from an *stochastic process* (Shashidhar 2006).

Aware of this limitation, the second approach directly models the time series as *stochastic processes*, concretely, as a *fractional Brownian process*. These are a family of stochastic processes that exhibit self-similarity on the 2D time series. The dependency between samples in these signals is expressed by the standard deviation as $\sigma_t = t^H$, where H is called Hurst exponent. H indicates the degree of positive correlation for $1/2 < H < 1$, or negative correlations for $0 < H < 1/2$, (Hurst 1956). The most popular estimator for the Hurst exponent is detrended fluctuation analysis (DFA). A DFA further apart from 0.5 means the time series presents long-term correlations and hence is more deterministic (Bashan et al. 2008). Additionally, a time series may be better described as the summation of several *fractional Brownian processes* with different Hurst exponents. Multifractal detrended fluctuation analysis (MFDFA estimates the spectrum of Hurst exponents. In a broad sense, the higher the spectrum of exponents, the more deterministic and the less complex the system is (Ihlen 2012).

High dimension *deterministic chaos* and low correlated *stochastic process* are hard to differentiate by the methods discussed above. For this surrogate tests are applied. These tests compare how similar variability indices are between the original signal and a copy of the signal where samples are randomly reordered (Shashidhar 2006). A more advanced method is noise limit (NL) which detects if the signal is chaotic and, if so, with what degree of complexity (Poon and Barahona 2001; Wysocki et al. 2006).

3.2.3.2   Studies on variability indices applied to tidal breathing

Table 3.2 presents a review of the studies on variability in tidal breathing associated with airway obstruction, maturation, sleep, and other factors. Due to the low number of studies on variability indices and the yet unclear effects of maturation this review includes studies in all ages. Searched by combining the names of respiratory conditions and variability indices.

Table 3.2 **Clinical studies on variability of tidal breathing:** Studies grouped by the main factor of study and sorted by age. Columns as in Table 3.1 subsubsection 3.2.2.2. Column *Signal* indicates the respiratory signal being analysed and its duration in square brackets. IBI stands for a interbreath interval signal and RR for respiratory rate signal. "*surr. Ln*" indicates surrogate testing with a Ln process.

| | Population | | | Methods | | | |
| | Compared | | Interv./ | | Signal | Indices | |
Authors	Groups(n)	Age	Cofac.	Device	[duration]	[domain]	Results
Airflow limitation							
1. Dames, Lopes and de Melo 2014	Healthy (16), COPD obstruction: None (11), Mild (11), Moderate (18), Severe (16), Acute (14)	50-80 years	None	PNT	*flow* [1 min]	SampEn *[i]*, RPDEn *[g]*	Entropy and variability in the tidal flow was respectively lower and higher in COPD compared to controls independently of the degree of obstruction. SampEn showed weak positive correlation with FEV1/FVC ($r = 0.42$). SampEn and SD were negatively correlated ($r = -0.50$). *Note* that here SD assesses spread around the mean amplitude.
2. Teulier et al. 2013	COPD (11)	48-79 years	BD	RIP	*flow*, IBI, Others [10 min]	NL *[f]*, LLE *[f]*, CV *[s]*	Complexity in tidal flow and variability in IBI increased after BD. Changes were <u>not</u> significant on the other signals.

3. Raoufy et al. 2016	Healthy (10), Asthma: Atopic (10), Uncontrol (10), Not-atopic (10)	21-39 years	None	RIP	IBI, V_t [60 min]	DFA [f], SampEn [i], LLE [f]	The IBI and V_t fluctuations showed decreased long-range correlation, increased regularity, and reduced sensitivity to initial conditions in patients with asthma, particularly in uncontrolled state.
4. Veiga et al. 2011	Healthy (11), Asthma obstruction: None (11), Mild (14), Moderate (14), Severe (12)	Adults	None	RIP, PNT	*flow* [120 sec]	ApEn [i], SD [s]	Entropy in the tidal flow was lower for asthmatics with obstruction. SD showed no differences between groups. ApEn showed weak positive correlation with FEV1/FVC ($r = 0.31$). ApEn and SD were negatively correlated ($r = -0.48$). *Note* that here SD assesses only spread around the mean amplitude.
5. Veiga et al. 2012	Healthy (12), Asthma obstruction: None (12), Mild (20), Moderate(18), Severe(12)	Adults	None	FOT	$R_{rs}5$ [60 sec]	ApEn [i], RPDEn [g], SD [s]	What they call $Z_{rs}5$ is $R_{rs}5$. Entropy in the respiratory impedance decreased with asthma severity, whereas SD increased. ApEn, RPDEn, and SD showed a repetitively weak negative, strong negative, and strong positive correlation with $R_{rs}5$ ($r = -0.43, -0.85, 0.88$). *Note* that here a higher SD indicates a larger difference in resistance between end and beginning of expiration. In this study RPDEn is equivalent to the SD.

6. Morris and Lane 1981	Healthy (15), Obstruction (51), Restriction (24)	Adults and Children	None	PNT	V_{PTEF}/V_E [10 breaths]	CV *[s]*	Individual patients with obstruction presented less breath-to-breath variability in the expiratory flow pattern than normal patients. CV of V_{PTEF}/V_E was 23% in healthy and 13% in the 23 most severely obstructed patients.
7. van der Ent et al. 1996	Healthy (26) Asthma (26) CF (12)	3-11 years	None	PNT	T_{PTEF}/T_E [15 breaths]	SD *[s]*, CV *[s]*	Healthy showed an slightly <u>lower</u> CV in T_{PTEF}/T_E than mild asthmatics (23.1% vs 26.5%), but significance was not tested. The SD of T_{PTEF}/T_E within one subject correlated positively with the mean of T_{PTEF}/T_E ($r = 0.67$).
8. V.-P. Seppä, A. S. Pelkonen, Kotaniemi-Syrjänen, Viik et al. 2016	Asthma: High risk (13), Low risk (14), Medicated (7)	3-7 years	None	IP	*flow*, TBFV [full night]	CSR_{min} *[g]*, NL_{min} *[f]*	Change in the TBFV shape between the first and second part of the night was stronger for the high risk compared to the low risk and high risk compared to medicated groups. The minimum NL (from 4-mins windows) was smaller for high risk compared to the lower risk groups. *Note* that here $NL = 0$ could indicate periodic breathing, but also excessive noise.
9. V.-P. Seppä, Paassilta et al. 2018	Healthy (39), Wheeze (70): Medicated, 2, 4 weeks off medication	1-6 years	None	IP	TBFV [full night]	$r_{15-45}IQR$ *[g]*	Variability between all-night TBFV late expiration shape was significantly higher for healthy compared to wheezes at all recorded weeks; and for wheezes on medication compared to off medication.

Maturation

10. Peng et al. 2002	Healthy (40)	22-56 years	Age, Gender	RIP	IBI [120 min]	DFA *[f]*, surr. *Ln*	Long-term correlation in IBI decreased in elderly men. However, this decrease was <u>not</u> found in women, perhaps due to the low number of subjects.
11. Stocks et al. 1994	Healthy (266)	1-19 months	Age, Sedation	RIP	T_{PTEF}/T_E [60 sec]	SD *[s]*	Variability and repeatability in T_{PTEF}/T_E was high on the first 6 weeks of live and stabilised thereafter. Sedation with triclofos sodium had <u>no</u> significant effects in T_{PTEF}/T_E.
12. Frey, Silverman and Suki 2001	Healthy measured at 1mo, 6mo, and 12mo (10); Wheezers at 12mo (10); CLD (10)	1-18 months	Age, BP	PNT	*flow*, T_{PTEF}/T_E [10 sec]	s *[e]*, kd *[e]*, CV *[s]*	Airflow became less regular (increased kd) from 1 month to 6 months, but change was <u>not</u> significant from 6 months to 12 months. Marginally increase in regularity (increased s) Wheezers, whereas s was significantly lower in infants with CLD of prematurity. Breath-to-breath CV on T_{PTEF}/T_E showed <u>no</u> significant changes. Measuring during REM may have influenced the results.

48

Sleep

13. Willemen et al. 2014	Meta-analysis	Adults	REM, NREM	RIP, Othe.	IBI, RR [-]	Multiple indices *[s]*	Variability in IBI and RR was significantly higher during the REM stage compared to NREM. MAD and IQR showed the best result to classify sleep stages across several studies.
14. Sako et al. 2001	Healthy (8)	23-26 years	REM, Stage IV Stage I	RIP	*Resp. effort* [204 sec]	CD *[f]*, surr. *Ln*	Complexity of tidal volume was significantly different between sleep stages as measured by CD. Complexity was least during stage IV sleep and greatest during REM.
15. Burioka et al. 2003	Healthy (8)	23-29 years	REM, Stage IV Stage I, Wake	RIP	*Resp. effort*, EEG [3 min]	ApEn *[i]*, surr. *Ln*	Entropy in the tidal respiratory effort and the EEG was lower during stage IV compared to other states of consciousness. ApEn of respiratory effort and EEG were positively correlated ($r = 0.494$).
16. Kantelhardt et al. 2003	Healthy (29)	26 ± 3 years	REM, Light, Deep, Wake	PNT	IBI, V_t [300 breaths]	DFA *[f]*	IBI, V_t presented long-range correlations during the REM stages and during wake states. In contrast, in the NREM stages, long-range correlations were absent.

17. Schumann et al. 2010	Healthy (180)	20-89 years	Wake, Deep, Light, REM, Age	Nasal flow	IBI, RR [-]	DFA2 [f]	IBI, RR presented long-term correlations only during wakefulness and REM sleep. RR long-term correlation increased with age in REM sleep and decreased during wake, while IBI long-term correlation decreased with age both during REM and wake.
18. Terrill et al. 2013	Infants (25)	3±2 months	REM, NREM	RIP	IBI [>400 breaths]	REC [g], SD [s], IQR [s], others	REC variability in IBI was significantly higher during REM stage. REC showed the best result to classify sleep stages. *Note* that REC shows similar results than IQR. It seems that here REC is convoluted way to measure the SD.
19. Isler et al. 2016	Healthy (49)	26-42 weaks	REM, NREM	RIP	IBI [full night]	SD [s]	Variability in IBI was significantly higher during REM stage compared to NREM. A fixed threshold was able to classify sleep stages reliably.

Other factors

20. Suyama et al. 2003	Healthy (8)	23-39 years	Hyper-capnia	RIP	*Resp. effort* [15 min]	CD [f] surr. *Ln*	Complexity of tidal respiratory effort decreased significantly after induced hypercapnia as measured by CD. Chemoreceptors influence the complexity of respiration.

21. Fiamma, Straus et al. 2007	Healthy (8)	24-26 years	Hyper-capnia, Hypo-capnia	PNT	*flow*, IBI, Others [10 min]	NL *[f]*, LLE *[f]*, KSE *[i]*, CD *[f]*, CV *[s]*	Induced hypercapnia reduced variability in most IBI indices and showed an increased in tidal flow complexity as measured by LLE and KSE. While, induced hypocapnia increased variability most in most IBI indices, but it showed reduced tidal flow complexity only for CV. NL showed <u>no</u> changes in tidal flow complexity.
22. Samara et al. 2009	Healthy (10)	19-34 years	Hyper-capnia, Re-sistive loads	PNT	*flow*, IBI [4-7 min]	LLE *[f]*, NL *[f]*, SD *[s]*	Adding a threshold load of $21 cmH2O \cdot l^{-1} \cdot s$ or a resistive load of $50 cmH2O \cdot l^{-1} \cdot s$ did <u>not</u> alter tidal flow complexity <u>nor</u> IBI variability. However, induced hypercapnia increased complexity and reduced variability.
23. Thibault et al. 2004	Healthy (7)	Adults	Resis-tive loads	PNT	*flow* [5 min]	LLE *[f]*	Complexity of tidal flow, measured by LLE, decreased with the successive increase of resistive loads: from 0 to 3.6 to 5.8 to 8.8 $cmH2O \cdot l^{-1} \cdot s$. However LLE increased from 8.8 to 13.1 $cmH2O \cdot l^{-1} \cdot s$.

3.2.3.3 Summary of observed influences in the variability indices

The common results from Table 3.2 are summarised next. To avoid repetition, the numbers in parentheses refer to the studies in Table 3.2. The possible mechanisms behind the associations of the following factors with the change in the variability indices are discuses together with the results of publications P.IV on section 6.1.

Influence of lower airway obstruction

    a. The results suggest that an increase in lower airway obstruction leads to a decrease in the variability of respiration. With a different degree of sensitivity, this decrease in respiration variability is reflected as a reduction in statistical variability (1, 6, 7, 9, 11, 12), spectral energy (12), entropy (1, 3, 4, 5), complexity (2, 3, 8), and long-term correlation (3) across the multiple respiratory signals: interbreath intervals (IBI) (2, 3), respiratory flow (1, 2, 8), respiratory impedance (5), TBFV shape (8,9), and TBFV indices (3, 6, 7, 11, 12).

    b. Three studies seem to contradict the previous observation (1, 4, 5). However, in one of them (5), the higher SD rather than time-related variability indicates a larger amplitude of the $R_{rs}5$ signal, which is due to the well known increased dependency between airways resistance and lung volume during asthma (Butler et al. 1960; Murakami et al. 2014). Similarly, in the other two (1, 4), the increase in SD with obstruction is most likely due to a higher amplitude of the flow signal, specifically PTEF (Benoist et al. 1994; Totapally et al. 2001), or other changes in shape (section 3.2.2.1).

Influence of sleep

    c. There is a clear consensus that variability on respiration is higher during REM sleep than during NREM, and that within NREM, it is lowest during N3 (deep sleep, stage IV). Most studies have showed this from the IBI signal either using statistical variability indices (12, 18, 19) or DFA (16, 17). Two others show this from the respiratory effort signal using entropy (15) and complexity (14) indices.

Influence of maturation

    d. Variability in respiration seems to increase with age. However, the results are inconclusive and may depend on the timescale, the signal, and the variability index. At

the scale of weeks, variability on respiratory flow only shows a decrease over the first month of life, depending on the method (11, 12). At the scale of years, DFA on IBI shows a decrease in long-term correlation with ageing (10, 17).

Other influences

e. Variability of respiration may be influenced by other respiratory conditions, such as upper airways obstruction (22, 13), but also by neural and hormonal disorders related to chemoreceptors (20, 21, 22).

f. Two studies seems to contradict the common observation that variability and complexity are correlated (20, 21). CV increases when other complexity indices are decreasing and vice versa.

3.3 Impedance pneumography

Impedance pneumography (IP) is a non-invasive technique that allow us to estimate lung aeration by means of four skin surface electrodes. The following subsections describe the working principle, the state-of-the-art and the advantages that it offers for the analysis of tidal breathing.

3.3.1   Bioimpedance basics

Any existing substance presents opposition to an electrical current when a voltage is applied. The characteristics of this opposition, known as electrical impedance, depends on the electrical properties of the material. Electrical impedance is measured by injecting an electrical current (I) and measuring the voltage response (U), or vice versa, and consequently applying Ohm's law (Z=U/I).

Bioimpedance refers to the electrical impedance of biological materials, which presents specific electrical properties (Grimes and Martinsen 2011). One of these properties is that, in biological materials, the electric current is principally carried by ions instead of electrons. For this reason, the measurement systems need to use electrodes as transducers between these two forms of current. Bioimpedance measurement systems typically employ a bipolar or tetrapolar electrode configuration. The bipolar configuration uses one pair of electrodes to connect both current and voltage. In contrast, the tetrapolar configuration uses two pairs of electrodes, one for current and one for voltage. The tetrapolar configuration is often pre-

ferred as it excludes the impedance of the electrodes from the measurement (Brown, Wilson and Bertemes-Filho 2000).

Bioimpedance measurements can be divided into two categories, frequency-domain and time-domain (Gracia, V.-P. Seppä, Viik and Hyttinen 2012). Frequency-domain measurements, also known as impedance spectroscopy, apply a signal composed of multiple frequencies and analyse the amplitude and the phase at each frequency to estimate the composition of the sampled material. Applications in this domain include body fat and muscle mass estimation (Kyle et al. 2004), the monitoring of wound healing (Kekonen et al. 2017), and in vitro cell analysis (Lehti-Polojärvi et al. 2018). Time-domain measurements record variations in the properties of the biological sample to derive a physiological signal. Commonly, these measurements apply one single frequency and analyse its changes in the amplitude. Impedance cardiography (Cybulski 2011) and IP are some examples of this. More advanced methods include a combination of frequency and time-domain measurements. For instance, electrical impedance tomography applies multiple impedance spectroscopy measurements over time and space to image body composition changes. This technique is used, for example, to monitor atelectasis in artificially ventilated patients (E. L. V. Costa, Gonzalez Lima and Amato 2009).

Given an impedance value, it is relatively easy to calculate the electrical properties of the measured material if the volume is regular and the properties are homogeneous. For example, impedance relates to the resistivity of a given volume as follows:

$$Z = \rho \cdot \frac{l}{A} \tag{3.3}$$

Here, ρ is the resistivity of the material, A is the area of current flow, and l is the length of the material. However, biological materials are highly heterogeneous and volumes in the human body are often irregular. *Lead field theory* describes how the electrical properties in each region in the material contributes to the measured impedance in an irregular volume (Malmivuo and Plonsey 1995). For example, impedance relation to resistivity is calculated as follows:

$$Z = \int_{V} \rho \cdot J_{LU} \bullet J_{LI} \cdot dV \tag{3.4}$$

Here, the impedance is the volumetric integral of the scalar product between the voltage lead field (J_{LU}) and the current lead field (J_{LI}) multiplied by the resistivity (ρ) at each point in the volume. The voltage and the current lead fields are vector fields defined as the intensity and

direction at each point in the volume caused by a theoretical unit current applied between the voltage or current electrode pairs respectively.

Figure 3.7-A shows an example of these lead fields applied to the thorax. The scalar product between each lead is defined by the angle they form at each point. The product is zero when they are perpendicular and maximum when they are parallel, being positive for the same direction and negative for opposing directions (Malmivuo and Plonsey 1995). The location of the electrodes affects the angles between lead fields, and therefore it is important to maximise the contribution of the target region to the measurement. Unfortunately, the contribution of unwanted regions can be decreased, but may be difficult to remove completely. Another source or artefact when recording in living organisms is movement. Movement alters the electrode-skin interface and the lead fields, thus interfering the measurement. The tetrapolar configuration helps to mitigate motion artefacts because the regions close to the electrodes form perpendicular angles between the lead fields Figure 3.7-A (Sahakian, Tompkins and Webster 1985).

3.3.2 Impedance pneumography technology

IP is a bioimpedance measurement technique that falls within the time-domain category. IP records variations in the electrical impedance of the thorax to derive a signal proportional to the lung volume. This technique is radically different from other non-invasive methods deriving lung volume from changes in the thoracic diameter, such as RIP, or optoelectronic plethysmography (Dellacà et al. 2003). In IP, respiratory changes emerge from microscopic changes in the lung parenchyma (Witsoe and Kinnen 1967). Although lung tissue is heterogeneous at the low scales, at a macroscopic level the tissue resistivity has been shown to change linearly with the proportion of air per unit volume (Nopp et al. 1997).

The first mention of respiration-induced changes in the thorax impedance appears in Atzler and Lehmann 1932. Where it is mentioned as an artefact to impedance cardiography. However, L. A. Geddes et al. 1962 were the first to find an application to this phenomena and give the technique its name. They implemented an IP system to remotely monitor the respiratory rate in astronauts. In the following decades, the technique saw a surge in interest, but it has declined in popularity until recent years. A search in *PubMed* with the term *"impedance pneumography"* reveals a steady rate of 30 publications per decade since the 60s. This declines to only 10 publications over the 2000s and rises back to 41 in the last decade. From these 41, 15 are actually associated with TUT. These improvements in the last
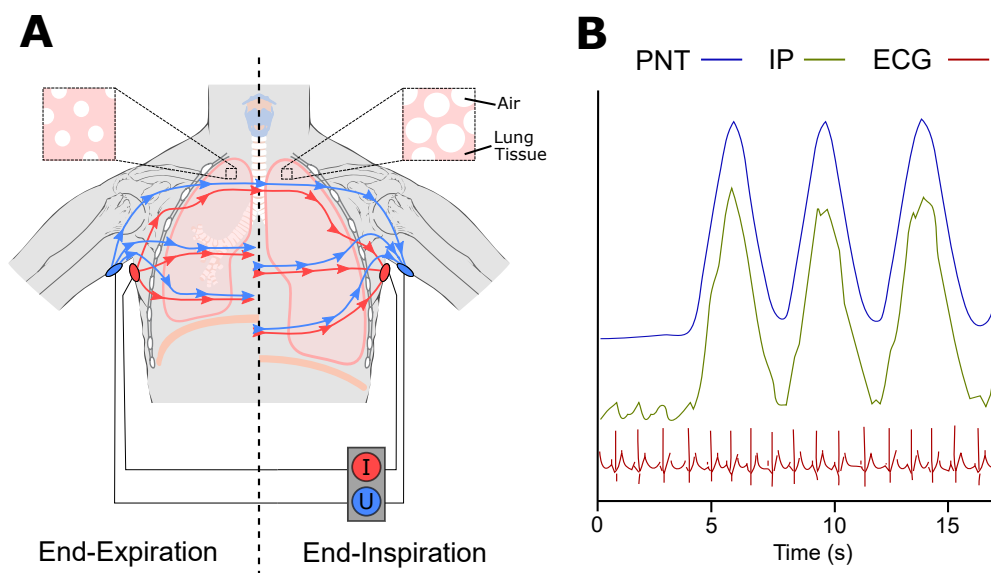
Figure 3.7 **A: Impedance pneumography working principle.** The electrical impedance of the thorax is measured as the ratio of a current (I) injected through a pair of electrodes in the midaxillary line and the voltage response (U) measured through another pair in the arms. The measured impedance depends on the resistivity of the different tissues and the angle formed by the voltage lead field (J_{LU}) (blue arrows) and the current lead field (J_{LI}) (red arrows)(equation 3.4). The resistivity of the lung parenchyma is proportional to its air content. The air content and hence the impedance are low at the end of expiration (left) and high at the end of inspiration (right). **B: Impedance pneumography raw signal.** The raw impedance signal is composed of two components. A large-amplitude component proportional to the lungs' air volume (PNT) and a small-amplitude component related to the thoracic blood, which is synchronised with the cardiac activity (ECG).

decade have transformed IP from a simple system to derive timing parameter at the bedside to a technology able to reliable derive respiratory flow and shape indices (V.-P. Seppä 2014). These specific developments are described next.

Recording device The majority of the previous studies were conducted using multipurpose impedance measurement devices. During his PhD., Vuorela 2011 developed a recording device customised for IP. By optimising the power consumption and the circuitry space Vuorela was able to embedded the measurement system into a portable device. The final version of this device uses a transimpedance amplifier as a current generator with a integrator feedback circuit for baseline correction. The excitation current is a 100 kHz sine wave as recommended (Nopp et al. 1997), from which the envelope of the voltage response is sampled at a 256 kHz (Vuorela et al. 2010). This device also records electrocardiogram

(ECG) at the same sampling rate. This device was turned into a CE marked product, named Ventica ®, and is commercialised by Revenio Group (*Ventica* 2019).

Removal of the cardiac component   The air density in lung tissue is not the only contributor to the changes in the thoracic impedance. At each heartbeat, the blood moves from the heart to the lungs and to the rest of the body and returns to the heart to start the cardiac cycle again. This, respectively, decreases and increases the thoracic impedance. These cardiac-related changes are known as cardiogenic oscillation (CGO) Figure 3.7-B. CGOs are the source of study for impedance cardiography but they are considered as an artefact in IP. It is possible to reduce the contribution of the systemic blood to the IP signals by choosing an adequate electrodes location. However, the lungs' blood circulation is intrinsic to the lung tissue and is therefore present in any electrode location (L. E. Geddes and L. E. Baker 1972). Moreover, a simple linear filter is not able to reliably separate the cardiac and the respiratory components, because they overlap in frequency.

Extensive work has been published on how to remove the respiratory component from the cardiac signal in impedance cardiography but few studies exist regarding the opposite problem (Pandey et al. 2011). Some of the few methods discussed include: setting a feature filter (()lynnFeatureFilteringDigital1977); subtracting signals recorded in two separated locations (Nakesch et al. 1994); and subtracting a CGO template at each heart beat, either a fixed template (Goldensohn and Zablow 1959) or an ensemble-averaged one (Wilson, Franks and Freeston 1982).

V.-P. Seppä, Hyttinen and Viik 2011 noticed that the shape of the CGOs changes with lung volume and improved Wilson's method to take this into account. In short, in the new method, the IP signal is split into sections defined by the R-peaks of the ECG signal. Sections are normalised in time, grouped into four groups, according to the lung volume at which they start, and averaged into CGO templates. The CGO templates are again resized to the duration of each R-peak interval and subtracted from the original IP signal.

Electrodes location   As mentioned, the resistivity in the lung tissue changes linearly with the proportion of air per unit volume (Nopp et al. 1997). However, this linearity may be lost if the lung moves relative to the electrodes as this reconfigures the lead field. The location of the electrodes is crucial to capture the linear changes in tissue aeration and not the displacement of the lungs in the abdomen (Kawakami et al. 1974).

Multiple studies suggest that placing the electrodes higher on the midaxillary line (L. Baker and L. Geddes 1966; L. A. Geddes et al. 1962) and over the 4th rib (Logic, Maksud and

Hamilton 1967) yields the highest linearity between lung volume and impedance change. V.-P. Seppä, Hyttinen, Uitto et al. 2013 showed that even in this configuration IP lost the linearity at low volume levels. They corrected this problem by moving one of the electrode pairs to the arms. Młyńczak et al. 2015 confirmed the linearity of this configuration in three different body postures.

Motion artefacts   The proposed methods to reduce motion artefacts in IP recordings include guarding electrodes to focus the sensitivity field out from the surface (Sahakian, Tompkins and Webster 1985); changing the location of the electrodes (Luo et al. 2002); or combining multiple IP signals, recorded at different electrode locations (Khambete, Brown and Smallwood 1999), at different excitation frequencies (Rosell, Cohen and Webster 2002), or a combination of both (Sahakian, Tompkins and Webster 1985).

These methods have shown to reduce the motion artefact but at the expense of losing linearity with lung volume. The best alternative to reducing motion artefacts is reducing motion itself. V.-P. Seppä, A. S. Pelkonen, Kotaniemi-Syrjänen, Viik et al. 2016 suggested recording ventilation while patients sleep. Publications P.II and P.III show that although on average 20 % of the night recordings in children become corrupted, the remaining 6 h to 7 h provides a good amount of information.

Deriving respiratory indices and respiratory flow   Since the early studies, it was noticed that the proportion ratio between lung volume and IP varies greatly between individuals (Logic, Maksud and Hamilton 1967). Two types of solution were proposed to correct this disparity; to derived a rule based on the anatomy of the subject (Allison, Holmes and Nyboer 1964; Valentinuzzi, L. A. Geddes and L. E. Baker 1971), or to calibrate the ratio for each individual based on PNT (Houtveen, Groot and de Geus 2006; Kubicek, Kinnen and Edin 1964; V.-P. Seppä, Hyttinen and Viik 2010).

It turned out that this ratio also presents intrasubject variations and any type of calibration is soon lost. This drawback is likely to be one of the reasons why IP has found only clinical applications for the monitoring of timing indices (Albisser and Carmichael 1974).

However, thanks to the abovementioned developments in instrumentation, electrodes location, and CGO filtering, V.-P. Seppä, A. S. Pelkonen, Kotaniemi-Syrjänen, Mäkelä et al. 2013 were able to obtain a high-quality volume-related IP which could be derived into a flow-related signal. Moreover, volume-related and flow-related signals can be split into respiratory cycles, see Schmidt et al. 1998 to form TBFV profiles. As described in subsection 3.2.2, meaningful relative shape indices can be derived from the flow signal and TBFV profiles

without the need for volume calibration. The IP flow-related signal and derived shape indices have shown a good agreement with mouth PNT in children (V.-P. Seppä, A. S. Pelkonen, Kotaniemi-Syrjänen, Mäkelä et al. 2013) and infants (Malmberg et al. 2017).

4   MATERIALS AND METHODS

This section firstly summarises the materials and methods common to the four studies, one on the improvement in the IP signal processing (P.I), and the three overnight studies (P.II, P.III, and P.IV). Details on the validation of the new processing method and the three overnight studies are presented in their respective sections.

Subjects: Publication P.I included 21 children 3-7 years old with lower respiratory tract symptoms; P.II 43 infants 6-24 months old with lower respiratory tract symptoms; P.III 70 children 1-6 years old with recurrent obstructive bronchitis after a three-month period of inhaled corticosteroids (ICS) treatment; and P.IV 20 healthy children 2-7 years old with no signs of obstruction or sleep apnoea.

Instrumentation: In publication P.I, P.II, and P.III, IP and ECG signals were recorded with a portable custom-made device similar to that described by Vuorela et al. 2010, whereas in P.IV a matching commercial version of the same devices was used (Ventica Recorder, Revenio Research Ltd., Finland). Additionally, in P.I, the direct mouth flow was measured with a PNT system (Masterscreen PFT, Jaeger, Germany). In P.II, all paediatric pulmonary function measurements were performed with a commercial equipment (Babybody Masterscreen, Jaeger GmbH, Würzburg, Germany), and doses of methacholine chloride were administered by using an inhalation-synchronised dosimeter (Spira Electro 2, Spira Respiratory Care Centre Ltd, Hämeen- linna, Finland). In P.IV, a polysomnograph (PSG) (EEG-1200, Nihon Kohden, CA, USA) was used to record 6 channel EEG, electrooculogram, peripheral oxygen saturation, nasal pressure, abdominal and thoracic plethysmography.

Preprocessing: In all publications, P.I-IV, signal processing and statistical analyses were performed using MATLAB software (MATLAB MathWorks, Natick, MA, USA). The heavy processing of overnight recordings was aided by the computational resources provided by CSC–IT Center for Science, Finland.

All recordings were visually inspected by trained researchers who were blind to patient information who discarded these sections corrupted by motion or other distortions. Accepted IP raw signals followed three processing steps: cardiac component removal aided by the ECG signal as described by V.-P. Seppä, Hyttinen and Viik 2011; differentiation of lung volume-oriented IP into a flow-oriented IP signal by a Savitzky-Golay (SG) filter (V. P. Seppä, Viik and Hyttinen 2010); and attenuation of remaining noise by means of the non-linear local projection filter (NLPF) described in publication P.I.

In P.I, these three steps were applied to the 1-minute recordings with a fixed embedding window of 1/5 s for the NLPF, while, in P.II-IV, steps were applied to 4-minutes windows with a dynamic embedding window of one third of the median respiratory period.

Tidal breathing indices: In P.II-IV, preprocessed flow and volume IP signals were split into respiratory cycles, as recommended by Schmidt et al. 1998. Consequently, cycles were averaged in the flow-volume domain, as described by Sato and Robbins 2001, by means of a 20-cycles moving window with 5-cycles overlap. In P.II and P.III, the shape of each averaged cycle was estimated by the conventional indices T_E, T_{PTEF}/T_E, V_{PTEF}/V_E, TEF50/PTEF, and TEF25/PTEF as well as the two new indices TEF05/PTEF and P_{FV} introduced in P.II. In P.IV, the variability of respiration was calculated as the IQR of the Pearson distances between the 15 % to 45 % exhaled volume ranges, namely EVI, as well as in the the 55 % to 85 % exhaled volume ranges.

Sleep segmentation: In P.II and P.III, REM and NREM were respectively estimated from the regions of higher and lower IBI variability by means of an automated method described in P.II. In P.III, night recordings were additionally divided in overlapping regions 3 hours long centred at each hour starting from sleep onset. In P.IV, wake, REM, N2, and N3 were defined by an experienced sleep technician using the Polysmith (Nihon Kohden,CA, USA) and Polaris (Nihon Kohden, CA, USA) software.

4.1 Improvement of the signal processing

The main limitation of the conventional processing, namely IP heart rate Savitzky-Golay (IP-HRSG), lies in the step differentiating volume-oriented IP into a flow-oriented IP. This step amplifies the noise remaining from the CGO-filter and the measurement. This noise can be reduced by shortening the SG-filter's fitting frame but at the cost of distorting the

shape of the flow signal (Schafer 2011). The proposed solution, named IP non-linear local projection filter (IP-NLPF), suggests lowering the fitting frame to maintain a low distorted flow and consequently attenuate the amplified noise by a NLPF (Hegger, Kantz and Schreiber 1999).

The performance of NLPF was compared to IP-HRSG by using an existing dataset recorded by Seppa, Uitto and Viik 2013. The dataset consisted on 64 raw IP signals with simultaneous mounted PNT flow. Each pair of signals was 1 minute long and had been recorded during four different stages of a methacholine challenge test.

Comparing the performance of the methods was challenging because the reference PNT was also contaminated with cardiac and measurement noise. Performance of the method was based on the ability to decrease the noise in the IP signal while maintaining the similarity with the reference PNT flow. For these four tests were conducted. Firstly, absolute sample-by-sample difference (Dss) measured the median sample-by-sample absolute difference in time-domain, between IP and PNT. Secondly, as absolute Dss is affected by the noise level of the PNT flow, noise-reduction factor (r) measured the reduction of noise of IP-NLPF relative to IP-HRSG. Thirdly, $\Delta P_{f_1 - f_2}$ measured the median point-to-point difference in a normalised power spectral density. $\Delta P_{f_1 - f_2}$ was measured at 5 different frequency bands. Putatively, high $\Delta P_{f_1 - f_2}$ values at high-frequency bands and low values at high-frequency bands indicate noise reduction and low shape distortion. Finally, absolute mean value of linearity (D_L) measured the average deviation from linearity. In short, comparing flows were plotted against each other and the median absolute difference of each point to a fitted line was calculated. A higher D_L denotes increased shape discrepancy rather than noise.

4.2 Shape analysis of nocturnal tidal breathing in wheezy infants

This cross-sectional study, presented as P.II, recruited 43 patients at Helsinki University Central Hospital (Finland) who were referred to infant lung function testing due to troublesome respiratory symptoms such as wheeze, cough and/or laborious breathing. Loose criteria of modified asthma predictive index (mAPI) were followed to classify children into three groups based on their risk of asthma, i.e. high risk (HR), intermediary risk (IR), and low risk (LR). In all patients, specific airway conductance (sGaw) was measured by the plethysmographic method and the maximum flow at FRC ($\dot{V}_{maxFRC}$) was determined using

the RTC technique. In addition, a subgroup of infants underwent a bronchial provocation test with methacholine where airway responsiveness was defined as the administered dose needed to reach a 40 % decrease in $\dot{V}_{maxFRC}$ (PD40).

After lung function testing, the IP device was set on the subjects for the overnight recording of IP and ECG signals at home. Nocturnal TBFV shape indices were derived from the recordings and classified as NREM or REM. for each subject, all night NREM and REM values were estimated as the median of all-night shape indices marked as NREM and REM respectively.

All-night NREM and REM median values were used to compare indices between sleep stages within subjects, to lung function testing parameters, and to asthma risk classification. These comparisons respectively used a Wilcoxon signed-rank test, a Spearman's rank correlation, and a Wilcoxon paired test.

4.3 Shape analysis of nocturnal tidal breathing in wheezy children

This longitudinal study, presented as P.III, recruited 70 children who visited the Tampere University Hospital (Finland) emergency room due to recurrent obstructive bronchitis and were prescribed 3 months of fluticasone propionate treatment.

Three overnight IP and ECG recordings were conducted at home. The first recording (Week -1) was performed one week before the end of the fluticasone treatment, and the second (Week 2) and third (Week 4) two and four weeks thereafter. Nocturnal TBFV shape indices were derived from the recordings and classified as NREM or REM. TBFV indices were derived and classified as NREM or REM. For each recording, for each subject, all night NREM and REM values were estimated as the median of all night shape indices marked as NREM and REM respectively. Additionally, for each recording, hourly progression for NREM and REM was estimated as the median of the NREM or REM indices within each of the hourly 3-hour-length bins.

All-night NREM, REM and hourly progression median values were used to compared between sleep phases within each recording, and between recording weeks within each subject. These comparisons respectively used a Wilcoxon signed-rank test and a Wilcoxon paired test.

4.4 Variability analysis of nocturnal tidal breathing in healthy children

This cross-sectional study, presented as P.IV, recruited 20 children who were clinically referred to a PSG study in the sleep laboratory at the Children's Hospital Srebrnjak (Croatia). The overnight measurement included a full PSG recording with video and a simultaneous IP and ECG measurement. For each IP recording, the variability of the TBFV profile was calculated between profiles in different sleep stages, between profiles in different sleep cycles of a sleep stage, between profiles in the same sleep cycle of a sleep stage, and between profiles before and after a body position change.

5 RESULTS

This chapter summarises the results of the four publications. Results for P.II, P.III, and P.IV, are grouped similarly to the literature summary (subsubsection 3.2.2.3 and subsubsection 3.2.3.3) to facilitate the discussion in section 6.1.

5.1 Improvement of the signal processing

Absolute Dss and relative r showed a significantly higher similarity in time-domain between PNT flow and IP flow derived by IP-NLPF than IP flow derived by IP-HRSG, for all methacholine test phases ($p < 0.01$). $\Delta P_{f_1-f_2}$ indicated that PNT and IP from IP-NLPF were similar in the low-frequency band but dissimilar at higher bands, probably due to noise in the PNT flow. In contrast, D_L remained significantly similar, or lower in the case of bronchodilator, for both processing methods. This suggests that IP-NLPF does not distort flow more than IP-HRSG. Figure 5.1 shows the results of the compared methods applied to one of the tested signals.
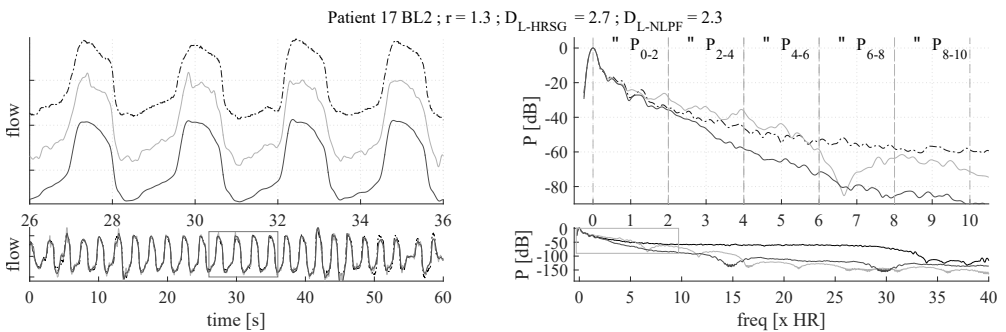
Figure 5.1   **Filter results comparison.** IP and PNT flow signals on the time (bottom-left) and frequency domains (bottom-right) for a representative 60s recording. Upper plots zoom a portion of the bottom plots indicated by a box. Dashed horizontal lines mark the six frequency bands used in the frequency analysis. Dashed dark line corresponds to the reference mouth PNT flow, solid grey to the output of IP-HRSG on IP, and solid dark to the output of IP-NLPF. Reproduced from P.I.

5.2 Shape analysis of nocturnal tidal breathing in wheezy infants

In wheezing infants, estimated REM and NREM sleep, and asthma risk affected the *early*, *middle*, and *late expiration* in TBFV profiles derived from overnight IP recordings differently. The most relevant observations in the TBFV profiles associated with airflow limitation and sleep stage are summarised next:
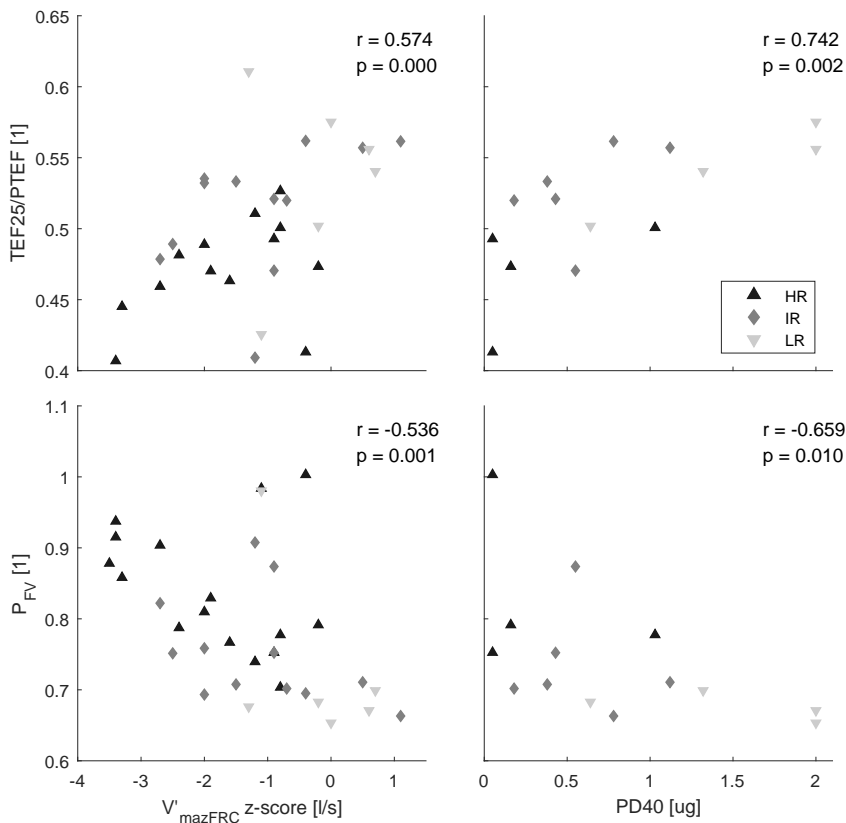

Figure 5.2 **Correlation between selected tidal expiration shape indices and lung function.** Indices TEF25/PTEF (upper plots) and P_{FV} (lower plots) correspond to the median values during all-night REM periods. $z\dot{V}_{maxFRC}$ (left plots) is the maximal flow at functional residual capacity (n=35). PD40 (right plots) is the dose of methacholine producing a 40% decrease in $z\dot{V}_{maxFRC}$ (n=14). Different shapes denote the risk group as high risk (HR), intermediary risk (IR), and low risk (LR). Spearman's rank correlation coefficient and its p-value indicated by r and p respectively. Reproduced from P.II.

Influence of airflow limitation

a. Higher asthma risk was associated with a decrease in the *early expiration* indices T_{PTEF}/T_E and V_{PTEF}/V_E during REM but not during NREM. This decrease was statistically significant between the LR and HR groups ($p = 0.018$ and $p = 0.009$ for T_{PTEF}/T_E and V_{PTEF}/V_E).

b. Higher asthma risk, airflow limitation, and hyperresponsiveness were associated with a decrease in the convexity of the *middle expiration* as measured by P_{FV}, TEF25/PTEF, and TEF50/PTEF. This decrease in convexity was more pronounced during REM, but also present during NREM. P_{FV} increased for both sleep phases, significantly for REM compared to IR ($p = 0.026$) and LR ($p = 0.033$), but for NREM only compared to IR ($p = 0.023$). TEF25/PTEF decreased significantly for REM compared to IR ($p = 0.012$) and LR ($p = 0.018$), but not for NREM. TEF50/PTEF decreased significantly only for REM compared to LR ($p = 0.021$) P_{FV} and TEF25/PTEF showed negative and positive correlations with $z\dot{V}_{maxFRC}$ and PD40 (Figure 5.2).

Influence of sleep

c. During REM, absolute values T_E and T_{PTEF} decreased when compared to NREM ($p < 0.05$). However, relative *early expiration* indices T_{PTEF}/T_E and V_{PTEF}/V_E remained similar during both sleep stages ($p > 0.05$). Except for the HR group which was likely to have been influenced by airflow limitation (**a.**).

d. *Middle expiration* indices P_{FV}, TEF25/PTEF and TEF50/PTEF remained similar during both sleep stages ($p > 0.05$), except for the HR group which was likely to have been influenced by airflow limitation (**b.**).

e. *Late expiration* index TEF05/PTEF was significantly lower during REM compared to NREM only for the LR group ($p = 0.021$).

f. Comparing this study with a previous study in almost the same group of patients during wakefulness shows a T_{PTEF}/T_E and V_{PTEF}/V_E decrease with sleep Malmberg et al. 2017.

5.3 Shape analysis of nocturnal tidal breathing in wheezy children

In wheezing children, estimated REM and NREM sleep, time from sleep onset, and exposure to treatment affected the *early*, *middle*, and *late expiration* in TBFV profiles derived from overnight IP recordings differently. Figure 5.3 presents the average hourly progression of NREM and REM values for four representative shape indices. The most relevant observation in the TBFV profiles associated with airflow limitation, sleep stage, and time from sleep onset are summarised next:

Influence of airflow limitation

a. Interruption of medication was associated with a decrease in the *early expiration* indices T_{PTEF}/T_E and V_{PTEF}/V_E. This decrease was significant during NREM and REM for V_{PTEF}/V_E ($p = 0.008$ and $p = 0.001$). Moreover, V_{PTEF}/V_E was significantly lower during NREM, for the whole night (Figure 5.3). Decrease in T_{PTEF}/T_E was significant only during NREM.

b. Interruption of medication was associated with a decrease in the convexity of the *middle expiration* as measured by P_{FV}, TEF50/PTEF, and TEF25/PTEF. Time from sleep onset analysis (Figure 5.3) shows that this decrease in convexity was more prominent during REM after 4 hours of sleep, although it was also significant during NREM.

c. Interruption of medication was associated with an earlier interruption of *late expiration* as suggested by the increase in TEF05/PTEF. This increase was more prominent during NREM and significant during the whole night.

Influence of sleep

d. *early expiration* remained similar during both sleep stages as measured by V_{PTEF}/V_E ($p > 0.05$). T_{PTEF}/T_E decreased during REM compared to NREM. However, we argued that this was due to changes in the *late expiration*.

e. *middle expiration* remained similar during both sleep stages as measured by P_{FV} ($p > 0.05$). TEF50/PTEF and TEF25/PTEF increased during REM compared
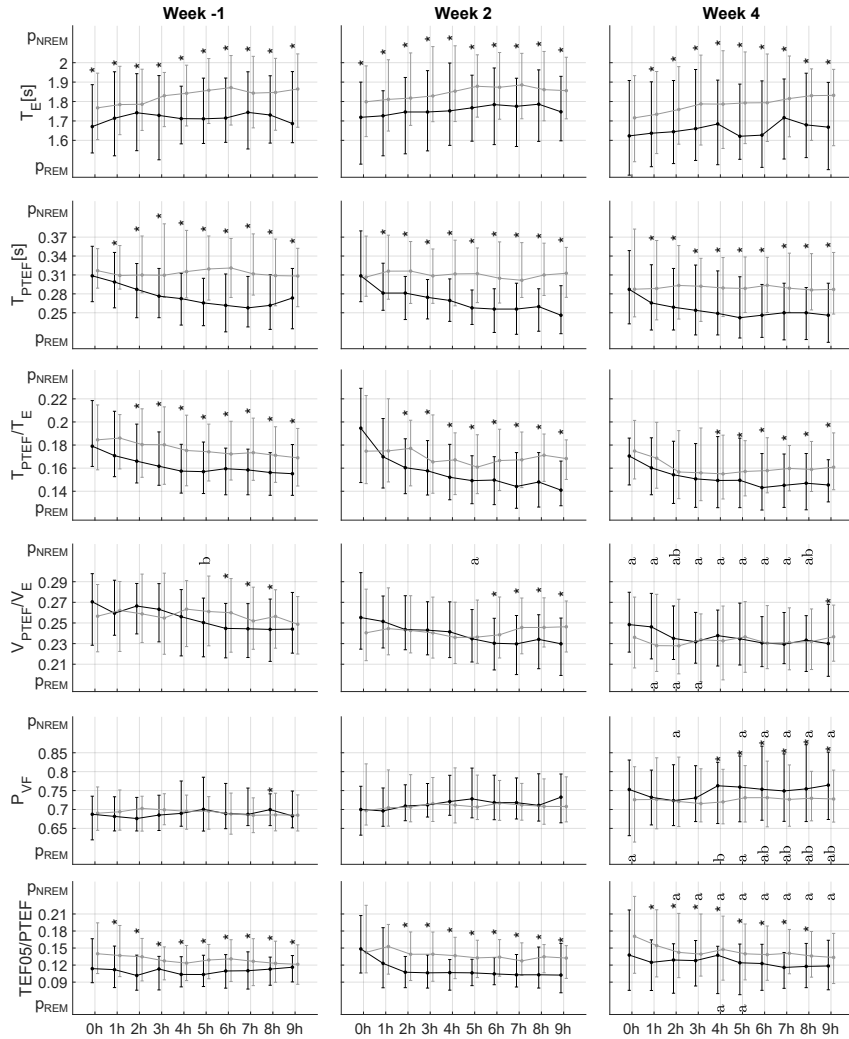
Figure 5.3 **Average hourly progression for selected indices grouped by recording week and sleep phase.** Each row of plots corresponds to a tidal expiration shape index and each column to a recording week. Within each plot, the x-axis marks the hours after sleep onset and the y-axis is the index value. Dots and whiskers indicate the median and the interquartile ranges of all patients at a given time for NREM (grey) and REM (black). *: significant difference ($p < 0.01$) between sleep stages; a: significant difference ($p < 0.05$) between Week -1 and Week 4; b: significant difference ($p < 0.05$) between Week 2 and Week 4. Letters on top of vertical lines for NREM (p_{NREM}) and letters on the bottom for REM (p_{REM}). Reproduced from P.III.

to NREM. However, we argued that this was due to an increase in PTEF. This similarity between sleep stages was broken during Week 4, four hours after sleep onset, likely due to airway obstruction.

f. *late expiration* was interrupted earlier during NREM than during REM, as suggested by the significantly higher in TEF05/PTEF. Moreover, Figure 5.3 suggest that this difference occurred during all night.

5.4 Variability analysis of nocturnal tidal breathing in healthy children

Variability in the TBFV shape not only differed between sleep stages, as previously described (**c.**), but these differences were larger when compared within and between sleep cycles of the same stage (Figure 5.4). Moreover, variability in the TBFV profiles was considerably higher in the early part than in the late part of expiration, as previously reported in V.-P. Seppä, Hult et al. 2019.

Influence of sleep

a. N3 stage presented the lowest variability of the night, in the the early expiation, when profiles were compared within the same sleep cycle. However, at the same time, the highest variability of the night occurred when profiles were compared between different N3 cycles. N2 stage presented similar results. Variability in the late expiration was higher during NREM than during REM and wake.

b. For REM, our results show that, despite the pronounced breath-to-breath variations in duration and amplitude, the normalised expiratory limb remains relatively similar within and between REM cycles.

c. Wake, unlike sleep, presented larger variability within the same cycle that between cycles. Nonetheless, this should be interpreted with care as the sample size was small.

d. Shape differences before and after a postural change were more pronounced during NREM than during REM and wake, especially for the later expiration.
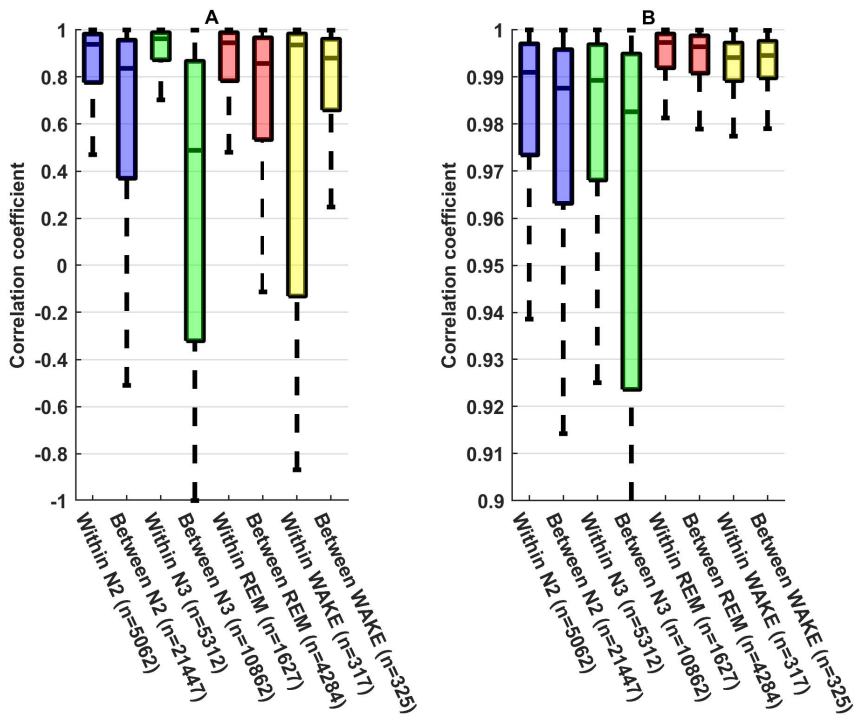
Figure 5.4 **Tidal breathing variability within and between sleep cycles of the same sleep stage.** Box-and-whiskers summarises the distribution of the Pearson correlation coefficients calculated between TBFV profiles. Each box-and-whisker groups the result from comparing these profiles falling in the same sleep cycle or those of the same sleep stages but falling in different sleep cycles within the same subject. Left and right plots correspond to variability the 15-45% and 55-85% exhaled volume ranges respectively. Reproduced from P.IV.

6 DISCUSSION

Previous works have empirically studied what changes in typically one non-respiratory factor, such as lower airway obstruction, sleep, or maturation causes a change in the respiratory indices (Table 3.1, Table 3.2). Similarly, the present thesis has empirically studied what changes when combining lower obstruction and sleep in infants and children causes a change in shape indices, as well as what changes in sleep in healthy children causes a change in variability indices.

The first section of this chapter discusses how, theoretically, these changes in non-respiratory factors translate into changes in the respiratory indices. We present the mechanisms explaining the connection between non-respiratory factors and indices. Some are novel, while others are summarised from the literature. Consequently, we examine these theoretical mechanisms under different scenarios combining one or more non-respiratory factors and compare them with the result from our studies and the literature. The two subsequent sections discuss the main limitations and possible improvements of IP technology for the assessment of lower airway obstruction. Lastly, specific limitations and improvements on the NLPF are described in more detailed in a separated section.

6.1 Interpretation of the tidal breathing indices

The diagram in Figure 6.1 summarises the pathway from lower airway obstruction to respiratory indices when using IP technology, and illustrates the many non-respiratory factors (in green), respiratory factors (in blue), and processing steps (in red) that influence this path. Hereafter, we define respiratory factors as those inherent to the respiratory process and the rendering of the breathing pattern. In contrast, non-respiratory factors are not necessary for respiration but may modify the breathing pattern by altering one or more of the respiratory factors.
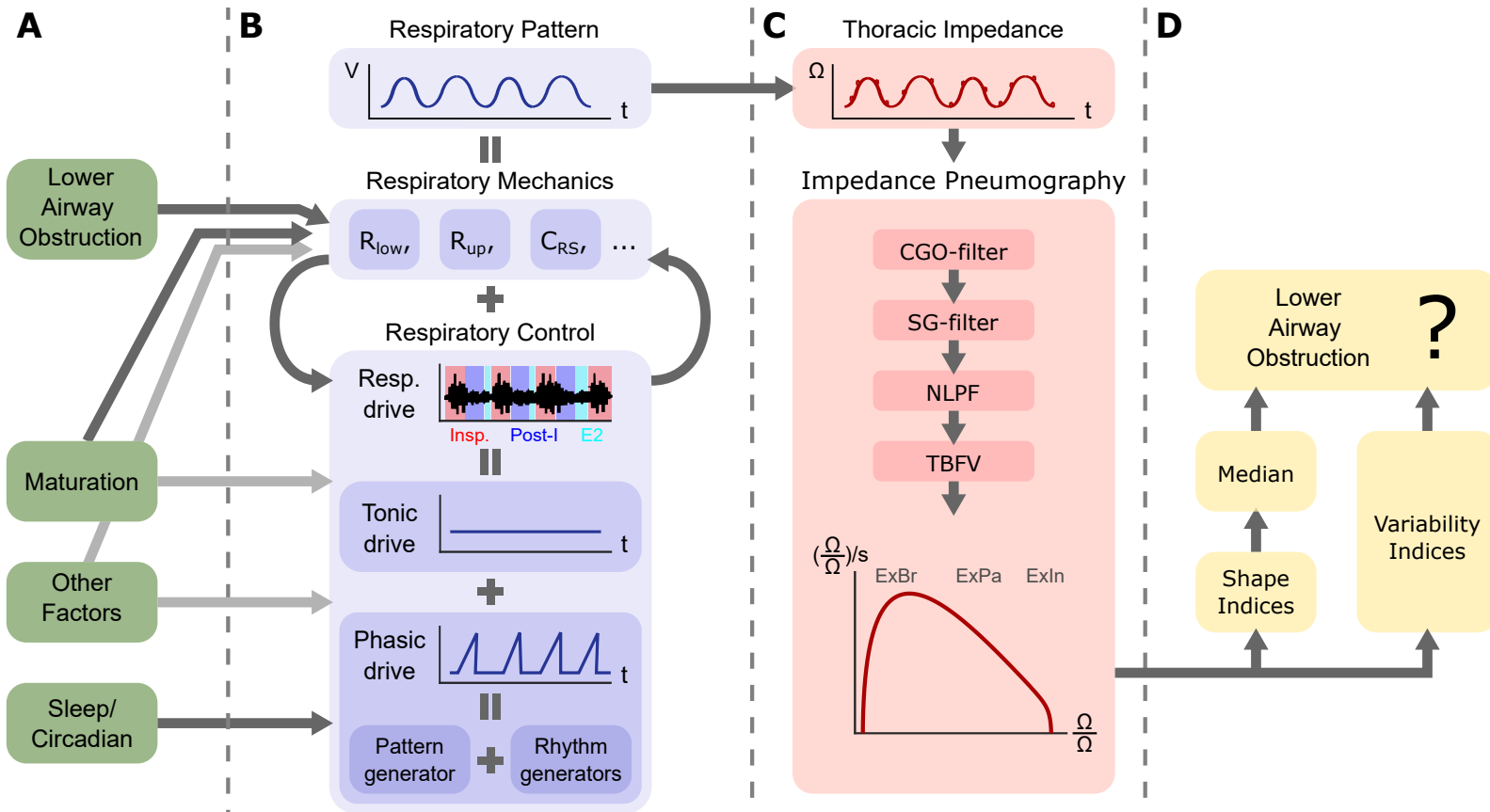
Figure 6.1 **Pathway from lower obstruction to respiratory indices derived from impedance pneumography (IP). A. Lower airway obstruction influences the respiratory factors:** An increase in lower airway obstruction directly raises the lower airway resistance. However, due to the feedback interaction between respiratory mechanics and respiratory control, a change in the lower airway resistance may also trigger changes in other respiratory factors. Moreover, sleep, maturation, and other non-respiratory factors, also influence this feedback loop, causing non-linear alterations in the breathing pattern (sections 3.1.3, 3.1.4, and 3.1.5). **B. Respiratory factors' influence in the tidal breathing indices:** The tidal breathing pattern is formed by the interaction of many mechanical, chemical, and neural respiratory factors. The rhythm and pattern generators originate the phasic drive stimuli which in combination with the tonic drive build the respiratory drive stimuli. The respiratory drive stimulates the respiratory musculature producing mechanical changes in the respiratory system. These active mechanical changes together with the passive mechanical characteristics of the respiratory system, such as airway resistance, ribcage compliance, etc., render the breathing pattern. All these respiratory factors have overlapping effects on the respiratory pattern. Hence, similar breathing patterns may originate under a dissimilar configuration of respiratory factors (sections 3.1.1 and 3.1.2). **C: The breathing pattern is recorded by IP:** Electrical impedance changes proportional to the respiratory pattern are recorded. These are processed to remove the cardiac component and derive the tidal breathing flow-volume loop (TBFV) profiles (section 3.3). **D. IP tidal flow is quantified into respiratory indices:** The different respiratory indices quantify different shape and variability properties of the TBFV profiles which putatively reflect changes caused by respiratory and non-respiratory factors (sections 3.2.2 and 3.2.3).

This diagram illustrates just how challenging the interpretation of the tidal breathing indices can be. Respiratory and non-respiratory factors interact with each other in non-linear ways. Moreover, their effects on the respiratory pattern often have overlap. Rather than jumping into the interpretation of our results, which combine the effects of multiple non-respiratory factors, we have decided to break this explanation down into simpler steps. Firstly, we explain the mechanisms by which respiratory factors reflect in different respiratory indices. Secondly, we describe how non-respiratory factors modify the respiratory factors and therefore reflect in the indices. For this second step we start with an scenario where only one non-respiratory factor is present and what happens when other non-respiratory factors are added. The results of these theoretical scenarios are then compared with the empirical results in our studies and the results in the literature.

6.1.1 Respiratory factors' influence in the tidal breathing indices

This subsection describes how the different respiratory indices quantify different features of the respiratory pattern, and therefore how they reflect different aspects of the respiratory factors. Different indices share similar mechanisms. For this reason, the explanation is divided into the following groups: *shape indices*, *variability of IBI*, and *variability of shape*. The mechanisms for *shape* and *variability of IBI* were partially mentioned in sections 3.2.2 and 3.2.2 but they are summarised here as they help to understand the latest group. The mechanisms behind the *variability of shape* indices are for the first time presented here with some ideas introduced in P.IV.

- *Shape indices:* Shape indices assess shape features averaged over several tidal expirations. Therefore, they reflect average mechanics and control characteristics over the studied period. The literature seems to agree that a less sharp *early expiration* with a later peak reflects a longer ExBr (Ent et al. 1998; Walraven et al. 2003). It is less clear, however, whether lower airway obstruction increases or decreases ExBr (subsection 3.1.5). *Middle expiration* is, at first, dominated by ExPa and, therefore, reflects the passive mechanical characteristics of the system. However, ExBr often extends well into this region (Shee, Ploy-Song-Sang and Milic-Emili 1985). A convex *middle expiration* is likely to be due to a prolonged ExBr. A concave *middle expiration* is probably the combination of a short ExBr and an increased in the volume-resistance coupling. An effect of airways hyperresponsiveness is the shortening of the distant airway's smooth muscle (An et al. 2007). This makes the airway's calibre more dependent on the lung volume, thus lowering airflow with expired volume at faster rates (Aliverti, Brusasco et al. 2002). *Late expiration* does not directly relate to obstruction, but obstruction-induced hyperinflation may cause an early ExIn (subsection 3.1.5). Because, sleep and maturation influence the control and the mechanics of breathing, both will produce average changes in the three regions of expiration.

- *Variability of IBI:* Indices assessing IBI reflect the variability in the respiratory drive, which is the same as the phasic drive except during REM. Mechanics may add a small discrepancy between IBI and the phasic drive, which is negligible. The literature hypothesises that obstruction decreases the adaptability of the system causing more regular IBIs, but it does not detail how this occurs. A possible explanation is that

increasing respiratory rate to maintain minute ventilation lowers the chance of having long breaths and thus IBIs became more self-similar (Fiamma, Straus et al. 2007). Nonetheless, many other non-respiratory factors affect the phasic drive, such as maturation, sleep, or neural disorders. Moreover, REM sleep causes the tonic drive to fluctuate, and therefore IBIs no longer reflect the phasic drive variations (Figure 3.3).

- *Variability of shape:* Indices assessing the variability of shape are a combination of the two previous factors. Rather than the phasic drive, these indices emphasise the breath-to-breath variations in the respiratory mechanics and the use of ExBr, ExPa, and ExIn. As with *variability of IBI*, the literature's vague explanation is that obstruction decreases the adaptability of the respiratory system causing a decrease in the variability. We, however, suggest a more concrete explanation. We believe that the variability in the TBFV profiles is affected by two elements, physical constraints on the flow-volume space and variations on the respiratory drive. As shown in Figures 3.5 and 6.2, in the flow-volume domain, the presence of lower obstruction reduces the space where breathing is possible. Narrower airways limit airflow at higher lung volumes. Lower muscle tone limits the space on the left side of the flow-volume domain, as breathing at a high volume becomes more difficult. Reducing the space in the flow-volume domain reduces the number of possible TBFV profiles. In the short-term, *variability of shape* may relate to the *variability of IBI*. Consecutive TBFV profiles vary if the respiratory drive varies. However, in the long term, a reduced number of possible profiles causes similar profiles to appear more often, thus decreasing the *variability of shape*. Similarly to *variability of IBI*, variations on the phasic or tonic drives will alter the short-term variability. Similarly to *shape analysis*, changes in mechanics and control reducing or increasing the valid flow-volume space will affect the long-term variability.

6.1.2 Non-respiratory factors' influence in the tidal breathing indices

The mechanisms described above are explored here under different scenarios combining multiple non-respiratory factors. Although this thesis has only studied the linear indices during obstruction and sleep and variability indices during sleep, here we also analyse other combinations of non-respiratory factors and indices.
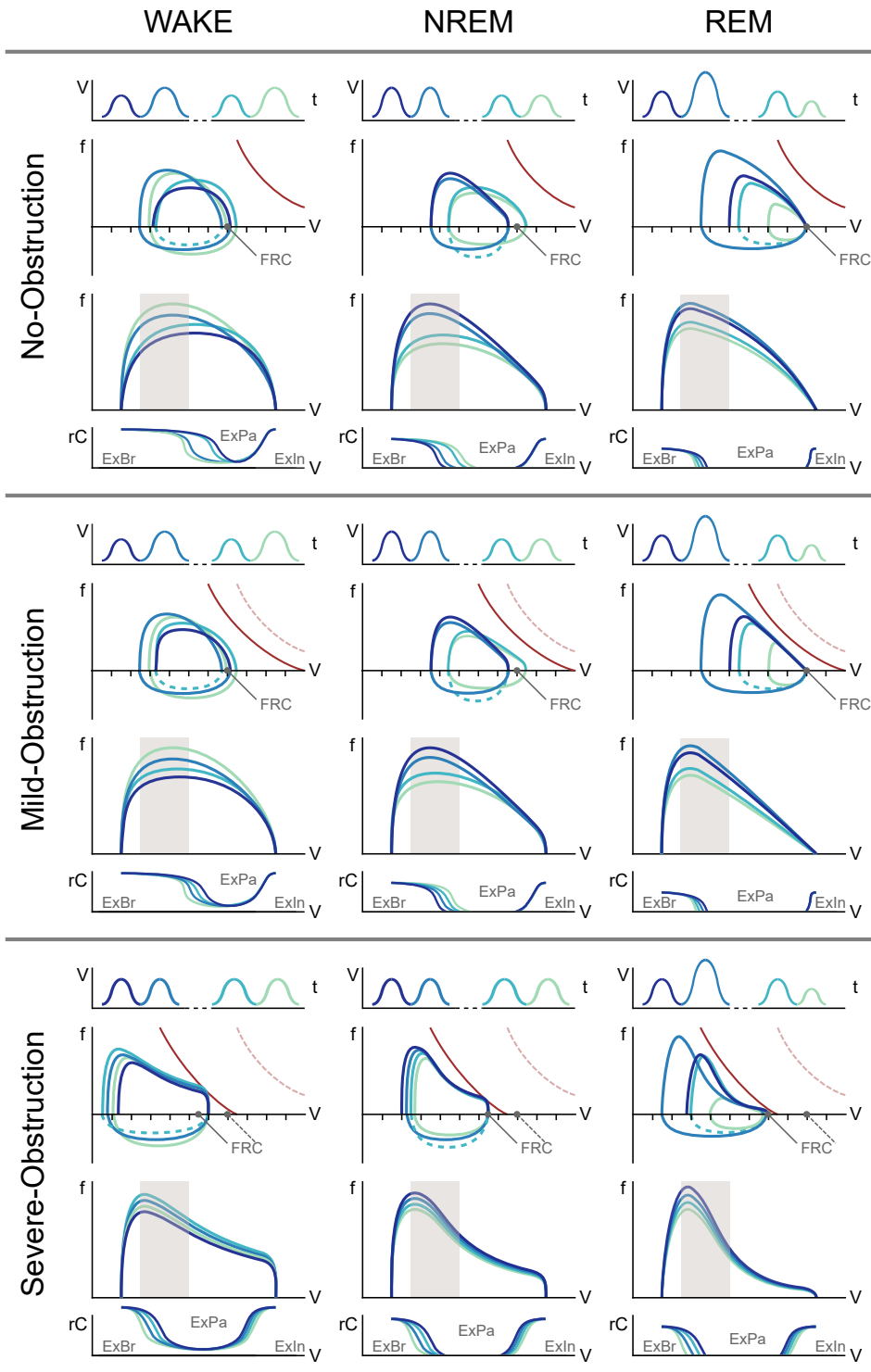
Figure 6.2 Changes in tidal breathing for obstruction degree and awareness state. Each obstruction degree vs. awareness state combination presents four different plots of the same two pairs of consecutive respiratory cycles. For NREM, the two pairs (separated by a dashed line) belong to different sleep cycles of the same stage. For WAKE and REM, they could belong to the same or different sleep cycles of the same stage. The cycles' decreasing hue indicates their order in time. The four plots from top to bottom: Volume-time plot illustrates the variability in IBI and tidal volume; In the flow-volume plot, forced partial expiration (red line) delimits the region of airflow limitation. Obstruction increases this region leading to an elevation of FRC (No-obstruction lines are dashed on the plots below for comparison); The normalised flow-volume plot illustrates the expiration profiles' shape and variability in the 15 % to 45 % range (grey box). Respiratory control-volume plot symbolises the strength and the duration of the stimulation of all the respiratory muscles. The overall strength decreases in NREM and REM but increases with obstruction to elevate FRC. Labels indicate the mechanical sub-phases of expiration, ExBr, ExPa, and ExIn.

This has a twofold purpose. First, understanding the effects of one non-respiratory factor on the indices helps us to understand the effects of two factors in combination. Second, showing that the abovementioned mechanisms also agree with other results in the literature increases their validity.

We start by describing how three different levels of obstruction may translate into the indices during awake patients. Consequently, this is repeated for two other awareness states, namely NREM sleep and REM sleep. This explanation is aided by the tidal breathing patterns illustrated in Figure 6.2. Lastly, we described how maturation and other factors may also influence the process. The theoretical effects in the indices are compared with the results in our studies, the results in the literature, otherwise left as a hypothesis.

WAKE Typically, during wakefulness, the tonic drive keeps a slightly elevated FRC and the phasic drive varies breath-by-breath adapting to metabolic demand. Expiration is generally controlled with a relatively short ExPa (subsection 3.1.1).

- **No obstruction:**

  - *Shape indices:* Typically, as most of the expiration is dominated by ExBr, profiles present a rounded *early expiration* and a convex *middle expiration* (item **a.** and **c.** in subsubsection 3.2.2.3).

  - *Variability of IBI:* Adaptation to metabolic demand is reflected as variable phasic drive and thus variables IBI and V_t (Raoufy et al. 2016).

– *Variability of shape:* A variable respiratory drive with no constraints in the flow-volume domain leads to variable profiles, as seen in the variability of shape indices (Frey, Silverman and Suki 2001) and the variability of profiles' shape (item **c.** in section 5.4).

- **Mild obstruction:** Mild obstruction reduces the valid space in the flow-volume domain, but there is still room for adaptation (Figure 3.5). Subjects may choose one, or combine both, of the two strategies mentioned in subsection 3.1.5. The ExBr-relaxation strategy maintains the same FRC and decreases ExBr to compensate for retardation in expiration added by the lower resistance. The hyperinflation strategy elevates the FRC to dilate the lower airway and increases ExBr to compensate for the recoiling force added by the elevated chest volume.

  – *Shape indices:* The hyperinflation strategy probably keeps the expiratory shape similar to that in no obstruction. In contrast, ExBr-relaxation strategy sifts the shape towards the characteristics of severe obstruction. Pellegrino and Brusasco 1997 suggest that balancing between these two strategies depends on the subject's physiology and pathophysiology rather than on the degree of obstruction. This subjectivity may explain the low correlations and the high overlap between groups on the studies assessing *early* and *middle expiration* indices (item **b.** and **d.** in subsubsection 3.2.2.3).

  – *Variability of IBI:* During wake, decrease in the variability of IBI and V_t (Raoufy et al. 2016; Teulier et al. 2013), may be explained by the changes in *variability of shape*, or the increase in respiratory rate.

  – *Variability of shape:* Likewise, choosing one strategy rules out a set of possible expiratory shapes, and thus decreases the variability of shape. However, subjects may still switch from one strategy to the other, or modulate how much of each strategy they use. Frey, Silverman and Suki 2001 showed a decrease in variability in the shape indices with increased obstruction.

- **Acute obstruction:** As obstruction increases the valid space in the flow-volume domain shrinks (Figure 3.5 C). This forces subjects to apply both of the compensatory strategies, hyperinflation and ExBr-relaxation. Subjects elevate the FRC to dilate the lower airway and decrease ExBr to avoid a slow expiration. This is probably achieved by an increase in muscle activity during inspiration and an early ExIn to avoid airway closure (MacBean et al. 2016; Morris, R. G. Madgwick, Frew et al. 1990).

- *Shape indices:* The short ExBr is reflected as a sharp *early expiration* with an early relative peak flow (short T_{PTEF}/T_E and V_{PTEF}/V_E) (item **a.** in subsubsection 3.2.2.3). The sort ExBr provides a large ExPa and the volume-resistance coupling causes a characteristic concave *middle expiration* (**c.** in subsubsection 3.2.2.3).

- *Variability of IBI:* During wake, decrease in the variability of IBI and V_t (Raoufy et al. 2016; Teulier et al. 2013), may be explained by the changes in *variability of shape*, or the increase in respiratory rate.

- *Variability of shape:* Modulating between strategies is tighter as both are utilised. With a lower room for manoeuvre, the expiratory shapes became more self-similar. This decreases further variability in shape and shape indices (Frey, Silverman and Suki 2001).

NREM   NREM sleep is characterised by a regular phasic drive and a decrease in the tonic drive. A reduced tonic drive decreases muscle contribution to respiration and lowers the FRC (subsection 3.1.3). A decrease in the FRC means that TBFV gets closer to the region of airflow limitation (red line in Figure 6.2).

- **No-obstruction:**

  - *Shape indices:* The decrease in tonic drive is likely to shorten the ExBr. A shorter ExBr leads to an earlier relative peak in the *early expiration* and a less convex *middle expiration*. These changes have been seen in sleep studies (item **e.** in subsubsection 3.2.2.3) and when comparing studies with matched groups (item **f.** in section 5.2).

  - *Variability analysis of IBIs:* The highly regular phasic drive characteristic of NREM sleep is reflected in the low variability of IBI. This is present in multiple studies (item **c.** in subsubsection 3.2.3.3).

  - *Variability analysis of shape:* The TBFV is closer to airflow limitation, but individuals still have a large space to adapt the breathing pattern. In the long term (between sleep cycles), the valid flow-volume space is large and allows for variability in shape similar to that in wake. However, in the short term (within sleep cycles), variability in shape is dominated by the regular phasic drive and, therefore, variability is the lowest of the whole night. (item **a.** in section 5.4).

- **Mild and acute obstruction:** The use of compensation strategies due to obstruction is presumably the same than during wake. However, during NREM, the effect of these strategies is added to the effects of lower muscle tone and low short-term variability.

    - *Shape indices:* During NREM, the *early expiration* is sharper and presents an earlier peak than during wake. The use of the ExBr-relaxation strategy makes *early expiration* even sharper but, like in wake, these changes are not linear with the degree of obstruction. This has been shown in children (item **a.** in section 5.3). Likewise, during NREM, *middle expiration* is less convex than during wake. The use of ExBr-relaxation strategy and the increase in the volume-resistance coupling make it even less convex, or turns it concave, and also these changes are not necessarily linear with obstruction. This is shown in children (item **b.** in section 5.3) and infants (item **b.** in section 5.2). The use of the hyperinflation strategy results in an increase of the ExIn in the *late expiration*. This can be seen in children (**c.** in 5.3) but not infants for the reasons described below in maturation.

    - *Variability of IBI:* Although there are no studies currently available, the behaviour may be similar than in *variability of shape*.

    - *Variability of shape:* In the short term (with sleep cycles), the regular phasic drive already causes a quite low variability of shape. Under such a regular stimulus, a further decrease in variability due to obstruction reducing the flow-volume space may not be noticeable. However, in the long term (between sleep cycles), reduced flow-volume space may contribute to decrease the full night variability (V.-P. Seppä, A. S. Pelkonen, Kotaniemi-Syrjänen, Viik et al. 2016)V.-P. Seppä, Paassilta et al. 2018.

REM   REM sleep is characterised by an irregular respiratory drive and a cease of the tonic drive. Muscle atony further lowers the muscle contribution to respiration and the FRC (subsection 3.1.3). A decrease in the FRC means that TBFV gets even closer to region of airflow limitation (red line in Figure 6.2).

- **No-obstruction:**

    - *Shape indices:* Due to muscle atony, most of the expiration is putatively passive (ExPa), with a short ExBr and ExIn. For this reason, we would expect a

sharper *early expiration* and a less concave *middle expiration* than in NREM. However, results suggest that they remain similar between sleep phases for infants (item **c.** in section 5.2) and children (item **d.** in section 5.3). This may be because breathing at a lower FRC lowers the thoracic recoil compensating for the decrease in ExBr. In the *late expiration*, the expected decrease in ExIn agrees with the results in infants (item **e.** in section 5.2) and children (item **f.** in section 5.3). Nonetheless, these should be interpreted with care as in P.II and P.III all subjects are diagnosed with wheeze. These observations assume that the subjects in the LR group and the Week -1 are close to healthy subjects.

– *Variability of IBI:* The tonic drive fluctuations alter the respiratory drive and are reflected in the high variability of IBI. This is present in multiple studies (item **c.** in subsubsection 3.2.3.3).

– *Variability of shape:* TBFV profiles get closer to the lower limit in flow-volume space. This reduces the valid flow-volume space, but the irregular respiratory drive causes large breath-to-breath variations. Compared to NREM, the decrease in flow-volume space leads to lower long-term variability in shape. However, in the short-term (within sleep cycles), variability in shape is dominated by the irregular respiratory drive and variability is higher than for NREM. (item **b.** in section 5.4).

- **Mild and acute obstruction:** The use of compensation strategies due to obstruction is presumably the same than during wake and NREM. However, during REM, due to the muscle atony, the hyperinflation strategy may be less effective and ExBr-relaxation strategy preferred.

  – *Shape indices:* As with in NREM, during REM, the use of the ExBr-relaxation strategy makes *early expiration* even sharper and with an earlier peak. This appears in children (item **a.** in section 5.3) and infants (**a.** in 5.3). Likewise, the use of ExBr-relaxation strategy and the increase in the volume-resistance coupling make the *middle expiration* less convex or turns it concave. This is shown in children (item **b.** in section 5.3) and infants (item **b.** in section 5.2). The hyperinflation strategy may be less effective during REM and, therefore, ExIn does not change significantly with obstruction in children (item **c.** in section 5.3) or infants (5.2). We hypothesise that as ExPa lasts longer during REM, *middle expiration* should be more sensitive to the effects of obstruction than wake

and NREM, and the opposite for *early expiration*. However, this presumption should be properly tested.

- *Variability of IBI:* Although there are no studies currently available, it may be difficult to detect a decrease in variability like for *variability of shape*.

- *Variability of shape:* In the short term (with sleep cycles), the irregular phasic drive causes a high variability of shape. Under such a regular stimulus, the effects of a reduced flow-volume space may not be noticeable. However, in the long term (between sleep cycles), reduced flow-volume space may contribute to decreasing the full night variability as seen in V.-P. Seppä, A. S. Pelkonen, Kotaniemi-Syrjänen, Viik et al. 2016V.-P. Seppä, Paassilta et al. 2018.

MATURATION Infants breathe at an elevated FRC. Therefore, their expiration is dominated by ExBr and ExIn, and ExPa is putatively shorter. In addition, the developing neural system leads to a variable respiratory drive. These effects overlap with the obstruction compensation strategies and sleep, thus challenging the assessment of obstruction.

- *Shape indices:* During wake, as ExBr and ExIn are already elevated, changes in the three parts of expiration caused by obstruction may go unnoticed. We believe that the degree of obstruction to force infants to resort to both compensation strategies is larger than in children. For this reason, studies fail to find a correlation between obstruction and shape indices under 12 months of age (item **g.** in subsubsection 3.2.2.3).

  During NREM, where the muscle tone is decreased but still present, the behaviour is similar than in wake. Obstruction does not significantly modify the shape indices in infants (item **a.** in section 5.2).

  During REM, muscle atony reduces the dominance of ExBr and ExIn. Then obstruction modifies the *early* and *middle expiration* indices in the same way as seen in children (item **a.** in section 5.2). However, ExIn still seems present, as it did not change significantly in our results (section 5.2).

- *Variability of IBI:* A higher variability in the respiratory drive in infants (item **d.** in subsubsection 3.2.3.3) may overlap with the other changes in variability due to obstruction and sleep, but again there are no studies on this.

- *Variability of shape:* In infants, the increased muscle control during expiration makes the shape of the TBFV profiles more variable (Hutten et al. 2010). This increased vari-

ability in shape may overlap with the other changes in variability due to obstruction and sleep, but there are no studies on this.

OTHER EFFECTS   In general, any effect that modifies any of the respiratory or non-respiratory factors may lead to non-linear changes in the respiratory pattern via the feedback interaction between control and mechanics (Figure 6.1). These include respiratory conditions other than lower obstruction, conditions of the nervous system, or even postural changes. These effects must be taken into account as they may overlap with obstruction changes or overwrite them completely.

- *Shape analysis:* Shape analysis may be sensitive to changes in the mechanical respiratory factors induced by other respiratory conditions. An example of this is the characteristic rectangular expiration shape associated with upper airway obstruction (item **h.** in subsubsection 3.2.2.3). Other respiratory restrictive diseases may also influence the shape by modifying the system compliance.

- *Variability of IBI:* Neural and chemical factors affecting the phasic drive are likely to be reflected in the variability of the IBI (item **f.** in subsubsection 3.2.3.3).

- *Variability of shape:* Variability of shape may be sensitive to both mechanics and phasic drive alterations in the short term. However, in the long term, variability seems to be dominated by the size of the valid space in the flow-volume domain. An example of this is the postural changes in item P.IV during NREM. A postural change may produce an immediate change from one shape to another shape within the possible profiles. However, despite local changes, a decrease in the number of possible profiles causes the issue that, in the long term, the profiles repeat, and therefore the variability is reduced (item **d.** in section 5.4).

6.2 Limitations of the method

The following points discuss the limitations of the presented method to assess lower airway obstruction. The main limitations lie on the analysis of tidal breathing. Although limitations in the use of IP technology and the analysis of nocturnal recordings are also presented.

Analysis of tidal breathing   Not only is the respiratory pattern the overlapping result of multiple respiratory factors, but these factors also interact with each other in non-linear

manners. Besides this, several non-respiratory factors influence these non-linear interactions. These multiple interacting factors make it practically impossible to know with precision the degree of obstruction by the sole interpretation of the tidal breathing pattern (J. H. Bates 1998).

Analysis of tidal breathing may not be able to replace the other obstruction assessment techniques. However, as it is easier to perform than the other methods, it may serve as a first-line analysis (Beydon et al. 2007). In the next section, we propose some improvements that may at least help to increase the certainty of the interpretation.

Variability indices   The variability indices, like the shape indices, present these limitations associated with the interpretation of the tidal breathing. In addition, some variability indices present limitations in the interpretation of the calculations.

Many of the *fractal* indices used on the early studies are sensitive to measurement noise and the non-stationarity properties of the physiological signals (Gao, Cao et al. 2007). Some of the latest indices have shown to work poorly for quasi-periodic signals like tidal flow (Gao, Hu et al. 2012). The first step in many *geometric*, *energetic*, and *informational* indices is to normalise the signal's standard deviation to make the result independent of the amplitude of the signal. However, the standard deviation of a flow signal not only depends on its amplitude but also its shape. A smooth sine-like flow has a larger SD than a flow signal with long expirations where samples concentrated around the abscissa. For this reason, some indices reflect the shape of the signals rather than their variability. This may explain some of the discrepancies seen in some studies (subsubsection 3.2.3.3 item **f.**).

Nocturnal analysis   In P.II and P.III, we used an indirect method to estimate the REM and NREM sleep stages. This method was a modification of than one presented by Isler et al. 2016, which shows a high agreement with polysomnography. However, the accuracy of the modified methods should as well be confirmed in a sleep study.

Impedance pneumography   The IP signal is an indirect estimation of mouth airflow. The agreement between IP and a reference PNT for the presented IP system has been proven high in publication P.I and in similar systems for infants and children (V.-P. Seppä, Hyttinen and Viik 2011; V.-P. Seppä, Hyttinen and Viik 2010). However, in the other publications, this agreement is assumed to remain during sleep.

The following factors associated with sleep could compromise this agreement. The pooling of blood in the lungs after sleep onset (Ballard, Pak and White 1991) could affect the cardiac

component of the IP signal. The increase in ECG variability during REM could compromise the performance of the CGO filter. The presences of PIRCM in small or obstructed infants during REM Gaultier et al. 1987 could modify the lungs' contribution of electrodes field.

6.3 Possible improvements

Mathematically speaking, trying to quantify lower airway obstruction based on a single index is an ill-posed problem (Hadamar 1902). The solution to the problem (the index value) is not unique to a set of initial conditions (respiratory and non-respiratory factors). Moreover, the solution does not change continuously with a change in the initial conditions. A technique to solve this type of problem is thought to be regularisation, which is simply the addition of more information to the problem. From this perspective, three groups of improvements are proposed, adding more indices, adding other physiological signals, and adding time information. These could be used alone or in combination.

Adding more indices   Rather than considering one index in isolation interpreting the combination of multiple indices may bring more information. In this direction, Leonhardt, Ahrens and Kecman 2010 have shown that, in infants, a support vector machine was able to classify several respiratory conditions based on multiple shape indices assessing the full shape of the TBFV profiles. Nonetheless, other researchers have found that shape indices are typically highly correlated and combining them adds little information (Schmalisch, R. R. Wauer et al. 2003). Shape and variability indices are hypothetically influenced by different mechanics (6.1). Therefore, combining these may provide more information than using them in isolation.

Adding other signals   Publications P.II and P.III, are initial approaches in this direction. They take into account the sleep stage to interpret the indices. The increase in amplitude of the rEMG signal has been related to induced obstruction (Maarsingh et al. 2004) and imposed load (MacBean et al. 2016), in children. In addition, trimming of the rEMG relative to mouth flow has been associated to chronic lung disease in newborns (Hutten et al. 2010). The rEMG could help to interpret the IP indices in two ways. On the time-domain, rEMG could be used to identify the region on the TBFV where passive exhale occurs and when ExIn starts. On the amplitude-domain, rEMG may be an indicator of hyperinflation.

If so, rEMG could distinguish the compensation strategy in use.

Another way to estimate the use of hyperinflation or the FRC could be by looking at the already available CGO signal. CGOs are known to decrease with the increase in total lung volume (V.-P. Seppä, Hyttinen and Viik 2011). Changes in the shape of the CGO could also be associated with transmural pressure due to an elevated FRC (Gracia, V.-P. Seppä and Viik 2015).

Adding time information Publications P.III and V.-P. Seppä, A. S. Pelkonen, Kotaniemi-Syrjänen, Viik et al. 2016 are initial approaches in this direction. They take into consideration the changes in lower obstruction associated with the early and late parts of the night.

Another time-related feature to explore could be assessing differences in short-term and long-term variability in the expiratory variability index (EVI)'s Pearson distance matrix, using RQA (Marwan et al. 2007).

6.4 Nonlinear projection filter

This section briefly describes the working principle of the NLPF to subsequently discuss the rationale on crossing the filter's configuration parameters. Moreover, a correction in the filter briefly mentioned in the publications is detailed here. Finally, some limitations and improvements in this method are mentioned.

As with many of the non-linear methods, NLPF operates in the phase-space. Hence the first step is to embed the IP flow signal into a phase-space by means of the time delays technique. Given the IP flow signal, sampled at τ_s intervals, $x_n = IP_{flow}(n\tau_s)$, $n = 1, ...N$ a delayed reconstruction in the m dimension is formed as $\mathbf{x}_n = [x_n, x_{n+\rho}, ..., x_{n+(m-1)\rho}]^T$ where ρ is an integer. The m coordinates of each point in $\mathbf{x}_n$ are samples from the time series separated by a delay time τ multiple of the sampling rate ($\tau = \rho\tau_s$). Therefore, each point in the m-dimensional space describes the shape of the time series within a window of length $\tau_w = (m-1)\tau$ moving at τ intervals. Consecutive points correspond to consecutive windows forming what is known as a phase-space trajectory (Kugiumtzis 1996). Areas of the time series similar in shape run close to each other in the phase space's trajectory.

The idea of the non-linear filter is, so to speak, to smooth the m-dimensional trajectory aided by the neighbouring regions in the phase space (Grassberger et al. 1993). In the case of the NLPF, introduced by Kantz, Schreiber et al. 1993, the time series is over-embedded in a

high dimension. This results in an unfolding of the noise around the main trajectory. For each point, the neighbouring points within a m-dimension sphere or radius rad are used to fit a lower dimension manifold $m_p < m$. Consequently, the original points are replaced by its projection on the fitted manifold. Finally, the filtered trajectory is reconstructed back into the time series. This process may be iterated i times.

6.4.1 On choosing the filter parameters

The next points discuss the rationale followed when choosing the NLPF parameters for the particular case of IP flow.

- *Downsampling rate τ_s*: Computing the manifold fit for each point is a demanding task. Decreasing the number of points by downsampling the flow signal lowers the computation demand. Since the SG-filter's cut-off-frequency falls around 21.5Hz (Schafer 2011), the IP flow signal could be decimated by a factor as low as 10 without losing information. Hence, the downsampling rate was set to τ_s = 25.6Hz.

- *Time window $\tau_w = (m - 1)\tau_s\rho$*: After fixing τ_s, τ_w can be chosen by setting the embedding dimension (m) and the embedding ratio ρ. Hegger, Kantz and Schreiber 1999 showed that a higher m leads to better noise averaging. They recommend to set ρ = 1 and choose a m that provides a τ_w of "reasonable length". What a "reasonable length" means for a quasi-periodic signal, such as IP flow, is better understood from the work of Kugiumtzis 1996. This describes the time window as the amount of information that is passed from the time series to each point in phase-space. A window much shorter than a cycle contains little information and therefore leads to points too close to each other and to the diagonal of the phase space. A window covering too many cycles contains too much information. A small displacement of one of these points by the NLPF will produce a great distortion of the signal. Moreover, a larger m increases computation.

  In publication P.I, m was set so that τ_w is around 1/15s. This value was fixed for all the recordings because they had similar respiratory rates. For publications P.II and P.III, however, m was adjusted for each of the 4-minute segments so that τ_w was 1/3 of the median of the IBIs in the segment.

- Radius rad: Neighbourhood radius was chosen to include the highest observed noise amplitude. This was around 30% of the signal's standard deviation. If the number of

neighbours was low, the defaults radius was extended to include at least of 20 samples.

- Projection dimension m_p: Lower projection dimension leads to larger changes on the signal. Putatively, a higher projection dimension needs additional iterations to achieve the same results. The lowest value was chosen $m_p = 2$.

- Iterations i: If the previous parameters are correctly chosen additional iterations soon converge to a stable solution. We found that $i > 3$ did not significantly improve the results.

6.4.2   Integrating volume from filtered flow

Publication P.I successfully tested the NLPF on the flow-related IP signal. However, in P.II the flow- and volume-related IP signals were needed. We discovered that when integrating the filtered IP flow back into volume introduced a low-frequency drift in the baseline of the signal. This error emerged from a tiny offset on the IP flow introduced by the NLPF. This offset is insignificant in the IP flow, but in the integration process, all the tiny deviations are added up, thus producing a significant drift on the volume signal.

We solved this problem by estimating the lower envelope of the IP volume before and after the filter and consequently adding their difference to the filtered IP volume. Estimation of the lower envelopes was made in three steps. First, the minimums at the expiration troughs were detected from a heavily band-pass filtered volume signal by means of a peak detector adjusted to the respiratory frequency. Second, time series made out of the detected troughs were smoothed using Matlab's "rlowess" method with five samples windows. Third, smoothed troughs were spline-interpolated to form the lower envelope.

6.4.3   Limitations and improvements

NLPF is a promising tool for biomedical signals as these are most often quasi-periodic. Nonetheless, the applications on the literature are primarily focused on the ECG signal either for noise reduction (Schreiber and D. T. Kaplan 1996a), artefacts rejection (Teixeira et al. 2006), separation of foetal ECG (Schreiber and D. T. Kaplan 1996b), or extraction of rEMG (Lu et al. 2009).

In the author's opinion, the main limitation of the NLPF method is that when the time series is embedded in the phase-space, the resulting trajectory has unequal sampled points. The high-frequency components of a time series, such as the beginning of expiratory flow

or the QRS complex, present widely spaced points in phase space. In contrast, the low-frequency regions, such as the respiratory pauses or the PR interval, points concentrate on the same area. This, unequally distribution of samples affects the performance of the NLPF. The sparse regions on the trajectory have fewer neighbours within the same *rad*, which may affect the manifold calculation. A solution for this could be to resample the trajectory to have equidistant samples in the phase-space before applying NLPF.

7 CONCLUSIONS

The following points present the conclusions for each of the partial aims (chapter 2). The subsequent paragraph presents the conclusions on the general aim of the thesis: the use of IP for the assessment of lower airway obstruction based on nocturnal tidal breathing.

- A NLPF applied to IP lowers the noise while maintaining the linearity with mount airflow. This benefits long-term IP recordings where visual selection of valid TBFV profiles is not feasible (P.I).

- In infants with a high risk of asthma compared to low risk, TBFV profiles determined from overnight IP recordings show a lower volume at exhalation peak flow during REM and a less convex middle expiration during NREM and REM.

- In children off-medication compared to on-medication, TBFV profiles determined from overnight IP recordings show a lower volume at exhalation peak flow, an earlier interruption of expiration, and a less convex middle expiration. In the last of these, changes are larger during REM after 4 h of sleep. In the firsts, changes are larger during NREM.

- In healthy children, TBFV profiles determined from overnight IP recordings show a less variable *early expiration* between cycles of REM than NREM sleep. However, within individual sleep cycles, TBFV curves during N3 are the least variable.

IP technology is an excellent tool for the recording of nocturnal TBFV profiles in infants and children. The IP system is easy to use at home on a regular bases. However, assessing lower airway obstruction from tidal breathing is still challenging. The shape and the variability of nocturnal TBFV profiles do change with lower airway obstruction but these changes are not necessarily linear to the degree of obstruction. Moreover, these changes are influenced by the subject's choice of compensation strategy, time from sleep onset, sleep stage, and maturation. We believe that, currently, tidal breathing analysis serves to estimate, but not to quantify, lower airway obstruction, and that IP technology holds great potential

as a first-line assessment method and for the frequent monitoring of patients. Nonetheless, future improvements in signal processing and the understanding of the tidal airflow signal can easily increase the accuracy of the method and find new applications.

REFERENCES

Agostoni, E. (1959). Volume-Pressure Relationships of the Thorax and Lung in the New-born. *Journal of Applied Physiology* 14.6, 909–913. DOI: 10.1152/jappl.1959.14.6.909.

Albisser, A. M. and Carmichael, A. B. (1974). Factors in Impedance Pneumography. en. *Medical and biological engineering* 12.5, 599–605. DOI: 10.1007/BF02477221.

Aliverti, A., Cala, S. J., Duranti, R., Ferrigno, G., Kenyon, C. M., Pedotti, A., Scano, G., Sliwinski, P., Macklem, P. T. and Yan, S. (1997). Human Respiratory Muscle Actions and Control during Exercise. *Journal of Applied Physiology* 83.4, 1256–1269. DOI: 10.1152/jappl.1997.83.4.1256.

Aliverti, A., Brusasco, V., Macklem, P. T. and Pedotti, A., eds. (2002). *Mechanics of Breathing: Pathophysiology, Diagnosis and Treatment*. en. Mailand: Springer-Verlag. DOI: 10.1007/978-88-470-2916-3.

Allison, R. D., Holmes, E. L. and Nyboer, J. (1964). Volumetric Dynamics of Respiration as Measured by Electrical Impedance Plethysmography. *Journal of Applied Physiology* 19.1, 166–173. DOI: 10.1152/jappl.1964.19.1.166.

An, S. S., Bai, T. R., Bates, J. H. T., Black, J. L., Brown, R. H., Brusasco, V., Chitano, P., Deng, L., Dowell, M., Eidelman, D. H., Fabry, B., Fairbank, N. J., Ford, L. E., Fredberg, J. J., Gerthoffer, W. T., Gilbert, S. H., Gosens, R., Gunst, S. J., Halayko, A. J., Ingram, R. H., Irvin, C. G., James, A. L., Janssen, L. J., King, G. G., Knight, D. A., Lauzon, A. M., Lakser, O. J., Ludwig, M. S., Lutchen, K. R., Maksym, G. N., Martin, J. G., Mauad, T., McParland, B. E., Mijailovich, S. M., Mitchell, H. W., Mitchell, R. W., Mitzner, W., Murphy, T. M., Paré, P. D., Pellegrino, R., Sanderson, M. J., Schellenberg, R. R., Seow, C. Y., Silveira, P. S. P., Smith, P. G., Solway, J., Stephens, N. L., Sterk, P. J., Stewart, A. G., Tang, D. D., Tepper, R. S., Tran, T. and Wang, L. (2007). Airway Smooth Muscle Dynamics: A Common Pathway of Airway Obstruction in Asthma. en. *European Respiratory Journal* 29.5, 834–860. DOI: 10.1183/09031936.00112606.

Aston, H., Clarke, J. and Silverman, M. (1994). Are Tidal Breathing Indices Useful in Infant Bronchial Challenge Tests?: *Pediatric pulmonology* 17.4, 225–230.

Atzler, E. and Lehmann, G. (1932). Über ein neues Verfahren zur Darstellung der Herztätigkeit (Dielektrographie). de. *Arbeitsphysiologie* 5.6, 636–680. DOI: 10.1007/BF02008706.

Baker, L. and Geddes, L. (1966). Transthoracic Current Paths in Impedance Spirometry. *Proc. Symp. Biomed. Eng*. Vol. 1, 181–186.

Baldwin, D. N., Pillow, J. J., Stocks, J. and Frey, U. (2006). Lung-Function Tests in Neonates and Infants with Chronic Lung Disease: Tidal Breathing and Respiratory Control. en. *Pediatric Pulmonology* 41.5, 391–419. DOI: 10.1002/ppul.20400.

Ballard, R. D., Irvin, C. G., Martin, R. J., Pak, J., Pandey, R. and White, D. P. (1990). Influence of Sleep on Lung Volume in Asthmatic Patients and Normal Subjects. en. *Journal of Applied Physiology* 68.5, 2034–2041.

Ballard, R. D. (1999). Sleep, Respiratory Physiology, and Nocturnal Asthma. *Chronobiology international* 16.5, 565–580.

Ballard, R. D., Pak, J. and White, D. P. (1991). Influence of Posture and Sustained Loss of Lung Volume on Pulmonary Function in Awake Asthmatic Subjects. *American Review of Respiratory Disease* 144.3_pt_1, 499–503. DOI: 10.1164/ajrccm/144.3_Pt_1.499.

Banovcin, P., Seidenberg, J. and Der Hardt, H. V. (1995). Assessment of Tidal Breathing Patterns for Monitoring of Bronchial Obstruction in Infants. en. *Pediatric Research* 38.2, 218–220. DOI: 10.1203/00006450-199508000-00014.

Bashan, A., Bartsch, R., Kantelhardt, J. W. and Havlin, S. (2008). Comparison of Detrending Methods for Fluctuation Analysis. *Physica A: Statistical Mechanics and its Applications* 387.21, 5080–5090. DOI: 10.1016/j.physa.2008.04.023.

Bates, J. H. (1998). Detecting Airways Obstruction from the Tidal Flow Profile. en. *European Respiratory Journal* 12.5, 1008–1009.

Bates, J. H., Schmalisch, G., Filbrun, D. and Stocks, J. (2000). Tidal Breath Analysis for Infant Pulmonary Function Testing. ERS/ATS Task Force on Standards for Infant Respiratory Function Testing. European Respiratory Society/American Thoracic Society. en. *European Respiratory Journal* 16.6, 1180–1192.

Bates, J. H., Irvin, C. G., Farré, R. and Hantos, Z. (2011). Oscillation Mechanics of the Respiratory System. en. *Comprehensive Physiology*. Ed. by R. Terjung. Hoboken, NJ, USA: John Wiley & Sons, Inc. DOI: 10.1002/cphy.c100058.

Bellia, V., Cuttitta, G., Insalaco, G., Visconti, A. and Bonsignore, G. (1989). Relationship of Nocturnal Bronchoconstriction to Sleep Stages. *American Review of Respiratory Disease* 140.2, 363–367. DOI: 10.1164/ajrccm/140.2.363.

Benoist, M. R., Brouard, J. J., Rufin, P., Delacourt, C., Waernessyckle, S. and Scheinmann, P. (1994). Ability of New Lung Function Tests to Assess Methacholine-Induced Airway Obstruction in Infants. en. *Pediatric Pulmonology* 18.5, 308–316. DOI: 10.1002/ppul.1950180508.

Berger, A. (1977). Regulation of Respiration. *N Engl J Med* 297, 194–201.

Beydon, N., Davis, S. D., Lombardi, E., Allen, J. L., Arets, H. G. M., Aurora, P., Bisgaard, H., Davis, G. M., Ducharme, F. M., Eigen, H., Gappa, M., Gaultier, C., Gustafsson, P. M., Hall, G. L., Hantos, Z., Healy, M. J. R., Jones, M. H., Klug, B., Lodrup Carlsen, K. C., McKenzie, S. A., Marchal, F., Mayer, O. H., Merkus, P. J. F. M., Morris, M. G., Oostveen, E., Pillow, J. J., Seddon, P. C., Silverman, M., Sly, P. D., Stocks, J., Tepper, R. S., Vilozni, D., Wilson, N. M. and on behalf of the American Thoracic Society/European Respiratory Society Working Group on Infant and Young Children Pulmonary Function Testing (2007). An Official American Thoracic Society/European Respiratory Society Statement: Pulmonary Function Testing in Preschool Children. *American Journal of Respiratory and Critical Care Medicine* 175.12, 1304–1345. DOI: 10.1164/rccm.200605-642ST.

Bisgaard, H. and Nielsen, K. G. (2005). Plethysmographic Measurements of Specific Airway Resistance in Young Children. eng. *Chest* 128.1, 355–362. DOI: 10.1378/chest.128.1.355.

Bohadana, A. B., Hannhart, B. and Teculescu, D. B. (2002). Nocturnal Worsening of Asthma and Sleep-Disordered Breathing. en. *Journal of Asthma* 39.2, 85–100. DOI: 10.1081/JAS-120002190.

Brancatisano, T. P., Dodd, D. S. and Engel, L. A. (1984). Respiratory Activity of Posterior Cricoarytenoid Muscle and Vocal Cords in Humans. eng. *Journal of Applied Physiology: Respiratory, Environmental and Exercise Physiology* 57.4, 1143–1149. DOI: 10.1152/jappl.1984.57.4.1143.

Brandsma, C.-A., Vries, M. de, Costa, R., Woldhuis, R. R., Königshoff, M. and Timens, W. (2017). Lung Ageing and COPD: Is There a Role for Ageing in Abnormal Tissue Repair? en. *European Respiratory Review* 26.146, 170073. DOI: 10.1183/16000617.0073-2017.

Bravi, A., Longtin, A. and Seely, A. J. (2011). Review and Classification of Variability Analysis Techniques with Clinical Applications. *Biomedical engineering online* 10.1, 90.

Brennan, M., Palaniswami, M. and Kamen, P. (2001). Do Existing Measures of Poincare Plot Geometry Reflect Nonlinear Features of Heart Rate Variability?: *IEEE Transactions on Biomedical Engineering* 48.11, 1342–1347. DOI: 10.1109/10.959330.

Brown, B. H., Wilson, A. J. and Bertemes-Filho, P. (2000). Bipolar and Tetrapolar Transfer Impedance Measurements from Volume Conductor. en. *Electronics Letters* 36.25, 2060–2062. DOI: 10.1049/el:20001439.

Brusasco, V. and Pellegrino, R. (2003). Invited Review: Complexity of Factors Modulating Airway Narrowing in Vivo: Relevance to Assessment of Airway Hyperresponsiveness. en. *Journal of Applied Physiology* 95.3, 1305–1313. DOI: 10.1152/japplphysiol.00001.2003.

Burioka, N., Cornélissen, G., Halberg, F., Kaplan, D. T., Suyama, H., Sako, T. and Shimizu, E. (2003). APproximate Entropy of Human Respiratory Movement during Eye-Closed Waking and Different Sleep Stages*. *CHEST Journal* 123.1, 80–86. DOI: 10.1378/chest.123.1.80.

Butler, J., Caro, C., Alcala, R. and Dubois, A. (1960). Physiological Factors Affecting Airway Resistance in Normal Subjects and in Patients with Obstructive Respiratory Disease. eng. *The Journal of clinical investigation* 39.4, 584–591. DOI: 10.1172/JCI104071.

Carlsen, K. H. and Carlsen, K. L. (1994). Tidal Breathing Analysis and Response to Salbutamol in Awake Young Children with and without Asthma. en. *European Respiratory Journal* 7.12, 2154–2159.

Carlsen, K. C. L., Pettersen, M. and Carlsen, K.-H. (2004). Is Bronchodilator Response in 2-Yr-Old Children Associated with Asthma Risk Factors? en. *Pediatric Allergy and Immunology* 15.4, 323–330. DOI: 10.1111/j.1399-3038.2004.00147.x.

Carlsen, K. L., Magnus, P. and Carlsen, K. H. (1994). Lung Function by Tidal Breathing in Awake Healthy Newborn Infants. en. *European Respiratory Journal* 7.9, 1660–1668.

Carroll, J. L. and Donnelly, D. F. (2013). Respiratory Physiology and Pathophysiology During Sleep. *Principles and Practice of Pediatric Sleep Medicine*. Elsevier Saunders, 179–192.

Catterall, J. R., Rhind, G. B., Stewart, I. C., Whyte, K. F., Shapiro, C. M. and Douglas, N. J. (1986). Effect of Sleep Deprivation on Overnight Bronchoconstriction in Nocturnal Asthma. en. *Thorax* 41.9, 676–680. DOI: 10.1136/thx.41.9.676.

Celli, B., MacNee, W., Agusti, A., Anzueto, A., Berg, B., Buist, A., Calverley, P., Chavannes, N., Dillard, T., Fahy, B., Fein, A., Heffner, J., Lareau, S., Meek, P., Martinez, F., McNicholas, W., Muris, J., Austegard, E., Pauwels, R., Rennard, S., Rossi, A., Siafakas, N., Tiep, B., Vestbo, J., Wouters, E. and ZuWallack, R. (2004). Standards for the Diagnosis and Treatment of Patients with COPD: A Summary of the ATS/ERS Position Paper. en. *European Respiratory Journal* 23.6, 932–946. DOI: 10.1183/09031936.04.00014304.

Chase, M. H. and Morales, F. R. (2005). Chapter 12 - Control of Motoneurons during Sleep. *Principles and Practice of Sleep Medicine (Fourth Edition)*. Ed. by M. H. Kryger, T. Roth and W. C. Dement. Philadelphia: W.B. Saunders, 154–168. DOI: 10.1016/B0-72-160797-7/50019-7.

Citterio, G., Agostoni, E., Del Santo, A. and Marazzini, L. (1981). Decay of Inspiratory Muscle Activity in Chronic Airway Obstruction. *Journal of Applied Physiology* 51.6, 1388–1397. DOI: 10.1152/jappl.1981.51.6.1388.

Clarke, J. R., Aston, H. and Silverman, M. (1994). Evaluation of a Tidal Expiratory Flow Index in Healthy and Diseased Infants. eng. *Pediatric Pulmonology* 17.5, 285–290. DOI: 10.1002/ppul.1950170504.

Colin, A., Wohl, M., Mead, J., Ratjen, F., Glass, G. and Stark, A. (1989). Transition from Dynamically Maintained to Relaxed End-Expiratory Volume in Human Infants. *Journal of Applied Physiology* 67.5, 2107–2111.

Collett, P. W., Brancatisano, T. and Engel, L. A. (1983). Changes in the Glottic Aperture during Bronchial Asthma. eng. *The American review of respiratory disease* 128.4, 719–723. DOI: 10.1164/arrd.1983.128.4.719.

Costa, E. L. V., Gonzalez Lima, R. and Amato, M. B. P. (2009). Electrical Impedance Tomography. en. *Yearbook of Intensive Care and Emergency Medicine*. Ed. by J.-L. Vincent. Yearbook of Intensive Care and Emergency Medicine. Berlin, Heidelberg: Springer, 394–404. DOI: 10.1007/978-3-540-92276-6_38.

Costa, M., Goldberger, A. L. and Peng, C.-K. (2005). Multiscale Entropy Analysis of Biological Signals. *Physical Review E* 71.2, 021906. DOI: 10.1103/PhysRevE.71.021906.

Coveney, P. V. and Fowler, P. W. (2005). Modelling Biological Complexity: A Physical Scientist's Perspective. *Journal of the Royal Society Interface* 2.4, 267–280. DOI: 10.1098/rsif.2005.0045.

Cunningham, D. J. C. (1973). The Control System Regulating Breathing in Man. en. *Quarterly Reviews of Biophysics* 6.4, 433–483. DOI: `10.1017/S003358350000158X`.

Cutrera, R., Filtchev, S. I., Merolla, R., Willim, G., Haluszka, J. and Ronchetti, R. (1991). Analysis of Expiratory Pattern for Monitoring Bronchial Obstruction in School-Age Children. en. *Pediatric Pulmonology* 10.1, 6–10. DOI: `10.1002/ppul.1950100103`.

Cybulski, G. (2011). Ambulatory Impedance Cardiography. *Ambulatory Impedance Cardiography*. Vol. 76. Berlin, Heidelberg: Springer Berlin Heidelberg, 39–56.

Czovek, D. (2019). Pulmonary Function Tests in Infants and Children. en. *Kendig's Disorders of the Respiratory Tract in Children*. Elsevier, 174–211.

Dames, K. K., Lopes, A. J. and de Melo, P. L. (2014). Airflow Pattern Complexity during Resting Breathing in Patients with COPD: Effect of Airway Obstruction. *Respiratory Physiology & Neurobiology* 192, 39–47. DOI: `10.1016/j.resp.2013.12.004`.

Del Negro, C. A., Funk, G. D. and Feldman, J. L. (2018). Breathing Matters. en. *Nature Reviews Neuroscience* 19.6, 351–367. DOI: `10.1038/s41583-018-0003-6`.

Dellacà, R. L., Aliverti, A., Lutchen, K. R. and Pedotti, A. (2003). Spatial Distribution of Human Respiratory System Transfer Impedance. en. *Annals of Biomedical Engineering* 31.2, 121–131. DOI: `10.1114/1.1541012`.

Dezateux, C. A., Stocks, J., Dundas, I., Jackson, E. A. and Fletcher, M. E. (1994). The Relationship between tPTEF:tE and Specific Airway Conductance in Infancy. en. *Pediatric Pulmonology* 18.5, 299–307. DOI: `10.1002/ppul.1950180507`.

Dolfin, T., Duffty, P., Wilkes, D., England, S. and Bryan, H. (1983). Effects of a Face Mask and Pneumotachograph on Breathing in Sleeping Infants. *American Review of Respiratory Disease* 128.6, 977–979. DOI: `10.1164/arrd.1983.128.6.977`.

Douglas, N. J., White, D. P., Pickett, C. K., Weil, J. V. and Zwillich, C. W. (1982). Respiration during Sleep in Normal Man. eng. *Thorax* 37.11, 840–844.

Durrington, H. J., Farrow, S. N., Loudon, A. S. and Ray, D. W. (2014). The Circadian Clock and Asthma. en. *Thorax* 69.1, 90–92. DOI: `10.1136/thoraxjnl-2013-203482`.

Eichenwald, E. C., Ungarelli, R. A. and Stark, A. R. (1993). Hypercapnia Increases Expiratory Braking in Preterm Infants. *Journal of Applied Physiology* 75.6, 2665–2670. DOI: `10.1152/jappl.1993.75.6.2665`.

Emralino, F. and Steele, A. M. (1997). Effects of Technique and Analytic Conditions on Tidal Breathing Flow Volume Loops in Term Neonates. en. *Pediatric Pulmonology* 24.2, 86–92. DOI: `10.1002/(SICI)1099-0496(199708)24:2<86::AID-PPUL3>3.0.CO;2-G`.

England, S. J., Ho, V. and Zamel, N. (1985). Laryngeal Constriction in Normal Humans during Experimentally Induced Bronchoconstriction. *Journal of Applied Physiology* 58.2, 352–356. DOI: 10.1152/jappl.1985.58.2.352.

Ent, C. van der, Grinten, C. van der, Meessen, N. E., Luijendijk, S. C., Mulder, P. G. and Bogaard, J. M. (1998). Time to Peak Tidal Expiratory Flow and the Neuromuscular Control of Expiration. en. *European Respiratory Journal* 12.3, 646–652.

Feldman, J. L., McCrimmon, D. R. and Morrison, S. F. (2013). Chapter 35 - Neural Control of Respiratory and Cardiovascular Functions. *Fundamental Neuroscience (Fourth Edition)*. Ed. by L. R. Squire, D. Berg, F. E. Bloom, S. du Lac, A. Ghosh and N. C. Spitzer. San Diego: Academic Press, 749–766. DOI: 10.1016/B978-0-12-385870-2.00035-4.

Ferris, B. G. and Pollard, D. S. (1960). Effect of Deep and Quiet Breathing on Pulmonary Compliance in Man. en. *The Journal of clinical investigation* 39.1, 143–149.

Fiamma, M.-N., Samara, Z., Baconnier, P., Similowski, T. and Straus, C. (2007). Respiratory Inductive Plethysmography to Assess Respiratory Variability and Complexity in Humans. *Respiratory Physiology & Neurobiology* 156.2, 234–239. DOI: 10.1016/j.resp.2006.12.001.

Fiamma, M.-N., Straus, C., Thibault, S., Wysocki, M., Baconnier, P. and Similowski, T. (2007). Effects of Hypercapnia and Hypocapnia on Ventilatory Variability and the Chaotic Dynamics of Ventilatory Flow in Humans. eng. *American Journal of Physiology. Regulatory, Integrative and Comparative Physiology* 292.5, R1985–1993. DOI: 10.1152/ajpregu.00792.2006.

Filippone, M., Narne, S., Pettenazzo, A., Zacchello, F. and Baraldi, E. (2000). Functional Approach to Infants and Young Children with Noisy Breathing: Validation of Pneumotachography by Blinded Comparison with Bronchoscopy. en. *American Journal of Respiratory and Critical Care Medicine* 162.5, 1795–1800. DOI: 10.1164/ajrccm.162.5.9912008.

Fleming, P. J., Levine, M. R. and Goncalves, A. (1982). Changes in Respiratory Pattern Resulting from the Use of a Facemask to Record Respiration in Newborn Infants. en. *Pediatric Research* 16.12, 1031–1034. DOI: 10.1203/00006450-198212000-00013.

Fleming, S., Thompson, M., Stevens, R., Heneghan, C., Plüddemann, A., Maconochie, I., Tarassenko, L. and Mant, D. (2011). Normal Ranges of Heart Rate and Respiratory Rate in Children from Birth to 18 Years of Age: A Systematic Review of Observational Studies. *The Lancet* 377.9770, 1011–1018. DOI: 10.1016/S0140-6736(10)62226-X.

Frey, U., Maksym, G. and Suki, B. (2011). Temporal Complexity in Clinical Manifestations of Lung Disease. en. *Journal of Applied Physiology* 110.6, 1723–1731. DOI: 10.1152/japplphysiol.01297.2010.

Frey, U., Silverman, M. and Suki, B. (2001). Analysis of the Harmonic Content of the Tidal Flow Waveforms in Infants. en. *Journal of Applied Physiology* 91.4, 1687–1693.

Fry, D. L., Ebert, R. V., Stead, W. W. and Brown, C. C. (1954). The Mechanics of Pulmonary Ventilation in Normal Subjects and in Patients with Emphysema. en. *The American Journal of Medicine* 16.1, 80–97. DOI: 10.1016/0002-9343(54)90325-3.

Gaffin, J. M., Shotola, N. L., Martin, T. R. and Phipatanakul, W. (2010). Clinically Useful Spirometry in Preschool-Aged Children: Evaluation of the 2007 American Thoracic Society Guidelines. *The Journal of asthma : official journal of the Association for the Care of Asthma* 47.7, 762–767. DOI: 10.3109/02770903.2010.485664.

Gao, J., Cao, Y., Tung, W.-w. and Hu, J. (2007). *Multiscale Analysis of Complex Time Series: Integration of Chaos and Random Fractal Theory, and Beyond*. English. 1 edition. Hoboken, N.J: Wiley-Interscience.

Gao, J., Hu, J., Mao, X. and Tung, W.-w. (2012). Detecting Low-Dimensional Chaos by the "Noise Titration" Technique: Possible Problems and Remedies. *Chaos, Solitons & Fractals* 45.3, 213–223. DOI: 10.1016/j.chaos.2011.12.004.

Gappa, M., Colin, A. A., Goetz, I. and Stocks, J. (2001). Passive Respiratory Mechanics: The Occlusion Techniques. en. *European Respiratory Journal* 17.1, 141–148.

Gaultier, C., Praud, J. P., Canet, E., Delaperche, M. F. and D'Allest, A. M. (1987). Paradoxical Inward Rib Cage Motion during Rapid Eye Movement Sleep in Infants and Young Children. eng. *Journal of developmental physiology* 9.5, 391–397.

Gaultier, C. (1995). Cardiorespiratory Adaptation during Sleep in Infants and Children. en. *Pediatric Pulmonology* 19.2, 105–117. DOI: 10.1002/ppul.1950190206.

Gauthier, M., Ray, A. and Wenzel, S. E. (2015). Evolving Concepts of Asthma. en. *American Journal of Respiratory and Critical Care Medicine* 192.6, 660–668. DOI: 10.1164/rccm.201504-0763PP.

Geddes, L. E. and Baker, L. E. (1972). Thoracic Impedance Changes Following Saline Injection into Right and Left Ventricles. *Journal of Applied Physiology* 33.2, 278–281. DOI: 10.1152/jappl.1972.33.2.278.

Geddes, L. A., Hoff, H. E., Hickman, D. M. and Moore, A. G. (1962). The Impedance Pneumography. eng. *Aerospace Medicine* 33, 28–33.

Gibson, P. G. and McDonald, V. M. (2015). Asthma-COPD Overlap 2015: Now We Are Six. en. *Thorax* 70.7, 683–691. DOI: 10.1136/thoraxjnl-2014-206740.

Gillespie, J. R. (1983). Mechanisms That Determine Functional Residual Capacity in Different Mammalian Species. EN. *American Review of Respiratory Disease* 126, S74–S77.

Goldensohn, E. S. and Zablow, L. (1959). An Electrical Impedance Spirometer. *Journal of Applied Physiology* 14.3, 463–464. DOI: 10.1152/jappl.1959.14.3.463.

Goldman, M. D. (2001). Clinical Application of Forced Oscillation. en. *Pulmonary Pharmacology & Therapeutics* 14.5, 341–350. DOI: 10.1006/pupt.2001.0310.

Gracia, J., Seppä, V.-P., Viik, J. and Hyttinen, J. (2012). Multilead Measurement System for the Time-Domain Analysis of Bioimpedance Magnitude. *Biomedical Engineering, IEEE Transactions on* 59.8, 2273–2280.

Gracia, J., Seppä, V.-P., Pelkonen, A., Kotaniemi-Syrjänen, A., Mäkelä, M., Malmberg, P. and Viik, J. (2017). Nonlinear Local Projection Filter for Impedance Pneumography. *EMBEC & NBC 2017*. IFMBE Proceedings. Springer, Singapore, 306–309. DOI: 10.1007/978-981-10-5122-7_77.

Gracia, J., Seppä, V.-P. and Viik, J. (2015). Multilead Impedance Pneumography and Forced Oscillation Technique for Assessing Lung Tissue Mechanical Properties. en. *Proceedins of the The 10th International Conference on Bioelectromagnetism*.

Gracia-Tabuenca, J., Seppä, V.-P., Jauhiainen, M., Kotaniemi-Syrjänen, A., Malmström, K., Pelkonen, A., Mäkelä, M. J., Viik, J. and Malmberg, L. P. (2019). Tidal Breathing Flow Volume Profiles during Sleep in Wheezing Infants Measured by Impedance Pneumography. *Journal of Applied Physiology* 126.5, 1409–1418. DOI: 10.1152/japplphysiol.01007.2018.

Gracia-Tabuenca, J., Seppä, V.-P., Jauhiainen, M., Paassilta, M., Viik, J. and Karjalainen, J. (2020). Tidal Breathing Flow Profiles during Sleep in Wheezing Children Measured by Impedance Pneumography. *Respiratory Physiology & Neurobiology* 271, 103312. DOI: 10.1016/j.resp.2019.103312.

Grassberger, P., Hegger, R., Kantz, H., Schaffrath, C. and Schreiber, T. (1993). On Noise Reduction Methods for Chaotic Data. en. *Chaos: An Interdisciplinary Journal of Nonlinear Science* 3.2, 127. DOI: 10.1063/1.165979.

Greenough, A., Pool, J. and Price, J. F. (1989). Changes in Functional Residual Capacity in Response to Bronchodilator Therapy among Young Asthmatic Children. en. *Pediatric Pulmonology* 7.1, 8–11. DOI: 10.1002/ppul.1950070104.

Grimes, S. and Martinsen, Ø. G. (2011). *Bioimpedance & Bioelectricity, Basics*. Academic Press.

Hadamar, J. (1902). Sur Les Problemes Aux Derivees Partielles et Leur Signification Physique. *Princeton University Bulletin*, 49–52.

Haddad, G. G., Epstein, R. A., Epstein, M. A., Leistner, H. L., Marino, P. A. and Mellins, R. B. (1979). Maturation of Ventilation and Ventilatory Pattern in Normal Sleeping Infants. eng. *Journal of Applied Physiology: Respiratory, Environmental and Exercise Physiology* 46.5, 998–1002. DOI: 10.1152/jappl.1979.46.5.998.

Haddad, G. G., Jeng, H. J., Lai, T. L. and Mellins, R. B. (1987). Determination of Sleep State in Infants Using Respiratory Variability. En. *Pediatric Research* 21.6, 556. DOI: 10.1203/00006450-198706000-00010.

Hammer, J. and Newth, C. J. L. (2009). Assessment of Thoraco-Abdominal Asynchrony. *Paediatric Respiratory Reviews* 10.2, 75–80. DOI: 10.1016/j.prrv.2009.02.004.

Harding, R., Johnson, P. and McClelland, M. E. (1980). Respiratory Function of the Larynx in Developing Sheep and the Influence of Sleep State. *Respiration Physiology* 40.2, 165–179. DOI: 10.1016/0034-5687(80)90090-0.

Hegger, R., Kantz, H. and Schreiber, T. (1999). Practical Implementation of Nonlinear Time Series Methods: The TISEAN Package. en. *Chaos: An Interdisciplinary Journal of Nonlinear Science* 9.2, 413–435. DOI: 10.1063/1.166424.

Henderson-Smart, D. J. and Read, D. J. (1979). Reduced Lung Volume during Behavioral Active Sleep in the Newborn. *Journal of Applied Physiology* 46.6, 1081–1085. DOI: 10.1152/jappl.1979.46.6.1081.

Hershenson, M. B., Colin, A. A., Wohl, M. E. B. and Stark, A. R. (1990). Changes in the Contribution of the Rib Cage to Tidal Breathing during Infancy. en. *American Review of Respiratory Disease* 141, 922–925. DOI: 10.1164/ajrccm/141.4_Pt_1.922.

Hetzel, M. R. and Clark, T. J. (1980). Comparison of Normal and Asthmatic Circadian Rhythms in Peak Expiratory Flow Rate. en. *Thorax* 35.10, 732–738. DOI: 10.1136/thx.35.10.732.

Hevroni, A., Goldman, A., Blank-Brachfeld, M., Abu Ahmad, W., Ben-Dov, L. and Springer, C. (2018). Use of Tidal Breathing Curves for Evaluating Expiratory Airway Obstruction in Infants. en. *Journal of Asthma* 55.12, 1331–1337. DOI: 10.1080/02770903.2017.1414234.

Hollier, C. A., Harmer, A. R., Maxwell, L. J., Menadue, C., Willson, G. N., Black, D. A. and Piper, A. J. (2014). Validation of Respiratory Inductive Plethysmography (LifeShirt) in

Obesity Hypoventilation Syndrome. *Respiratory Physiology & Neurobiology* 194, 15–22. DOI: `10.1016/j.resp.2014.01.014`.

Homma, I. and Masaoka, Y. (2008). Breathing Rhythms and Emotions: Breathing and Emotion. en. *Experimental Physiology* 93.9, 1011–1021. DOI: `10.1113/expphysiol.2008.042424`.

Horner, R. L. (2017). Chapter 15 - Respiratory Physiology: Central Neural Control of Respiratory Neurons and Motoneurons During Sleep. *Principles and Practice of Sleep Medicine (Sixth Edition)*. Ed. by M. Kryger, T. Roth and W. C. Dement. Elsevier, 155–166.e5. DOI: `10.1016/B978-0-323-24288-2.00015-5`.

Houtveen, J. H., Groot, P. F. and de Geus, E. J. (2006). Validation of the Thoracic Impedance Derived Respiratory Signal Using Multilevel Analysis. *International journal of psychophysiology* 59.2, 97–106.

Hudgel, D. W. and Devadatta, P. (1984). Decrease in Functional Residual Capacity during Sleep in Normal Humans. *Journal of Applied Physiology* 57.5, 1319–1322. DOI: `10.1152/jappl.1984.57.5.1319`.

Hudgel, D. W., Martin, R. J., Johnson, B. and Hill, P. (1984). Mechanics of the Respiratory System and Breathing Pattern during Sleep in Normal Humans. en. *Journal of Applied Physiology* 56.1, 133–137. DOI: `10.1152/jappl.1984.56.1.133`.

Hult, A., Juraški, R. G., Gracia-Tabuenca, J., Partinen, M., Plavec, D. and Seppä, V.-P. (2019). Sources of Variability in Expiratory Flow Profiles during Sleep in Healthy Young Children. *Respiratory Physiology & Neurobiology* 274, 103352. DOI: `10.1016/j.resp.2019.103352`.

Hurst, H. E. (1956). The Problem of Long-Term Storage in Reservoirs. *Hydrological Sciences Journal* 1.3, 13–27.

Hutchison, A. A., Wozniak, J. A., Choi, H. G., Conlon, M., Otto, R. A., Abrams, R. M. and Kosch, P. C. (1993). Laryngeal and Diaphragmatic Muscle Activities and Airflow Patterns after Birth in Premature Lambs. *Journal of Applied Physiology* 75.1, 121–131. DOI: `10.1152/jappl.1993.75.1.121`.

Hutten, G. J., Eykern, L. A. van, Latzin, P., Thamrin, C., Aalderen, W. M. van and Frey, U. (2010). Respiratory Muscle Activity Related to Flow and Lung Volume in Preterm Infants Compared With Term Infants. en. *Pediatric Research* 68.4, 339–343. DOI: `10.1203/PDR.0b013e3181eeeaf4`.

Hyatt, R. E., Schilder, D. P. and Fry, D. L. (1958). Relationship between Maximum Expiratory Flow and Degree of Lung Inflation. eng. *Journal of Applied Physiology* 13.3, 331–336. DOI: 10.1152/jappl.1958.13.3.331.

Iber, C., Simon, P., Skatrud, J. B., Mahowald, M. W. and Dempsey, J. A. (1995). The Breuer-Hering Reflex in Humans. Effects of Pulmonary Denervation and Hypocapnia. *American Journal of Respiratory and Critical Care Medicine* 152.1, 217–224. DOI: 10.1164/ajrccm.152.1.7599827.

Ihlen, E. A. F. (2012). Introduction to Multifractal Detrended Fluctuation Analysis in Matlab. *Frontiers in Physiology* 3, 141. DOI: 10.3389/fphys.2012.00141.

Irvin, C. G., Pak, J. and Martin, R. J. (2000). Airway–Parenchyma Uncoupling in Nocturnal Asthma. *American Journal of Respiratory and Critical Care Medicine* 161.1, 50–56. DOI: 10.1164/ajrccm.161.1.9804053.

Isler, J. R., Thai, T., Myers, M. M. and Fifer, W. P. (2016). An Automated Method for Coding Sleep States in Human Infants Based on Respiratory Rate Variability. en. *Developmental Psychobiology* 58.8, 1108–1115. DOI: 10.1002/dev.21482.

Joseph, V., Pequignot, J. M. and Van Reeth, O. (2002). Neurochemical Perspectives on the Control of Breathing during Sleep. *Respiratory Physiology & Neurobiology* 130.3, 253–263. DOI: 10.1016/S0034-5687(02)00012-9.

Kantelhardt, J. W., Penzel, T., Rostig, S., Becker, H. F., Havlin, S. and Bunde, A. (2003). Breathing during REM and Non-REM Sleep: Correlated versus Uncorrelated Behaviour. *Physica A: Statistical Mechanics and its Applications* 319, 447–457.

Kantz, H. and Schreiber, T. (2004). *Nonlinear Time Series Analysis*. English. Cambridge, UK; New York: Cambridge University Press.

Kantz, H., Schreiber, T., Hoffmann, I., Buzug, T., Pfister, G., Flepp, L. G., Simonet, J., Badii, R. and Brun, E. (1993). Nonlinear Noise Reduction: A Case Study on Experimental Data. en. *Physical Review E* 48.2, 1529–1538. DOI: 10.1103/PhysRevE.48.1529.

Kaplan, J. L. and Yorke, J. A. (1979). Chaotic Behavior of Multidimensional Difference Equations. *Functional Differential Equations and Approximation of Fixed Points*. Ed. by H.-O. Peitgen and H.-O. Walther. Vol. 730. Berlin, Heidelberg: Springer Berlin Heidelberg, 204–227. DOI: 10.1007/BFb0064319.

Katz, E. S., Marcus, C. L. and White, D. P. (2006). Influence of Airway Pressure on Genioglossus Activity during Sleep in Normal Children. *American Journal of Respiratory and Critical Care Medicine* 173.8, 902–909. DOI: 10.1164/rccm.200509-1450OC.

Kawakami, K., Watanabe, A., Ikeda, K., Kanno, R. and Kira, S. (1974). An Analysis of the Relationship between Transthoracic Impedance Variations and Thoracic Diameter Changes. en. *Medical and biological engineering* 12.4, 446–453. DOI: 10.1007/BF02478600.

Kekonen, A., Bergelin, M., Eriksson, J.-E., Vaalasti, A., Ylänen, H. and Viik, J. (2017). Bioimpedance Measurement Based Evaluation of Wound Healing. en. *Physiological Measurement* 38.7, 1373–1383. DOI: 10.1088/1361-6579/aa63d6.

Khambete, N. D., Brown, B. H. and Smallwood, R. (1999). Movement Artefact Rejection in Impedance Pneumography Using Six Strategically Placed Electrodes. *Physiol. Meas. 21 (2000) 79-88*.

Knill, R. L. and Clement, J. L. (1985). Ventilatory Responses to Acute Metabolic Acidemia in Humans Awake, Sedated, and Anesthetized with Halothane. eng. *Anesthesiology* 62.6, 745–753. DOI: 10.1097/00000542-198506000-00008.

Kosch, P. C., Davenport, P. W., Wozniak, J. A. and Stark, A. R. (1985). Reflex Control of Expiratory Duration in Newborn Infants. en. *Journal of Applied Physiology* 58.2, 575–581. DOI: 10.1152/jappl.1985.58.2.575.

— (1986). Reflex Control of Inspiratory Duration in Newborn Infants. en. *Journal of Applied Physiology* 60.6, 2007–2014. DOI: 10.1152/jappl.1986.60.6.2007.

Kosch, P. C., Hutchinson, A. A., Wozniak, J. A., Carlo, W. A. and Stark, A. R. (1988). Posterior Cricoarytenoid and Diaphragm Activities during Tidal Breathing in Neonates. *Journal of Applied Physiology* 64.5, 1968–1978. DOI: 10.1152/jappl.1988.64.5.1968.

Kosch, P. C. and Stark, A. R. (1984). Dynamic Maintenance of End-Expiratory Lung Volume in Full-Term Infants. en. *Journal of Applied Physiology* 57.4, 1126–1133. DOI: 10.1152/jappl.1984.57.4.1126.

Krimsky, W. R. and Leiter, J. C. (2005). Physiology of Breathing and Respiratory Control during Sleep. en. *Seminars in Respiratory and Critical Care Medicine* 26.1, 5–12. DOI: 10.1055/s-2005-864197.

Kubicek, W. G., Kinnen, E. and Edin, A. (1964). Calibration of an Impedance Pneumograph. *Journal of Applied Physiology* 19.3, 557–560. DOI: 10.1152/jappl.1964.19.3.557.

Kugiumtzis, D. (1996). State Space Reconstruction Parameters in the Analysis of Chaotic Time Series — the Role of the Time Window Length. *Physica D: Nonlinear Phenomena* 95.1, 13–28. DOI: 10.1016/0167-2789(96)00054-1.

Kuna, S. T., Smickley, J. S. and Vanoye, C. R. (1997). Respiratory-Related Pharyngeal Constrictor Muscle Activity in Normal Human Adults. *American Journal of Respiratory and Critical Care Medicine* 155.6, 1991–1999. DOI: 10.1164/ajrccm.155.6.9196107.

Kuna, S. T., Smickley, J. S. and Insalaco, G. (1990). Posterior Cricoarytenoid Muscle Activity during Wakefulness and Sleep in Normal Adults. *Journal of Applied Physiology* 68.4, 1746–1754. DOI: 10.1152/jappl.1990.68.4.1746.

Kyle, U. G., Bosaeus, I., De Lorenzo, A. D., Deurenberg, P., Elia, M., Gómez, J. M., Heitmann, B. L., Kent-Smith, L., Melchior, J.-C., Pirlich, M., Scharfetter, H., Schols, A. M. W. J. and Pichard, C. (2004). Bioelectrical Impedance Analysis—Part I: Review of Principles and Methods. en. *Clinical Nutrition* 23.5, 1226–1243. DOI: 10.1016/j.clnu.2004.06.004.

Lehti-Polojärvi, M., Koskela, O., Seppänen, A., Figueiras, E. and Hyttinen, J. (2018). Rotational Electrical Impedance Tomography Using Electrodes with Limited Surface Coverage Provides Window for Multimodal Sensing. en. *Measurement Science and Technology* 29.2, 025401. DOI: 10.1088/1361-6501/aa97f1.

Leonhardt, S., Ahrens, P. and Kecman, V. (2010). Analysis of Tidal Breathing Flow Volume Loops for Automated Lung-Function Diagnosis in Infants. *IEEE Transactions on Biomedical Engineering* 57.8, 1945–1953. DOI: 10.1109/TBME.2010.2046168.

Levitzky, M. G. (2018). *Pulmonary Physiology, Ninth Edition*. English. 9 edition. McGraw-Hill Education / Medical.

Lewis, M. J., Short, A. L. and Lewis, K. E. (2006). Autonomic Nervous System Control of the Cardiovascular and Respiratory Systems in Asthma. *Respiratory Medicine* 100.10, 1688–1705. DOI: 10.1016/j.rmed.2006.01.019.

Lødrup, K. C., Mowinckel, P. and Carlsen, K. H. (1992). Lung Function Measurements in Awake Compared to Sleeping Newborn Infants. en. *Pediatric Pulmonology* 12.2, 99–104. DOI: 10.1002/ppul.1950120208.

Lodrup-Carlsen, K. C. and Carlsen, K. H. (1993). Lung Function in Awake Healthy Infants: The First Five Days of Life. en. *European Respiratory Journal* 6.10, 1496–1500.

Logic, J. L., Maksud, M. G. and Hamilton, L. H. (1967). Factors Affecting Transthoracic Impedance Signals Used to Measure Breathing. *Journal of Applied Physiology* 22.2, 251–254. DOI: 10.1152/jappl.1967.22.2.251.

Lu, G., Brittain, J.-S., Holland, P., Yianni, J., Green, A. L., Stein, J. F., Aziz, T. Z. and Wang, S. (2009). Removing ECG Noise from Surface EMG Signals Using Adaptive Filtering. *Neuroscience Letters* 462.1, 14–19. DOI: 10.1016/j.neulet.2009.06.063.

Lumb, A. B. and Nunn, J. F. (1991). Respiratory Function and Ribcage Contribution to Ventilation in Body Positions Commonly Used during Anesthesia. eng. *Anesthesia and analgesia* 73.4, 422–426. DOI: 10.1213/00000539-199110000-00010.

Luo, S., Afonso, V. X., Webster, J. G. and Tompkins, W. J. (2002). The Electrode System in Impedance-Based Ventilation Measurement. *Biomedical Engineering, IEEE Transactions on* 39.11, 1130–1141.

Maarsingh, E. J. W., van Eykern, L. A., Sprikkelman, A. B. and van Aalderen, W. M. C. (2004). Histamine Induced Airway Response in Pre-School Children Assessed by a Non-Invasive EMG Technique. *Respiratory Medicine* 98.4, 363–372. DOI: 10.1016/j.rmed.2003.10.014.

MacBean, V., Jolley, C. J., Sutton, T. G., Deep, A., Greenough, A., Moxham, J. and Rafferty, G. F. (2016). Parasternal Intercostal Electromyography: A Novel Tool to Assess Respiratory Load in Children. en. *Pediatric Research* 80.3, 407–414. DOI: 10.1038/pr.2016.89.

Malmberg, L. P., Seppä, V.-P., Kotaniemi-Syrjänen, A., Malmström, K., Kajosaari, M., Pelkonen, A. S., Viik, J. and Mäkelä, M. J. (2017). Measurement of Tidal Breathing Flows in Infants Using Impedance Pneumography. en. *European Respiratory Journal* 49.2, 1600926. DOI: 10.1183/13993003.00926-2016.

Malmivuo, J. and Plonsey, R. (1995). *Bioelectromagnetism - Principles and Applications of Bioelectric and Biomagnetic Fields*. Oxford University Press, USA. DOI: 10.1093/acprof:oso/9780195058239.001.0001.

Marchal, F. and Crance, J.-P. (1987). Measurement of Ventilatory System Compliance in Infants and Young Children. en. *Respiration Physiology* 68.3, 311–318. DOI: 10.1016/S0034-5687(87)80016-6.

Marchal, F., Schweitzer, C. and Moreau-Colson, C. (2002). Respiratory Impedance Response to a Deep Inhalation in Children with History of Cough or Asthma. en. *Pediatric Pulmonology* 33.6, 411–418. DOI: 10.1002/ppul.10093.

Martin, J., Powell, E., Shore, S., Emrich, J. and Engel, L. A. (1980). The Role of Respiratory Muscles in the Hyperinflation of Bronchial Asthma. *American Review of Respiratory Disease* 121.3, 441–447. DOI: 10.1164/arrd.1980.121.3.441.

Marwan, N., Carmen Romano, M., Thiel, M. and Kurths, J. (2007). Recurrence Plots for the Analysis of Complex Systems. *Physics Reports* 438.5–6, 237–329. DOI: 10.1016/j.physrep.2006.11.001.

Miller, M. R. (2005). Standardisation of Spirometry. en. *European Respiratory Journal* 26.2, 319–338. DOI: 10.1183/09031936.05.00034805.

Mitchell, R. A. and Severinghaus, J. W. (1967). Cerebrospinal Fluid and the Regulation of Respiration. en-US. *Anesthesia & Analgesia* 46.1, 134.

Młyńczak, M., Niewiadomski, W., Żyliński, M. and Cybulski, G. (2015). Verification of the Respiratory Parameters Derived from Impedance Pneumography during Normal and Deep Breathing in Three Body Postures. en. *6th European Conference of the International Federation for Medical and Biological Engineering*. Ed. by I. Lacković and D. Vasic. IFMBE Proceedings. Cham: Springer International Publishing, 881–884. DOI: 10.1007/978-3-319-11128-5_219.

Mols, G., Brandes, I., Kessler, V., Lichtwarck-Aschoff, M., Loop, T., Geiger, K. and Guttmann, J. (1999). Volume-Dependent Compliance in ARDS: Proposal of a New Diagnostic Concept. en. *Intensive Care Medicine* 25.10, 1084–1091. DOI: 10.1007/s001340051016.

Morris, M. J. and Lane, D. J. (1981). Tidal Expiratory Flow Patterns in Airflow Obstruction. en. *Thorax* 36.2, 135–142. DOI: 10.1136/thx.36.2.135.

Morris, M. J., Madgwick, R. G., Frew, A. J. and Lane, D. J. (1990). Breathing Muscle Activity during Expiration in Patients with Chronic Airflow Obstruction. *European Respiratory Journal* 3.8, 901–909.

Morris, M. J., Madgwick, R. G. and Lane, D. J. (1995). Analysis of Tidal Expiratory Flow Pattern in the Assessment of Histamine-Induced Bronchoconstriction. en. *Thorax* 50.4, 346–352. DOI: 10.1136/thx.50.4.346.

Morris, M. J., Madgwick, R., Collyer, I., Denby, F. and Lane, D. (1998). Analysis of Expiratory Tidal Flow Patterns as a Diagnostic Tool in Airflow Obstruction. *European Respiratory Journal* 12.5, 1113–1117. DOI: 10.1183/09031936.98.12051113.

Mortola, J. P., Fisher, J. T., Smith, B., Fox, G. and Weeks, S. (1982). Dynamics of Breathing in Infants. en. *Journal of Applied Physiology* 52.5, 1209–1215. DOI: 10.1152/jappl.1982.52.5.1209.

Mortola, J. P. (2004). Breathing around the Clock: An Overview of the Circadian Pattern of Respiration. *European Journal of Applied Physiology* 91.2-3, 119–129. DOI: 10.1007/s00421-003-0978-0.

Muller, N., Bryan, A. C. and Zamel, N. (1981). Tonic Inspiratory Muscle Activity as a Cause of Hyperinflation in Asthma. *Journal of Applied Physiology* 50.2, 279–282. DOI: 10 . 1152/jappl.1981.50.2.279.

Muller, N., Volgyesi, G., Becker, L., Bryan, M. H. and Bryan, A. C. (1979). Diaphragmatic Muscle Tone. *Journal of Applied Physiology* 47.2, 279–284. DOI: 10 . 1152 / jappl . 1979.47.2.279.

Murakami, K., Habukawa, C., Kurosawa, H. and Takemura, T. (2014). Evaluation of Airway Responsiveness Using Colored Three-Dimensional Analyses of a New Forced Oscillation Technique in Controlled Asthmatic and Nonasthmatic Children. English. *Respiratory Investigation* 52.1, 57–64. DOI: 10.1016/j.resinv.2013.07.003.

Naimark, A. and Cherniack, R. M. (1960). Compliance of the Respiratory System and Its Components in Health and Obesity. *Journal of Applied Physiology* 15.3, 377–382. DOI: 10.1152/jappl.1960.15.3.377.

Nakesch, H., Pfützner, H., Ruhsam, C., Nopp, P. and Futschik, K. (1994). Five-Electrode Field Plethysmography Technique for Separation of Respiration and Cardiac Signals. *Medical and Biological Engineering and Computing* 32, 65–70.

Nopp, D. P., Harris, N. D., Zhao, T.-X. and Brown, B. H. (1997). Model for the Dielectric Properties of Human Lung Tissue against Frequency and Air Content. en. *Medical and Biological Engineering and Computing* 35.6, 695–702. DOI: 10.1007/BF02510980.

Notter, R. H. (2000). *Lung Surfactants: Basic Science and Clinical Applications*. en. CRC Press.

Oosterhoff, Y., Koëter, G. H., De Monchy, J. G. R. and Postma, D. S. (1993). Circadian Variation in Airway Responsiveness to Methacholine, Propranolol, and AMP in Atopic Asthmatic Subjects. *American Review of Respiratory Disease* 147.3, 512–517. DOI: 10 . 1164/ajrccm/147.3.512.

Openshaw, P., Edwards, S. and Helms, P. (1984). Changes in Rib Cage Geometry during Childhood. *Thorax* 39.8, 624–627.

Orem, J., Norris, P. and Lydic, R. (1978). Laryngeal Abductor Activity during Sleep. *Chest* 73.2, Supplement, 300–301. DOI: 10.1378/chest.73.2_Supplement.300.

Otis, A. B., Fenn, W. O. and Rahn, H. (1950). Mechanics of Breathing in Man. en. *Journal of Applied Physiology* 2.11, 592–607.

Pandey, V. K., Pandey, P. C., Burkule, N. J. and Subramanyan, L. R. (2011). Adaptive Filtering for Suppression of Respiratory Artifact in Impedance Cardiography. *2011 Annual In-*

ternational Conference of the IEEE Engineering in Medicine and Biology Society, 7932–7936. DOI: 10.1109/IEMBS.2011.6091956.

Papastamelos, C., Panitch, H. B., England, S. E. and Allen, J. L. (1995). Developmental Changes in Chest Wall Compliance in Infancy and Early Childhood. *Journal of Applied Physiology* 78.1, 179–184. DOI: 10.1152/jappl.1995.78.1.179.

Parmelee, A., Stern, E. and Harris, M. (1972). Maturation of Respiration in Prematures and Young Infants. en. *Neuropediatrics* 3.03, 294–304. DOI: 10.1055/s-0028-1091768.

Pellegrino, R., Violante, B. and Brusasco, V. (1996). Maximal Bronchoconstriction in Humans. Relationship to Deep Inhalation and Airway Sensitivity. *American Journal of Respiratory and Critical Care Medicine* 153.1, 115–121. DOI: 10.1164/ajrccm.153.1.8542103.

Pellegrino, R. and Brusasco, V. (1997). On the Causes of Lung Hyperinflation during Bronchoconstriction. en. *European Respiratory Journal* 10.2, 468–475.

Pellegrino, R., Violante, B., Nava, S., Rampulla, C., Brusasco, V. and Rodarte, J. R. (1993). Expiratory Airflow Limitation and Hyperinflation during Methacholine-Induced Bronchoconstriction. *Journal of Applied Physiology* 75.4, 1720–1727. DOI: 10.1152/jappl.1993.75.4.1720.

Peng, C.-K., Mietus, J. E., Liu, Y., Lee, C., Hausdorff, J. M., Stanley, H. E., Goldberger, A. L. and Lipsitz, L. A. (2002). Quantifying Fractal Dynamics of Human Respiration: Age and Gender Effects. en. *Annals of Biomedical Engineering* 30.5, 683–692. DOI: 10.1114/1.1481053.

Perez, W. and Tobin, M. J. (1985). Separation of Factors Responsible for Change in Breathing Pattern Induced by Instrumentation. eng. *Journal of Applied Physiology (Bethesda, Md.: 1985)* 59.5, 1515–1520. DOI: 10.1152/jappl.1985.59.5.1515.

Peterson-Carmichael, S., Seddon, P. C., Cheifetz, I. M., Frerichs, I., Hall, G. L., Hammer, J., Hantos, Z., van Kaam, A. H., McEvoy, C. T., Newth, C. J. L., Pillow, J. J., Rafferty, G. F., Rosenfeld, M., Stocks, J. and Ranganathan, S. C. (2016). An Official American Thoracic Society/European Respiratory Society Workshop Report: Evaluation of Respiratory Mechanics and Function in the Pediatric and Neonatal Intensive Care Units. *Annals of the American Thoracic Society* 13.2, S1–S11. DOI: 10.1513/AnnalsATS.201511-730ST.

Phillipson, E. A. (1978). Respiratory Adaptations in Sleep. en. *Annual review of Physiology* 40.1, 133–156.

Pincus, S. M. (1991). Approximate Entropy as a Measure of System Complexity. *Proceedings of the National Academy of Sciences of the United States of America* 88.6, 2297–2301.

Polak, A. G., Wysoczański, D. and Mroczka, J. (2019). Effects of Homogeneous and Heterogeneous Changes in the Lung Periphery on Spirometry Results. *Computer Methods and Programs in Biomedicine* 173, 139–145. DOI: 10.1016/j.cmpb.2019.03.014.

Poon, C.-S. and Barahona, M. (2001). Titration of Chaos with Added Noise. en. *Proceedings of the National Academy of Sciences* 98.13, 7107–7112. DOI: 10.1073/pnas.131173198.

Rabbette, P. S., Fletcher, M. E., Dezateux, C. A., Soriano-Brucher, H. and Stocks, J. (1994). Hering-Breuer Reflex and Respiratory System Compliance in the First Year of Life: A Longitudinal Study. *Journal of Applied Physiology* 76.2, 650–656. DOI: 10.1152/jappl.1994.76.2.650.

Raoufy, M. R., Ghafari, T., Darooei, R., Nazari, M., Mahdaviani, S. A., Eslaminejad, A. R., Almasnia, M., Gharibzadeh, S., Mani, A. R. and Hajizadeh, S. (2016). Classification of Asthma Based on Nonlinear Analysis of Breathing Pattern. en. *PLOS ONE* 11.1, e0147976. DOI: 10.1371/journal.pone.0147976.

Richman, J. S. and Moorman, J. R. (2000). Physiological Time-Series Analysis Using Approximate Entropy and Sample Entropy. *American Journal of Physiology-Heart and Circulatory Physiology* 278.6, H2039–H2049. DOI: 10.1152/ajpheart.2000.278.6.H2039.

Richter, D. W. and Smith, J. C. (2014). Respiratory Rhythm Generation In Vivo. en. *Physiology* 29.1, 58–71. DOI: 10.1152/physiol.00035.2013.

Robinson, P. D., Stocks, J., Marchal, F., Nielsen, K. G., Thompson, B. R., Tomalak, W. and Kirkby, J. (2015). Poor Standardisation of Plethysmographic Specific Airways Resistance Measurement despite Widespread Use. en. *European Respiratory Journal* 46.6, 1811–1814. DOI: 10.1183/13993003.00377-2015.

Rosell, J., Cohen, K. P. and Webster, J. G. (2002). Reduction of Motion Artifacts Using a Two-Frequency Impedance Plethysmograph and Adaptive Filtering. *Biomedical Engineering, IEEE Transactions on* 42.10, 1044–1048.

Sachis, P. N., Armstrong, D. L., Becker, L. E. and Bryan, A. C. (1981). The Vagus Nerve and Sudden Infant Death Syndrome: A Morphometric Study. English. *The Journal of Pediatrics* 98.2, 278–280. DOI: 10.1016/S0022-3476(81)80661-0.

Sahakian, A. V., Tompkins, W. J. and Webster, J. G. (1985). Electrode Motion Artifacts in Electrical Impedance Pneumography. *IEEE Transactions on Biomedical Engineering* BME-32.6, 448–451. DOI: 10.1109/TBME.1985.325453.

Sahn, S.A. (1988). The Pleura. *The American review of respiratory disease* 1.138, 184–234.

Sako, T., Burioka, N., Suyama, H., Nomura, T., Takeshima, T. and Shimizu, E. (2001). Nonlinear Behavior of Human Respiratory Movement during Different Sleep Stages. eng. *Chronobiology International* 18.1, 71–83.

Samara, Z., Raux, M., Fiamma, M.-N., Gharbi, A., Gottfried, S. B., Poon, C.-S., Similowski, T. and Straus, C. (2009). Effects of Inspiratory Loading on the Chaotic Dynamics of Ventilatory Flow in Humans. *Respiratory Physiology & Neurobiology* 165.1, 82–89. DOI: 10.1016/j.resp.2008.10.015.

Sato, J. and Robbins, P. A. (2001). Methods for Averaging Irregular Respiratory Flow Profiles in Awake Humans. en. *Journal of Applied Physiology* 90.2, 705–712.

Sauerland, E. K. and Harper, R. M. (1976). The Human Tongue during Sleep: Electromyographic Activity of the Genioglossus Muscle. *Experimental Neurology* 51.1, 160–170. DOI: 10.1016/0014-4886(76)90061-3.

Schafer, R. W. (2011). On the Frequency-Domain Properties of Savitzky-Golay Filters. en. *2011 Digital Signal Processing and Signal Processing Education Meeting (DSP/SPE)*. Sedona, AZ, USA: IEEE, 54–59. DOI: 10.1109/DSP-SPE.2011.5739186.

Schmalisch, G., Wilitzki, S. and Wauer, R. (2005). Differences in Tidal Breathing between Infants with Chronic Lung Diseases and Healthy Controls. en. *BMC Pediatrics* 5.1, 36. DOI: 10.1186/1471-2431-5-36.

Schmalisch, G., Wauer, R. R., Foitzik, B. and Patzak, A. (2003). Influence of Preterm Onset of Inspiration on Tidal Breathing Parameters in Infants with and without CLD. *Respiratory Physiology & Neurobiology* 135.1, 39–46. DOI: 10.1016/S1569-9048(03)00029-6.

Schmidt, M., Foitzik, B., Wauer, R., Winkler, F. and Schmalisch, G. (1998). Comparative Investigations of Algorithms for the Detection of Breaths in Newborns with Disturbed Respiratory Signals. en. *Computers and Biomedical Research* 31.6, 413–425. DOI: 10.1006/cmbr.1998.1493.

Schreiber, T. and Kaplan, D. T. (1996a). Nonlinear Noise Reduction for Electrocardiograms. *Chaos: An Interdisciplinary Journal of Nonlinear Science* 6.1, 87–92. DOI: 10.1063/1.166148.

— (1996b). Signal Separation by Nonlinear Projections: The Fetal Electrocardiogram. *Physical Review E* 53.5, R4326–R4329. DOI: 10.1103/PhysRevE.53.R4326.

Schumann, A. Y., Bartsch, R. P., Penzel, T., Ivanov, P. C. and Kantelhardt, J. W. (2010). Aging Effects on Cardiac and Respiratory Dynamics in Healthy Subjects across Sleep Stages. *Sleep* 33.7, 943–955.

Sears, T. A. (1977). 6 - Some Neural and Mechanical Aspects of Singing. *Music and the Brain*. Ed. by M. Critchley and R. A. Henson. Butterworth-Heinemann, 78–94. DOI: 10.1016/B978-0-433-06703-0.50013-9.

Seely, A. J. and Macklem, P. T. (2004). Complex Systems and the Technology of Variability Analysis. *Critical Care* 8.6, R367. DOI: 10.1186/cc2948.

Senaratna, C. V., Perret, J. L., Lodge, C. J., Lowe, A. J., Campbell, B. E., Matheson, M. C., Hamilton, G. S. and Dharmage, S. C. (2017). Prevalence of Obstructive Sleep Apnea in the General Population: A Systematic Review. *Sleep Medicine Reviews* 34, 70–81. DOI: 10.1016/j.smrv.2016.07.002.

Seppa, V.-P., Uitto, M. and Viik, J. (2013). Tidal Breathing Flow-Volume Curves with Impedance Pneumography during Expiratory Loading. *2013 35th Annual International Conference of the IEEE Engineering in Medicine and Biology Society (EMBC)*, 2437–2440. DOI: 10.1109/EMBC.2013.6610032.

Seppä, V. P., Viik, J. and Hyttinen, J. (2010). Assessment of Pulmonary Flow Using Impedance Pneumography. *IEEE Transactions on Biomedical Engineering* 57.9, 2277–2285. DOI: 10.1109/TBME.2010.2051668.

Seppä, V.-P., Hyttinen, J. and Viik, J. (2011). A Method for Suppressing Cardiogenic Oscillations in Impedance Pneumography. en. *Physiological Measurement* 32.3, 337. DOI: 10.1088/0967-3334/32/3/005.

Seppä, V.-P. (2014). Development and Clinical Application of Impedance Pneumography Technique. en. PhD thesis.

Seppä, V.-P., Hult, A., Gracia-Tabuenca, J., Paassilta, M., Viik, J., Plavec, D. and Karjalainen, J. (2019). Airway Obstruction Is Associated with Reduced Variability in Specific Parts of the Tidal Breathing Flow–Volume Curve in Young Children. en. *ERJ Open Research* 5.2, 00028–2019. DOI: 10.1183/23120541.00028-2019.

Seppä, V.-P., Hyttinen, J., Uitto, M., Chrapek, W. and Viik, J. (2013). Novel Electrode Configuration for Highly Linear Impedance Pneumography. *Biomedizinische Technik/Biomedical Engineering* 58.1. DOI: 10.1515/bmt-2012-0068.

Seppä, V.-P., Hyttinen, J. and Viik, J. (2010). Agreement Between Impedance Pneumography and Pneumotachograph in Estimation of a Tidal Breathing Parameter. English. *CHEST* 138.4, 816A. DOI: 10.1378/chest.10384.

Seppä, V.-P., Paassilta, M., Gracia, J., Hult, A., Viik, J., Plavec, D. and Karjalainen, J. (2018). Tidal Breathing Variability during Sleep Is a Sensitive Marker of Disease Control in Small Children with Recurrent Wheeze. *ERS*. Paris.

Seppä, V.-P., Pelkonen, A. S., Kotaniemi-Syrjänen, A., Mäkelä, M. J., Viik, J. and Malmberg, L. P. (2013). Tidal Breathing Flow Measurement in Awake Young Children by Using Impedance Pneumography. *Journal of Applied Physiology* 115.11, 1725–1731. DOI: 10.1152/japplphysiol.00657.2013.

Seppä, V.-P., Pelkonen, A. S., Kotaniemi-Syrjänen, A., Viik, J., Mäkelä, M. J. and Malmberg, L. P. (2016). Tidal Flow Variability Measured by Impedance Pneumography Relates to Childhood Asthma Risk. en. *European Respiratory Journal*, ERJ-00989–2015. DOI: 10.1183/13993003.00989-2015.

Shannon, C. E. (1948). A Mathematical Theory of Communication. *The Bell System Technical Journal* 27.3, 379–423. DOI: 10.1002/j.1538-7305.1948.tb01338.x.

Sharp, J. T., Druz, W. S., Balagot, R. C., Bandelin, V. R. and Danon, J. (1970). Total Respiratory Compliance in Infants and Children. *Journal of Applied Physiology* 29.6, 775–779. DOI: 10.1152/jappl.1970.29.6.775.

Shashidhar, A. (2006). Generalized Volterra-Wiener and Surrogate Data Methods for Complex Time Series Analysis. PhD thesis. Massachusetts Institute of Technology.

Shee, C. D., Ploy-Song-Sang, Y. and Milic-Emili, J. (1985). Decay of Inspiratory Muscle Pressure during Expiration in Conscious Humans. en. *Journal of Applied Physiology* 58.6, 1859–1865.

Small, M., Judd, K., Lowe, M. and Stick, S. (1999). Is Breathing in Infants Chaotic? Dimension Estimates for Respiratory Patterns during Quiet Sleep. en. *Journal of Applied Physiology* 86.1, 359–376.

Stark, A. R., Cohlan, B. A., Waggener, T. B., Frantz, I. D. and Kosch, P. C. (1987). Regulation of End-Expiratory Lung Volume during Sleep in Premature Infants. en. *Journal of Applied Physiology* 62.3, 1117–1123. DOI: 10.1152/jappl.1987.62.3.1117.

Stocks, J., Dezateux, C. A., Jackson, E. A., Hoo, A. F., Costeloe, K. L. and Wade, A. M. (1994). Analysis of Tidal Breathing Parameters in Infancy: How Variable Is TPTEF:TE? en. *American Journal of Respiratory and Critical Care Medicine* 150.5, 1347–1354. DOI: 10.1164/ajrccm.150.5.7952563.

Suki, B., Hantos, Z., Daroczy, B., Alkaysi, G. and Nagy, S. (1991). Nonlinearity and Harmonic Distortion of Dog Lungs Measured by Low-Frequency Forced Oscillations. *Journal of Applied Physiology* 71.1, 69–75. DOI: 10.1152/jappl.1991.71.1.69.

Suki, B., Bates, J. H. T. and Frey, U. (2011). Complexity and Emergent Phenomena. eng. *Comprehensive Physiology* 1.2, 995–1029. DOI: 10.1002/cphy.c100022.

Sutherland, E. R. (2005). Nocturnal Asthma. *Journal of Allergy and Clinical Immunology* 116.6, 1179–1186. DOI: 10.1016/j.jaci.2005.09.028.

Suyama, H., Burioka, N., Sako, T., Miyata, M. and Shimizu, E. (2003). Reduction of Correlation Dimension in Human Respiration by Inhaling a Mixture Gas of 5% Carbon Dioxide and 95% Oxygen. eng. *Biomedicine & Pharmacotherapy = Biomedecine & Pharmacotherapie* 57 Suppl 1, 116s–121s.

Teague, W. G., Tustison, N. J. and Altes, T. A. (2014). Ventilation Heterogeneity in Asthma. *Journal of Asthma* 51.7, 677–684. DOI: 10.3109/02770903.2014.914535.

Teixeira, A. R., Tomé, A. M., Stadlthanner, K. and Lang, E. W. (2006). Nonlinear Projective Techniques to Extract Artifacts in Biomedical Signals. *2006 14th European Signal Processing Conference*, 1–5.

Terrill, P. I., Wilson, S. J., Suresh, S., Cooper, D. M. and Dakin, C. (2013). Characterising Non-Linear Dynamics in Nocturnal Breathing Patterns of Healthy Infants Using Recurrence Quantification Analysis. *Computers in Biology and Medicine* 43.4, 231–239. DOI: 10.1016/j.compbiomed.2013.01.005.

Teulier, M., Fiamma, M.-N., Straus, C. and Similowski, T. (2013). Acute Bronchodilation Increases Ventilatory Complexity during Resting Breathing in Stable COPD: Toward Mathematical Biomarkers of Ventilatory Function?: *Respiratory Physiology & Neurobiology* 185.2, 477–480. DOI: 10.1016/j.resp.2012.09.006.

Thamrin, C., Frey, U., Kaminsky, D. A., Reddel, H. K., Seely, A. J. E., Suki, B. and Sterk, P. J. (2016). Systems Biology and Clinical Practice in Respiratory Medicine. The Twain Shall Meet. en. *American Journal of Respiratory and Critical Care Medicine* 194.9, 1053–1061. DOI: 10.1164/rccm.201511-2288PP.

Thibault, S., Calabrese, P., Benchetrit, G. and Baconnier, P. (2004). Effects of Resistive Loading on Breathing Variability. en. *Post-Genomic Perspectives in Modeling and Control of Breathing*. Springer, Boston, MA, 293–298. DOI: 10.1007/0-387-27023-X_44.

Thurlbeck, W. M. (1982). Postnatal Human Lung Growth. en. *Thorax* 37.8, 564–571. DOI: 10.1136/thx.37.8.564.

Totapally, B. R., Demerci, C., Zureikat, G. and Nolan, B. (2001). Tidal Breathing Flow-Volume Loops in Bronchiolitis in Infancy: The Effect of Albuterol [IS-RCTN47364493]. en. 6.2, 6.

Troyer, A. de and Loring, S. H. (2011). Action of the Respiratory Muscles. en. *Comprehensive Physiology*. American Cancer Society, 443–461. DOI: 10.1002/cphy.cp030326.

Tully, A., Brancatisano, A., Loring, S. H. and Engel, L. A. (1990). Relationship between Thyroarytenoid Activity and Laryngeal Resistance. *Journal of Applied Physiology* 68.5, 1988–1996. DOI: 10.1152/jappl.1990.68.5.1988.

Tusiewicz, K., Moldofsky, H., Bryan, A. C. and Bryan, M. H. (1977). Mechanics of the Rib Cage and Diaphragm during Sleep. en. *Journal of Applied Physiology* 43.4, 600–602. DOI: 10.1152/jappl.1977.43.4.600.

Valentinuzzi, M. E., Geddes, L. A. and Baker, L. E. (1971). The Law of Impedance Pneumography. en. *Medical and biological engineering* 9.3, 157–163. DOI: 10.1007/BF02474811.

van der Ent, C. K., Brackel, H. J., van der Laag, J. and Bogaard, J. M. (1996). Tidal Breathing Analysis as a Measure of Airway Obstruction in Children Three Years of Age and Older. *American Journal of Respiratory and Critical Care Medicine* 153.4, 1253–1258. DOI: 10.1164/ajrccm.153.4.8616550.

Veiga, J., Lopes, A. J., Jansen, J. M. and Melo, P. L. (2012). Fluctuation Analysis of Respiratory Impedance Waveform in Asthmatic Patients: Effect of Airway Obstruction. en. *Medical & Biological Engineering & Computing* 50.12, 1249–1259. DOI: 10.1007/s11517-012-0957-x.

Veiga, J., Lopes, A. J., Jansen, J. M. and Melo, P. L. (2011). Airflow Pattern Complexity and Airway Obstruction in Asthma. en. *Journal of Applied Physiology* 111.2, 412–419. DOI: 10.1152/japplphysiol.00267.2011.

Venegas, J. G., Winkler, T., Musch, G., Vidal Melo, M. F., Layfield, D., Tgavalekos, N., Fischman, A. J., Callahan, R. J., Bellani, G. and Scott Harris, R. (2005). Self-Organized Patchiness in Asthma as a Prelude to Catastrophic Shifts. en. *Nature* 434.7034, 777–782. DOI: 10.1038/nature03490.

Ventica (2019). https://www.ventica.net/.

Vuorela, T., Seppä, V.-P., Vanhala, J. and Hyttinen, J. (2010). Design and Implementation of a Portable Long-Term Physiological Signal Recorder. *IEEE Transactions on Information Technology in Biomedicine* 14.3, 718–725. DOI: 10.1109/TITB.2010.2042606.

Vuorela, T. (2011). Technologies for Wearable and Portable Physiological Measurement Devices - Tampere University of Technology. PhD thesis.

Walraven, D., van der Grinten, C. P. M., Bogaard, J. M., van der Ent, C. K. and Luijendijk, S. C. M. (2003). Modeling of the Expiratory Flow Pattern of Spontaneously Breathing Cats. *Respiratory Physiology & Neurobiology* 134.1, 23–32. DOI: 10.1016/S1569-9048(02)00206-9.

Weibel, E. R., Cournand, A. F. and Richards, D. W. (1963). *Morphometry of the Human Lung*. en. Vol. 1. Berlin Heidelberg: Springer-Verlag.

Wheatley, West, S., Cala, S. J. and Engel, L. A. (1990). The Effect of Hyperinflation on Respiratory Muscle Work in Acute Induced Asthma. en. *European Respiratory Journal* 3.6, 625–632.

Widdicombe, J. G. (1961). The Activity of Pulmonary Stretch Receptors during Bronchoconstriction, Pulmonary Oedema, Atelectasis and Breathing against a Resistance. *The Journal of Physiology* 159.3, 436–450.

Willemen, T., Deun, D. V., Verhaert, V., Vandekerckhove, M., Exadaktylos, V., Verbraecken, J., Huffel, S. V., Haex, B. and Sloten, J. V. (2014). An Evaluation of Cardiorespiratory and Movement Features With Respect to Sleep-Stage Classification. *IEEE Journal of Biomedical and Health Informatics* 18.2, 661–669. DOI: 10.1109/JBHI.2013.2276083.

Wilson, A. J., Franks, C. I. and Freeston, I. L. (1982). Methods of Filtering the Heart-Beat Artefact from the Breathing Waveform of Infants Obtained by Impedance Pneumography. en. *Medical and Biological Engineering and Computing* 20.3, 293–298. DOI: 10.1007/BF02442795.

Witsoe, D. A. and Kinnen, E. (1967). Electrical Resistivity of Lung at 100 kHz. *Medical and Biological Engineering and Computing* 5.3, 239–248.

World Health Organization (2018). *World Health Statistics 2018: Monitoring Health for the SDGs*. English.

Wysocki, M., Fiamma, M.-N., Straus, C., Poon, C.-S. and Similowski, T. (2006). Chaotic Dynamics of Resting Ventilatory Flow in Humans Assessed through Noise Titration. *Respiratory Physiology & Neurobiology* 153.1, 54–65. DOI: 10.1016/j.resp.2005.09.008.

Young, S., Arnott, J., Le Souef, P. N. and Landau, L. I. (1994). Flow Limitation during Tidal Expiration in Symptom-Free Infants and the Subsequent Development of Asthma. en.

PUBLICATION

P.I

Nonlinear Local Projection Filter for Impedance Pneumography

J. Gracia, V.-P. Seppä, A. Pelkonen, A. Kotaniemi-Syrjänen, M. Mäkelä, P. Malmberg and J. Viik

Nonlinear Local Projection Filter for Impedance Pneumography

J. Gracia[1], V-P. Seppä[1], A. Pelkonen[2], A. Kotaniemi-Syrjänen[2], M. Mäkelä[2], P. Malmberg[2] and J. Viik[1]

[1] BioMediTech Institute and Faculty of Biomedical Sciences and Engineering, Tampere University of Technology, Tampere, Finland
[2] Department of Allergology, University Central Hospital, Helsinki, Finland

Abstract— **The ability of impedance pneumography (IP) for recording tidal flow during long periods of free breathing make it a promising tool for assessing temporal complexity of respiration. However, techniques quantifying complexity may be sensitive to the noise in the IP signal resulting from the current processing method. A nonlinear local projection filter (NLPF) is presented as the solution to the current linear processing method, failing to reduce noise without distorting the flow signal. Current and proposed NLPF methods were applied to and existing data set of raw IP recorded in 21 infants during a methacholine challenge test. Methods' performance was compared in a battery of test using mouth flow as a reference. NLPF achieved lower sample-by-sample error, and higher frequency attenuation, while linearity with mouth flow was maintained. Therefore, we concluded that NLPF superiorly reduces noise without distorting respiratory information.**

Keywords— **Impedance pneumography, nonlinear filter, noise reduction ,lung function**

I. INTRODUCTION

Latest trend in respiratory medicine sees respiration as a complex homokinetic process. According to this, the degree of adaptivity of the respiratory system, exhibited degree of complexity in breathing paterns over minutes or hours, represents a more accurate indicator of disease than traditional lung function measured at a single moment [1, 2]. In this context, impedance pneumography (IP), using skin electrodes to monitor tidal flow during long terms of free breathing, emerges as a promising tool to assess respiration adaptivity.

However, limitations of the current processing method to reduce signals' noise may compromises the accuracy of the techniques used to quantify respiration complexity [3]. Specifically, in current IP's processing, measurement noise is amplified during the differentiation of recorded volumetric IP into flow performed by a linear Savitzky-Golay filter (SG). Noise can be attenuated by shortening the SG's fitting frame, but at the price of smoothing out fast transitions in the expiratory part of the flow.

As a solution, we propose to set a sort SG's frame, to keep flow integrity, and consequently, to reduce the noise with a non-linear projection filter (NLPF). NLPF distinguishes signals based on their predictability at different time scales. Respiratory signal is fairly predictable in the time spam of a breath, being easily unfold in a 2 dimensional phase space. Whereas, higher dimensions are needed to embed the trajectory of noise occurring in sorter time scales. NLPF exploits this principle to separate uncorrelated signals overlaping in frequency. The target signal is over-embedded into a high dimension space. Subsequently, each point is protected into a lower dimension manifold define as the best fit of the local neighbouring samples. Result is a lower dimension representation of the original signal.

Performance of the proposed and current methods is compared using an existing 64 signals data set, containing reference mount flow.

II. MATERIALS AND METHODS

A. Data set:

The set of signals was previously recorded by Seppä et al. [4]. It contained simultaneous recordings of direct mouth pneumotachograph ($\dot{V}_{PNT}$), IP (V_{IPraw}), and electrocardiogram (*ECG*), lasting 60 s. Recordings were performed in 21 sitting children aged 3-7 years, during tidal breathing in four different stages of a methacholine challenge test. Two base line recordings performed before the test (BL1 and BL2), one during methacholine-induced bronchoconstriction (MIB), and a last one 10 min after inhalation of a bronchodilator (BRD). Corrupted tracings were rejected after visual inspection, leaving a total of 64 recordings.

B. Current HRSG:

For each IP raw signal (V_{IPraw}), the cardiac component was removed using an ensemble average method developed for this purpose [5].

Resulting volumetric component of the IP signal was ran through a SG filter of order 2 and a fitting frame duration proportional to each recording's hear rate. Specifically, fitting frame was one fifth of the median of the R-R intervals, thus being on the range of 100 to 170 ms. This outputted a flow related signal named $\dot{V}_{IP-HRSG}$.
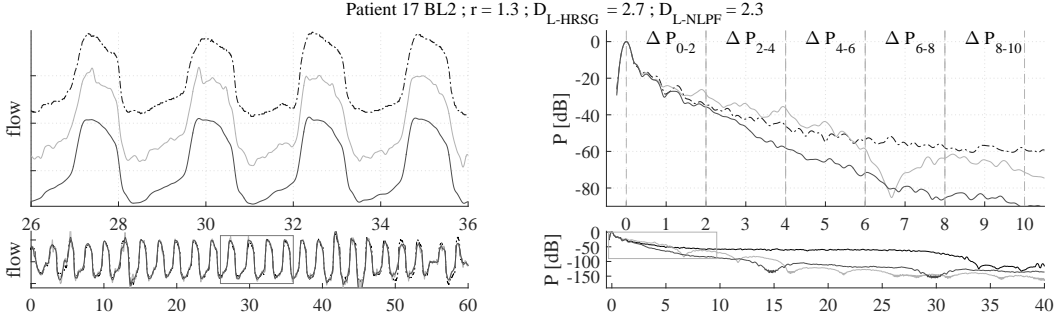
Fig. 1: Time and frequency results for a representative 60 s recording. Lower left plot overlaps reference mouth flow ($\dot{V}_{PNT}$:- · - · -); HRSG method output ($\dot{V}_{IP-HRSG}$:——); and NLPF method output ($\dot{V}_{IP-NLPF}$:——). Upper left plot show a zoomed 10 s section, where signals have been unfolded for clarity. Lower right plot shows the normalised power spectral density for the same signals. Upper left plot shows a zoomed 10xHR wide section. Dashed lines mark the six frequency bands used for the frequency analysis. Upper text denote calculated parameters for this specific recording.

C. Proposed NLPF:

Signals at the output of the CGO filter, were ran through a SG filter with fixed fitting frame duration of 66.4 ms (1/15 s). This resulted in a less distorted but noisier flow signal.

In order to reduce the computational cost of the nonlinear filter the SG's output was previously decimate by a factor 10. Prior to decimation a low pass anti-aliasing filter with cut of frequency $13Hz$ was applied. This decimation processes involved non significant lost of information as the first zero of the SG filter frequency response falls around $21.5Hz$ [6].

NLPF was applied using the *"ghkss"* function from the TISEAN package [7]. Embedding dimension was fixed to 18 and time delay to 1 sample. This made a embedding window in the range of 1/3 a and 1/4 of the respiratory cycle as recomende in literature [8]. Neighbourhood radius was chosen to include the highest observed noise amplitude -that being 30% of signal's standard deviation-, or containing a minimum of 20 samples. Samples were projected in to a two dimensions linear manifold. This process was iterated 2 times. Resulting signal was resampled to the original frequency ($256Hz$) by spline interpolation and named $\dot{V}_{IP-NLPF}$.

D. Comparison analysis

Agreement with PNT. Agreement of both processing outputs with the reference mouth flow was assessed for each measurement using the parameters described by Seppä et. al [4]. Average discrepancy between signals was measured by the sample-by-sample absolute difference (*Dss*). Calculated as the median of $d(n) = |\dot{V}_{PNT}(n) - \dot{V}_{IP}(n)|$, with n all signals' samples. Discrepancies at different phases of respiration was assessed using a deviation from linearity plot. Briefly,

$\dot{V}_{PNT}$ and $\dot{V}_{IP}$ were normalized to their median tidal inspiratory flow (TPIF). Perpendicular residuals of a linear regression between the two flows were calculated. Residuals were grouped into 10 bins of size 25% of the $\dot{V}_{PNT}$ range. Median for each bin were defined as $D_{bin,m}$ with $m = 1..10$. Average deviation from linearity (D_L) was then computed as the mean of all $D_{bin,m}$.

Noise reduction. Parameter *Dss* is conditioned by the noise level in $\dot{V}_{PNT}$. Therefore, comparing HRSG and NLPF based on the difference on this absolute value may not show the true noise reduction when noise level in $\dot{V}_{PNT}$ is high.

We used the *noise reduction factor*, *r*, -originally intended for synthetic signals- suggested by Kapan and Schreiber [9] to assess the noise reduction in $\dot{V}_{IP-NLPF}$ relative to $\dot{V}_{IP-HRSG}$.

$$r = \sqrt{\frac{\langle(\dot{V}_{PNT}(n) - \dot{V}_{IP-HRSG}(n))^2\rangle}{\langle(\dot{V}_{PNT}(n) - \dot{V}_{IP-NLPF}(n))^2\rangle}}$$

A factor higher that 1 shows the proportion of noised removed by NLPF respect to the noise removed by HRSG.

Frequency analysis. Reduction distribution in frequency was assessed as the differences in power spectral of both outputs $\dot{V}_{IP-HRSG}$ and $\dot{V}_{IP-NLPF}$ respect the reference $\dot{V}_{PNT}$ at five different frequency bands. Power spectral density was estimated for each signal using an 8192 points Welch method with a $5s$ non-overlapping Hanning window. To allow comparison, spectra were normalised by centring the frequency to the respiratory frequency and scaling it to make the heart frequency one. Peak power was also normalized to zero for all signals. Differences between $P_{PNT} - P_{IP-HRSG}$ and $P_{PNT} - P_{IP-NLPF}$ were averaged within five equally sized bands between 0xHR and 10xHR (see Fig. 1). These parame-

Table 1: Linearity, noise, and frequency parameters

	BL1		BL2		MIB		BRD	
	IP-HRSG	IP-NLPF	IP-HRSG	IP-NLPF	IP-HRSG	IP-NLPF	IP-HRSG	IP-NLPF
Dss	5.7 ± 1.2	5.3 ± 1.0 *	6.7 ± 1.9	5.9 ± 1.7 *	6.9 ± 1.4	6.2 ± 1.6 *	7.5 ± 2.0 ‡	7.0 ± 2.0 *
D_L	2.4 ± 1.0	2.4 ± 1.0	3.0 ± 1.3	2.8 ± 1.4	2.6 ± 0.9	2.5 ± 0.9	3.1 ± 1.4	2.6 ± 1.4 *
r	1.1 ± 0.1		1.4 ± 0.7		1.2 ± 0.3 *		1.3 ± 0.6 †	
$\Delta P_{0.0-10.0}$	-5.1 ± 6.9	-10.5 ± 9.6*	-2.9 ± 8.4	-11.1 ± 10.0*	-4.7 ± 7.5	-9.9 ± 9.5*	-3.4 ± 8.4	-10.4 ± 9.4*

Values are means±SD. BL1 baseline 1; BL2 baseline 2; MIB methacholine-induced bronchoconstriction; BRD,broncodilator; IP-HRSG current processing method; IP-NLPF presented processing method; *$P < 0.05$, ‡$P < 0.01$, between mean BL1 and BL2 and the corresponding value; †$P < 0.015$ between MIB and BRD; *$P < 0.01$ between IP-HRSG and IP-NLPF
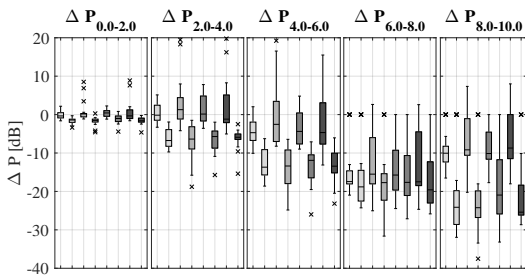

Fig. 2: Frequency attenuation $\Delta P_{f_1-f_2}$ across patients for SGHR and NLPF, grouped by methacholine phase and frequency band. Separated plots denote frequency bands. Colours correspond to phases as: ▪ BL1, ▪ BL2, ▪ MIB, and ▪ BRD. Pairs of equal colour plotboxes results for SGHR left and NLPF right.Boxes denote the 25th-75th percentiles; middle lines the median; whiskers extreme values; and crosses outliers;

ter are refereed in the text as $\Delta P_{f_1-f_2}$, where f_1 and f_2 denote the frequency band in multiples of the hear rate (xHR). Average of all five bands is named ΔP_{0-10}.

Statistical analysis. A paired Wilcoxon signed rank test was used for comparing the changes in Dss, D_L, r, and all ΔP between methods with in each phase; and between phases with in each method.

III. RESULTS

Time plot of both methods' output and mouth flow for a representative recording is shown in Fig.1. $\dot{V}_{IP-NLPF}$ appeared smoother than $\dot{V}_{IP-HRSG}$ without loosing the resemblance with $\dot{V}_{PNT}$.

Power spectra for the same recordings are presented in Fig.1. Characteristics drops in power occurred at $30Hz$ for P_{PNT} due to denoising low pass filter; at multiples of $26Hz$ for P_{NLPF} due to down-sapling; and at multiples of $6.8xHR$

caused by the heart rate dependent frame in the SG filter [6].

Results for attenuation in the five frequency bands ($\Delta P_{f_1-f_2}$) for the outputs of SGHR and NLPF is summarized as boxplots separated by methacholine test phases in 2. Each boxplot represents the distribution across patients. Positive values for HRSG in the lower bands indicate that outputted respiratory component is contaminated with additional noise compared to mouth flow. Whereas, negative values for NLPF suggest that noise level is reduced even under the noise levels of PNT. For high frequency bands (ΔP_{6-8}, ΔP_{8-10}, and higher) both showed noise attenuation, being NLPF higher.

Mean and standard deviation (mean±SD) of all parameters along patients for both processing methods are grouped in Table. 1 for the four methacholine test phases. Apart from these reported by Seppä et al. in Dss, statistically significant differences between groups were found in r for mean BL1 and BL2 vs. MIB (P=0.035), but not vs. BRD (P=0.79), and in a lesser extent for BRD vs. MIB (P=0.14). Significant differences between methods was found for all groups in Dss and $\Delta P_{f_1-f_2}$, and in BRD for D_L.

Deviation from linearity plots for $\dot{V}_{PNT}$ vs. $\dot{V}_{IP-HRSG}$ and $\dot{V}_{IP-NLPF}$ are shown in Fig 3. NLPF presented means slightly closer to 0 for all flow levels and phases, except under -100, where high means and percentiles were cause by the low number of samples on these bins.

IV. DISCUSION

Statistical significant decreases in Dss, all ΔPs between methods, and one r, suggest that NLPF method further reduces the stochastic noise in the IP flow when compared to the current HRSG method. Moreover, not significant changes -or decrease for BRD- in D_L confirms that removed components are uncorrelated to the mouth air flow.

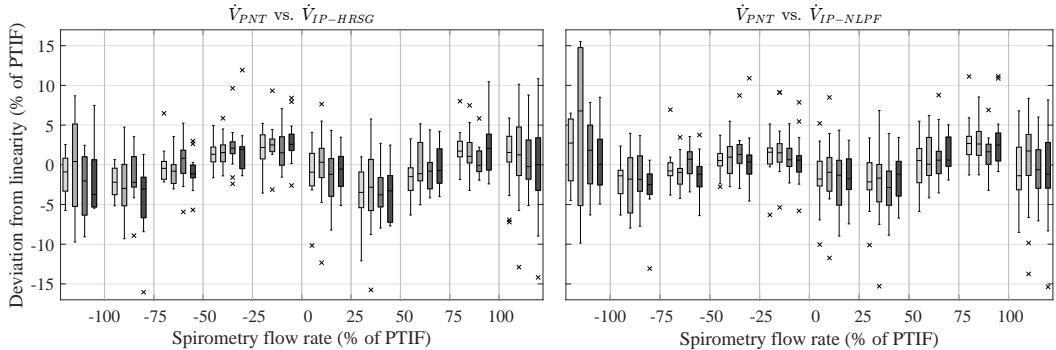Statistically significant difference in r for MIB relative

Fig. 3: Deviation from linearity plot for $\dot{V}_{PNT}$ vs. $\dot{V}_{IP-HRSG}$ (left) and $\dot{V}_{PNT}$ vs. $\dot{V}_{IP-NLPF}$ (right). Boxes denote the 25th-75th percentiles; middle lines the median; whiskers extreme values; and crosses outliers; Colours correspond to phases as: ■ BL1, ■ BL2, ■ MIB, and ■ BRD.

to the other phases was likely due to the increase in heart rate during this phase. Wilcoxon signed rank tests for differences in median, these being 1.22, 1.18, and 1.09 for MIB, BRD and mean BL1 and BL2 respectively. Whereas, median heart rate for the same phases was $91.94bpm$, $87.27bpm$, and $88.27bpm$. Increased hear rate meant a shorter fitting frame in HRSG leading to noisier $\dot{V}_{IP-HRSG}$, and thus higher r. This difference did not appear in Dss. Presumably, because this parameters was affected by the noise in $\dot{V}_{PNT}$. Otherwise, performance of NLPF was not degraded by possible differences in breathing due to obstruction.

Five cases were found with r moderately lower than 1, indicating a better performance of HRSG. Visual inspection showed that rare events on tidal breathing were the source of error for NLPF. For example, a breathing cycle with an abnormal shape than the rest of the recording, or a sudden spike on breathing. We believe that if applied to signals longer than $60s$, these errors won't dismiss the performance of NLPF. These rear event will not be attenuated if they repeat. Moreover, if they appear only once, can be consider as an stochastic phenomena and its attenuation is justified for the variability analysis techniques. Nonetheless, further research must be done in this direction.

V. CONCLUSIONS

The use of a NLPF allows to decrease the fitting frame of the SG filter for deriving a lower noise differentiate IP signal while maintain linearity with the mouth flow. This improvement opens new possibilities for IP instrumentation in the assessment of temporal complexity of the respiratory system.

VI. CONFLICT OF INTEREST

V.-P. Seppä and J. Viik are shareholders in Tide Medical Oy that holds patents relating to impedance pneumography. V.-P. Seppä is an employee of Revenio Group Oyj that commercialises impedance pneumography technology.

VII. ACKNOWLEDGEMENT

REFERENCES

1. Thamrin C, et al . Systems Biology and Clinical Practice in Respiratory Medicine. The Twain Shall Meet *AJRCCM.* 2016;194:1053–1061.
2. Frey U, Geoffrey G, Suki B. Temporal complexity in clinical manifestations of lung disease *J Appl Physiol.* 2011;110:1723–1731.
3. Bravi A, Longtin A, et al . Review and classification of variability analysis techniques with clinical applications *BioMed Eng.* 2011;10:90.
4. Sepp V-P, et al . Tidal breathing flow measurement in awake young children by using impedance pneumography *J Appl Physiol.* 2013;115:1725–1731.
5. Seppä V-P, Hyttinen J, Viik J. A method for suppressing cardiogenic oscillations in impedance pneumography *P Meas.* 2011;32:337.
6. Schafer R. On the frequency-domain properties of Savitzky-Golay filters in *Proc. 2011 DSP/SPE Workshop*:54–59 2011.
7. Hegger R, Kantz H., Schreiber T. Practical implementation of nonlinear time series methods: The TISEAN package *Chaos.* 1999;9:413.
8. Kugiumtzis D. State space reconstruction parameters in the analysis of chaotic time series *Physica D..* 1996;95:13–28.
9. Schreiber T, Kaplan D. Nonlinear noise reduction for electrocardiograms *Chaos.* 1996;6:87–92.

PUBLICATION

P.II

Tidal Breathing Flow Volume Profiles during Sleep in Wheezing Infants Measured by Impedance Pneumography

J. Gracia-Tabuenca, V.-P. Seppä, M. Jauhiainen, A. Kotaniemi-Syrjänen, K. Malmström, A. Pelkonen, M. J. Mäkelä, J. Viik and L. P. Malmberg

RESEARCH ARTICLE

Tidal breathing flow volume profiles during sleep in wheezing infants measured by impedance pneumography

Javier Gracia-Tabuenca,[1] Ville-Pekka Seppä,[1] Milla Jauhiainen,[1] Anne Kotaniemi-Syrjänen,[2] Kristiina Malmström,[2] Anna Pelkonen,[2] Mika Mäkelä,[2] Jari Viik,[1] and L. Pekka Malmberg[2]

[1]*Faculty of Biomedical Sciences and Engineering, Tampere University of Technology, Tampere, Finland; and* [2]*Department of Allergology, University Central Hospital, Helsinki, Finland*

Submitted 14 November 2018; accepted in final form 5 February 2019

Gracia-Tabuenca J, Seppä VP, Jauhiainen M, Kotaniemi-Syrjänen A, Malmström K, Pelkonen A, Mäkelä M, Viik J, Malmberg LP. Tidal breathing flow volume profiles during sleep in wheezing infants measured by impedance pneumography. *J Appl Physiol* 126: 1409–1418, 2019. First published February 14, 2019; doi: 10.1152/japplphysiol.01007.2018.—Overnight analysis of tidal breathing flow volume (TBFV) loops, recorded by impedance pneumography (IP), has been successfully applied in the home monitoring of children with wheezing disorders. However, little is known on how sleep physiology modifies the relationship between TBFV profiles and wheeze. We studied such interactions in wheezing infants. Forty-three infants recruited because of recurrent lower airway symptoms were divided into three groups based on their risk of asthma: high (HR), intermediate (IR), or low (LR). Sedated patients underwent infant lung function testing including assessment of airway responsiveness to methacholine at the hospital and a full-night recording of TBFV profiles at home with IP during natural sleep. Overnight TBFV indexes were estimated from periods of higher and lower respiration variability, presumably belonging to active [rapid eye movement (REM)] and quiet [non-REM (NREM)] sleep, respectively. From 35 valid recordings, absolute time indexes showed intrasubject sleep phase differences. Peak flow relative to time and volume were lower in HR compared with LR only during REM, suggesting altered expiratory control. Indexes estimating the concavity/convexity of flow decrease during exhalation suggested limited flow during passive exhale in HR compared with LR, similarly during NREM and REM. Moreover, during REM convexity was negatively correlated with maximal flow at functional residual capacity and methacholine responsiveness. We conclude that TBFV profiles determined from overnight IP recordings vary because of sleep phase and asthma risk. Physiological changes during REM, most likely decrease in respiratory muscle tone, accentuate the changes in TBFV profiles caused by airway obstruction.

NEW & NOTEWORTHY Impedance pneumography was used to investigate overnight tidal breathing flow volume (TBFV) indexes and their interactions with sleep phase [rapid eye movement (REM) vs. non-REM] at home in wheezing infants. The study shows that TBFV indexes vary significantly because of sleep phase and asthma risk of the infant and that during REM the changes in TBFV indexes caused by airway obstruction are accentuated and better associated with lung function of the infant.

bronchial hyperresponsiveness; impedance pneumography; infants; lung function; tidal breathing; wheezing

---

Address for reprint requests and other correspondence: J. Gracia-Tabuenca, SM319, Korkeakoulunkatu 10, FI-33720, Tampere, Finland (e-mail: javier. graciatabuenca@tuni.fi).

INTRODUCTION

Analysis of tidal flow volume (TBFV) loops is one of the most convenient lung function testing techniques for infants, whose lack of cooperation limits performance of conventional spirometry (3). Assessing TBFV profiles overnight at home, rather than during short periods at the hospital, could bring new insights in diseases with circadian worsening such as asthma (5). Impedance pneumography (IP) is a noninvasive method that enables for the first time continuous recording of TBFV profiles overnight (41). IP uses four surface skin electrodes to record changes in the thoracic electrical impedance, which are proportional to changes in respiratory lung volume. Other noninvasive methods, such as respiratory inductive plethysmography, lack the precision to derive tidal flow (17), whereas IP has shown high correspondence between IP and pneumotachograph recorded in children and infants with and without induced bronchoconstriction (27, 40).

TBFV profiles are shaped by the complex interactions between the passive mechanical properties of the respiratory system and the active control of respiratory musculature (2). During expiration, passive characteristics include thoraco-pulmonary recoil and airway resistance (32). In infants, the immature chest wall is highly compliant. If expiration was solely passive, lung volume would rapidly decrease to a critically low resting volume, allowing little time for gas exchange and causing end-expiratory airway closure (31). To avoid this, infants employ different active mechanisms. From the beginning of expiration, infants support the fast passive exhale by prolonging the postinspiratory inspiratory activity (PIIA) of intercostal and diaphragm muscles and, more typically neonatally (10), by increasing laryngeal airway resistance. Toward the end, infants recruit respiratory musculature to interrupt expiration and start the following breath before reaching resting volume. Interaction of all these mechanisms dynamically maintains an elevated functional residual capacity (FRC) (19, 22, 23). Airway obstruction has a direct effect on the passive respiratory mechanics and an indirect effect on respiratory control. Narrower airways increase resistance, slowing passive exhale. However, active adaptation to this mechanical deficiency is less well understood. In adults, it has been speculated that PIIA is shortened to accommodate the slower passive exhale (30). What seems empirically consistent is that obstructed infants more often present early expiratory peaks and concave TBFV profiles (9, 16, 36).

Likely because of the lack of noninvasive recording systems, little is known about how sleep physiology may affect TBFV profiles. Compared with the awake state, sleep presents a lower intercostal, diaphragm, and upper airway muscle tone, which is further reduced during rapid eye moment (REM) (24a). In infants, this lower intercostal tone is known to expose the low compliance of the chest wall (11) and increase the contribution of the diaphragm to respiration (15). These natural changes in musculature most likely influence TBFV profiles.

The aim of this study was to assess the ability of TBFV profiles, determined from home overnight IP recordings, to detect airway obstruction in wheezing infants and classify infants by their risk of asthma. It also investigated the extent to which REM and non-REM (NREM) sleep, respectively defined as regions of higher and lower respiration variability, affect this ability.

MATERIALS AND METHODS

Study subjects and data collection. The study included 43 infants who were referred for infant lung function testing because of troublesome respiratory symptoms such as wheeze, cough, and/or laborious breathing and who underwent infant lung function tests. Short-acting beta2-agonists were withheld for at least 12 h preceding the tests.

A standardized questionnaire, including questions on parental asthma, was filled in by the parents, and the probability of persistent asthma was estimated on the basis of these and clinical records. We applied loose criteria of the modified Asthma Predictive Index (mAPI): Children with a history of multiple episodes of wheeze (at least 2) and who fulfilled one of the major criteria (parental history of asthma, atopic dermatitis, sensitization to respiratory allergens), were considered to have a high risk

(HR) of asthma. Those children who did not have a history of wheeze or did not fulfill any of the above major criteria were considered to have low risk (LR). Infants who fell between the criteria of HR and LR were considered to have intermediate risk (IR).

Before the lung function measurements, the infants were clinically examined to exclude current respiratory infection. The infants were sedated with orally administered chloral hydrate (50–100 mg/kg; maximum dose 1,000 mg). All measurements were performed with commercial pediatric pulmonary function equipment (Babybody Masterscreen; Jaeger, Würzburg, Germany) as described previously (24, 28). FRC and specific airway conductance (sGaw) was assessed by the plethysmographic method and the maximum flow at FRC ($\dot{V}_{maxFRC}$) was determined with the rapid thoracoabdominal compression (RTC) technique (43). The lung function data were converted to z scores adjusting for weight, length, and/or sex (18). z scores below -1.96 in sGaw or $\dot{V}_{maxFRC}$ were defined as abnormal and indicative of reduced lung function.

A subgroup of infants underwent a bronchial provocation test with methacholine in which increasing doses of methacholine chloride were administered with an inhalation-synchronized dosimeter (Spira Electro 2; Spira Respiratory Care Centre, Hämeenlinna, Finland), as described previously (24). The procedure was continued until a 40% decrease in $\dot{V}_{maxFRC}$ was observed or the maximum dose of methacholine had been administered. From the dose-response curves, the dose of methacholine producing a 40% decrease in $\dot{V}_{maxFRC}$ (PD40) was calculated with logarithmic interpolation.

After lung function testing, the impedance pneumograph was installed on the subjects for overnight continuous recording of IP and ECG signals. The current-feeding electrodes were placed on both sides of the thorax on the midaxillary line at the height of the fifth intercostal space and the voltage measurement electrodes on the arms opposing the other electrode pair as described previously (38).
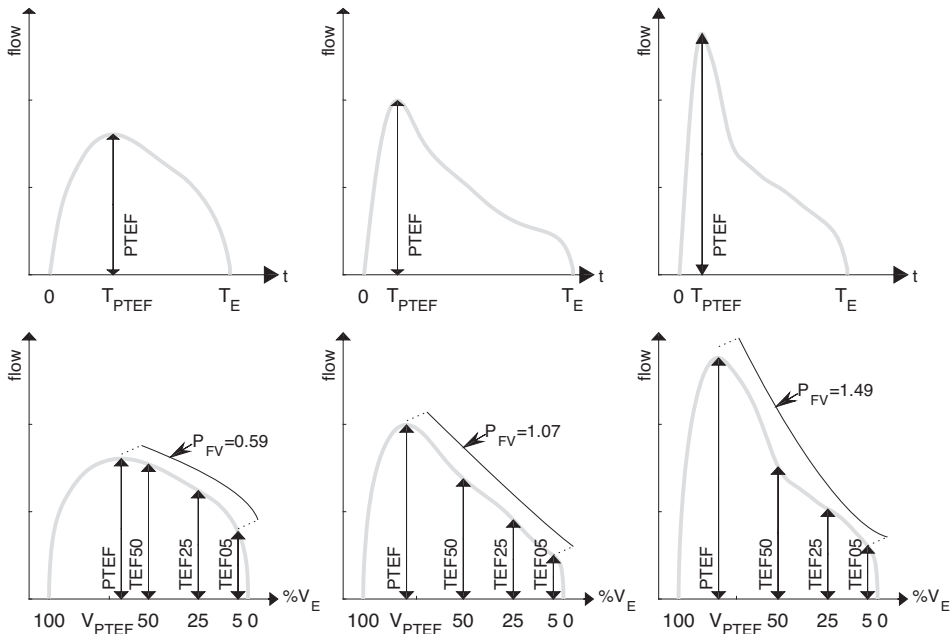

Fig. 1. TBFV indexes for 3 representative expiration limbs. Plots for flow-time domain (*top*) and flow-volume domain (*bottom*), normalized to area 1 and volume 1, respectively. Light gray lines represent the expiration signals, arrowed lines measured distances, and solid lines the power fitted line. Power fit line displaced for clarity; dotted lines indicate the fitting location. See GLOSSARY for abbreviations.

The study was approved by the institutional pediatric committee of Helsinki University Central Hospital (approval no. 53/13/03/03/2012). The tests were conducted after written informed consent was received from the parents.

Data preprocessing. All signal processing and statistical analyses were performed with MATLAB software (MATLAB R2017a; Math-Works, Natick, MA). A trained researcher, who was blind to patient information, visually discarded those sections corrupted by motion or other distortions within each recording. A specifically developed algorithm filtered the cardiac component out of the IP sections (39). This process yielded a lung volume-oriented IP signal, which was differentiated into a flow-oriented IP signal with a Savitzky-Golay filter. Remaining noise was consequently mitigated by means of a nonlinear projection filter applied in 4-min windows (12). Cleaned flow and volume signals were split into respiratory cycles with "Algorithm 4" described by Schmidt et al. (36a) in which time and volume thresholds were dynamically adjusted within 4-min windows as 0.3 times the median of all respiratory period and 0.3 times the median of all tidal volumes. Split respiratory cycles were transformed to TBFV profiles. The resulting TBFV profiles were averaged in the flow-volume domain, as described by Sato and Robbins (35), by means of a 20-TBFV moving window with 5-TBFV overlap.

Tidal breathing indexes. Without previous calibration, absolute volume or flow rate cannot be derived from IP. For this reason, each averaged TBFV profile was normalized to unit volume and flow was scaled accordingly (35). For each profile the following distances were measured as recommended (3): expiratory time (T_E), peak tidal expiratory flow (PTEF), time to peak tidal expiratory flow (T_{PTEF}), and tidal expiratory flow when 50%, 25%, and 5% of tidal volume remains in the lungs (TEF50, TEF25, and TEF05, respectively). Additionally, we suggested a new measure of shape, named P_{FV}. It is calculated as the exponent of a power function fitted to the section between PTEF and TEF05 as $v(f) = Af^{P_{FV}}$. Figure 1 shows measurements in three different TBFV profiles. These measurements combined or alone were used to estimate active and passive characteristics of expiration, as follows.

The balance between active expiratory braking and passive exhale was estimated based on conventional measures T_{PTEF}, T_{PTEF}/T_E, and V_{PTEF}/V_E. A shorter T_{PTEF} has been linked to the faster decay of the PIIA (8). Since T_{PTEF} varies with maturation (45), more often, relative ratios T_{PTEF}/T_E and V_{PTEF}/V_E are used for intersubject comparison. Putatively, these ratios reflect the proportion of active and passive exhale on a TBFV (30). For example, a low T_{PTEF}/T_E indicates that a
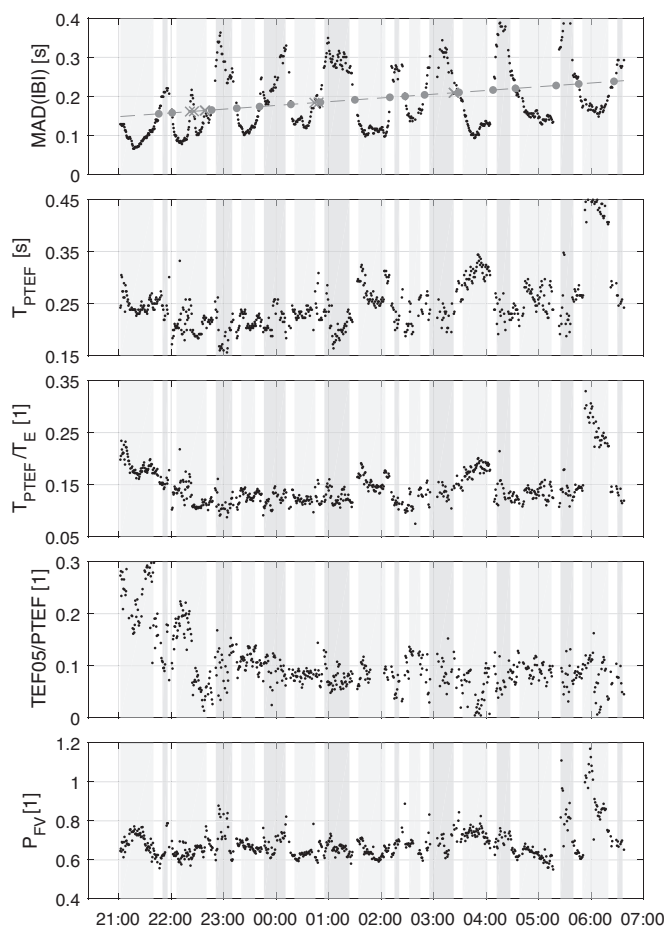

Fig. 2. Overnight evolution of some TBFV indexes for a representative patient. *x*-Axes show the time in hours. *y*-Axes show the values for 5 different indexes. Grey and light gray boxes highlight the estimated NREM and REM periods, respectively. First plot [MAD(IBI)] shows how sleep periods were estimated. Dashed line shows the linear fit; circles and crosses indicate valid and rejected crossings, respectively. See GLOSSARY for abbreviations.

larger portion of the expiration was passive, because of decrease in PIIA (lower T_{PTEF}), delay of expiration interruption (higher T_E), or both. Empirically, decrease in both ratios has shown correspondence with increased obstruction (9, 36).

The influence of passive mechanical characteristics was estimated from TEF50/PTEF, TEF25/PTEF, and P_{FV}. Relative ratios TEF50/PTEF and TEF25/PTEF reflect flow in the middle to late portion of the expiration, where the influence of PIIA is supposedly lower. Increased airway resistance is thought to cause lower flow during this period, leading to lower ratios (16). The suggested index, P_{FV}, rather than two points, takes into account the full portion of uninterrupted decreasing flow against volume. P_{FV} is 1 for a linear decrease, between 1 and 0 for a convex decrease, and >1 for a concave decrease. Putatively, increase in P_{FV} is associated with an increase in obstruction.

TEF05/PTEF was used as an estimation of early expiration interruption similar to previous works (7, 36). Putatively, a lower flow close to the end of exhale suggests that exhale continued without interruption until volume was close to resting volume, and vice versa.

Sleep segmentation. Several studies, summarized by Willimen et al. (47), have shown that an increase in the variability of respiratory frequency is a reliable estimator for REM versus NREM sleep. Similar studies have also been conducted in infants (20). In light of this, we developed an automated method to separate the overnight areas with higher and lower respiration variability. For each patient the interbreath interval signal (IBI) was formed as the time distances between begining of inspirations. At each time location of the averaged TBFV profiles, respiration variability was calculated as the median absolute deviation (MAD) of the intervals within the preceding and following 2.5-min region. An example of the resulting MAD(IBI) signal overnight for a representative patient is shown in the first plot of Fig. 2.

Instead of defining a constant linear threshold as Isler et al. (20), we fitted a line to the full signal that was then set as a threshold. Consequently, crossing points on the threshold line were marked. If time between two consecutive crossings was <10 min, both crossings were rejected. Sections between valid crossings were marked as REM if most samples were over the line and NREM otherwise. Samples

within 5 min around the valid crossing were removed for further analysis.

Statistical analysis. For each subject, we calculated the median of all-night TBFV indexes within the REM sections as well as the median of all TBFV indexes within the NREM sections. The same was done for the mean IBI, mean heart rate, and MAD(IBI). P_{FV} indexes for which the fitted function had a determination coefficient below 0.95 were omitted. Median values were used to assess differences between groups and sleep phases. A Wilcoxon signed-rank test assessed differences between NREM and REM within subjects separately for the three groups. A Wilcoxon rank sum test assessed group differences separately for NREM and REM; Bonferroni correction was applied ($n = 3$). Moreover, correlations between TBFV indexes and between TBFV indexes and lung function indexes were calculated with Spearman's rank correlation. Population characteristics and lung function between groups were compared by Kruskal-Wallis test for continuous variables or χ^2/Fisher's exact test for categorical variables, both with Bonferroni correction ($n = 3$).

RESULTS

Out of the 43 overnight recordings, 8 were rejected because of battery or electrode problems. Successfully recorded infants were classified in the three above-described groups according to their risk of asthma, leading to 8 infants in LR, 12 in IR, and 15 in HR groups. Table 1 summarizes the characteristics and lung function of each group. Night recordings were on average 9.74 h (SD 0.84) long. On average 28.34% (SD 6.71) of the night recordings were discarded for being corrupted or falling between sleep phases. On average 32.45% (SD 6.70) of the accepted data was classified as REM, with no significant differences between groups. Table 2 summarizes the median values during all-night NREMs and REMs for all patients for all parameters and significant differences between sleep phases and groups. Figure 3 plots the median values for four selected indexes.

REM relative to NREM for all groups showed, evidently, an increased IBI variability [MAD(IBI)] and, expectedly, a higher

Table 1. *Characteristics of study infants*

	LR	IR	HR
Subjects	8	12	15
Male	4 (50)	9 (75)	11 (73)
Age, mo	14.81 (7.27–23.57)	13.23 (6.70–21.10)	14.47 (7.50–23.83)
Gestational age, wk	41.43 (40.00–42.29)[a]	38.57 (30.86–41.71)[b]	39.70 (36.29–42.0)[a,b]
Weight, kg	10.14 (8.60–12.60)	10.15 (7.70–12.60)	11.01 (7.40–15.00)
Skin prick test positive	1 (13)	2 (20)	6 (40)
Atopic eczema	1 (13)[a]	6 (55)	13 (87)[a]
Parental smoking	1 (13)	3 (25)	5 (33)
Parental asthma	4 (50)	5 (42)	8 (53)
Dominant respiratory symptom			
Cough	8 (100)[a]	8 (67)	5 (33)[a]
Wheeze	0 (0)	2 (17)	4 (27)
Dyspnea	0 (0)	2 (17)	6 (40)
Physician-diagnosed wheeze	0 (0)[a]	12 (100)[b]	15 (100)[a,b]
Inhaled corticosteroids	0 (0)	0 (0)	1 (7)
FRC, ml	231.3 (157.4–318.8)	230.4 (147.1–347.4)	208.3 (132.4–278.6)
FRC-z	1.04 (−1.30 to 3.80)	0.95 (−1.20 to 3.40)	−0.14 (−1.90 to 1.80)
sGaw, $kPa^{-1}\cdot s^{-1}$	2.61 (1.55–4.81)	3.41 (1.08–15.18)	3.09 (0.74–10.68)
sGaw-z	0.26 (−2.80 to 5.80)	2.18 (−3.80 to 31.18)	1.39 (−4.40 to 21.10)
$\dot{V}_{maxFRC}$, ml/s	289.33 (145.0–401.0)[a]	196.17 (75.0–365.0)	150.93 (29.0–320.0)[a]
$\dot{V}_{maxFRC}$-z	−0.22 (−1.30 to 0.70)[a]	−1.10 (−2.70 to 1.10)	−1.90 (−3.50 to −0.20)[a]
PD40, mg	1.49 (0.64–2.00)[a]	0.57 (0.18–1.12)	0.32 (0.05–1.03)

Data are presented as *n*, *n* (%), or mean (range). HR, high risk; IR, intermediate risk; LR, low risk. *P* values between groups determined by Kruskal-Wallis test (continuous variables) or χ^2/Fisher's exact test (categorical variables). Differences between paired groups with $P < 0.05$ after Bonferroni correction: [a]LR vs. HR; [b]IR vs. HR. See GLOSSARY for rest of abbreviations.

Table 2. *Median TBFV parameters during estimated NREM and REM sections overnight*

	LR	IR	HR
Subjects	8	12	15
t_{REM}/t_{Total}, %	0.31 (0.27 0.38)	0.34 (0.29 0.38)	0.33 (0.25 0.36)
MAD(IBI), s			
NREM	0.10 (0.09 0.11)*	0.11 (0.10 0.12)†	0.10 (0.09 0.11)‡
REM	0.26 (0.21 0.29)*	0.27 (0.22 0.31)†	0.25 (0.25 0.28)‡
Heart rate, beats/min			
NREM	102.93 (97.15 113.93)*	105.59 (97.55 112.98)†	104.83 (98.45 108.97)†
REM	111.00 (101.93 119.06)*	109.78 (105.65 119.28)†	109.41 (105.51 114.67)†
Respiratory rate, breaths/min			
NREM	23.36 (22.14 26.71)	23.15 (21.96 27.90)	23.26 (21.25 25.15)
REM	23.89 (21.60 27.92)	24.64 (21.37 29.37)	24.24 (22.24 25.94)
T_E, s			
NREM	1.54 (1.34 1.71)	1.63 (1.28 1.67)*	1.61 (1.44 1.84)†
REM	1.46 (1.23 1.63)	1.43 (1.15 1.63)*	1.50 (1.29 1.63)†
T_{PTEF}, s			
NREM	0.28 (0.26 0.29)*	0.26 (0.23 0.28)*	0.25 (0.23 0.30)‡
REM	0.25 (0.22 0.26)*	0.20 (0.19 0.26)*	0.21 (0.18 0.22)‡
T_{PTEF}/T_E			
NREM	0.18 (0.15 0.21)	0.17 (0.16 0.19)	0.16 (0.14 0.19)†
REM	0.17 (0.17 0.18)ᵃ	0.17 (0.14 0.17)	0.15 (0.13 0.16)†ᵃ
V_{PTEF}/V_E			
NREM	0.25 (0.22 0.27)	0.25 (0.24 0.27)	0.25 (0.23 0.27)†
REM	0.26 (0.25 0.27)ᵃ	0.25 (0.23 0.26)	0.24 (0.22 0.24)†ᵃ
TEF50/PTEF			
NREM	0.84 (0.81 0.87)	0.86 (0.83 0.88)	0.84 (0.78 0.86)†
REM	0.86 (0.80 0.88)ᵃ	0.83 (0.77 0.85)	0.78 (0.76 0.81)†ᵃ
TEF25/PTEF			
NREM	0.55 (0.52 0.58)	0.54 (0.52 0.58)	0.48 (0.45 0.56)*
REM	0.55 (0.49 0.57)ᵃ	0.53 (0.48 0.55)ᵇ	0.47 (0.42 0.49)*ᵃ,ᵇ
P_{FV}			
NREM	0.70 (0.67 0.79)	0.72 (0.69 0.76)ᵇ	0.78 (0.75 0.84)ᵇ
REM	0.68 (0.66 0.76)ᵃ	0.73 (0.70 0.79)ᵇ	0.81 (0.77 0.90)ᵃ,ᵇ
TEF05/PTEF			
NREM	0.15 (0.12 0.25)*	0.15 (0.10 0.17)	0.10 (0.06 0.17)
REM	0.11 (0.09 0.13)*	0.13 (0.09 0.14)	0.09 (0.06 0.14)

Values are medians (0.25 0.75 quartiles) and are stratified according to the 3 risk groups: low risk (LR), intermediate risk (IR), and high risk (HR). Indexes as described in text. Significant differences between sleep phases within each group tested by Wilcoxon signed-rank test: *$P < 0.05$, †$P < 0.01$, ‡$P < 0.001$. Significant differences between LR and HR: ᵃ$P < 0.05$. Significant differences between IR and HR: ᵇ$P < 0.05$, within the same sleep phases tested by Wilcoxon rank sum test. All P values after Bonferroni correction. See GLOSSARY for rest of abbreviations.

heart rate (42). T_E and T_{PTEF} were significantly shorter during REM for all groups, except for T_E in the LR group. However, their time and volume ratios (T_{PTEF}/T_E and V_{PTEF}/V_E) remained similar across sleep stages, except for the HR group, where they decreased significantly during REM. Relative flow indexes (TEF50/PTEF, TEF25/PTEF, and P_{FV}) remained similar to NREM, except for the HR group. For the HR group, TEF50/PTEF decreased significantly during REM ($P = 0.006$), TEF25/PTEF less significantly ($P = 0.012$), and P_{FV} nonsignificantly ($P = 0.07$). TEF05/PTEF deceased during REM significantly only for the LR group.

Differences between groups were not significant for heart rate, respiratory frequency, or respiration variability in any sleep stage. Neither absolute T_E nor T_{PTEF} was significantly different between groups. However, T_{PTEF}/T_E and V_{PTEF}/V_E were significantly lower for the HR group compared with the LR group during REM ($P = 0.018$ and $P = 0.009$, respectively) but not during NREM. Similarly, TEF50/PTEF and TEF25/PTEF showed a significant decrease in relative late flow during REM for the HR group compared with infants in the LR group ($P = 0.018$ and $P = 0.021$, respectively). Decrease was also significant for HR versus IR, but only for TEF25/PTEF ($P = 0.012$). P_{FV} was significantly increased in the HR group compared with LR and IR groups during both

sleep stages, indicating that the number and degree of concave profiles increased for subjects in the HR group compared with LR and IR groups during both sleep phases.

Table 3 summarizes the correlations of TBFV indexes against lung function indexes and infant age. Heart rate and respiratory rate decreased with maturation, as reported elsewhere (37). Low correlation with age was also seen for T_E. The number and degree of concave profiles during REM, assessed by P_{FV}, showed a significant correlation with lung function expressed as sGaw, sGaw-z, $\dot{V}_{maxFRC}$, and $\dot{V}_{maxFRC}$-z. Less strongly, TEF50/PTEF and TEF25/PTEF showed similar correlations with $\dot{V}_{maxFRC}$ and $\dot{V}_{maxFRC}$-z. Additionally, during REM decreases in $\dot{V}_{maxFRC}$-z were associated with an early flow peak relative to volume (V_{PTEF}/V_E). Finally, airway responsiveness to methacholine, assessed by PD40, correlated positively with TEF25/PTEF and negatively with P_{FV}, both indicating a decrease in relative late flow in hyperresponsive infants, illustrated in Fig. 4.

DISCUSSION

This study evidences the feasibility of IP for the home recording of tidal flow in infants and posterior analysis of TBFV profiles. It also demonstrates that dividing the night into
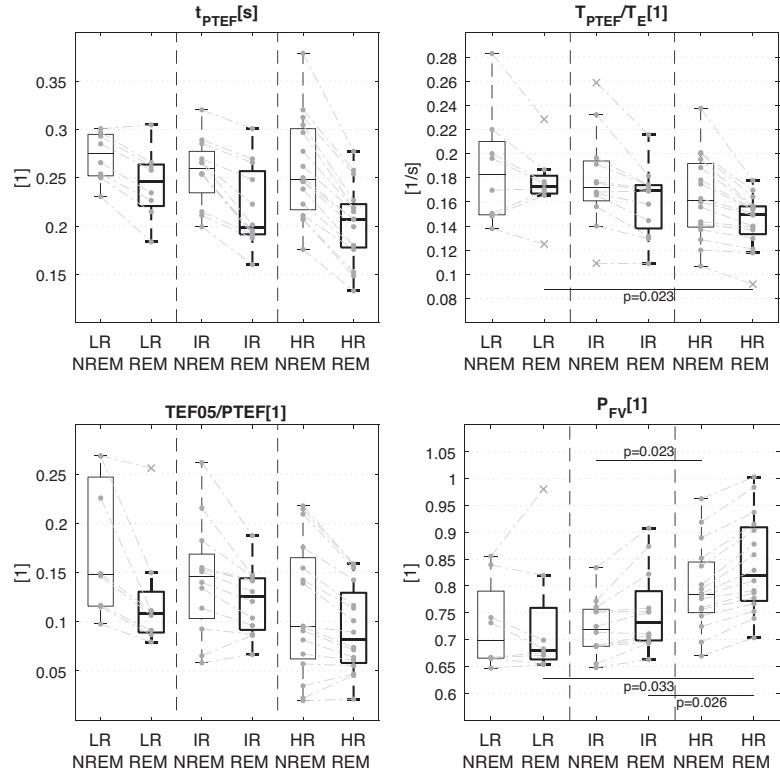
Fig. 3. Median values for 4 TBFV indexes. In each plot, a pair of points connected by dashed lines represents 1 subject. Values are the median of the index during all-night NREMs and REMs, for left and right points, respectively. Point pairs are divided into 3 groups: low risk (LR), intermediate risk (IR), and high risk (HR). For each group and sleep phase a corresponding box plot is overlaid. For outliers, the point is replaced by a cross. P value from a Wilcoxon signed-rank test with Bonferroni correction ($n = 3$) between groups within sleep phases is shown if $P <$ 0.05: NREM comparison, *top*; REM, *bottom*. See GLOSSARY for abbreviations.

regions of higher and lower IBI variability, as an estimation of REM and NREM sleep, reveals intrasubject differences in absolute time indexes (T_{PTEF} and T_E). Moreover, we found that relative TBFV indexes distinguished groups of infants with different risks of asthma and correlated well with conventional lung function, even with airway responsiveness to methacholine. Specifically, conventional TBFV indexes T_{PTEF}/T_E and V_{PTEF}/V_E, influenced by respiratory control and passive mechanics, differentiated high-risk patients only during REM. A newly introduced index, P_{FV}, mostly influenced by passive expiration, showed the most significant differentiated medians between groups, as assessed by a Wilcoxon signed-rank test. P_{FV} also presented the strongest correlation to lung function for both sleep phases, although with slightly better results for REM. In contrast, TEF05/PTEF, assessing control on late expiration, showed no significant relation to lung function or sleep.

Shortening of absolute time values T_{PTEF} and T_E during REM showed differences in expiration between sleep phases in wheezing infants. Lower times were likely related to reduction of respiratory muscle tone during REM. Lower PIIA of diaphragm may be reflected as a shorter T_{PTEF} (8). Although T_E depends on many factors, consistently lower T_E during REM may be explained by the atony of the intercostal muscles. Inhibition of the intercostal muscles relaxes the chest wall compliance, leading to a faster deflation of the lungs (31). A

decrease in T_E during REM has been reported previously in healthy infants (14). Nonetheless, this muscle tone decreased from NREM to REM did not result in a reduction of ratios T_{PTEF}/T_E and V_{PTEF}/V_E.

Ratios T_{PTEF}/T_E and V_{PTEF}/V_E estimate the relative contributions of actively controlled and passive expiration to the TBFV profile. However, these indexes may not be direct indicators for airway obstruction. Different levels of obstruction combined with different adaptive breathing mechanisms may present similar ratios. The present results suggest that during NREM wheezing infants employ a different breathing strategy to compensate for obstruction, thus resulting in similar T_{PTEF}-to-T_E and V_{PTEF}-to-V_E ratios for different levels of obstruction and risk groups. However, during REM lower muscle tone limits the active breathing control and obstruction is reflected as an increase of passive expiration, particularly in the HR group.

Comparing the present results with one of our previous studies (27), T_{PTEF}/T_E and V_{PTEF}/V_E were lower during natural sleep than during sedation, even under methacholine-induced bronchoconstriction. Decrease in relative peak flow from awake state to sleep has also been reported by Lødrup et al. in newborns (25), and it is likely due to the fall in muscle tone. The literature is controversial regarding the utility of T_{PTEF}/T_E and V_{PTEF}/V_E in awake or sedated infants to indicate airway obstruction (45). It is possible that, as in

Table 3. *Correlations between respiratory parameters and subject age and lung function parameters*

	Age	FRC	FRC-z	sGaw	sGaw-z	$\dot{V}_{maxFRC}$	$\dot{V}_{maxFRC}$-z	PD40
MAD(IBI), s								
NREM	0.37	0.29	0.11	0.07	0.10	0.02	−0.13	0.34
REM	0.29	0.19	0.09	0.24	0.22	0.02	−0.06	0.29
Heart rate, beats/min								
NREM	−0.79‡	−0.55†	−0.38	−0.22	−0.33	−0.53*	−0.33	−0.35
REM	−0.85‡	−0.55†	−0.32	−0.10	−0.22	−0.47*	−0.23	−0.07
Respiratory rate, breaths/min								
NREM	−0.37	−0.24	−0.20	−0.04	−0.04	0.02	0.13	−0.03
REM	−0.44*	−0.37	−0.32	−0.18	−0.20	−0.17	−0.06	0.07
T_E, s								
NREM	0.31	0.11	0.07	0.06	0.05	−0.11	−0.21	0.21
REM	0.43*	0.33	0.25	0.15	0.17	0.13	0.02	0.08
T_{PTEF}/T_E								
NREM	−0.13	−0.03	−0.06	−0.02	0.01	0.29	0.36	−0.00
REM	−0.00	0.04	0.09	0.08	0.09	0.33	0.41	0.60
V_{PTEF}/V_E								
NREM	−0.31	−0.23	−0.07	0.03	−0.00	−0.01	0.09	−0.11
REM	−0.09	−0.15	0.02	0.34	0.34	0.40	0.49*	0.54
TEF50/PTEF								
NREM	−0.16	−0.02	0.15	0.13	0.12	0.16	0.21	0.02
REM	0.13	0.07	0.18	0.39	0.39	0.51*	0.54*	0.59
TEF25/PTEF								
NREM	0.00	0.12	0.11	0.16	0.20	0.39	0.41	0.27
REM	0.34	0.31	0.37	0.36	0.41	0.62†	0.60†	0.74*
P_{FV}								
NREM	−0.04	−0.12	−0.18	−0.38	−0.40	−0.45*	−0.42	−0.34
REM	−0.42	−0.34	−0.37	−0.48*	−0.52*	−0.65‡	−0.57†	−0.66
TEF05/PTEF								
NREM	−0.01	0.20	0.08	−0.15	−0.09	0.27	0.31	0.13
REM	0.11	0.28	0.24	−0.29	−0.22	0.12	0.15	0.37

Correlation tested by Spearman's rank correlation. *$P < 0.01$, †$P < 0.001$, ‡$P < 0.0001$. All comparisons contained 35 samples except those against PD40, which contained 14. See GLOSSARY for abbreviations.

NREM, during the awake state the contribution of active breathing control may confound the effects of altered airway mechanics during obstruction. The present results suggest that assessing T_{PTEF}/T_E and V_{PTEF}/V_E during REM rather than NREM or awake state may serve as a better indicator for respiratory disease.

Correlation of P_{FV} with lung function recorded at the hospital indicates that infants with airflow limitation and increased airway resistance ($\dot{V}_{maxFRC}$-z and sGaw-z) and increased airway responsiveness to methacholine (PD40) present more concave and less convex profiles overnight. Visual inspection of the time series revealed concave profiles concentrated in regions, but their location was not consistent between subjects. P_{FV} is supposedly more influenced by passive expiration and less by the active breathing mechanisms operating at the beginning or the end of expiration. This may explain why P_{FV} differentiated groups during both sleep phases independently of V_{PTEF}/V_E and TEF05/PTEF. Nonetheless, active control may still have a small influence on this index, as correlation is slightly better during REM, where active mechanisms are supposedly lower. TEF50/PTEF and TEF25/PTEF assessing the TBFV profile at instantaneous time points may be more affected by active control than P_{FV}, as group differentiation and correlation to lung function were low during NREM. In contrast, during REM, TEF25/PTEF showed correlations as high as P_{FV}.

Few studies have reported TEF50/PTEF or TEF25/PTEF in sedated wheezing infants. Compared with our results, Hevroni et al. (16) reported higher values for both indexes in infants with recurrent respiratory symptoms, but TBFV loops were recorded while infants were sedated, and not all the infants were wheezy. Concordantly, they found TEF50/PTEF or TEF25/PTEF to be associated with lung function expressed as $\dot{V}_{maxFRC}$.

TEF05/PTEF showed no significant relation to obstruction. In young infants the shape of later expiration may reflect breathing strategy rather than impaired breathing (36), which may decrease with maturation (7). Within subjects, we expected a lowering of TEF05/PTEF caused by lower muscle tone during REM compared with NREM, as seen in preterm newborns (44). This was the case for several individuals (Fig. 3), but the differences were not significant at the group level, at least for IR and HR. Inconclusive results may reflect the importance of dynamic maintenance of FRC in infants, regardless of obstruction or adaptation to obstruction.

The methods introduced in this study present some limitations. First, the determination of sleep phases is based on an indirect method rather than conventional polysomnography. This method is almost identical to that of Isler et al. (20), who reported sensitivity and specificity of 83% and 78% for REM and 78% and 83% for NREM compared with standard polysomnography classification. We assume that our method presents a similar performance and is not affected by respiratory conditions. Second, TBFV indexes are indirect estimators of physiological changes such as PIIA, passive exhale, and FRC and as such always subject to changes in both respiratory control and lung mechanics. Although correspondences have been proven in laboratory conditions, other mechanisms, such

Fig. 4. Association between selected TBFV indexes and lung function indexes. TBFV indexes TEF25/PTEF (*top*) and P_{FV} (*bottom*) are median values during all-night REM periods. $\dot{V}_{maxFRC}$–z (*left*) is the maximal flow at functional residual capacity ($n = 35$). PD40 (*right*) is the dose of methacholine producing a 40% decrease in $\dot{V}_{maxFRC}$ ($n = 14$). Different color and shapes denote the risk groups. See GLOSSARY for abbreviations.
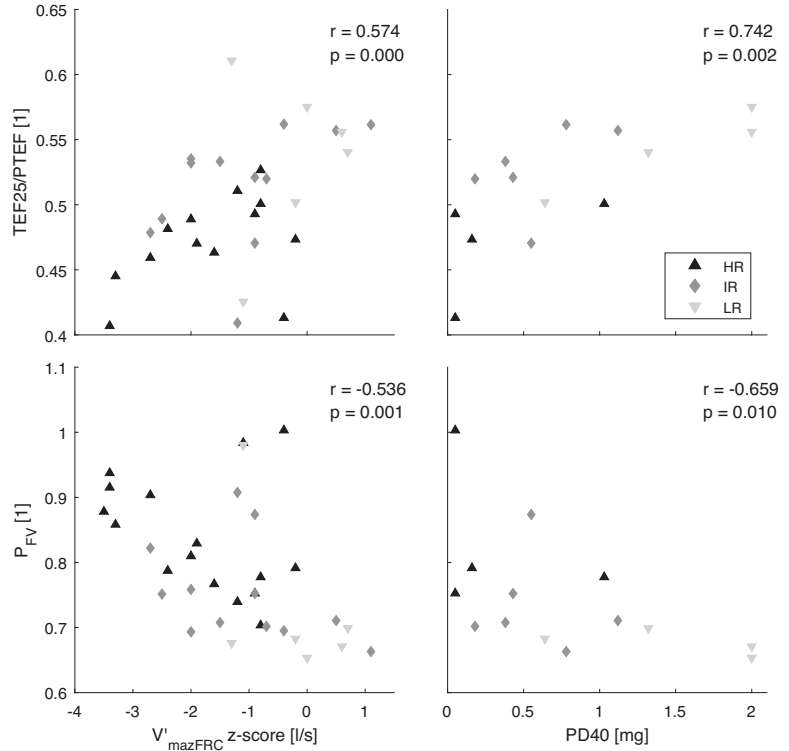
as increase of upper airway resistance, could affect these relationships. For example, expiratory braking in the form of "grunting" is a typical adaptation of breathing pattern of infants in respiratory distress (34). However, in the present sample of infants the disease was stable and severe respiratory distress was unlikely. Third, airway narrowing is assumed to be evenly distributed along both sleep phases, and therefore the full-night median is a fair indicator. In adults, obstruction has been reported to increase toward the end of the night (4), where REM is more frequent (42), whereas in infants sleep distribution is more uniform (42). Moreover, visual inspection of the time series showed an even distribution of sleep phases and not favored regions for changes in the TBFV indexes. Finally, we assumed that physiological changes during sleep do not affect the linearity of IP to mouth flow. Paradoxical inward rib cage motion is a phenomenon known to occur in healthy infants in which a high-compliance chest collapses under inspiratory effort. Paradoxical inward rib cage motion is more common during REM (11), especially under airway obstruction (1), and its presence decreases with maturation. Although IP reflects changes in electrical resistance and not in volume, displacement of the volume toward the abdomen away from the electrodes may result in loss of linearity.

The methods used as reference, mAPI and RTC, have been suggested to present some limitations when applied to infants. mAPI is intended for children over 2 yr of age (6). Arguably, the index could be extended to younger patients, since it already considers historical data before 2 yr of age (13), when wheezing episodes and symptoms are already recurrent (33). Nonetheless, until the index is validated the group classification on this study should be interpreted with care. Lung function testing based on RTC requires the previous sedation of the infants. Sedation with chloral hydrate has been reported to alter lung function parameters such as respiratory rate and tidal volume (21, 26). Nonetheless, the principal lung function parameter employed in the study, $\dot{V}_{maxFRC}$, seems not to be affected (46). TBFV indexes were derived during natural sleep and therefore unaffected by sedation. These limitations of current asthma assessment methods highlight the potential of nocturnal IP TBFV analysis for lung function testing. Unlike classification indexes, such as mAPI, analysis of TBFV is based on quantitative rather than qualitative assessment. Unlike other quantitative methods, such as RTC, IP requires no sedation and can be performed at home.

To summarize, TBFV profiles are shaped by the passive mechanical properties and active muscular control of the respiratory system. Respiratory condition not only alters passive characteristics but also triggers active adaptation strategies that are age and sleep stage dependent. We found that TBFV profiles reflected sleep stage variations and that the respiratory adaptation for natural changes during sleep stages differs in wheezing infants depending on their risk of asthma. We conclude that analysis of TBFV profiles overnight, and in particular during REM, may improve the clinical usefulness of IP to

identify infants with high risk of asthma and to assess their lung function.

GLOSSARY

FRC	Functional residual capacity
FRC-z	Adjusted functional residual capacity
IBI	Interbreath interval
MAD(IBI)	Median absolute deviation of IBI
mean(IBI)	Mean of IBI
NREM	Non-rapid eye movement
PD40	Provocative dose producing a 40% decrease in $\dot{V}_{maxFRC}$
P_{FV}	Exponential decrease of flow vs. volume from PTEF to TEF05.
PIIA	Postinspiratory inspiratory activity
REM	Rapid eye movement
sGaw	Specific airway conductance
sGaw-z	Adjusted specific airway conductance
TBFV	Tidal breathing flow volume
T_E	Time of expiration (s)
TEF05	Tidal expiratory flow at 5% remaining volume
TEF25	Tidal expiratory flow at 25% remaining volume
TEF50	Tidal expiratory flow at 50% remaining volume
T_{PTEF}	Time to peak tidal expiratory flow (s)
t_{REM}/t_{Total}	Percentage of night spent on REM
V_E	Expired volume
$\dot{V}_{maxFRC}$	Maximum flow at FRC
$\dot{V}_{maxFRC}$-z	Adjusted maximum flow at FRC
V_{PTEF}	Expired volume to peak tidal expiratory flow

REFERENCES

1. **Allen JL, Wolfson MR, McDowell K, Shaffer TH.** Thoracoabdominal asynchrony in infants with airflow obstruction. *Am Rev Respir Dis* 141: 337–342, 1990. doi:10.1164/ajrccm/141.2.337.

2. **Baldwin DN, Pillow JJ, Stocks J, Frey U.** Lung-function tests in neonates and infants with chronic lung disease: tidal breathing and respiratory control. *Pediatr Pulmonol* 41: 391–419, 2006. doi:10.1002/ppul.20400.

3. **Bates JH, Schmalisch G, Filbrun D, Stocks J.** Tidal breath analysis for infant pulmonary function testing. ERS/ATS Task Force on Standards for Infant Respiratory Function Testing. *Eur Respir J* 16: 1180–1192, 2000. doi:10.1034/j.1399-3003.2000.16f26.x.

4. **Bellia V, Cuttitta G, Insalaco G, Visconti A, Bonsignore G.** Relationship of nocturnal bronchoconstriction to sleep stages. *Am Rev Respir Dis* 140: 363–367, 1989. doi:10.1164/ajrccm/140.2.363.

5. **Bohadana AB, Hannhart B, Teculescu DB.** Nocturnal worsening of asthma and sleep-disordered breathing. *J Asthma* 39: 85–100, 2002. doi:10.1081/JAS-120002190.

6. **Castro-Rodríguez JA, Holberg CJ, Wright AL, Martinez FD.** A clinical index to define risk of asthma in young children with recurrent wheezing. *Am J Respir Crit Care Med* 162: 1403–1406, 2000. doi:10.1164/ajrccm.162.4.9912111.

7. **Colin AA, Wohl ME, Mead J, Ratjen FA, Glass G, Stark AR.** Transition from dynamically maintained to relaxed end-expiratory volume in human infants. *J Appl Physiol (1985)* 67: 2107–2111, 1989. doi:10.1152/jappl.1989.67.5.2107.

8. **van der Ent CK, van der Grinten CP, Meessen NE, Luijendijk SC, Mulder PG, Bogaard JM.** Time to peak tidal expiratory flow and the neuromuscular control of expiration. *Eur Respir J* 12: 646–652, 1998. doi:10.1183/09031936.98.12030646.

9. **Filippone M, Narne S, Pettenazzo A, Zacchello F, Baraldi E.** Functional approach to infants and young children with noisy breathing: validation of pneumotachography by blinded comparison with bronchoscopy. *Am J Respir Crit Care Med* 162: 1795–1800, 2000. doi:10.1164/ajrccm.162.5.9912008.

10. **Fisher JT, Mortola JP, Smith JB, Fox GS, Weeks S.** Respiration in newborns: development of the control of breathing. *Am Rev Respir Dis* 125: 650–657, 1982.

11. **Gaultier C, Praud JP, Canet E, Delaperche MF, D'Allest AM.** Paradoxical inward rib cage motion during rapid eye movement sleep in infants and young children. *J Dev Physiol* 9: 391–397, 1987.

12. **Gracia J, Seppä VP, Pelkonen A, Kotaniemi-Syrjänen A, Mäkelä M, Malmberg P, Viik J.** Nonlinear local projection filter for impedance pneumography. In: *EMBEC & NBC 2017*, edited by Eskola H, Väisänen O, Viik J, Hyttinen J. Singapore: Springer, 2017, p. 306–309.

13. **Guilbert TW, Morgan WJ, Zeiger RS, Mauger DT, Boehmer SJ, Szefler SJ, Bacharier LB, Lemanske RF Jr, Strunk RC, Allen DB, Bloomberg GR, Heldt G, Krawiec M, Larsen G, Liu AH, Chinchilli VM, Sorkness CA, Taussig LM, Martinez FD.** Long-term inhaled corticosteroids in preschool children at high risk for asthma. *N Engl J Med* 354: 1985–1997, 2006. doi:10.1056/NEJMoa051378.

14. **Haddad GG, Epstein RA, Epstein MA, Leistner HL, Marino PA, Mellins RB.** Maturation of ventilation and ventilatory pattern in normal sleeping infants. *J Appl Physiol* 46: 998–1002, 1979. doi:10.1152/jappl.1979.46.5.998.

15. **Hershenson MB, Colin AA, Wohl ME, Stark AR.** Changes in the contribution of the rib cage to tidal breathing during infancy. *Am Rev Respir Dis* 141: 922–925, 1990. doi:10.1164/ajrccm/141.4_Pt_1.922.

16. **Hevroni A, Goldman A, Blank-Brachfeld M, Abu Ahmad W, Ben-Dov L, Springer C.** Use of tidal breathing curves for evaluating expiratory airway obstruction in infants. *J Asthma* 55: 1331–1337, 2018. doi:10.1080/02770903.2017.1414234.

17. **Hollier CA, Harmer AR, Maxwell LJ, Menadue C, Willson GN, Black DA, Piper AJ.** Validation of respiratory inductive plethysmography (LifeShirt) in obesity hypoventilation syndrome. *Respir Physiol Neurobiol* 194: 15–22, 2014. doi:10.1016/j.resp.2014.01.014.

18. **Hoo AF, Dezateux C, Hanrahan JP, Cole TJ, Tepper RS, Stocks J.** Sex-specific prediction equations for Vmax_FRC in infancy: a multicenter collaborative study. *Am J Respir Crit Care Med* 165: 1084–1092, 2002. doi:10.1164/ajrccm.165.8.2103035.

19. **Hutten GJ, van Eykern LA, Latzin P, Kyburz M, van Aalderen WM, Frey U.** Relative impact of respiratory muscle activity on tidal flow and

end expiratory volume in healthy neonates. *Pediatr Pulmonol* 43: 882–891, 2008. doi:10.1002/ppul.20874.

20. **Isler JR, Thai T, Myers MM, Fifer WP.** An automated method for coding sleep states in human infants based on respiratory rate variability. *Dev Psychobiol* 58: 1108–1115, 2016. doi:10.1002/dev.21482.

21. **Jackson EA, Rabbette PS, Dezateux C, Hatch DJ, Stocks J.** The effect of triclofos sodium sedation on respiratory rate, oxygen saturation, and heart rate in infants and young children. *Pediatr Pulmonol* 10: 40–45, 1991. doi:10.1002/ppul.1950100109.

22. **Kosch PC, Davenport PW, Wozniak JA, Stark AR.** Reflex control of expiratory duration in newborn infants. *J Appl Physiol (1985)* 58: 575–581, 1985. doi:10.1152/jappl.1985.58.2.575.

23. **Kosch PC, Stark AR.** Dynamic maintenance of end-expiratory lung volume in full-term infants. *J Appl Physiol* 57: 1126–1133, 1984. doi:10.1152/jappl.1984.57.4.1126.

24. **Kotaniemi-Syrjänen A, Malmberg LP, Pelkonen AS, Malmström K, Mäkelä MJ.** Airway responsiveness: associated features in infants with recurrent respiratory symptoms. *Eur Respir J* 30: 1150–1157, 2007. doi:10.1183/09031936.00158106.

24a.**Kryger M, Roth T, Dement W.** Central neural control of respiratory neurons and motoneurons during sleep. In: *Principles and Practice of Sleep Medicine* (6th ed.). Philadelphia, PA: Elsevier, 2017.

25. **Lødrup KC, Mowinckel P, Carlsen KH.** Lung function measurements in awake compared to sleeping newborn infants. *Pediatr Pulmonol* 12: 99–104, 1992. doi:10.1002/ppul.1950120208.

26. **Mallol J, Sly PD.** Effect of chloral hydrate on arterial oxygen saturation in wheezy infants. *Pediatr Pulmonol* 5: 96–99, 1988. doi:10.1002/ppul.1950050206.

27. **Malmberg LP, Seppä VP, Kotaniemi-Syrjänen A, Malmström K, Kajosaari M, Pelkonen AS, Viik J, Mäkelä MJ.** Measurement of tidal breathing flows in infants using impedance pneumography. *Eur Respir J* 49: 1600926, 2017. doi:10.1183/13993003.00926-2016.

28. **Malmberg LP, von Wright L, Kotaniemi-Syrjänen A, Malmström K, Pelkonen AS, Mäkelä MJ.** Methacholine-induced lung function changes measured with infant body plethysmography. *Pediatr Pulmonol* 46: 362–368, 2011. doi:10.1002/ppul.21375.

30. **Morris MJ, Lane DJ.** Tidal expiratory flow patterns in airflow obstruction. *Thorax* 36: 135–142, 1981. doi:10.1136/thx.36.2.135.

31. **Mortola JP, Fisher JT, Smith B, Fox G, Weeks S.** Dynamics of breathing in infants. *J Appl Physiol Respir Environ Exerc Physiol* 52: 1209–1215, 1982. doi:10.1152/jappl.1982.52.5.1209.

32. **Otis AB, Fenn WO, Rahn H.** Mechanics of breathing in man. *J Appl Physiol* 2: 592–607, 1950. doi:10.1152/jappl.1950.2.11.592.

33. **Pennington AF, Strickland MJ, Freedle KA, Klein M, Drews-Botsch C, Hansen C, Darrow LA.** Evaluating early-life asthma definitions as a marker for subsequent asthma in an electronic medical record setting. *Pediatr Allergy Immunol* 27: 591–596, 2016. doi:10.1111/pai.12586.

34. **Reuter S, Moser C, Baack M.** Respiratory distress in the newborn. *Pediatr Rev* 35: 417–429, 2014. doi:10.1542/pir.35-10-417.

35. **Sato J, Robbins PA.** Methods for averaging irregular respiratory flow profiles in awake humans. *J Appl Physiol (1985)* 90: 705–712, 2001. doi:10.1152/jappl.2001.90.2.705.

36. **Schmalisch G, Wauer RR, Foitzik B, Patzak A.** Influence of preterm onset of inspiration on tidal breathing parameters in infants with and without CLD. *Respir Physiol Neurobiol* 135: 39–46, 2003. doi:10.1016/S1569-9048(03)00029-6.

36a.**Schmidt M, Foitzik B, Wauer RR, Winkler F, Schmalisch G.** Comparative investigations of algorithms for the detection of breaths in newborns with disturbed respiratory signals. *Comput Biomed Res* 31: 413–425, 1998. doi:10.1006/cbmr.1998.1493.

37. **Scholle S, Wiater A, Scholle HC.** Normative values of polysomnographic parameters in childhood and adolescence: cardiorespiratory parameters. *Sleep Med* 12: 988–996, 2011. doi:10.1016/j.sleep.2011.05.006.

38. **Seppä VP, Hyttinen J, Uitto M, Chrapek W, Viik J.** Novel electrode configuration for highly linear impedance pneumography. *Biomed Tech (Berl)* 58: 35–38, 2013. doi:10.1515/bmt-2012-0068.

39. **Seppä VP, Hyttinen J, Viik J.** A method for suppressing cardiogenic oscillations in impedance pneumography. *Physiol Meas* 32: 337–345, 2011. doi:10.1088/0967-3334/32/3/005.

40. **Seppä VP, Pelkonen AS, Kotaniemi-Syrjänen A, Mäkelä MJ, Viik J, Malmberg LP.** Tidal breathing flow measurement in awake young children by using impedance pneumography. *J Appl Physiol (1985)* 115: 1725–1731, 2013. doi:10.1152/japplphysiol.00657.2013.

41. **Seppä VP, Pelkonen AS, Kotaniemi-Syrjänen A, Viik J, Mäkelä MJ, Malmberg LP.** Tidal flow variability measured by impedance pneumography relates to childhood asthma risk. *Eur Respir J* 47: 1687–1696, 2016. [Erratum in *Eur Respir J* 48: 285, 2016.] doi:10.1183/13993003.00989-2015.

42. **Sheldon SH, Ferber R, Kryger MH (Editors).** *Principles and Practice of Pediatric Sleep Medicine* (2nd ed.). London: Elsevier Saunders, 2014.

43. **Sly PD, Tepper R, Henschen M, Gappa M, Stocks J.** Tidal forced expirations. ERS/ATS Task Force on Standards for Infant Respiratory Function Testing. *Eur Respir J* 16: 741–748, 2000. doi:10.1034/j.1399-3003.2000.16d29.x.

44. **Stark AR, Cohlan BA, Waggener TB, Frantz ID 3rd, Kosch PC.** Regulation of end-expiratory lung volume during sleep in premature infants. *J Appl Physiol (1985)* 62: 1117–1123, 1987. doi:10.1152/jappl.1987.62.3.1117.

45. **Stocks J, Dezateux CA, Jackson EA, Hoo AF, Costeloe KL, Wade AM.** Analysis of tidal breathing parameters in infancy: how variable is TPTEF: TE? *Am J Respir Crit Care Med* 150: 1347–1354, 1994. doi:10.1164/ajrccm.150.5.7952563.

46. **Turner DJ, Morgan SE, Landau LI, LeSouëf PN.** Methodological aspects of flow-volume studies in infants. *Pediatr Pulmonol* 8: 289–293, 1990. doi:10.1002/ppul.1950080414.

47. **Willemen T, Van Deun D, Verhaert V, Vandekerckhove M, Exadaktylos V, Verbraecken J, Van Huffel S, Haex B, Vander Sloten J.** An evaluation of cardiorespiratory and movement features with respect to sleep-stage classification. *IEEE J Biomed Health Inform* 18: 661–669, 2014. doi:10.1109/JBHI.2013.2276083.

PUBLICATION

P.III

Tidal Breathing Flow Profiles during Sleep in Wheezing Children Measured by Impedance Pneumography

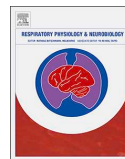J. Gracia-Tabuenca, V.-P. Seppä, M. Jauhiainen, M. Paassilta,
J. Viik and J. Karjalainen

Publication reprinted with the permission of the copyright holders

Tidal breathing flow profiles during sleep in wheezing children measured by impedance pneumography

Javier Gracia-Tabuenca[a,*], Ville-Pekka Seppä[b], Milla Jauhiainen[a], Marita Paassilta[c], Jari Viik[a], Jussi Karjalainen[c]

[a] Faculty of Medicine and Health Technology, Tampere University, Korkeakoulunkatu 10, FI-33720, Tampere, Finland
[b] Revenio Research Ltd., Äyritie 22, FI-01510, Vantaa, Finland
[c] Allergy Centre, Tampere University Hospital, Teiskontie 35 PL 2000, FI-33521, Tampere, Finland

ARTICLE INFO

ABSTRACT

For the first time, impedance pneumography (IP) enables a continuous analysis of the tidal breathing flow volume (TBFV), overnight. We studied how corticosteroid inhalation treatments, sleep stage, and time from sleep onset modify the nocturnal TBFV profiles of children. Seventy children, 1–5 years old and with recurrent wheezing, underwent three, full-night TBFVs recordings at home, using IP. The first recorded one week before ending a 3-months inhaled corticosteroids treatment, and remaining two, 2 and 4 weeks after treatment. TBFV profiles were grouped by hour from sleep onset and estimated sleep stage. Compared with on-medication, the off-medication profiles showed lower volume at exhalation peak flow, earlier interruption of expiration, and less convex middle expiration. The differences in the first two features were significant during non-rapid eye movement (NREM), and the differences in the third were more prominent during REM after 4 h of sleep. These combinations of TBFV features, sleep phase, and sleep time potentially indicate airflow limitation in young children.

1. Introduction

Tidal breathing flow volume (TBFV) analysis has been proposed as an alternative for detecting lower-airway obstruction in young children who are unable to cooperate with forced spirometry (Beydon et al., 2007). However, interpretation of TBFV profiles, particularly the expiratory limb, is challenging (Bates, 1998). Expiration is shaped not only by passive mechanical characteristics such as thoracopulmonary recoil and airway resistance (Otis et al., 1950), but also by the active braking during the early part of expiration and the active interruption of the expiration ending (Hutten et al., 2008). Airway narrowing directly alters passive characteristics, which triggers subject-dependent active adaptation strategies (Baldwin et al., 2006; Maarsingh et al., 2000; Morris and Lane, 1981). Moreover, passive and active characteristics are influenced by other factors such as instrumentation (Fleming et al., 1982), awareness state (Lodrup-Carlsen and Carlsen, 1993), and other respiratory conditions (Leonhardt et al., 2010).

Impedance pneumography (IP) allows the continuous recording of the tidal flow overnight, providing several advantages to TBFV profile analysis. Firstly, IP uses four surface skin electrodes to derive the respiratory flow noninvasively, from changes in the thoracic electrical impedance, which is proportional to lung aeration. Hence, unlike conventional pneumography (PNT) (Fleming et al., 1982), IP does not corrupt the shape of the TBFV profiles. Secondly, sleep is characterised by a decrease in respiratory musculature tone, which is accentuated further during the rapid eye movement (REM) stage (Horner, 2010). It has been hypothesized that a decrease in muscle tone increases the contribution of passive characteristics to the TBFV profile, revealing signs of obstruction (Gracia-Tabuenca et al., 2019). Thirdly, diseases such as asthma are influenced by many neural, hormonal, and autoimmune circadian factors. Asthma symptoms worsen late at night and early in the morning (Bohadana et al., 2002). Assessment of the nocturnal TBFV profiles recorded at home may reveal symptoms that go unnoticed by tests conducted in hospitals.

Previous studies have proven the feasibility of using IP to derive TBFV profiles during night sleep (Gracia-Tabuenca et al., 2019; Seppä et al., 2016) and the strong agreement between IP and PNT results in children (Seppä et al., 2013b) and infants (Malmberg et al., 2017), even under induced bronchoconstriction. The effect of interactions between asthma risk and sleep physiology on the shape of TBFV profiles has been studied for infants (Gracia-Tabuenca et al., 2019), but not for older children. During the first year of life, development of the thoracic

---

Table 1
Characteristics of studied children.

Groups	Current asthma			Skin prick	
	CA-N	CA-P	CA-Y	Nonatopic	Atopic
Subjects	16	16	36	40	28
Age [mo]	51.45	54.27	41.10	43.87	51.23
	(18.23 77.07)	(40.07 80.70)	(15.73 78.63)	(17.77 67.50)	(15.73 80.70)
Male	12	10	22	26	18
Broncho-Week -1	2	0	2	2	2
Broncho-Week 2	1	4	7	9	3
Broncho-Week 4	3	6	7	11	5

Subjects were classified according to two classification criteria: current asthma and skin-prick test. The first criteria consist on tree groups: no current asthma (CA-N), probable current asthma (CA-P), and current asthma (CA-Y). The second criteria consist on two groups: nonatopic and atopic. Age (in months) is given as the median (range). The entries for Broncho-Week -1, Broncho-Week 2, and Broncho-Week 4 are the number of subjects who used a bronchodilator in Week -1, Week 2, and Week 4, respectively. No significant difference was found between groups within each criterion for any characteristic as determined by the Kruskal–Wallis test (continuous variables) or the χ^2/Fisher's exact test (categorical variables).

cage (Allen and Gripp, 2002) and the nervous system (Rabbette et al., 1994) modifies breathing strategy. For example, dynamic maintenance of end-expiratory volume decreases (Colin et al., 1989), thoracoabdominal asynchrony (Guilleminault et al., 1982) decreases, and respiratory apnoeas become less common (Flores-Guevara et al., 1982). It is unknown if these developmental changes affect the results observed in infants. Finally, lower airway obstruction increases with night progression, at least in adults with and without asthma (Bellia et al., 1989). However, whether TBFV profiles change with night progression has not been studied.

The present longitudinal study assessed the effect that the interruption of medication had on the TBFV profiles obtained from overnight IP recordings taken at home, for a group of wheezing children. It also investigated the extent to which the time from sleep onset, as well as REM and non-REM sleep stages, influenced these changes. These two main sleep stages were respectively estimated from regions of high and low respiration variability.

2. Materials and methods

### 2.1. Study subjects and data collection

Seventy children (age = 2.5 (0.9–5.7) years old (median and range)), who were prescribed 3 months of fluticasone propionate treatment –based on Finnish guidelines for obstructive bronchitis– were enrolled in our study at Tampere University Hospital. Each patient had IP and electrocardiography (ECG) signals recorded at home for three nights. The first recording (Week -1) was performed 1 week before conclusion of the fluticasone treatment, and the second (Week 2) and third (Week 4) recordings were performed 2 and 4 weeks after treatment ended. Recordings were obtained using a custom-designed device developed at Tampere University of Technology (Seppä et al., 2013b). Electrode placement was as previously described (Seppä et al., 2013a). On the first recording day (Week -1), a trained nurse placed the electrodes and the device on the patient at the hospital and instructed the parents on the procedure. For the following recordings (Week 2 and Week 4), the parents placed and activated the device at home. A nurse contacted the families to confirm the planned recording nights. In all cases, the device started recording before the patient went to sleep and recorded until after the patient woke up the next morning. On each recording day, parents photographed the electrode locations and noted the time of sleep onset, wake-up time, periods of nocturnal awakening, times of bronchodilator intake, and respiratory symptoms, usually coughing, sneezing, and rhinorrhoea. Patients were classified according to the following two classification criteria. For the first classification criteria, a paediatric pulmonologist followed the patients for 6 months after the last recording and classified them as current asthma (CA-Y) if

they had been prescribed a regular asthma controller, reported difficult nocturnal coughing, exercise-induced coughing, or shortness of breath relieved by the bronchodilator; possible current asthma (CA-P) if they did not fulfil the preceding criteria but were prescribed intermittent controller medication for treating asthma symptoms; and no current asthma (CA-N) otherwise. For the second classification criterion, patients were classified as atopic if they responded positively in a skin-prick test against egg, cat, dog, birch, or timothy, or nonatopic otherwise. Classification criterion, demographic data, and bronchodilator use are summarised in Table 1. The Regional Ethics Committee of Tampere University Hospital approved the research protocol (Ethics Committee Code R14027), and the ethical guidelines of the Declaration of Helsinki were followed.

2.2. Data preprocessing

All the recordings were visually inspected by trained researchers who were blind to patient information. The researchers discarded sections corrupted by motion or other distorting events such as coughing, moving, or talking. Accepted sections of the recordings were automatically processed to derive minute-by-minute TBFV profiles, as previously detailed (Gracia-Tabuenca et al., 2019). In short, the ECG signal was used to filter out the cardiac artefact from the raw IP signal (Seppä et al., 2011). A Savitzky–Golay filter differentiated the resulting lung volume-oriented IP signal into a flow-oriented IP signal (Seppä et al., 2010), the remaining noise of which was further attenuated using a nonlinear projection filter (Gracia et al., 2017). Cleaned-up flow and volume IP signals were split into respiratory cycles, as recommended by Schmidt et al. (1998), and cycles were transformed into TBFV profiles. Resulting TBFV profiles were averaged in the flow-volume domain, as described by Sato and Robbins (2001), using a 20-TBFV moving window with a 5-TBFV overlap. Each averaged TBFV profile was normalised to unit volume and flow-scaled, making its time integral equal to 1 (Sato and Robbins, 2001).

For each profile, the following expiratory indices were measured as recommend by Bates et al., 2000; and Beydon et al., 2007: expiratory time (T_E), time to peak tidal expiratory flow (T_{PTEF}), their ratio (T_{PTEF}/T_E), equivalent volume ratio (V_{PTEF}/V_E), tidal expiratory flow when 50%, 25%, and 5% of the tidal volume remains in the lungs relative to peak tidal expiratory flow (TEF50/PTEF, TEF25/PTEF, and TEF05/PTEF, respectively). In addition, the index P_{FV} was calculated as the exponent of a power function fitted between PTEF and TEF05, as described previously (Gracia-Tabuenca et al., 2019). Fig. 1 shows the indices measured in four representative profiles.
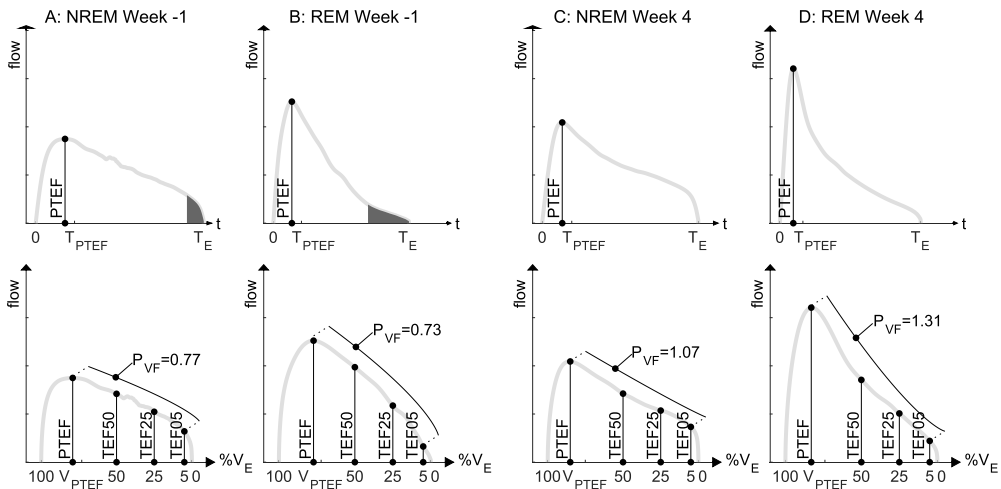
Fig. 1. TBFV indices for four representative expiration limbs from the same patient extracted from NREM Week -1 (A), REM Week -1 (B), NREM Week 4 (C), and REM Week 4 (D). Upper plots show flow-time domain and lower plots show flow-volume domain. Volume is normalized to 1 and flow is scaled to have area of 1 in the flow-time domain. Light grey lines represent the expiration signals, vertical solid lines between points show distances, and solid line curves are the power-fitted curves, which are displaced for clarity and the dotted lines project where the curves should be located. The grey areas in the flow-time plots (A) and (B) are regions with the same area. They show that integrating the same volume (V) took a longer time in (B) than in (A) because the flow (Q) was lower ($V = \int Q \mathrm{d}t$).
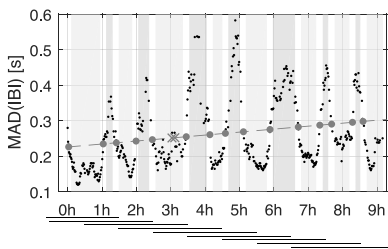
Fig. 2. Two sleep segmentation methods: (upper) segments of high and low respiratory rate variability are shown as grey and light-grey boxes, respectively; (lower) solid lines indicate time from sleep onset in 3-h segments. The procedure presented in the text is based on the dotted-line signal (MAD(IBI)). The dashed line is the linear fit and the black dots are valid crossings. The abscissa shows the time from sleep onset in hours.

2.3. Sleep segmentation

The overnight recordings were segmented on the basis of two different methods: regions of high and low respiratory rate variability and time from sleep onset. Regions of high and low variability were automatically defined using a method similar to that proposed by Isler et al. (2016). In short, a respiration variability time series was formed using the median absolute deviation (MAD) of the interbreath intervals (IBI) within a moving 5-min 50% overlap window. Subsequently, a line was fitted to the variability time series and crossing points were marked. Regions of 5 min around the crossing points were discarded. The remaining sections with the most samples over the fitted line were defined as REM and NREM otherwise. An example of the process is shown in Fig. 2. Although this implementation could not be validated against polysomnography, the performance of our method was putatively similar to that of the Isler et al. method (see the Discussion section). The time from sleep onset regions were defined as 3-h bins centred at each hour starting from sleep onset. A representative recording is shown in Fig. 2. Sleep-onset time was set automatically as the beginning of the first segment that had no motion artefacts for more than 5 min. Only

one automatic sleep onset was detected more than an hour before the time annotated by the parents. It was considered an error and the annotated time was used.

2.4. Statistical analysis

In each recording, we calculated for each index the median of all-night values within the REM sections and the median of all-night values within the NREM sections. Similarly, in each recording, we calculated for each index and for each hourly bin the median of the REM values and the median of the NREM values within each 3-h bin. If the number of indices within a bin was fewer than 20, that bin was rejected. The same two procedures were followed for IBI, heart rate, and MAD(IBI) signals. The following tests were performed on both: all-night medians (Table 2) and hourly bin medians (Fig. 3). Wilcoxon rank sum was used to assess the differences between the REM and NREM medians within each recording, separately for the three recording weeks. The same test was used to assess the differences between recording weeks for each subject, separately for REM and NREM. The differences between groups within each classification criterion and between bronchodilator use and no use were assessed for each index, in each sleep stage, and in each recording day using the Wilcoxon rank sum test. The characteristics of the subjects between groups were compared using the Kruskal–Wallis test for continuous variables or the χ^2/Fisher's exact test for categorical variables (Table 1). Bonferroni correction was applied in all tests. Moreover, Spearman rank correlation coefficients were calculated between all-night median values and patient age for all weeks (Table 3).

3. Results

Twenty-two recordings were rejected due to battery or electrode problems, or malfunctioning of the prototype recorders. For the accepted recordings, the starting time was at a mean of 9:20 pm (± 1:05) and lasted 9.95 (± 1.11) h (mean value (standard deviation). Of the accepted data, 28.33% (± 4.47%) was discarded for being corrupted or occurring between sleep stages, and 25.17% (± 5.93%) was classified as REM, slightly higher than reported by Traeger et al. (2005). Table 2

Table 2

Median of the TBFV parameters during estimated NREM and REM sections overnight. Values are grouped according to the recording week.

		Week -1	Week 2	Week 4
Subjects		62	64	62
T_{REM}/T_{Total} [%]		0.25 (0.22 0.29)	0.24 (0.21 0.28)	0.24 (0.21 0.29)
MAD(IBI) [s]	NREM	0.13 (0.12 0.14)	0.13 (0.11 0.15)	0.13 (0.12 0.14)
	REM	0.28 (0.25 0.34) *	0.30 (0.26 0.33) *	0.29 (0.25 0.34) *
Heart rate [bpm]	NREM	83.30 (77.37 89.86)	83.53 (75.47 92.11)	84.94 (79.66 92.95)
	REM	89.90 (82.54 95.80) *	89.07 (81.85 97.04) *	89.41 (84.91 97.91)*
Mean(IBI) [bpm]	NREM	19.33 (18.32 22.35)	19.57 (17.89 21.85)	20.47 (18.21 23.04)
	REM	20.44 (18.17 22.01)	19.92 (18.40 22.69)	20.93 (18.93 23.62)
T_E [s]	NREM	1.85 (1.65 2.00)	1.87 (1.71 2.04)	1.82 (1.59 2.00)
	REM	1.71 (1.59 1.92) *	1.75 (1.59 1.96) *	1.64 (1.50 1.94) *
T_{PTEF} [s]	NREM	0.32 (0.27 0.37)	0.32 (0.27 0.37)	0.29 (0.24 0.34) a
	REM	0.27 (0.24 0.32) *	0.27 (0.24 0.29) *	0.26 (0.22 0.29) *
T_{PTEF}/T_E	NREM	0.17 (0.15 0.20)	0.17 (0.14 0.20)	0.16 (0.14 0.19) a
	REM	0.16 (0.14 0.19) *	0.15 (0.13 0.18) *	0.15 (0.13 0.18) *
V_{PTEF}/V_E	NREM	0.25 (0.22 0.29)	0.24 (0.21 0.28)	0.23 (0.20 0.27) a
	REM	0.26 (0.23 0.28)	0.24 (0.21 0.26)	0.23 (0.21 0.27) a
TEF50/PTEF	NREM	0.87 (0.84 0.89)	0.85 (0.80 0.88)	0.84 (0.79 0.88) a, Br
	REM	0.85 (0.81 0.88) *	0.81 (0.79 0.86) *	0.80 (0.76 0.87) *, a, b, Br
TEF25/PTEF	NREM	0.57 (0.53 0.61)	0.57 (0.51 0.60)	0.53 (0.48 0.60)
	REM	0.54 (0.52 0.57) *	0.52 (0.48 0.56) *	0.50 (0.45 0.56) *, a, b, Br
P_{VF}	NREM	0.68 (0.64 0.73)	0.69 (0.65 0.78)	0.71 (0.66 0.80) a, Br
	REM	0.69 (0.65 0.75)	0.72 (0.67 0.78)	0.75 (0.68 0.85) *, a, b, Br
TEF05/PTEF	NREM	0.13 (0.09 0.16)	0.14 (0.10 0.18)	0.14 (0.10 0.21) a
	REM	0.11 (0.09 0.14) *	0.11 (0.08 0.13) *	0.12 (0.08 0.16) *, a

Values are given as median (0.25 0.75 (quartiles)). Columns are recording weeks: Week -1 is one week before end of treatment, Week 2 is two weeks after end of treatment, and Week 4 is 4 weeks after end of treatment. Indices are defined in the text. *: significant difference ($p < 0.01$) between sleep stages within each week. a: significant difference ($p < 0.05$) between Week -1 and Week 4. b: significant difference ($p < 0.05$) between Week 2 and Week 4. Significant differences were calculated using the Wilcoxon signed sum test. Br: significant difference ($p < 0.01$) between subjects who used a bronchodilator that recording day and subjects who did not, calculated using the Wilcoxon rank sum test. Bonferroni correction ($n = 3$) was applied to all p values.

shows that neither faulty recordings nor sleep efficiency depended on the recording week, and summarises all-night medians for each index and recording week. Hourly bin medians for six selected indices and three recording weeks are summarised in Fig. 3.

MAD (IBI), heart rate, and respiratory rate showed similar results in on-medication and off-medication recording weeks. Evidently, IBI variability was higher during REM than during NREM the whole night. Only respiratory variability, respiratory rate, and T_E presented a weak but significant correlation ($p < 0.05$) with the patients' age for some combinations of sleep stage and recording day. However, heart rate had a significant correlation with age ($p < 0.001$) for all stages and ages (Table 3). The correlation of age with heart rate, and less significantly with respiratory rate, agrees with published results (Scholle et al., 2011).

For the on-medication recordings (Week -1), absolute times T_E and T_{PTEF} were both significantly shorter during REM for the whole night. However, their overnight median trends were different. The T_E median slightly increased overnight for both sleep stages, whereas the T_{PTEF} median was constant for NREM and decreased for REM in the first part of the night. As expected, the overnight median trend for T_{PTEF}/T_E was the combination of the trend of T_{PTEF} and the inverted trend of T_E. For V_{PTEF}/V_E, the trend of T_E was no longer present, but both NREM and REM presented a trend similar to that of T_{PTEF}. However, unlike with T_{PTEF}, for V_{PTEF}/V_E, the NREM and REM median trends overlapped with each other and, therefore, showed no significant differences overnight. On the end side of the TBFV profiles, TEF05/PTEF was significantly lower for REM than for NREM during the whole night. In the middle part of the profiles, P_{VF} showed a constant median during the whole night for NREM and REM. On the other hand, TEF50/PTEF and TEF25/PTEF showed a decreasing trend, similar to that of V_{PTEF}/V_E, and a sleep-stage differentiation similar to that of TEF05/PTEF. The time progression of TEF50/PTEF and TEF25/PTEF seemed to be a combination of V_{PTEF}/V_E and TEF05/PTEF (not shown in Fig. 3).

A comparison of the indices for on-medication (Week -1) with those for off-medication (Week 2 and Week 4) showed there were no significant differences in IBI variability, heart rate, and respiratory rate. Overnight median trends for T_E, T_{PTEF}, T_{PTEF}/T_E, and V_{PTEF}/V_E presented night progressions for off-medication similar to those for on-medication. However, in the Week 4 recordings, all-night medians for T_{PTEF}, T_{PTEF}/T_E, and V_{PTEF}/V_E were significantly lower during NREM. The most significant difference was observed for V_{PTEF}/V_E ($p = 0.0019$), which also showed a significant decrease for all hourly bin medians. Likewise, TEF05/PTEF increased in the Week 4 recordings for both sleep stages, but the increase was statistically significant for all hourly bin medians only for NREM. Unlike in Week -1, P_{VF} significantly increased in Week 4 for both sleep stages, but only in the second half of the night. Moreover, the increase in P_{VF} was higher for REM than for NREM.

Current asthma and skin-prick test classifications showed no significant differences for any index in any sleep stage on any recording day. However, the use of a bronchodilator showed significant differences ($p < 0.01$) in Week 4 for both sleep stages for all the indices in the middle part except TEF25/PTEF in NREM. Counterintuitively, the values of subjects who used a bronchodilator suggest that they presented greater obstruction than subject who did not use: during REM, P_{VF} was 0.89 (0.83 1.04) (median (interquartile range)) for bronchodilator use vs. no use 0.71 (0.67 0.77); TEF25/PTEF was 0.44 (0.39 0.46) vs. 0.53 (0.50 0.57); and TEF50/PTEF was 0.74 (0.68 0.77) vs. 0.82 (0.79 0.87). Similarly, during NREM, P_{VF} was 0.82 (0.73 0.92) vs 0.69 (0.64 0.74) and TEF50/PTEF was 0.77 (0.75 0.81) vs. 0.85 (0.80 0.89).

4. Discussion

This study demonstrated that dividing the night into regions of higher and lower IBI variability, as an estimation of REM and NREM sleep, presented differences in the TBFV indices for both on-medication and off-medication recordings in children. Moreover, when assessed at different times from sleep onset, certain indices presented a decreasing averaged trend during REM. In addition, the interruption of treatment
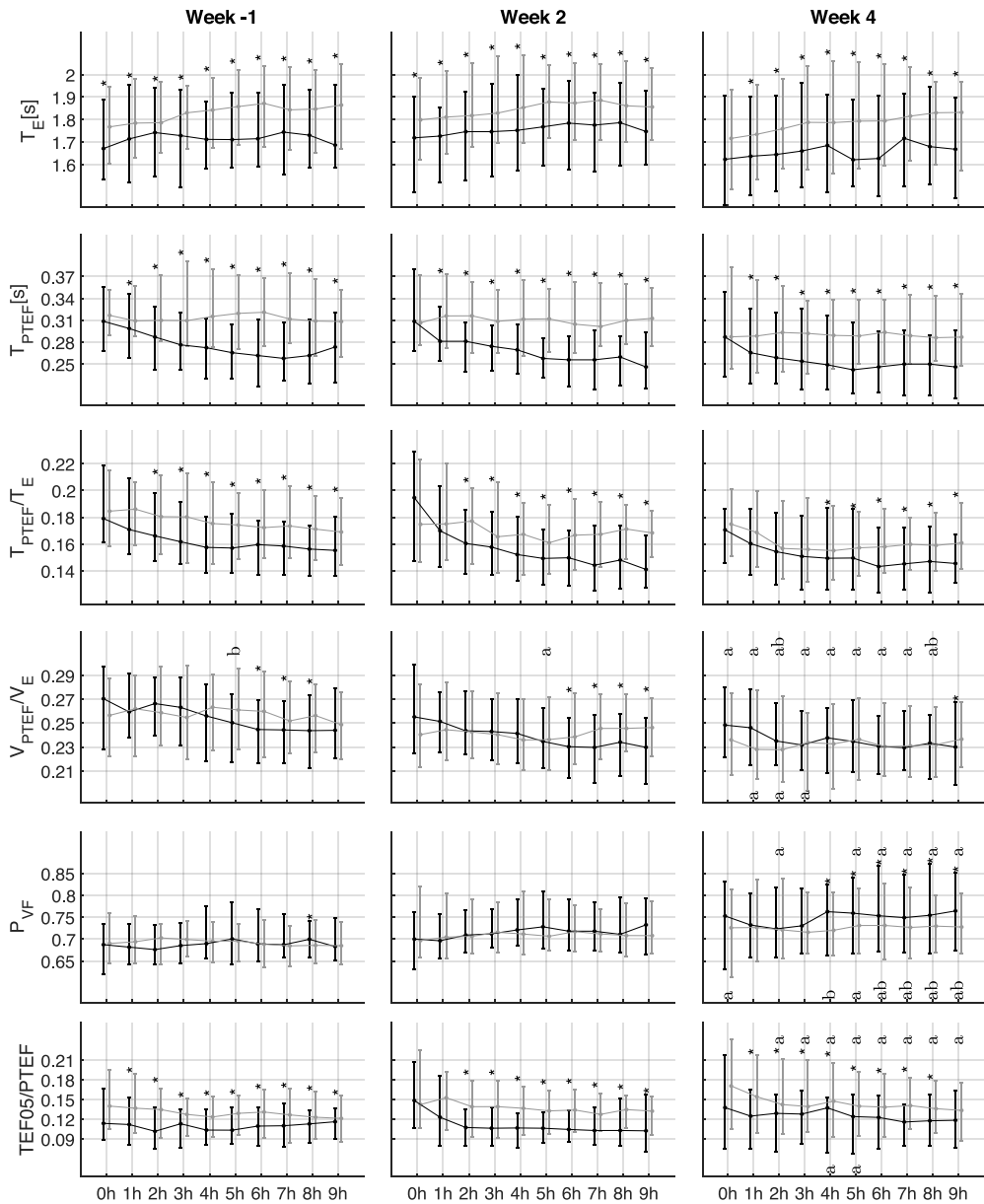
Fig. 3. Averaged hourly progression of several indices grouped by recording week and sleep stage. Rows correspond to an index and the columns to a recording week. Within each plot, the *x*-axis is the time from sleep onset (in hours) and the *y*-axis is the index value. Dots and vertical lines are median and interquartile ranges of all patients at a given time for NREM (grey) and REM (black). *: significant difference ($p < 0.01$) between sleep stages; a: significant difference ($p < 0.05$) between Week -1 and Week 4; b: significant difference ($p < 0.05$) between Week 2 and Week 4. Letters on top of vertical lines for NREM and letters on bottom for REM. All p values were calculated using the Wilcoxon signed sum test after Bonferroni corrections ($n = 3$).

had a different effect on the early and late parts of the expiratory TBFV profile than on the middle part. Changes in the early and late expiration were significant during the whole night for NREM. Changes in the middle expiration were significant in the second part of the night and larger for REM.

Lower T_E and T_{PTEF} values for REM than for NREM have been

observed in healthy and wheezing infants (Gracia-Tabuenca et al., 2019; Haddad et al., 1979), but not in adolescents (Tabachnik et al., 1981). We found that the ratio T_{PTEF}/T_E was lower for REM than for NREM but that V_{PTEF}/V_E was similar for both sleep stages. Such different results for these similar ratios can be explained by comparing the late part of expiration on the time and volume domains. For example,

Table 3

Spearman correlation coefficients between selected indices and patient age during NREM and REM recorded in the week under treatment (Week -1).

		Week -1	Week 2	Week 4
MAD(IBI) [s]	NREM	0.29 (0.02) *	0.35 (0.01) *	0.13 (0.33)
	REM	−0.01 (0.97)	0.10 (0.45)	−0.01 (0.96)
Heart rate [bpm]	NREM	−0.42 (0.00) ‡	−0,40 (0.00) ‡	−0.49 (0.00) ‡
	REM	−0.42 (0.00) ‡	−0.44 (0.00) ‡	−0.50 (0.00) ‡
Respiration rate [bpm]	NREM	0.17 (0.17)	0.13 (0.03) *	0.20 (0.13)
	REM	0.26 (0.04) *	0.23 (0.04) *	0.33 (0.01) *
T_E [s]	NREM	0.17 (0.19)	0.13 (0.30)	0.19 (0.14)
	REM	0.21 (0.09)	0.23 (0.07)	0.34 (0.01) *

Correlation tested using Spearman's rank correlation rho (ρ). *: $p < 0.0001$, ‡: $p < 0.0001$. The indices not included in the table had a nonsignificant correlation with $p > 0.05$.

the profiles in Fig. 1(A) and (B) present similar V_{PTEF}/V_E, but T_{PTEF}/T_E is lower in (B) because in the late part, expiratory airflow is low. Hence, a longer time is needed to produce the same change in volume as in (A), where the flow is higher. Thus, our results suggest that for REM sleep, the later part of exhalation was interrupted less often, whereas for NREM, exhalation was interrupted more often before reaching resting volume, as is also suggested by a higher TEF05/PTEF during REM. Shorter and uninterrupted exhalation during REM may be due to the natural decrease in respiratory musculature tone in this sleep stage (Horner, 2010). Intercostal atony in REM leads to a more compliant chest that deflates faster (Mortola et al., 1982; Otis et al., 1950). Intercostal atony together with a lower diaphragm tone decreases the functional residual capacity (FRC) (Henderson-Smart and Read, 1979). This decrease has been linked to uninterrupted or late interruption of expiration (Morris et al., 1998; Schmalisch et al., 2003).

The overnight decreasing trend in the REM bin medians, which is shared by T_{PTEF}, T_{PTEF}/T_E, V_{PTEF}/V_E, TEF50/PTEF, and TEF25/PTEF, may have been caused by a shortening of post-inspiration inspiratory activity (PIIA) during the night. For individuals of all ages, a decrease in T_{PTEF}, and therefore in T_{PTEF}/T_E and V_{PTEF}/V_E, is commonly understood as a shortening of PIIA (van der Ent et al., 1998). Shorter PIIA would also explain the lower TEF50/PTEF and TEF25/PTEF values because decreased expiratory braking leads to higher PTEF (Walraven et al., 2003). The shortening of PIIA during the night may be due to multiple factors such as a decrease in respiratory musculature tone during the night, as seen in asthmatic adults (Steier et al., 2011); an adaptation to a circadian increase in airway resistance (Bellia et al., 1989); or other circadian factors (Bohadana et al., 2002). In any case, changes in the sleep stage or night progression did not seem to affect the number of concave profiles, as assessed by P_{VF}, or the interruption of expiration, as assessed by TEF05/PTEF, at least for Week -1.

Changes in the off-medication TBFV profiles compared to the on-medication TBFV profiles were presumably caused by an increased number of children presenting airflow limitation. Such changes in the early, middle, and late parts of expiration agreed with the changes related to airflow limitation reported in the following studies. In the early part, the significant decrease in V_{PTEF}/V_E, T_{PTEF}/T_E, and T_{PTEF} was potentially caused by a shortening of PIIA. It has been speculated that individuals with airway obstruction have short PIIA braking to accommodate for the slower passive expiration (Carlsen and Carlsen, 1994; van der Ent et al., 1996). In the late part, the significant increase in TEF05/PTEF may be due to the early interruption of expiration with the purpose of elevating the FRC to increase airway calibre (Greenough et al., 1989; Wheatley et al., 1990). In the middle part, the significant increase in P_{VF} was most likely due to an increase in concavity, as observed in infants (Benoist et al., 1994) and adults (Williams et al., 1998). Bronchodilator use decreases airway obstruction, thus putatively making the TBFV profiles less concave. However, our results show that profiles were more concave the days where bronchodilator

was used. This apparent contradiction can be explained as follows. Bronchodilator use occurred mostly before the recording period and its effects are known to wear off after a few hours. Therefore, any changes in the profiles because of bronchodilator use were likely averaged out over the rest of the recording. Under these assumptions, bronchodilator use indicates that on that recording day, parents notice airflow limitation and applied the medication, but for most of the recording bronchodilator had no effects. This, together with the lack of correspondence between indices and classification criteria, suggests that nocturnal TBFV analysis may better reflect occasional worsening of asthma rather than the presence of the condition.

Why early and late indices differ during all hourly bins for NREM but not for REM can be explained by the decrease in respiratory musculature tone during REM. During NREM, active strategies to compensate for obstruction, such as shortening PIIA or interrupting expiration, are potentially reflected as changes in early and late expiration. However, during REM, decreased musculature tone reduces the strength of active strategies. Why middle expiration differs during the second half of the night more strongly for REM can be explained by the increase in lower airway resistance with night progression (Bellia et al., 1989) and the decreased musculature tone in REM. During the first half of the night, active strategies compensate for lower airway resistance, so middle expiration is less affected. The increased resistance overnight, despite active compensation, is reflected as an increase in concave middle expiration. During REM, as the decreased musculature tone reduces the strength of active strategies, the concavity of middle expiration is accentuated.

Our study has the following limitations. Firstly, the REM and NREM regions were not based on conventional polysomnography but on an indirect classification based on IBI variability. We assumed that the accuracy of our method was similar to that of Isler et al. (2016) or greater than this because we rejected the 5 min between stages where misclassification is higher. The sensitivity and specificity of the method of Isler et al. compared against standard polysomnographic classification, is 83% and 78% for REM and 78% and 83% for NREM. Additionally, Willemen et al. (2014) have summarised several studies on adults which found accuracies greater than 80% when variability in respiratory rate was used to separate REM from NREM sleep Secondly, we assumed that IP maintains a high linearity with mouth airflow overnight. Physiological changes during NREM and REM could degrade the strong agreement between IP and PNT results shown for awake children. Finally, our study group was rather heterogeneous. Some patients may not have responded to the medication, some may not have presented asthma, and it is unlikely that all nonmedicated asthmatics would have suffered from airflow limitation on the recording nights. In addition, our study included a few children younger than 2 years. Before this age, maturation affects the shape of the TBFV profiles in the late (Colin et al., 1989) and early parts (Frey et al., 2001). However, in a previous study, we demonstrated that airflow limitation is reflected as an increased concavity of the middle part in infants (Gracia-Tabuenca et al., 2019). The current IP technique also has its limitations. Patient movement may cause the detachment of the electrodes or contamination of the recordings. In this study, 22 of the 210 recordings had to be rejected. Although the correspondence between IP and PNT is independent of posture (Seppä et al., 2010), posture could affect respiratory mechanics and hence TBFV shapes (Mayer et al., 2003). Alternative electrodes such as textile electrodes and the effects of sleeping posture should be researched further.

5. Conclusion

We conclude that the analysis of TBFV profiles derived from nocturnal home IP recordings, holds the potential to monitor nocturnal symptoms in wheezing children. The IP system is easy to use at home on regular bases allowing for a frequent monitoring of patients' symptoms. Regular assessment may serve to identify children with nocturnal

airflow limitation aiding clinicians to take informed treatment adjustments. We observed that the IP of young children with recurrent wheezing, who were recorded overnight, was influenced by medication, sleep stage, and time from sleep onset. Two indicators may suggest the presence of airflow limitation in children. Firstly, an increase in the concavity of the middle expiration during REM in the second half of the night, likely caused by the natural decrease in respiratory musculature tone and circadian factors, and, secondly, changes in early and late expiration, assessed by V_{PTEF}/V_E and TEF05/PTEF, respectively, during NREM sleep, likely caused by active obstruction compensatory strategies.

Funding

Declaration of Competing Interest

V.-P. Seppä and J. Viik are shareholders in Tide Medical Oy, which holds patents related to impedance pneumography. V.-P. Seppä is an employee of Revenio Group Oyj, which commercializes impedance pneumography technology.

Acknowledgement

References

Allen, J.U., Gripp, K.A., 2002. Development of the thoracic cage. Chernick-Mellins Basic Mechanisms of Pediatric Respiratory Disease. pp. 51–124.

Baldwin, D.N., Pillow, J.J., Stocks, J., Frey, U., 2006. Lung-function tests in neonates and infants with chronic lung disease: tidal breathing and respiratory control. Pediatr. Pulmonol. 41, 391–419. https://doi.org/10.1002/ppul.20400.

Bates, J.H., 1998. Detecting airways obstruction from the tidal flow profile. Eur. Respir. J. 12, 1008–1009.

Bates, J.H., Schmalisch, G., Filbrun, D., Stocks, J., 2000. Tidal breath analysis for infant pulmonary function testing. ERS/ATS task force on standards for infant respiratory function testing. European Respiratory Society/American Thoracic Society. Eur. Respir. J. 16, 1180–1192.

Bellia, V., Cuttitta, G., Insalaco, G., Visconti, A., Bonsignore, G., 1989. Relationship of nocturnal bronchoconstriction to sleep stages. Am. Rev. Respir. Dis. 140, 363–367. https://doi.org/10.1164/ajrccm/140.2.363.

Benoist, M.R., Brouard, J.J., Rufin, P., Delacourt, C., Waernessyckle, S., Scheinmann, P., 1994. Ability of new lung function tests to assess methacholine-induced airway obstruction in infants. Pediatr. Pulmonol. 18, 308–316. https://doi.org/10.1002/ppul.1950180508.

Beydon, N., Davis, S.D., Lombardi, E., Allen, J.L., Arets, H.G.M., Aurora, P., Bisgaard, H., Davis, G.M., Ducharme, F.M., Eigen, H., Gappa, M., Gaultier, C., Gustafsson, P.M., Hall, G.L., Hantos, Z., Healy, M.J.R., Jones, M.H., Klug, B., Lodrup Carlsen, K.C., McKenzie, S.A., Marchal, F., Mayer, O.H., Merkus, P.J.F.M., Morris, M.G., Oostveen, E., Pillow, J.J., Seddon, P.C., Silverman, M., Sly, P.D., Stocks, J., Tepper, R.S., Vilozni, D., Wilson, N.M., on behalf of the American Thoracic Society/European Respiratory Society Working Group on Infant and Young Children Pulmonary Function Testing, 2007. An official American Thoracic Society/European Respiratory Society statement: pulmonary function testing in preschool children. Am. J. Respir. Crit. Care Med. 175, 1304–1345. https://doi.org/10.1164/rccm.200605-642ST.

Bohadana, A.B., Hannhart, B., Teculescu, D.B., 2002. Nocturnal worsening of asthma and sleep-disordered breathing. J. Asthma 39, 85–100. https://doi.org/10.1081/JAS-120002190.

Carlsen, K.H., Carlsen, K.L., 1994. Tidal breathing analysis and response to salbutamol in awake young children with and without asthma. Eur. Respir. J. 7, 2154–2159.

Colin, A.A., Wohl, M.E.B., Mead, J., Ratjen, F.A., Glass, G., Stark, A.R., 1989. Transition from dynamically maintained to relaxed end-expiratory volume in human infants. J. Appl. Physiol. 67, 2107–2111.

van der Ent, C.K., van der Grinten, C., Meessen, N.E., Luijendijk, S.C., Mulder, P.G., Bogaard, J.M., 1998. Time to peak tidal expiratory flow and the neuromuscular control of expiration. Eur. Respir. J. 12, 646–652.

Fleming, P.J., Levine, M.R., Goncalves, A., 1982. Changes in respiratory pattern resulting from the use of a facemask to record respiration in newborn infants. Pediatr. Res. 16, 1031–1034. https://doi.org/10.1203/00006450-198212000-00013.

Flores-Guevara, R., Plouin, P., Curzi-Dascalova, L., Radvanyi, M.-F., Guidasci, S., Pajot, N., Monod, N., 1982. Sleep apneas in normal neonates and infants during the first 3 months of Life1. Neuropediatrics 13, 21–28. https://doi.org/10.1055/s-2008-1059630.

Frey, U., Silverman, M., Suki, B., 2001. Analysis of the harmonic content of the tidal flow waveforms in infants. J. Appl. Physiol. 91, 1687–1693.

Gracia, J., Seppä, V.-P., Pelkonen, A., Kotaniemi-Syrjänen, A., Mäkelä, M., Malmberg, P., Viik, J., 2017. Nonlinear local projection filter for impedance pneumography. In: EMBEC & NBC 2017, IFMBE Proceedings. Springer, Singapore. pp. 306–309. https://doi.org/10.1007/978-981-10-5122-7_77.

Gracia-Tabuenca, J., Seppä, V.-P., Jauhiainen, M., Kotaniemi-Syrjänen, A., Malmström, K., Pelkonen, A., Mäkelä, M.J., Viik, J., Malmberg, L.P., 2019. Tidal breathing flow volume profiles during sleep in wheezing children measured by impedance pneumography. J. Appl. Physiol. https://doi.org/10.1152/japplphysiol.01007.2018.

Greenough, A., Pool, J., Price, J.F., 1989. Changes in functional residual capacity in response to bronchodilator therapy among young asthmatic children. Pediatr. Pulmonol. 7, 8–11. https://doi.org/10.1002/ppul.1950070104.

Guilleminault, C., Winkle, R., Korobkin, R., Simmons, B., 1982. Children and nocturnal snoring: evaluation of the effects of sleep related respiratory resistive load and daytime functioning. Eur. J. Pediatr. 139, 165–171.

Haddad, G.G., Epstein, R.A., Epstein, M.A., Leistner, H.L., Marino, P.A., Mellins, R.B., 1979. Maturation of ventilation and ventilatory pattern in normal sleeping infants. J. Appl. Physiol. 46, 998–1002. https://doi.org/10.1152/jappl.1979.46.5.998.

Henderson-Smart, D.J., Read, D.J., 1979. Reduced lung volume during behavioral active sleep in the newborn. J. Appl. Physiol. 46, 1081–1085. https://doi.org/10.1152/jappl.1979.46.6.1081.

Horner, R.L., 2010. Respiratory physiology: central neural control of respiratory neurons and motoneurons during sleep. Principles and Practice of Sleep Medicine. Saunders, pp. 237–249.

Hutten, G.J., van Eykern, L.A., Latzin, P., Kyburz, M., van Aalderen, W.M., Frey, U., 2008. Relative impact of respiratory muscle activity on tidal flow and end expiratory volume in healthy neonates. Pediatr. Pulmonol. 43, 882–891. https://doi.org/10.1002/ppul.20874.

Isler, J.R., Thai, T., Myers, M.M., Fifer, W.P., 2016. An automated method for coding sleep states in human infants based on respiratory rate variability. Dev. Psychobiol. 58, 1108–1115. https://doi.org/10.1002/dev.21482.

Leonhardt, S., Ahrens, P., Kecman, V., 2010. Analysis of tidal breathing flow volume loops for automated lung-function diagnosis in infants. IEEE Trans. Biomed. Eng. 57, 1945–1953. https://doi.org/10.1109/TBME.2010.2046168.

Lodrup-Carlsen, K.C., Carlsen, K.H., 1993. Lung function in awake healthy infants: the first five days of life. Eur. Respir. J. 6, 1496–1500.

Maarsingh, E.J.W., van Eykern, L.A., Sprikkelman, A.B., Hoekstra, M.O., van Aalderen, W.M.C., 2000. Respiratory muscle activity measured with a noninvasive EMG technique: technical aspects and reproducibility. J. Appl. Physiol. 88, 1955–1961.

Malmberg, L.P., Seppä, V.-P., Kotaniemi-Syrjänen, A., Malmström, K., Kajosaari, M., Pelkonen, A.S., Viik, J., Mäkelä, M.J., 2017. Measurement of tidal breathing flows in infants using impedance pneumography. Eur. Respir. J. 49, 1600926. https://doi.org/10.1183/13993003.00926-2016.

Mayer, O.H., Clayton, R.G., Jawad, A.F., McDonough, J.M., Allen, J.L., 2003. Respiratory inductance plethysmography in healthy 3- to 5-year-old children*. Chest 124, 1812–1819. https://doi.org/10.1378/chest.124.5.1812.

Morris, M.J., Lane, D.J., 1981. Tidal expiratory flow patterns in airflow obstruction. Thorax 36, 135–142. https://doi.org/10.1136/thx.36.2.135.

Morris, M.J., Madgwick, R.G., Collyer, I., Denby, F., Lane, D.J., 1998. Analysis of expiratory tidal flow patterns as a diagnostic tool in airflow obstruction. Eur. Respir. J. 12, 1113–1117. https://doi.org/10.1183/09031936.98.12051113.

Mortola, J.P., Fisher, J.T., Smith, B., Fox, G., Weeks, S., 1982. Dynamics of breathing in infants. J. Appl. Physiol. 52, 1209–1215. https://doi.org/10.1152/jappl.1982.52.5.1209.

Otis, A.B., Fenn, W.O., Rahn, H., 1950. Mechanics of breathing in man. J. Appl. Physiol. 2, 592–607.

Rabbette, P.S., Fletcher, M.E., Dezateux, C.A., Soriano-Brucher, H., Stocks, J., 1994. Hering-Breuer reflex and respiratory system compliance in the first year of life: a longitudinal study. J. Appl. Physiol. 76, 650–656. https://doi.org/10.1152/jappl.1994.76.2.650.

Sato, J., Robbins, P.A., 2001. Methods for averaging irregular respiratory flow profiles in awake humans. J. Appl. Physiol. 90, 705–712.

Schmalisch, G., Wauer, R.R., Foitzik, B., Patzak, A., 2003. Influence of preterm onset of inspiration on tidal breathing parameters in infants with and without CLD. Respir. Physiol. Neurobiol. 135, 39–46. https://doi.org/10.1016/S1569-9048(03)00029-6.

Schmidt, M., Foitzik, B., Wauer, R.R., Winkler, F., Schmalisch, G., 1998. Comparative investigations of algorithms for the detection of breaths in newborns with disturbed respiratory signals. Comput. Biomed. Res. 31, 413–425. https://doi.org/10.1006/cbmr.1998.1493.

Scholle, S., Wiater, A., Scholle, H.C., 2011. Normative values of polysomnographic parameters in childhood and adolescence: cardiorespiratory parameters. Sleep Med. 12, 988–996. https://doi.org/10.1016/j.sleep.2011.05.006.

Seppä, V.-P., Hyttinen, J., Uitto, M., Chrapek, W., Viik, J., 2013a. Novel electrode configuration for highly linear impedance pneumography. Biomed. Technol. Eng. 58. https://doi.org/10.1515/bmt-2012-0068.

Seppä, V.-P., Hyttinen, J., Viik, J., 2011. A method for suppressing cardiogenic oscillations in impedance pneumography. Physiol. Meas. 32, 337. https://doi.org/10.1088/0967-3334/32/3/005.

Seppä, V.-P., Pelkonen, A.S., Kotaniemi-Syrjänen, A., Mäkelä, M.J., Viik, J., Malmberg, L.P., 2013b. Tidal breathing flow measurement in awake young children by using impedance pneumography. J. Appl. Physiol. 115, 1725–1731. https://doi.org/10.1152/japplphysiol.00657.2013b.

Seppä, V.-P., Pelkonen, A.S., Kotaniemi-Syrjänen, A., Viik, J., Mäkelä, M.J., Malmberg, L.P., 2016. Tidal flow variability measured by impedance pneumography relates to childhood asthma risk. Eur. Respir. J. https://doi.org/10.1183/13993003.00989-2015. ERJ-00989-2015.

Seppä, V.-P., Viik, J., Hyttinen, J., 2010. Assessment of pulmonary flow using impedance pneumography. IEEE Trans. Biomed. Eng. 57, 2277–2285. https://doi.org/10.1109/TBME.2010.2051668.

Steier, J., Jolley, C.J., Polkey, M.I., Moxham, J., 2011. Nocturnal asthma monitoring by chest wall electromyography. Thorax 66, 609–614. https://doi.org/10.1136/thx.2010.152462.

Tabachnik, E., Muller, N.L., Bryan, A.C., Levison, H., 1981. Changes in ventilation and chest wall mechanics during sleep in normal adolescents. J. Appl. Physiol. 51, 557–564. https://doi.org/10.1152/jappl.1981.51.3.557.

Traeger, N., Schultz, B., Pollock, A.N., Mason, T., Marcus, C.L., Arens, R., 2005. Polysomnographic values in children 2-9 years old: additional data and review of the literature. Pediatr. Pulmonol. 40, 22–30. https://doi.org/10.1002/ppul.20236.

van der Ent, C.K., Brackel, H.J.L., Mulder, P., Bogaard, J.M., 1996. Improvement of tidal breathing pattern analysis in children with asthma by on-line automatic data processing. Eur. Respir. J. 9, 1306–1313. https://doi.org/10.1183/09031936.96.09061306.

Walraven, D., van der Grinten, C.P.M., Bogaard, J.M., van der Ent, C.K., Luijendijk, S.C.M., 2003. Modeling of the expiratory flow pattern of spontaneously breathing cats. Respir. Physiol. Neurobiol. 134, 23–32. https://doi.org/10.1016/S1569-9048(02)00206-9.

Wheatley, West, S., Cala, S.J., Engel, L.A., 1990. The effect of hyperinflation on respiratory muscle work in acute induced asthma. Eur. Respir. J. 3, 625–632.

Willemen, T., Deun, D.V., Verhaert, V., Vandekerckhove, M., Exadaktylos, V., Verbraecken, J., Huffel, S.V., Haex, B., Sloten, J.V., 2014. An evaluation of cardiorespiratory and movement features with respect to sleep-stage classification. IEEE J. Biomed. Health Inform. 18, 661–669. https://doi.org/10.1109/JBHI.2013.2276083.

Williams, E.M., Madgwick, R.G., Morris, M.J., 1998. Tidal expired airflow patterns in adults with airway obstruction. Eur. Respir. J. 12, 1118–1123. https://doi.org/10.1183/09031936.98.12051118.

PUBLICATION

P.IV

Sources of Variability in Expiratory Flow Profiles during Sleep in Healthy Young Children

A. Hult, R. G. Juraški, J. Gracia-Tabuenca, M. Partinen, D. Plavec and V.-P. Seppä

Sources of variability in expiratory flow profiles during sleep in healthy young children

Anton Hult[a], Romana Gjergja Juraški[b,c], Javier Gracia-Tabuenca[d], Markku Partinen[e,f], Davor Plavec[c,g], Ville-Pekka Seppä[a,*]

[a] Revenio Research Ltd., Vantaa, Finland
[b] Sleep Laboratory, Srebrnjak Children's Hospital, Zagreb, Croatia
[c] Medical Faculty, University JJ Strossmayer, Osijek, Croatia
[d] Faculty of Medicine and Health Technology, Tampere University, Tampere, Finland
[e] Helsinki Sleep Clinic, Vitalmed Research Center, Helsinki, Finland
[f] Department of Clinical Neurosciences, University of Helsinki, Helsinki, Finland
[g] Research Department, Srebrnjak Children's Hospital, Zagreb, Croatia

ABSTRACT

Standard lung function tests are not feasible in young children, but recent studies show that the variability of expiratory tidal breathing flow-volume (TBFV) curves during sleep is a potential indirect marker of lower airway obstruction. However, the neurophysiological sources of the TBFV variability in normal subjects has not been established.

We investigated sleep stages and body position changes as potential sources for the TBFV curve variability. Simultaneous impedance pneumography (IP), polysomnography (PSG) and video recordings were done in 20 children aged 1.4–6.9 years without significant respiratory disorders during sleep.

The early part of expiratory TBFV curves are less variable between cycles of REM than NREM sleep. However, within individual sleep cycles, TBFV curves during N3 are the least variable. The differences in TBFV curve shapes between sleep stages are the main source of overnight variability in TBFV curves and the changes in body position have a lesser impact.

1. Introduction

Objective evidence of airway obstruction is essential for the diagnosis and monitoring of asthma (Global Initiative for Asthma, 2018). Usually lung function is tested by spirometry, but for subjects with limited cognitive or physical capabilities, such as patients with developmental disabilities, elderly or young children, the spirometric respiratory maneuvers are too demanding. However, tidal breathing flow profiles also contain information regarding the presence of airway obstruction.

Because tidal breathing variability analysis is still in its early phases as a field, studies so far have taken varied approaches leading to different measurement duration and technique, differing study populations (age and cognitive state, i.e. sleep or awake) and various extracted parameters from the tidal breathing flow-volume (TBFV) curves. Despite the differences in study methods, the overall finding has been that reduced tidal breathing variability is associated with airway obstruction in asthmatic adults (Veiga et al., 2011) and asthmatic children (Seppä et al., 2016), in adults with COPD (Dames et al., 2014; Motamedi-Fakhr et al., 2016; Niérat et al., 2017) and infants with bronchopulmonary dysplasia (Usemann et al., 2019).

Recently, we showed that such lack of variability distinguishes children with recurrent wheeze (asthma) from healthy children also during sleep at night when measured using impedance pneumography (IP) (Seppä et al., 2019). We also discovered that the obstruction-related reduction in tidal breathing variability is mostly associated with a specific part of the expiration, namely, 15–45% of expired volume. Moreover, obstruction-related changes in the TBFV curves were recently shown to be sleep stage-associated (Gracia-Tabuenca et al., 2019).

Based on the aforementioned findings, this IP measurement method may have a significant impact on the clinical practice of assessing lower airway obstructions (wheeze, asthma) in young children who cannot be easily assessed with any other method at the moment. Thus, it is

important to explore the underlying neurophysiological mechanisms of a new method like this. The aim of this study is to investigate the sources of variability in expiratory TBFV curves during sleep to better understand the neurophysiological origins of the normal (healthy) TBFV curve variability. In this study, we investigated sleep stages and body position changes as sources for the normal TBFV curve variability. Firstly, we explored if there is temporal synchrony in how the different parts (volume ranges) of the expiratory TBFV curves change throughout the night. Secondly, we assessed how similar the TBFV curves are within and between different sleep stages, and lastly, we analyzed the potential effect of body position changes on the TBFV curve variability.

2. Materials and methods

2.1. Subjects

The study recruited children who were clinically referred to a polysomnography (PSG) study and healthy children without any relevant symptoms. The inclusion criteria for the referred group was age 1–7 years, both sexes, referral to PSG and a signed informed consent. The inclusion criteria for the healthy children were: age 2–7 years, both sexes, healthy at the time of inclusion based on history and clinical examination according to the investigator's judgment and the signed informed consent. All the children that met the inclusion criteria were in the range of normal regarding the apnea-hypopnea index, since subjects who had signs of obstruction or sleep apnea during the PSG were excluded.

The main exclusion criteria were history or risk of asthma, chronic conditions that may alter breathing pattern, continuous upper airway airflow limitation, or other significant clinical findings in the PSG (full list available at https://clinicaltrials.gov/ct2/show/NCT03408990).

One overnight measurement was done for each subject in a sleep laboratory at the Children's Hospital Srebrnjak, Zagreb, Croatia between January 2018 and December 2018. The study was approved by the local ethics committee, guardians of all subjects gave a written informed consent, and the Declaration of Helsinki and Good Clinical Practice were followed.

2.2. Measurement setup

The overnight measurement included a full PSG recording with video and a simultaneous TBFV curve shape measurement using IP equipment. IP is a method for indirect measurement of lung tissue aeration (volume) changes through skin electrodes. With correct electrode placement strategy (Seppä et al., 2013a) and signal processing (Seppä et al., 2011), the method can record TBFV curve shapes accurately in young children (Seppä et al., 2013b; Malmberg et al., 2017).

The PSG study was done by using the EEG-1200 (Nihon Kohden, CA, USA), the signals (6 channel electroencephalogram, electrooculogram, peripheral oxygen saturation, nasal pressure, abdominal and thoracic plethysmography) were analyzed using the Polysmith (Nihon Kohden, CA, USA) and Polaris (Nihon Kohden, CA, USA) softwares by an experienced sleep technician. The PSG-signals were analyzed in 30-second epochs. The IP measurement was done using a Ventica Recorder (Revenio Research Ltd., Finland), providing the following signals: IP, electrocardiogram (ECG) and accelerometer. Sleep staging was done according to the current AASM guideline (Berry et al., 2018). Apneic and hypopneic events were identified from the PSG signals. The changes in body position during the night were annotated from a video recording by a human operator.

2.3. Signal processing & calculating TBFV curves

IP signal processing to derive TBFV curves was done with a commercially available software (Ventica Analytics 2.0.1, Revenio Research Ltd., Finland) and the subsequent analysis of the curves was done using MATLAB (R2017b, MathWorks Inc., USA).

The Ventica Analytics software provides averaged TBFV curves, calculated by averaging raw TBFV curves in a moving 5-minute window, with 2.5-minute steps. Before generating the TBFV curves, distorted parts of the IP, ECG and accelerometer signals were discarded at the beginning of the signal processing. The resulting TBFV curves represent normal breathing, where sighs, coughs, crying etc. have been excluded.

We were only interested in the exhale part of the TBFV curves, based on the findings from previous studies, where it was shown that it is possible to differentiate between healthy subjects and asthmatics with the help of the exhale part (Gracia-Tabuenca et al., 2019; Seppä et al., 2019). Here we analyzed two ranges of interest, namely, 15–45% and 55–85% of expired volume. The earlier (15–45%) part is used in the expiratory variability index (EVI) parameter derived by the Ventica Analytics software and it has been shown to be the best at differentiating between wheezy and healthy children (Seppä et al., 2019). The latter (55–85%) part was included because it presumably represents mostly passive expiration (post-inspiratory muscle activity has ceased) and Gracia-Tabuenca et al. (2019) showed that parameters derived from that part show significant differences between asthma risk categories in young children.

To make sure that the analysis was accurate it had to be ensured that the Ventica-signals and the PSG-signals were synchronized so that the parameters derived and calculated from these signals were comparable. Both the PSG and Ventica measurements were started as simultaneously as possible, leading to at most a difference of some seconds in the start times. The temporal synchronization was done by manually comparing the breathing signals from both sources, finding multiple reference points seen in both signals (for ex. distortion caused by movement) and iteratively searching for the correct time shift for the PSG-signal so that the signals are aligned.

2.4. TBFV curve analysis

2.4.1. Averaged TBFV curves and their mutual correlation

To ensure that averaged TBFV curves only belong to one sleep stage, we rejected these averaged TBFV curves resulting from 5-minute windows situated partially in two different sleep stages. For each recording, then the Pearson correlation was calculated between all of the accepted averaged TBFV curves for the 15–45% and 55–85% ranges of the exhaled volume. This process results in two separate correlation matrices, which show how similar or different the TBFV curves are between different points in time during the night (Fig. 2). These matrices from all recordings were the base for the different analyses presented in Fig. 1.

2.4.2. Time-synchrony of change in different parts of TBFV curves

In order to assess whether the changes in the TBFV curve shape occur at the same time in different parts of the exhaled TBFV curve, we calculated the Pearson correlations between all the averaged TBFV curves of a measurement night within ranges of 30% of exhaled volume (0–30%, 5–35%, 10–40% all the way to 70–100%). This resulted in a correlation matrix for each range, where the axes are the sleep time and the correlation coefficients indicate how similar or different the averaged TBFV curves were at different points of the night. After establishing the correlations between the TBFV curves within each volume range, the cross-correlation between the correlation matrices of different ranges was calculated to find out if the changes occur synchronously in time in different parts of the TBFV curve. If the correlation between two ranges (i.e. 0–30% and 5–35%) is high, it means that the changes in the TBFV curve happens at similar points in time during the night. If the correlation is close to 0, it means that the TBFV curve changes occur at different time points in the two compared ranges of the curve.
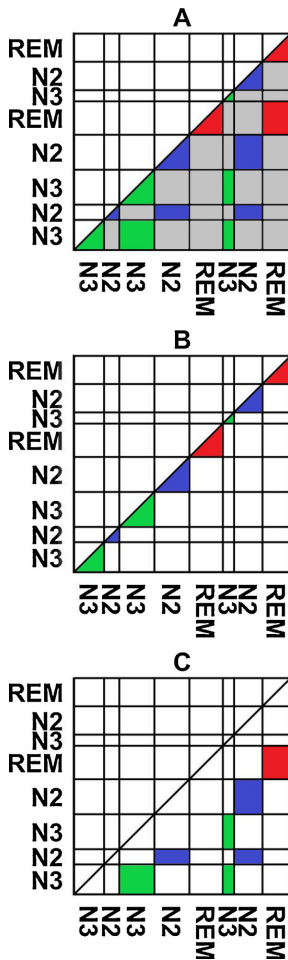
Fig. 1. The sleep stage analyses of this study explained visually, based on the correlation matrix resulting from calculating the Pearson correlation between the accepted averaged TBFV curves of the night. The x- and y-axes represent the sleep time. The non-white cells in the matrices indicate that the data within the cell (correlation values) are part of the analysis. The non-grey colored areas represent the data behind the same colored boxes in Figs. 4 and 5, where N2 is shown in blue, N3 in green, and REM in red. Panel A shows the data behind Fig. 4, B and C show respectively the within sleep stage cycle and between cycle correlations of Fig. 5.

2.4.3. TBFV curve variability within and between sleep stage cycles

To better understand if there are certain types of breathing patterns in the sleep stages and whether they differ from one sleep stage to another, the averaged TBFV curves of the whole night were divided according to sleep stages (wake, N1, N2, N3 and REM) and the cross-correlations were calculated between the curves. These results show us if the TBFV curve variability differs in different sleep stages. We also extracted the averaged TBFV curve correlations within single sleep stage cycles to understand if the curve patterns behave differently within cycles in comparison to all sleep stages combined.

2.4.4. Effect of body position change on averaged TBFV curves

In addition to purely analyzing the averaged TBFV curves in regards of sleep stages, we also analyzed the effect of changes in body position
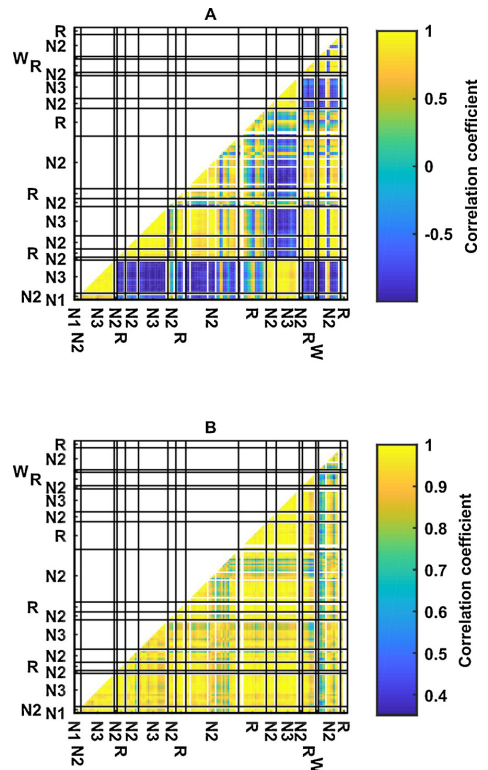
Fig. 2. Example of night-time correlation between TBFV curves in one individual. Both axes represent linear time from sleep onset (bottom left) to awakening (top right). The black lines represent a change in sleep stages. The sleep stages of the night are specified on both axes. Panels A and B represent TBFV curve parts of 15–45% and 55–85% of exhaled volume, respectively.

on the averaged TBFV curves throughout the night. This analysis was broken down into sleep stages, to better see if body position change has different outcomes on breathing in different sleep stages. The analysis was done by taking the last averaged TBFV curve before a change in position (averaging window ends before change in position) and the first curve after (averaging window begins after change in position), and calculating the correlation between the two curves. If the averaged TBFV curve before the position change is in a different sleep stage than the first curve after the change, they were discarded from the analysis. The reason for this is to enable assessing solely body position change effect without simultaneous sleep stage change effect.

2.5. Statistical analysis

Pearson correlation was used in all correlation calculations between the averaged TBFV curves. This method was the same as used by Seppä et al. (2019) and was able to differentiate between healthy subjects and asthmatics. All tests of difference between multiple data groups were done using the Kruskal–Wallis test.

3. Results

Fig. 2 illustrates the correlation matrices from a representative recording. This example shows several typical features: 1) Latter part of the TBFV curve (panel B) is generally more stable (higher absolute

correlations) than the earlier part (panel A), 2) effect of sleep stage changes (especially stage 3 non-REM sleep; N3) on the curve shape is more prominent in the early part, and 3) the early part of the TBFV curve during N3 is very similar within one cycle (next to the matrix diagonal), but can be quite different between two cycles of N3 (away from the diagonal).

3.1. Patient characteristics and polysomnographic findings

20 subjects (8 female) aged 4.0 (1.4–6.9) (median and range) years were included in the study. 7 of the children had been referred to a polysomnography (PSG) study on clinical grounds and other were healthy volunteers.

N1, N2, N3, REM and wake stages constituted 2.2 (1.7)% (mean, SD), 43.6 (5.4)%, 28.1 (4.5)%, 21.0 (5.1)%, 5.1 (5.5)% of sleep duration, respectively. These agree with previously reported values for proportions of sleep stages during sleep (Traeger et al., 2005). Because N1 constituted such a small part of the sleep time, it was not analyzed any further. Also the impact of apneic/hypopneic events were not analyzed because they were so rare and short in duration.

3.2. Time-synchrony of change in different parts of TBFV curves

As expected, the changes in the expiratory TBFV curve occurred more synchronously between overlapping, adjacent parts (above the black diagonal line in Fig. 3) and the synchronicity gradually reduced as the overlap reduced (towards the black line). More interesting is the synchronicity between non-overlapping curve parts. Unexpectedly, the highest degree of asynchrony was not found between the parts that are farthest away from each other (bottom right in Fig. 3), but between the range 15–45% and all the other parts. This means that 15–45% is the most independent range in terms of timing of changes in the curve. In fact, a change in the last parts of the curve (after 55% of exhaled volume) is more likely to be accompanied by a simultaneous change in the earliest parts (before 40%) than in the middle parts of the curve.

3.3. Variability of TBFV curve shapes in sleep stages

For both TBFV curve ranges, REM and wake stage showed higher correlations and lower variability (curves more similar to each other) than N2 or N3 (Fig. 4) when comparing TBFV curves from all the cycles of the same sleep stage. Curves from REM and wake stage were also mutually similar to each other. Slightly paradoxically, in the latter

Fig. 3. Mean time synchrony of changes between different parts in the averaged TBFV curves. High correlation means that the curve parts are likely to change shape at the same time during sleep. Low correlation means that they may change independently of each other. The area below the diagonal black line has only non-overlapping curve parts. The correlation coefficient values have been transformed logarithmically, to emphasize the differences.

curve range, curves during N2 and N3 were better correlated with curves from REM than within N2 or N3 (Fig. 4, panel B). The variability in TBFV curves was significantly different between sleep stages in both curve ranges ($p < 0.0001$).

Interesting properties were discovered when the curve comparisons were done either only within individual sleep stage cycles or between different cycles of the same sleep stage (Fig. 5); The range 15–45% N3 showed even slightly higher correlations than REM *within cycles*, but, on the contrary, very low correlation between separate cycles. In practice this means that the 15–45% part of the TBFV curve is remarkably stable during each continuous cycle of N3 sleep, but can have significantly different shape between different cycles of N3 sleep. For the latter range 55-85 % such behaviour was not clearly present. Moreover, the REM and wake stages showed highest median correlations irrespective of analysis type (within/between cycles) for the latter range. Significant differences were found in both curve ranges, when comparing the correlation distributions shown in Fig. 5 ($p < 0.0001$).

3.4. Effect of body position change on TBFV curves

There were expected differences in the rate of movement in different sleep stages with N2, N3, REM and awake having 1.5, 0.4, 2.2, 0.5 movements per hour (mean), respectively.

The correlations in the 15–45% part of curves compared right before and after a movement event (Fig. 6) were lower than the correlations within each cycle of a certain sleep stage (Fig 5) which indicates that body position changes do have an effect on the TBFV curve shape. The effect was, however, smaller than what was caused by a change in sleep stage, especially for N3. Only the latter curve range showed statistical significance when comparing the effect of body position in different sleep stages ($p < 0.0001$), while in the early part of the curve there was no significance.

For the latter part of the curve the body position change seemed to have less effect on the curve shape (again comparing Figs. 6 and 5). If changes in body position would not have had any effect on the TBFV curve shape, the distributions in Fig. 6 should have been the same as the within sleep cycle distributions in Fig. 5. This analysis only included body position changes that occurred without a simultaneous sleep stage change.

4. Discussion

Our findings display that the different parts of the TBFV curves show a degree of independence since they change shape asynchronously in time. An interesting result was that the degree of synchronicity is not the smallest between the earliest and latest parts of the curve. Instead, the last parts of the curve show a higher degree of synchronicity with the earliest parts than with the middle parts. This finding corroborates the special properties of the 15–45% part since it was also found to be the most susceptible for a reduction in its variability in the presence of lower airway obstruction (Seppä et al., 2019). This finding may be associated with the fact that the middle parts of the curve have been found to exhibit a higher absolute level of variability than the other parts (Seppä et al., 2019).

We found the curve shape variability to be considerably higher in the early part than in the late part of the curve which is in line with our previous findings (Seppä et al., 2019). This may be to some extent attributed to the approach we have taken in quantifying the variability (linear correlation between curves) and to the general shape of the expiratory TBFV curves. Namely, the flow peak of the curve occurs during the early section whereas the latter section is characterized by a monotonic decay of flow rate. This renders the earlier part of the curve more susceptible to variation (low correlation values between curves) because even if the curve shape remained the same around the peak flow region, small movements in the peak flow location (within the fixed window of 15–45%) cause a marked drop in the curve correlation
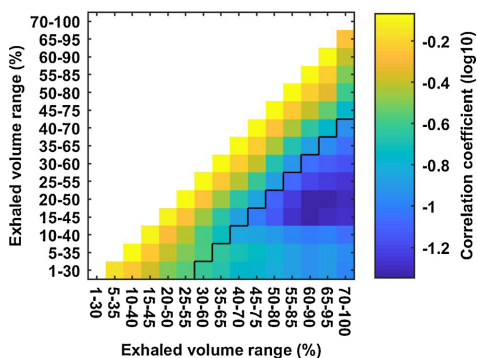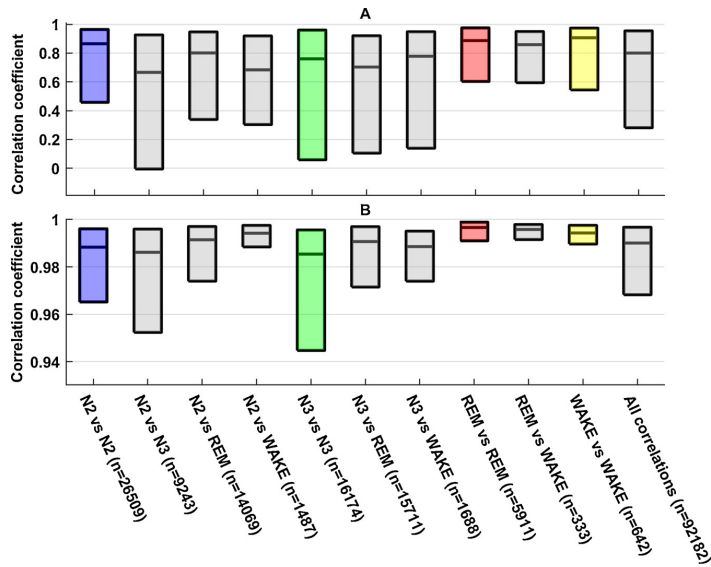
Fig. 4. Correlation between averaged TBFV curves, divided in sleep stages. Correlation values from all the subjects pooled together. Panels A and B represent TBFV curve parts of 15–45% and 55–85% of exhaled volume, respectively.
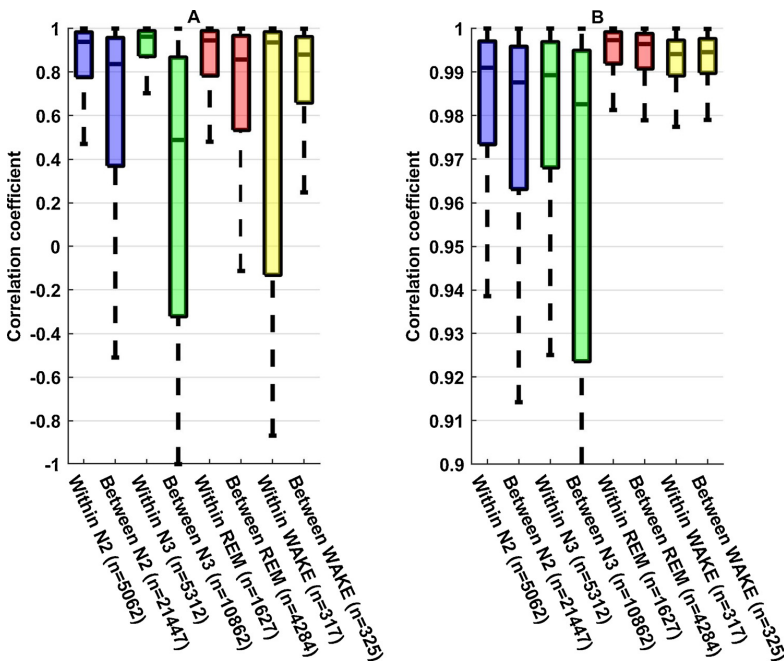

Fig. 5. Correlation between averaged TBFV curves, divided in sleep stages, showing the correlation within individual sleep stage cycles and between different cycles of the same sleep stage. Correlation values from all the subjects pooled together. Panels A and B represent TBFV curve parts of 15–45% and 55–85% of exhaled volume, respectively.

value. Such an effect is naturally less prominent in the late part of the curve due to the monotonic shape of the curve. This should, however, only affect the general level of the correlation values between the early and late parts and the interpretation of the effect of sleep stages or body position changes is still valid and comparable for both curve parts.

The expiratory limb of the TBFV curves is shaped by a multitude of factors: passive, such as the combined recoil of lungs and thoracic cage

and the caliber of lower and upper airways (Otis et al., 1950); and active, such as post-inspiratory inspiratory activity (PIIA), glottal breaking, and expiration interruption (Richter and Smith, 2014). These factors have a different contribution to the early and late part of the curves. The early part is most likely dominated by PIIA and glottal breaking, whereas the late part is mostly passive unless expiration is interrupted before reaching resting volume (typical in newborns) (van
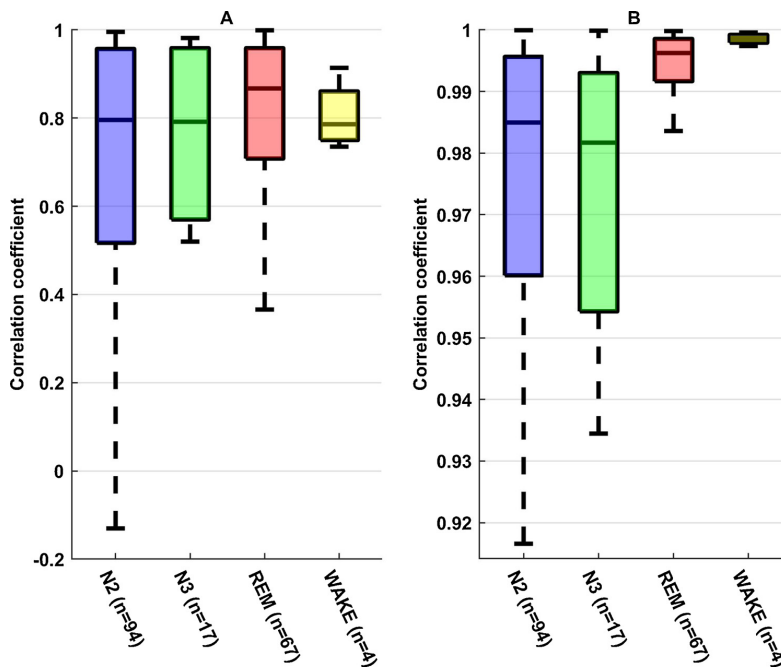
Fig. 6. Correlation between averaged TBFV curves right before and after a body position change. Results here should be compared to the correlation level presented in Fig. 5 within sleep stage cycle. Panels A and B represent TBFV curve parts of 15–45% and 55–85% of exhaled volume, respectively.

der Ent et al., 1998; Hutten et al., 2008). Shee et al. (1985) showed that in awake healthy adults at 23% of the total expiratory time, 50% of the muscle activity is still present and that only at 79% of the expiratory time the activity ceases completely. Similar values were found by Mortola et al. (1984) for sleeping newborns. The decay time of PIIA means that the early section in our analysis is likely to be affected more by PIIA and the latter less if at all, suggesting that the latter curve shape would be more determined by the passive airway and chest wall mechanics. However, also the adductor and abductor muscles in the pharynx and larynx affect the upper airway patency and thus may also affect TBFV curves. They show both phasic (in concert with the respiratory cycles) (England et al., 1985) and tonic (continuous) activity and the activity level depends on sleep stage (Carroll and Donnelly, 2014).

When comparing TBFV curves from all cycles of the same sleep stage throughout the night, we found both early and late parts to be generally less variable during REM than NREM sleep. An interesting feature is that, for the early part (15–45%), the lowest variability occurs within the same N3 sleep cycles, but at the same time, the highest variability appears between different N3 cycles of the night. NREM and in particular N3 is characterized by remarkably regular respiration and decreased muscle tone. Regular respiration in N3 is seen as a low variability in breath-to-breath amplitude and in frequency (Rostig et al., 2005), as well as in a low complexity in the short-term (3 minutes) flow signal (Burioka et al., 2003). Our results show that also the expiratory TBFV is regular during the same NREM cycle. This suggests that the above-mentioned factors shaping expiration remain stable within a NREM cycle. However, our results also show that expiration shape changes between NREM cycles. This suggest that there is more than one configuration of factors that produce a regular within cycle respiration. At different NREM cycles across the night, respiratory control may be attracted into different configurations of factors providing regular respiration (Donaldson, 1992), and for this reason, TBFV profiles between

NREM cycles appear dissimilar.

The lower variability of the curve shape during REM in comparison to NREM might be unexpected considering that REM sleep is characterized by significantly higher variability in respiration rhythm (Willemen et al., 2014). The source of this variability is caused by REM-dependent alterations in the motoneurons relaying the respiratory drive (Horner, 2010). Despite the pronounced breath-to-breath variations in duration and amplitude of the respiratory stimulus, our results show that the expiratory limb remains relatively similar within and between REM cycles. This may be explained by the decrease in tone in upper and lower respiratory musculature during REM, which leads to an increase in upper airways resistance (increased collapsibility), a decrease in the contribution of the rib-cage to respiration, and a lower functional residual capacity (Gaultier, 1995). These neurophysiological limitations during REM translate into a reduction in the dynamic range for the factors shaping the expiratory profile. Constricted factors increase the chances of profiles being similar within and between REM cycles across the night.

Because of the small sample size, it is difficult to analyze the results in the awake state. Putatively, in healthy individuals, muscle tone is high, most of the expiration is controlled (PIIA or glottal breaking) and the last part is passive (Morris et al., 1998). Moreover, the respiratory drive is modulated breath-to-breath to adapt to changing metabolic demand. Therefore, large variations in the early part within and between cycles may be due to a longer and variable active control of expiration. Whereas, low variation in the late part reflect a similar shorter passive exhale.

The interpretation of TBFV as a product of a given configuration of factors also serves to explain why a change in posture leads to higher differences during NREM than REM. During NREM, a postural change may perturb the stable factor configuration and displace respiratory control into another stable factor configuration. If the new configuration is different from the one before the perturbation, curve shapes will

present low correlation. During REM, the reduced dynamic range of the factors increases the chances that after a movement perturbation the curve shape will be similar to the preceding ones.

Since the averaged TBFV curves seemed to behave differently in different sleep stages, as demonstrated by the correlation distributions in Fig. 4, the TBFV curve variability of the whole night is affected by the relative amount of each sleep stage. As discovered in previous studies, the overall variability in tidal breathing patterns (from shorter recordings) was lowered during obstruction (Veiga et al., 2011; Dames et al., 2014; Frey and Bielicki, 2017; Fouzas et al., 2017; Hmeidi et al., 2018; Usemann et al., 2019). A similar lowering of the overall TBFV curve variability of the whole night could be achieved if the proportions of N2 or REM would grow in regards to the other sleep stages, since the averaged TBFV curves are least variable during these sleep stages. However, it is yet unclear whether the obstruction-related reduction in TBFV curve variability is more prominent in certain sleep stages or if it affects all stages equally. Hypothetically, following the above-mentioned interpretation, lower airway obstruction also reduces the dynamic range of some of the factors shaping TBFV. For instance, to ensure airways patency lungs are hyper-inflated by means of PIIA and glottal breaking (Pellegrino and Brusasco, 1997). Constricted factors would reduce the number of possible stable configurations between different NREM cycles, as well as lowering the chances of TBFV profiles being different within a cycle of any sleep stage or after motion perturbations.

It is also worth noting that the proportion of REM sleep decreases with age, taking approximately 30% of the sleep time in toddlers, while in adolescence and adulthood the time spent in REM sleep is around 20–25%. The proportion of REM sleep in the night decreases once more when reaching the age of 70 and onward. From birth to the age of 20, the percentage of time spent in N3 decreases rapidly from approximately 25% to around 15%. N3 sleep practically disappears after reaching the age of 60. (Carroll and Donnelly, 2014; Cardinali, 2018)

In addition to natural change due to aging, there are also sleep disorders and other conditions which hinder normal sleep (Anders and Eiben, 1997; Moore et al., 2006; Parish, 2009). All of these things which can affect the amount of time spent in different sleep stages also indirectly affect the breathing patterns, which may result in increased or decreased variability of breathing for the night. This has to be taken into consideration when assessing the cause of decreased tidal breathing variability, since in addition to lower airway obstructions, there could be other factors in play as well.

This study has some limitations. The types of body position changes are not stratified in any way although it is apparent that, for instance, a movement of the leg is likely to have less impact on breathing than complete change in sleeping position from side to side. Additionally, our sample size is relatively small but there was no patient group with lower airway obstruction included, thus providing group homogeneity. To better understand the mechanisms that drive the known reduction in tidal breathing variability in presence of lower airway obstruction future sleep studies should include patients with uncontrolled asthma and monitor their respiratory muscle activity in addition to PSG.

5. Conclusions

The late part (55–85% of exhaled volume) of the TBFV curves is significantly more stable than the early part (15–45%). Changes in the curve shape show higher temporal synchronicity between the beginning and end of the curve than with the 15-45 % part. For the early part of the TBFV curves, cycles of REM sleep are less variable than those of NREM, when comparing all cycles of the same sleep stage throughout the night. However, when analyzing the variability only within individual cycles of the same sleep stage, N3 is the least variable. Similar behaviour is not observed for the late part of the curve where REM is less variable than the NREM stages both between and within sleep stage cycles. Body position changes affect predominantly the early part of the

curve, but not as strongly as the sleep stage changes, which based on our findings are the main source of variability in the TBFV curves of the night in healthy subjects.

6. Conflict of interest statement

7. Author contributions

AH, VPS and DP conceived and designed the study. RGJ and DP collected the data. AH, VPS and MP designed and performed the analysis. AH, VPS and JGT wrote the paper. All authors contributed to manuscript revision, read and approved the submitted version.

8. Funding

Acknowledgments

References

Anders, T.F., Eiben, L.A., 1997. Pediatric sleep disorders: a review of the past 10 years. J. Am. Acad. Child Adolesc. Psychiatry 36, 9–20. https://doi.org/10.1097/00004583-199701000-00012.

Berry, R.B., Albertartio, C.L., Harding, S.M., 2018. The AASM Manual for the Scoring of Sleep and Associated Events: Rules, Terminology and Technical Specifications. American Academy of Sleep Medicine, Darien, IL.

Burioka, N., Cornélissen, G., Halberg, F., Kaplan, D.T., Suyama, H., Sako, T., Shimizu, E., 2003. Approximate entropy of human respiratory movement during eye-closed waking and different sleep stages. Chest 123, 80–86. https://doi.org/10.1378/chest.123.1.80.

Cardinali, D.P., 2018. The Timed Autonomic Nervous System. in: Autonomic Nervous System. Springer International Publishing, Cham 19–54. https://doi.org/10.1007/978-3-319-57571-1.

Carroll, J.L., Donnelly, D.F., 2014. Respiratory physiology and pathophysiology during sleep. In: Sheldon, S.H., Ferber, R., Kryger, M.H., Gozal, D. (Eds.), Principles and practice of pediatric sleep medicine, 2nd ed. Elsevier, pp. 179–194.

Dames, K.K., Lopes, A.J., de Melo, P.L., 2014. Airflow pattern complexity during resting breathing in patients with COPD: Effect of airway obstruction. Respir. Physiol. Neurobiol. 192, 39–47. https://doi.org/10.1016/j.resp.2013.12.004.

Donaldson, G., 1992. The chaotic behaviour of resting human respiration. Respir. Physiol. 88, 313–321. https://doi.org/10.1016/0034-5687(92)90005-H.

England, S.J., Ho, V., Zamel, N., 1985. Laryngeal constriction in normal humans during experimentally induced bronchoconstriction. J. Appl. Physiol. 58, 352–356. https://doi.org/10.1152/jappl.1985.58.2.352.

Fouzas, S., Theodorakopoulos, I., Delgado-Eckert, E., Latzin, P., Frey, U., 2017. Breath-to-breath variability of exhaled CO_2 as a marker of lung dysmaturity in infancy. J. Appl. Physiol. 123, 1563–1570. https://doi.org/10.1152/japplphysiol.00372.2017.

Frey, U., Bielicki, J.A., 2017. Fluctuation metrics as novel endpoints for clinical trials in asthma. Am. J. Respir. Crit. Care Med. 195, 967–968. https://doi.org/10.1164/rccm.201611-2286ED.

Gaultier, C., 1995. Cardiorespiratory adaptation during sleep in infants and children. Pediatric Pulmonol. 19, 105–117. https://doi.org/10.1002/ppul.1950190206.

Global Initiative for Asthma, 2018. Global Strategy for Asthma Management and Prevention.

Gracia-Tabuenca, J., Seppä, V.P., Jauhiainen, M., Kotaniemi-Syrjänen, A., Malmström, K.,

Pelkonen, A., Mäkelä, M.J., Viik, J., Malmberg, L.P., 2019. 2019. Tidal breathing volume profiles during sleep in wheezing infants measured by impedance pneumography. Journal of Applied Physiology. https://doi.org/10.1152/japplphysiol.01007.2018.. URL: https://www.physiology.org/doi/10.1152/japplphysiol.01007.2018.

Hmeidi, H., Motamedi-Fakhr, S., Chadwick, E.K., Gilchrist, F.J., Lenney, W., Iles, R., Wilson, R.C., Alexander, J., 2018. Tidal breathing parameters measured by structured light plethysmography in children aged 2-12 years recovering from acute asthma/wheeze compared with healthy children. Physiol. Rep. 6, e13752. https://doi.org/10.14814/phy2.13752.

Horner, R.L., 2010. in:Principles and Practice of Sleep Medicine. Respir. Physiol. 237–249.

Hutten, G.J., van Eykern, L.A., Latzin, P., Kyburz, M., van Aalderen, W.M., Frey, U., 2008. Relative impact of respiratory muscle activity on tidal flow and end expiratory volume in healthy neonates. Pediatr. Pulmonol. 43, 882–891. https://doi.org/10.1002/ppul.20874.

Malmberg, L.P., Seppä, V.P., Kotaniemi-Syrjänen, A., Malmström, K., Kajosaari, M., Pelkonen, A.S., Viik, J., Mäkelä, M.J., 2017. Measurement of tidal breathing flows in infants using impedance pneumography. Eur. Respir. J. 49, 1600926. https://doi.org/10.1183/13993003.00926-2016.

Moore, M., Allison, D., Rosen, C.L., 2006. A review of pediatric nonrespiratory sleep disorders. Chest 130, 1252–1262. https://doi.org/10.1378/chest.130.4.1252.

Morris, M., Madgwick, R., Collyer, I., Denby, F., Lane, D., 1998. Analysis of expiratory tidal flow patterns as a diagnostic tool in airflow obstruction. Eur. Respir. J. 12, 1113–1117. https://doi.org/10.1183/09031936.98.12051113.

Mortola, J.P., Milic-Emili, J., Noworaj, A., Smith, B., Fox, G., Weeks, S., 1984. Muscle pressure and flow during expiration in infants. Am. Rev. Respir. Dis. 129, 49–53. https://doi.org/10.1164/arrd.1984.129.1.49.

Motamedi-Fakhr, S., Wilson, R.C., Iles, R., 2016. Tidal breathing patterns derived from structured light plethysmography in COPD patients compared with healthy subjects. Med. Dev.: Evid. Res. 10, 1–9. https://doi.org/10.2147/MDER.S119868.

Niérat, M.C., Dubé, B.P., Llontop, C., Bellocq, A., Layachi Ben Mohamed, L., Rivals, I., Straus, C., Similowski, T., Laveneziana, P., 2017. Measuring ventilatory activity with structured light plethysmography (SLP) reduces instrumental observer effect and preserves tidal breathing variability in healthy and COPD. Front. Physiol. 8, 316. https://doi.org/10.3389/fphys.2017.00316.

Otis, A.B., Fenn, W.O., Rahn, H., 1950. Mechanics of breathing in man. J. Appl. Physiol. 2, 592–607. https://doi.org/10.1152/jappl.1950.2.11.592.

Parish, J.M., 2009. Sleep-related problems in common medical conditions. Chest 135, 563–572. https://doi.org/10.1378/chest.08-0934.

Pellegrino, R., Brusasco, V., 1997. On the causes of lung hyperinflation during bronchoconstriction. Eur. Respir. J. 10, 468–475. https://doi.org/10.1183/09031936.97.10020468.

Richter, D.W., Smith, J.C., 2014. Respiratory rhythm generation in vivo. Physiology 29, 58–71. https://doi.org/10.1152/physiol.00035.2013.

Rostig, S., Kantelhardt, J.W., Penzel, T., Cassel, W., Peter, J.H., Vogelmeier, C., Becker, H.F., Jerrentrup, A., 2005. Nonrandom variability of respiration during sleep in healthy humans. Sleep 28, 411–417. https://doi.org/10.1093/sleep/28.4.411.

Seppä, V.P., Hyttinen, J., Viik, J., 2011. A method for suppressing cardiogenic oscillations in impedance pneumography. Physiol. Measure. 32, 337–345. https://doi.org/10.1088/0967-3334/32/3/005.

Seppä, V.P., Hyttinen, J., Uitto, M., Chrapek, W., Viik, J., 2013a. Novel electrode configuration for highly linear impedance pneumography. Biomed. Eng. 58. https://doi.org/10.1515/bmt-2012-0068.

Seppä, V.P., Pelkonen, A.S., Kotaniemi-Syrjänen, A., Mäkelä, M.J., Viik, J., Malmberg, L.P., 2013b. Tidal breathing flow measurement in awake young children by using impedance pneumography. J. Appl. Physiol. 115, 1725–1731. https://doi.org/10.1152/japplphysiol.00657.2013.

Seppä, V.P., Pelkonen, A.S., Kotaniemi-Syrjänen, A., Viik, J., Mäkelä, M.J., Malmberg, L.P., 2016. Tidal flow variability measured by impedance pneumography relates to childhood asthma risk. Eur. Respir. J. 47, 1687–1696. https://doi.org/10.1183/13993003.00989-2015.

Seppä, V.P., Hult, A., Gracia-Tabuenca, J., Paassilta, M., Viik, J., Plavec, D., Karjalainen, J., 2019. Airway obstruction is associated with reduced variability in specific parts of the tidal breathing flow-volume curve in young children. ERJ Open Res. 5, 00028–02019. https://doi.org/10.1183/23120541.00028-2019.

Shee, C.D., Ploy-Song-Sang, Y., Milic-Emili, J., 1985. Decay of inspiratory muscle pressure during expiration in conscious humans. J. Appl. Physiol. 58, 1859–1865.

Traeger, N., Schultz, B., Pollock, A.N., Mason, T., Marcus, C.L., Arens, R., 2005. Polysomnographic values in children 2-9 years old: additional data and review of the literature. Pediatr. Pulmonol. 40, 22–30. https://doi.org/10.1002/ppul.20236.

Usemann, J., Suter, A., Zannin, E., Proietti, E., Fouzas, S., Schulzke, S., Latzin, P., Frey, U., Fuchs, O., Korten, I., Anagnostopoulou, P., Gorlanova, O., Frey, U., Latzin, P., Proietti, E., Usemann, J., 2019. Variability of tidal breathing parameters in preterm infants and associations with respiratory morbidity during infancy: a cohort study. J. Pediatr. 205, 61–69. https://doi.org/10.1016/j.jpeds.2018.10.002.

van der Ent, C., van der Grinten, C., Meessen, N., Luijendijk, S., Mulder, P., Bogaard, J., 1998. Time to peak tidal expiratory flow and the neuromuscular control of expiration. Eur. Respir. J. 12, 646–652. https://doi.org/10.1183/09031936.98.12030646.

Veiga, J., Lopes, A.J., Jansen, J.M., Melo, P.L., 2011. Airflow pattern complexity and airway obstruction in asthma. J. Appl. Physiol. 111, 412–419. https://doi.org/10.1152/japplphysiol.00267.2011.

Willemen, T., Deun, D.V., Verhaert, V., Vandekerckhove, M., Exadaktylos, V., Verbraecken, J., Huffel, S.V., Haex, B., Sloten, J.V., 2014. An evaluation of cardiorespiratory and movement features with respect to sleep-stage classification. IEEE J. Biomed. Health Inform. 18, 661–669. https://doi.org/10.1109/JBHI.2013.2276083.